Development of a platform technology for the cell-free synthesis and functional characterization of toxic proteins with clinical and diagnostic relevance:

Applications of bacterial enterotoxins, ribosome-inactivating proteins and viral cytotoxins

Univ.-Diss. by

Franziska Ramm

to be awarded the academic degree of
“doctor rerum naturalium” (Dr. rer. nat.)

submitted to the
Department of Biology, Chemistry, Pharmacy
Institute of Chemistry and Biochemistry
of the

Freie Universität Berlin

Conducted at the
Fraunhofer Institute for Cell Therapy and Immunology,
Branch Bioanalytics and Bioprocesses (IZI-BB),
Potsdam-Golm, Germany

Fraunhofer
IZI-BB

Berlin 2022

Reviewer: 1. Dr. Stefan Kubick

2. Prof. Dr. Markus Wahl

Date for the thesis defence: October 20th 2022

Eidesstattliche Erklärung

Hiermit erkläre ich, Franziska Ramm, an Eides statt, dass die eingereichte Arbeit mit dem Titel „Development of a platform technology for the cell-free synthesis and functional characterization of toxic proteins with clinical and diagnostic relevance: Applications of bacterial enterotoxins, ribosome-inactivating proteins and viral cytotoxins“ oder wesentliche Teile derselben in keinem anderen Verfahren zur Erlangung eines akademischen Grades vorgelegt worden sind. Ich versichere darüber hinaus, dass bei der Anfertigung der Dissertation die Grundsätze zur Sicherung guter wissenschaftlicher Praxis der DFG eingehalten wurden, die Dissertation in allen Teilen von mir selbständig und ohne fremde Hilfe angefertigt wurde, andere als die von mir angegebenen Quellen und Hilfsmittel nicht benutzt worden sind und die den benutzten Werken wörtlich oder sinngemäß entnommenen Stellen als solche kenntlich gemacht wurden. Veröffentlichungen von Teilen der vorliegenden Dissertation sind von mir wie folgt vorgenommen worden und an den jeweiligen Stellen zitiert worden.

Weiter erkläre ich, dass ich nicht schon anderweitig einmal die Promotionsabsicht angemeldet oder ein Promotionseröffnungsverfahren beantragt habe.

Berlin,

_____

(Franziska Ramm)

Acknowledgements

With the following words, I would like to express my thanks and gratitude to all of whom supported me and this work. Firstly, I would like to express my gratitude to Dr. Stefan Kubick for giving me the opportunity to conduct my doctoral thesis in his group and for his supervision. Secondly, I would like to express my gratitude to Prof. Dr. Markus Wahl for supervising this doctoral thesis.

I would like to thank the Fraunhofer-Gesellschaft for the Talenta scholarship and the IZI-BB for welcoming me at the institute. A great thanks belongs to the whole “Cell-free Protein Synthesis” research group for the continuous help and support as well as motivating talks. Especially, I would like to thank Dr. Anne Zemella, Jeffrey Schloßhauer, Dana Wenzel, Lisa Haueis, Jessica Ullrich, Dr. Dominik Jescheck, Hoai Anh Trinh and Nathanaël Rakotoarinoro. Life as a PhD student wouldn’t have been the same. I always had a place to go when I needed advice, concerning both my professional career and work as well as personal matters. A great thanks goes to Dr. Marlitt Stech, Dr. Lena Thoring and Dr. Anne Zemella for the fruitful discussions and suggestions throughout the thesis. Moreover, I would like to thank the OE330 and Dana Wenzel for preparing the cell-free lysates. Further, I would like to thank Beate Morgenstern and Anika Anderson for introducing me to the cell culture and organizing the daily routines in the cell culture lab. Further, I would like to address Dr. Srujan Dondapati for the introduction to electrophysiology and the help on the measurements.

Kind and special thanks go to the students I supervised, which were a big help in the lab. I would like to thank Hoai Anh Trinh for the synthesis of Hepatitis E Virus proteins, Lena Jack for establishing the synthesis of the AB_5 toxins, Pauline Löffler for the preparation of the IL-13 constructs, Danny Kaser for optimizing CytK, Anna Schöntag for studying the superantigens, Lukas Hübner for working on the IL-13-Shiga clickable immunotoxin and Benjamin Skorupa for the synthesis of SARS-CoV2 spike proteins. Furthermore, I would like to express my gratitude to Dr. Hendrik Frentzel from the BfR for the cooperation in the *Bacillus cereus* projects, to Prof. Dr. Fuchs who provided the toxin sequences as well the Saponin and surgeons from the Charité-Universitätsmedizin Berlin (Prof. Dr. Ervens, Dr. Koerdt, Dr. Kreutzer) for the sampling of tumor probes.

Additionally, I would like to express my gratefulness to Dr. Anne Zemella, Dr. Marlitt Stech and Dr. Stefan Kubick for reviewing this manuscript.

At last, this work would not have been possible without the loving support of my family, friends and my husband Timo not only throughout this thesis but also throughout my entire studies. Thank you for the enduring patience and encouragement.

Abstract

A toxin can be described as a foreign substance that inflicts damages to living organisms. Naturally occurring proteinaceous toxins can derive from bacteria, fungi, plants, animal venoms and even viruses. Identifying the toxins' underlying mechanisms of action has been a major research interest in order to develop inhibitors against their effects. Nonetheless, various findings have sparked the use of toxic moieties for the medical benefit resulting in treatment options as for example for cancers.

To gain novel insights into the structure and function of a toxin, the toxin itself has to be synthesized. *In vivo* production can involve high laboratory safety standards as well as a low total protein amount since the toxin might harm the overexpressing cell. An alternative to circumvent these drawbacks is cell-free protein synthesis (CFPS). Within this doctoral thesis CFPS was established as a platform technology for the production and application of proteinaceous toxins in diagnostic and medical fields.

As a first step, various bacterial toxins were analyzed. The mechanisms of action of the tripartite pore-forming toxins (PFT) Hbl and Nhe were studied by hemolytic activity assays, cell-based toxicity assessments and electrophysiological recordings. Next, the PFT CytK was analyzed to identify its potential as a biological nanopore that can be used as a diagnostic tool. This thesis identified the CytK1 variant as a candidate for a nanopore development. Further, two AB_5 toxins, namely the cholera toxin and the heat-labile enterotoxin, were modified. These modified toxins could be fluorescently labeled and tested for their functional activity. These data are a proof-of-concept for using CPFS for intracellular trafficking of toxins and coupling of payloads for drug delivery.

In a second step, a targeted toxin combining the plant-derived toxin Dianthin and the epidermal growth factor (EGF) was assessed for its potency as a potential cancer therapeutic. The medical benefit of this Dianthin-EGF targeted toxin was demonstrated on human squamous cell carcinoma samples. 0.1 nM Dianthin-EGF in combination with an endosomal escape enhancer suppressed the growth of carcinoma colonies by almost 50%.

As a third and last step, CFPS was assessed for its potential as a rapid response system against novel viral pathogens using SARS-CoV2 viral proteins. All SARS-CoV2 proteins could be synthesized and analyzed. The cytotoxic behaviors of the nsp1 and envelope protein were determined. The nucleocapsid protein was quantitatively detected by specific antibodies thereby facilitating cell-free systems for the validation of available antibodies.

All in all, this thesis successfully developed a platform technology for the cell-free synthesis, functional characterization and application of toxic proteins in clinical and diagnostic fields.

Zusammenfassung

Ein Toxin ist ein Fremdstoff, der lebenden Organismen Schaden zufügt. Natürliche proteinogene Toxine können von Bakterien, Pilzen, Pflanzen, Tiergiften und sogar Viren stammen. Die Identifizierung der zugrundeliegenden Wirkungsmechanismen bildet die Grundlage, um Stoffe zu entwickeln, die diese Toxine hemmen. Andererseits können toxische Komponenten auch für medizinische Zwecke eingesetzt werden. Um neue Erkenntnisse über die Struktur und Funktion eines Toxins zu erlangen, muss dieses zunächst hergestellt werden. Die *In-vivo*-Produktion von Toxinen kann zu hohen Sicherheitsstandards im Labor führen. Des Weiteren kann dies mit einer geringen Gesamtproteinmenge einhergehen, da das Toxin die Wirts-Zelle schädigen könnte. Eine Alternative zu dieser nachteilhaften Methode ist die zellfreie Proteinsynthese. Im Rahmen dieser Dissertation wurde die zellfreie Proteinsynthese als Plattformtechnologie für die Herstellung und Applikation von proteinogenen Toxinen in diagnostischen und medizinischen Bereichen etabliert.

Im ersten Schritt wurden diverse bakterielle Toxine analysiert. Die Wirkmechanismen der hetero-multimeren porenbildenden Toxine Hbl und Nhe wurden durch Hämolyse-Studien, zellbasierte Toxizitätsuntersuchungen und elektrophysiologische Messungen untersucht. Anschließend wurde das homo-multimere porenbildende Toxin CytK analysiert, um seinen Nutzen als biologische Nanopore zu überprüfen und es damit als diagnostisches Werkzeug einzusetzen. Die CytK1-Variante wurde dabei als ein potenzieller Kandidat identifiziert. Darüber hinaus wurden das Choleratoxin und das hitzelabile Enterotoxin, zwei Vertreter der AB_5-Toxine, modifiziert. Diese modifizierten Toxine konnten mit Fluoreszenzfarbstoffen markiert und anschließend auf ihre funktionelle Aktivität hin getestet werden. Diese Daten bilden einen *Proof-of-Concept* für die Verwendung zellfrei modifizierter Toxine für die Verfolgung des intrazellulären Transports von Toxinen und die Kopplung von Wirkstoffen an Toxindomänen für die Verabreichung von Medikamenten.

In einem zweiten Schritt wurde ein zielgerichtetes Toxin, ein sogenanntes *targeted toxin*, auf seine Wirksamkeit als potenzielles Krebstherapeutikum untersucht. Das ursprünglich aus Pflanzen gewonnene Toxin Dianthin und der humane epidermale Wachstumsfaktor (EGF) wurden hierzu kombiniert und zellfrei hergestellt. Der medizinische Nutzen dieses Dianthin-EGF-Toxins wurde an menschlichen Plattenepithelkarzinomproben nachgewiesen. Kleinstmengen von Dianthin-EGF in Kombination mit einem „Endosomal Escape-Enhancer“ verringerten das Wachstum der Karzinomkolonien um fast 50%.

In einem dritten und letzten Teil wurde die zellfreie Proteinsynthese als sogenanntes *rapid response* System (Schnellantwort) gegen neuartige virale Krankheitserreger validiert. Hierfür wurden die viralen Proteine des neuartigen Coronavirus (SARS-CoV2) verwendet. Alle Proteine konnten hergestellt und analysiert werden. Das zytotoxische Verhalten des

nsp1 Proteins sowie des Hüllproteins wurde bestimmt. Des Weiteren wurde das Nukleokapsidprotein durch spezifische Antikörper quantitativ nachgewiesen. Diese Ergebnisse zeigen, dass das zellfreie Proteinsynthesesystem somit die Validierung verfügbarer Antikörper erleichtert.

Zusammenfassend wurde in der vorliegenden Arbeit eine Plattformtechnologie für die zellfreie Synthese und anschließende funktionelle Charakterisierung und Anwendung proteinogener Toxine für den klinischen und diagnostischen Bereich erfolgreich entwickelt.

List of abbreviations

ADP ..... Adenosine diphosphate
aHL ..... α-Hemolyin
Amp ..... Ampicillin
ANOVA ..... Analysis of variance
APS ..... Ammonium persulfate
ATP ..... Adenosine triphosphate
AzF ..... p-Azido-L-Phenylalanine
B. cereus ..... *Bacillus cereus*
BfR ..... Bundesinstitut für Risikobewertung
bp ..... base pairs
BSA ..... Bovine serum albumin
$CaCl_2$ ..... Calcium chloride
cAMP ..... Cyclic adenosine monophosphate
CECF ..... Continuous-exchange cell-free system
CFPS ..... Cell-free protein synthesis
CHAPS ..... 3-((3-cholamidopropyl)-dimethylammonio)-1-propanesulfonate
Cho ..... Cholesterol
CHO ..... Chinese Hamster Ovary
CIP ..... Calf intestinal alkaline phosphatase
CLSM ..... Confocal laser scanning microscopy
CO_2 ..... Carbon dioxide
CrPV ..... Cricket paralysis virus
CTP ..... Cytidine triphosphate
Ctx ..... Cholera toxin
$CuSO_4$ $5H_2O$ ..... Copper(II) sulfate pentahydrate
CytK ..... Cytotoxin K
ddH_2O ..... Bidestilled water
DDM ..... Dodecyl -D-maltoside
DMEM ..... Dulbecco Modified Eagle Medium
DMSO ..... Dimethyl sulfoxide
DNA ..... Deoxyribonucleic acid
DPhPC 1,2-diphytanoyl-sn-glycero-3-phosphocholine
DT ..... Diphtheria toxin
DTT ..... Dithiothreitol
E. coli ..... *Escherichia coli*
eAzFRS ..... *E. coli* tyrosine-tRNA-synthetase
EDTA ..... Ethylene diamine tetraacetic acid
EGF ..... Epidermal growth factor
EGFR ..... Epidermal growth factor receptor
EGTA ..... Ethylene glycol tetra acetic acid
Endo H ..... Endoglycosidase H
ER ..... endoplasmic reticulum
eYFP ..... Enhanced yellow fluorescent protein
FBS ..... Fetal bovine serum
GTP ..... Guanosine triphosphate
H2SO4 ..... Sulfuric acid
Hbl ..... Hemolysin BL
HCl ..... Hydrochloric acid
HEK293 ..... Human embryonic kidney cells
HEPES ..... Hydroxyethyl-piperazineethane sulfonic acid
Hifi ..... HotStart HiFidelity DNA Polymerase
IC_{50} ..... Half maximal inhibitory effect
IPTG ..... Isopropyl-β-D-thiogalactopyranoside

IRES ..... Internal ribosome entry sites
KCl ..... Potassium chloride
KOAc ..... Potassium acetate
KOH ..... Potassium hydroxide
LB ..... Lysogeny broth
LT ..... Heat-labile enterotoxin
LUC ..... Luciferase
MECA ..... Multi-Electrode Cavity Array
Mel ..... Melittin
MEM ..... Minimum Essential Medium
MERS-CoV ..... Middle East respiratory syndrome coronavirus
MF ..... Microsomal fraction
$Mg(OAc)_2$ ..... Magnesium acetate
$MgCl_2$ ..... Magnesium chloride
$MgSO_4$ ..... Magnesium sulfate
mRNA ..... messenger ribonucleic acid
MTT ..... 3-(4,5-dimethylthiazol-2-yl)-2,5-diphenyltetrazolium bromide
NaAsc ..... Sodium ascorbate
NaCl ..... Sodium chloride
NaH_2PO_4 ..... Sodium dihydrogen phosphate
NaN_3 ..... Sodium azide
NaOAc ..... Sodium acetate
Nat-SP ..... Native signal peptide
ncAA ..... Non-canonical amino acids
NEAAs ..... Non-essential amino acids
Nhe ..... Non-hemolytic enterotoxin
nsp ..... Non-structural proteins
ORFs ..... Open reading frames
P. pastoris ..... *Pichia pastoris*
PBS ..... Phosphate-buffered saline
PCR ..... Polymerase chain reaction
PE ..... Pseudomonas exotoxin
Pen/Strep ..... Penicillium/Streptomycin
Pen/Strep/Ampho ..... Penicillium/Streptomycin/Amphotericin B
PFTs ..... Pore-forming toxins
PNGase F ..... Peptide-N-Glycosidase F
PolyG ..... Poly guanin
polyPEG ..... Poly-dispersed poly-ethylene glycol
pPa ..... p-propargyloxy-L-Phenylalanine
PTMs ..... Post-translational modifications
PURE ..... Protein synthesis using recombinant elements
RdRp ..... RNA-dependent RNA-polymerase
RIP ..... Ribosome inactivating proteins
RLU ..... Relative light units
RNA ..... Ribonucleic acid
rpm ..... Revolutions per minute
S. cerevisiae ..... *Saccharomyces cerevisiae*
SARS-CoV ..... Severe acute respiratory syndrome coronavirus
SARS-CoV2 ..... Severe acute respiratory syndrome coronavirus type 2
SDS ..... Sodium dodecyl sulphate
SDS-PAGE ..... Sodium dodecyl sulphate polyacrylamide gel electrophoresis
*Sf*21 ..... *Spodoptera frugiperda* 21
SN ..... Supernatant
SN2 ..... Second supernatant
SOC ..... Super optimal broth with catabolite repression
SRP ..... Signal recognition particle

Strep.....Streptavidin
TBE .....Tris base borate EDTA
TBS ..... Tris-buffered saline
TBST .....TBS-Tween
TCA ..... Trichloroacetic acid
TDH ..... Thermostable direct hemolysin
TEMED ..... *Tetramethylethylenediamine*
TGF ..... Transforming growth factor
THPTA..... Tris(3-hydroxypropyltriazolylmethyl)amine
TM ..... Translation mixture
TMB.....Tetramethylbenzidine
TMR..... Tetramethylrhodamine
Tris .....Tris(hydroxymethyl)-aminomethane
tRNA.....Transfer ribonucleic acid
UTP .....Uridine triphosphate
VLP.....Virus-like particles
WT.....Wild type

Table of Contents

1 Introduction

1.1 Preface - Toxic proteins

A toxic compound is defined as a xenobiotic substance that causes damage to a living organism[1]. Toxicity is generally associated with chemical substances or side effects of medical compounds, but naturally occurring substances can cause toxic effects as well. Such substances can derive from bacteria, fungi or even viruses, and are present in plants as self-defense mechanisms or are part in venoms from poisonous animals such as snakes, spiders or jellyfish. On the one hand, these naturally occurring toxins are proteinaceous compounds that are pre-synthesized in the organisms and cause hazardous effects in animals or human beings after their exposure[1,2]. On the other hand, when a host organism is infected by a virus, cytotoxic effects can occur. Such effects are triggered as the virus itself encodes a cascade of proteins which are translated in the host organism and collectively these proteins harm the host[3]. Either way, proteinaceous substances cause toxic or even lethal events and are the main virulence factors of the pathogen. Therefore, the scientific world was focused on identifying toxic compounds and finding antidotes against them. A complexity of various toxic proteins presenting tremendous mechanisms of action was discovered. In the 15th century Theophrastus Bombast von Hohenheim (Paracelsus) implied that the dose of a substance defines its toxicity and at a certain dosage everything can be toxic[4]. With that in mind, the idea sparked that the toxic effect could also be used for a medical benefit, resulting in Paul Ehrlich`s magic bullet concept in the early 1900s[5]. A new era of research started using toxins to target diseases such as cancers, resulting in targeted toxins.

1.2 Synthesis of proteinaceous toxins

When studying toxic proteins a major difficulty is the availability of the toxin itself. Moreover, toxins are part of the dual-use regulation VO (EU) 2021/821 and therefore the production of toxins is limited to research purposes and to low scale productions[6]. Hence, data on the expression of toxic proteins are generally only available for single research projects.

Ordinarily, toxins can either be directly extracted from the organism that naturally expresses it or it is synthetically synthesized. Animal toxins are usually contained in venoms comprising a variety of toxins. Such venoms normally derive from the respective organism itself as for example by applying pressure to the venomous glands or electric stimulation of spiders, snakes or bees[7,8].

The generation of synthetically synthesized toxins is rather difficult. Standard operating procedures in bioproduction of recombinant proteins generally focus on prokaryotic and

eukaryotic cell-based expression systems[9–12]. Unfortunately, a variety of toxins target eukaryotic cells, which results in inefficient protein yields in eukaryotic systems and also results in dangerous handling procedures for human beings. Data on cell-based expression of toxins is rather limited, which might be caused by the fact that these so-called difficult-to-express proteins cannot be synthesized in high yields or in an active manner as they might harm living eukaryotic cells. Thus, toxins are usually synthesized in cell-based prokaryotic expression systems. When toxins, generally bacterial toxins, are obtained by cultivating bacterial strains, higher laboratory standards might occur as various strains encode endotoxins themselves as described by technical rules for biological agents TRBA 466[13]. Therefore, in many cases toxins are synthesized as inactive fragments such as only synthesizing the binding domains or targeted toxins with truncated fragments are developed[9,14,15]. Another possibility is the synthetic production of peptide fragments as for example by solid-phase synthesis[16,17].

When expressing cytotoxic viral proteins in cell-based systems high laboratory standards are needed as well, as a zoonosis could occur. Especially when handling novel zoonotic viruses, there is a high risk for a human pathogenic disease[18], which further enlarges the necessary safety standards.

All of these procedures have major drawbacks. Cell-based and naturally isolated toxins are in need of a series of purification methods to further study the specific toxin of interest[9] as various byproducts such as other endogenous proteins are present in the extracted mixture. Moreover, they are cost-intensive measures and can be harmful to the respective living organisms. Synthetic peptides are mainly limited in their size. An alternative to circumvent these obstacles is presented by cell-free protein synthesis.

1.2.1 Cell-free protein synthesis

Cell-free protein synthesis (CFPS), which is also termed *in vitro* translation, uses a cell lysate rather than viable cells. The method dates back to the early 1960s when Matthaei and Nirenberg established the basis for the *Escherichia coli* (*E. coli*) based lysate[19]. Interestingly, their original idea was to study the translation machinery and this concept was further developed to the lysate as it is known today. Since then, decades of research resulted in a variety of different lysates originating from prokaryotes as well as eukaryotes and CFPS has established itself as an efficient alternative to conventional *in vivo* protein synthesis. The lysate used comprises all essential components that are needed for the successful translation of a protein. In order to obtain an active cell lysate, the cell line of interest is grown, usually as a suspension culture, and fermented[20]. The harvested cells are disrupted and the extracts are further processed. The cell disruption and processing are crucial steps in the lysate generation. Cell membranes and the nuclei of the cell itself are removed from the lysate. Essential components for the translation machinery such as

ribosomes, initiation/ elongation/ termination factors and chaperones maintain within the crude lysate[20]. Endogenous nucleic acids are depleted from crude cell extract by a micrococcal nuclease[21]. For a functional protein synthesis, the cell lysate is further supplemented with energy in the form of adenosine triphosphate (ATP), an energy regeneration system, canonical amino acids and a nucleic acid template for the protein of interest[20,22,23]. As the cell-free system is an open system, any kind of supplement can be added to the reaction, which allows for the adaptation of the reaction conditions to the protein's individual needs.

The choice of the template defines the synthesis mode to be applied. A circular or linear deoxyribonucleic acid (DNA) template can be used in a so-called coupled mode (Figure 1), where transcription and translation run in parallel[20,24]. Linear DNA templates as derived from a polymerase chain reaction (PCR) can be necessary whenever a template has to be modified as for example when adding a purification tag, specific regulatory sequences or mutating the gene of interest. Such modifications are especially important when using toxin encoding templates, as cloning procedures harbor major challenges[25–27]. The generation of a genetically modified organism by cloning procedures would lead to higher safety levels in the laboratory.

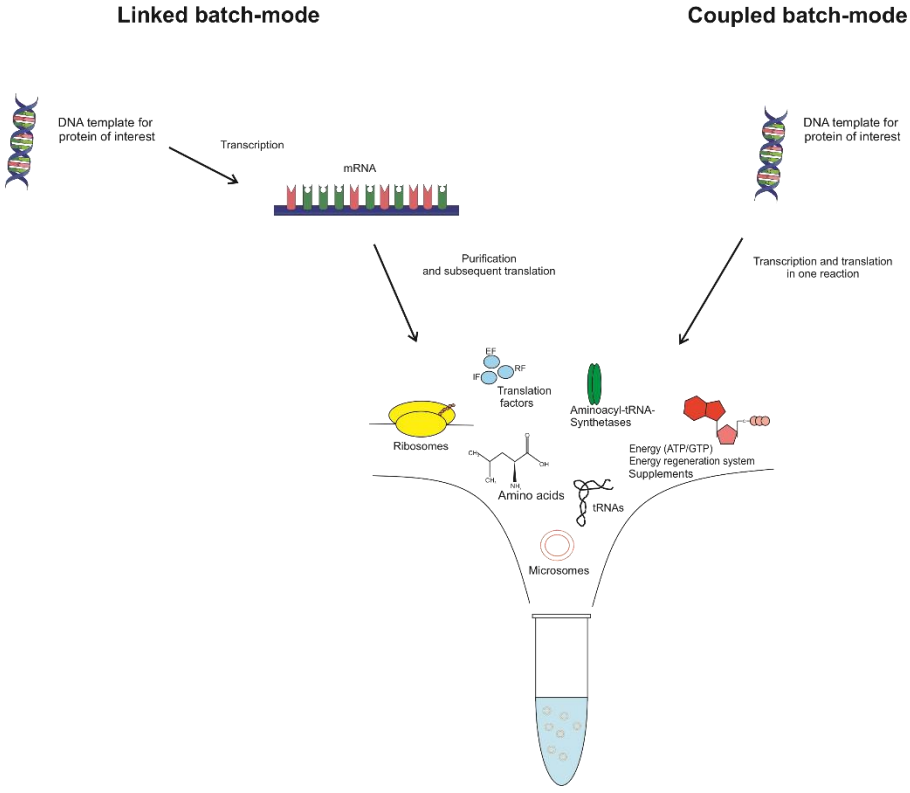

Figure 1: Batch-based cell-free protein synthesis.

The second synthesis mode is the so-called linked system. A previously transcribed and purified messenger ribonucleic acid (mRNA) is supplemented to the cell-free system[28] (Figure 1).

Cell-free syntheses can be further divided into different reaction modes. The easy to handle mode is the batch-based reaction, which takes place in a single tube as shown in Figure 1. Such a reaction is not only easy to prepare but also time efficient as the synthesis takes place within 90 min to 3 hours[29]. The total protein yields are limited as the energy supply is continuously consumed and inhibitory phosphate complexes are formed[30]. To circumvent these drawbacks, a two chambered system was developed. The reaction and feeding chamber are divided by a semi-permeable dialysis membrane[31] (Figure 2). This system therefore enables that inhibitory byproducts cannot accumulate within the reaction and the reaction itself is continuously supplied with energy, amino acids, buffer and salt components. Hence, this mode was called a continuous-exchange cell-free system (CECF) and permits a synthesis of up to 72 h[32,33].

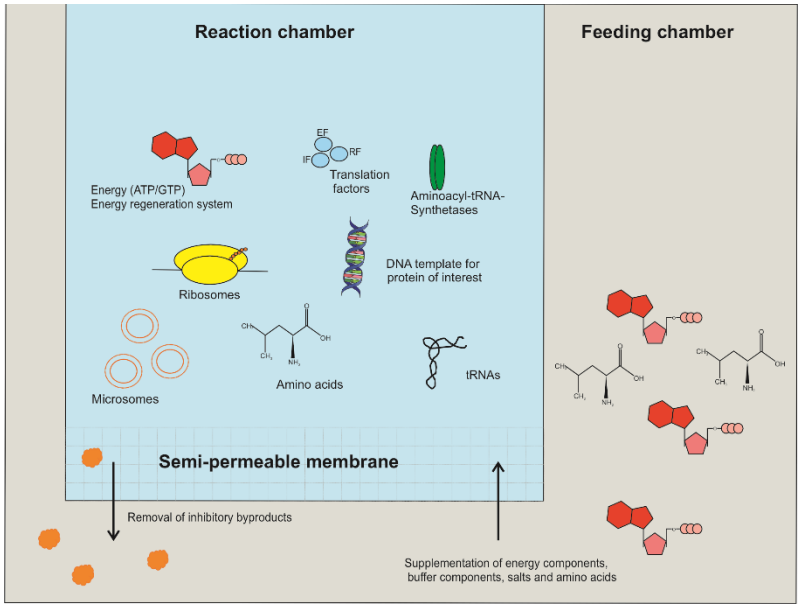

Figure 2: CECF based cell-free reaction.

1.2.1.1 Cell-free systems

The general basis of CFPS is the translationally active cell lysate. Even though lysates originate from different cell types, the basic principle of the reaction maintains the same. Until today lysates derive from diverse cell types including prokaryotic, fungal, plant, insect and even mammalian cells. The first cell-free system was based on an idea from the 1960s where an *E. coli* lysate was used to study the translation machinery[19]. The potential of this system has been enhanced ever since and is nowadays known as the high yield cell-free system[29,34]. Even though there are a number of prokaryotic systems such as from

Vibrio natriegens and *Bacillus subtilis*, the *E. coli* system is the most developed and used prokaryotic system[34]. Unfortunately, impurities from the lysate including endogenous proteins led to difficulties in downstream applications and background noise in functionality assays. This resulted in the development of a modified protein synthesis using recombinant elements (PURE) *E. coli* system. *E. coli* components needed for CFPS are purified or modified before they are supplemented to the lysate[35]. This lysate resulted in optimized results with lower background noise. Another drawback of prokaryotic cell-free systems is the lack of post-translational modifications (PTMs), which, if present in the protein of interest, are essential to the proper folding and functionality of a protein. The missing endogenous membranous structures could be the cause of the lack in PTMs. Further, membranes are of utmost importance for membrane proteins as the insertion of the protein into the membrane allows for their correct folding. In order to circumvent these missing features, supplementation of different components during and after the reaction was performed. Detergents, liposomes, so-called nanodiscs or even microsomal structures were added when synthesizing membrane proteins and redox-systems were supplemented[36]. With the help of these modifications disulfide bridging as well as minor artificial glycosylation patterns could be generated[34].

The development and optimization of eukaryotic cell-free systems was the next step to establish CFPS as an alternative to conventional *in vivo* production systems. In comparison to prokaryotic systems, eukaryotic systems generally do not yield protein amounts as high as in an *E. coli* system, but PTMs are more easily accessible[29,34]. Eukaryotic systems offer many PTMs such as glycosylation, disulfide bridging and signal peptidase cleavage[34]. A wide range of different eukaryotic lysates has been developed and the developmental process is still ongoing to establish the best suited lysate. The choice of the cell-free lysate depends upon the protein of interest and its individual characteristics as each individual system has its benefits and drawbacks[29,34].

The first eukaryotic lysate originates from the reticulocytes of anaemic rabbits and is called the rabbit reticulocyte system. It was first used for protein synthesis in 1958[37]. Unfortunately, this system has low total protein yields and membranous structures have to be additionally supplemented to the synthesis[34]. Recent studies have shown that the inclusion of different internal ribosome entry sites (IRES) site can lead to a 10-fold increase in protein yields[38].

Eukaryotic systems that were established since then have focussed on surpassing the low total protein yields and focussed on including membranous vesicles. One of the most prominent and well-characterized eukaryotic system is the insect cell derived system, namely the *Spodoptera frugiperda* 21 (*Sf*21) cell-free system[28,39]. This lysate paved the way for the following cell-free systems as many optimizations were performed which could

be transferred to other eukaryotic systems. The most striking feature of this lysate are the endogenous microsomes, which are natural membranous structures derived from the endoplasmic reticulum (ER). These vesicles allow for signal peptide cleavage, co-translational translocation and PTMs such as glycosylation, disulfide bridging and phosphorylation[34]. Therefore, this system is essential for the synthesis of post-translationally modified proteins and membrane proteins which can be synthesized in the presence of a natural membranous surrounding[40]. In comparison to prokaryotic systems, the total protein yield was low in the beginning, but the introduction of the melittin (Mel) signal peptide and the shift from a cap-dependent translation to a cap-independent translation by the introduction of an IRES from the cricket paralysis virus (CrPV). This improved the translation initiation process within the lysate to a competitive system. A 100-fold increase of the protein yield to up to 285 µg/mL could be obtained[41].

In order to establish cell-free systems as a methodology for the production of pharmaceutical proteins a lysate based on Chinese Hamster Ovary (CHO) cells came into focus. This cell-free system contains endogenous microsomal structures allowing the accessibility of all the relevant PTMs carried out by the ER[20,34]. Tremendous increases in total protein yields of up to 980 µg/mL could be achieved by the usage of the CrPV IRES and the CECF manner[40,42] facilitating the CHO cell-free system as a high yield protein production system.

To date, CFPS is rarely used for the production of therapeutics, but using a mammalian cell-free lysate derived from cultured human cell lines might be beneficious for such applications. The codon usage in such systems would match to the therapeutically relevant protein of interest and it could be shown that this leads to the ability to synthesize highly complex proteins[43]. Human cell lines used for lysate preparation are human embryonic kidney cells (HEK293)[44], the cervical cancer cell line HeLa[43] and the myelogenous leukemia cell line K562[40]. Only few studies using lysates derived from human cell lines have been published and the systems yet have to be standardized and optimized. As human lysates contain endogenous microsomal structures and are therefore able to post-translationally modify proteins[34,40], these systems are promising for future developments.

Apart from mammalian and insect based systems other alternatives have been developed in parallel in the beginnings of CFPS. Two plant cell derived lysates have already been established. In the early 1970s the wheat germ cell-free extract was first introduced[45] and continuous optimizations as well as the use of the CECF system have led to a high yield cell-free system with yields ranging up to a scale of mg/mL[46]. Nonetheless, a major drawback of this system, is the lack of PTMs as no endogenous microsomal structures

are present[34]. The second plant based cell-free system is the tobacco BY-2 cell lysate which might overcome this bottleneck as newer studies have optimized the lysate preparation in order to synthesize glycosylated proteins also containing disulfide bridges[47,48].

Another option are fungal lysates as the cultivation of these cells is cost-efficient. The optimization of fungal cell-free lysates resulted in various stable cell-free synthesis systems such as from yeasts like *Saccharomyces cerevisiae (S. cerevisiae)*[49] or *Pichia pastoris (P. pastoris)*[50]. Even though in the beginning the total protein yields were rather low compared to other cell-free systems, recent studies have shown that within a few hours protein yields of up to 50 µg/mL could be achieved[50]. This suggests that they are promising candidates for high-yielding systems. In addition to that, fungal systems are promising as they display PTMs[34].

In the end, the proteins characteristics and its mechanism of action define the choice of the lysate. The downstream application such as cell-based assays or high-throughput screenings can further define the choice of the lysate.

1.2.1.2 Current applications of cell-free protein synthesis

Dating back to the beginnings of CFPS, cell-free systems were used to study the effect of individual proteins on the translation machinery. Proteins known to inhibit a certain pathway within the transcription/ translation process, such as ribosomes, were added to the cell-free synthesis of a model protein and it was investigated whether the synthesis rate decreased[51,52]. Since then CFPS has become a more prominent instrument in diagnostic and therapeutic applications. The open nature of CFPS allows for individual adaptations to the proteins need but also to the downstream application in which the protein of interest will be used. A tremendous amount of proteins has already been synthesized by cell-free synthesis. Membrane proteins[33,40,41,53], glycoproteins[40], antibodies[48] and even toxic proteins[54] were expressed, offering the opportunity to characterize individual proteins and identify their mechanism of action. This is why also therapeutically relevant proteins such as the epidermal growth factor receptor (EGFR)[41] have already been synthesized in cell-free systems. Further, CFPS is a scalable system offering syntheses ranging from small scale reactions in microwell plates to reactions in liter batches. The scalability of the system, the possibility to use PCR templates and the versatility of the reaction modes and formats allow for high-throughput-screenings[34,55]. Such screenings could either be the screening of different modified templates such as mutants or templates harboring different signal peptides and allow for the screening of pharmaceutically relevant inhibitors.

As already mentioned, a major advantage of CFPS is the easy modification of templates allowing to study different templates, such as mutants or a protein carrying different purification tags[26], in a parallel and reproducible manner. CFPS further enables the modification of the protein itself. A site-directed modification of a protein can be performed by the insertion of a so-called amber stop codon into the genetic template[56]. Using this technique non-canonical amino acids (ncAA) can be integrated into the protein of interest and therefore the genetic code is extended. This results in novel possibilities for protein modification and protein engineering. An orthogonal system is used where a reaction does not integrate the natural components of the system into the amber stop codon during protein translation. In this case a suppressor transfer ribonucleic acid (tRNA) addressing the amber codon and a corresponding aminoacyl-tRNA-synthetase are used and supplemented to the reaction. An orthogonal system has to maintain certain criteria. On the one hand, the orthogonal synthetase should not be aminoacylated by the endogenous tRNA in the system and on the other hand the orthogonal tRNA should not be detected by the endogenous synthetase. The same principle applies to the ncAA. The ncAA should only be detected by the orthogonal synthetase and not by the endogenous one[57,58]. Addressing the amber stop codon by the suppressor-tRNA competes with the termination of the translation which results in two protein products, namely the terminated and the full-length protein. An optimized orthogonal system will lead to higher amounts of full-length rather than terminated protein. Subsequently, the incorporation of ncAAs can be used to label the protein site-specifically at the desired position. The choice of the ncAA defines the label that can be inserted into the protein, as each ncAA harbors chemically reactive side chains[29]. The general construct of an orthogonal system is presented in Figure 3. Studies have shown that this technique was successfully established for CFPS for glycoengineering erythropoietin[59] or even antibody-drug conjugates[60].

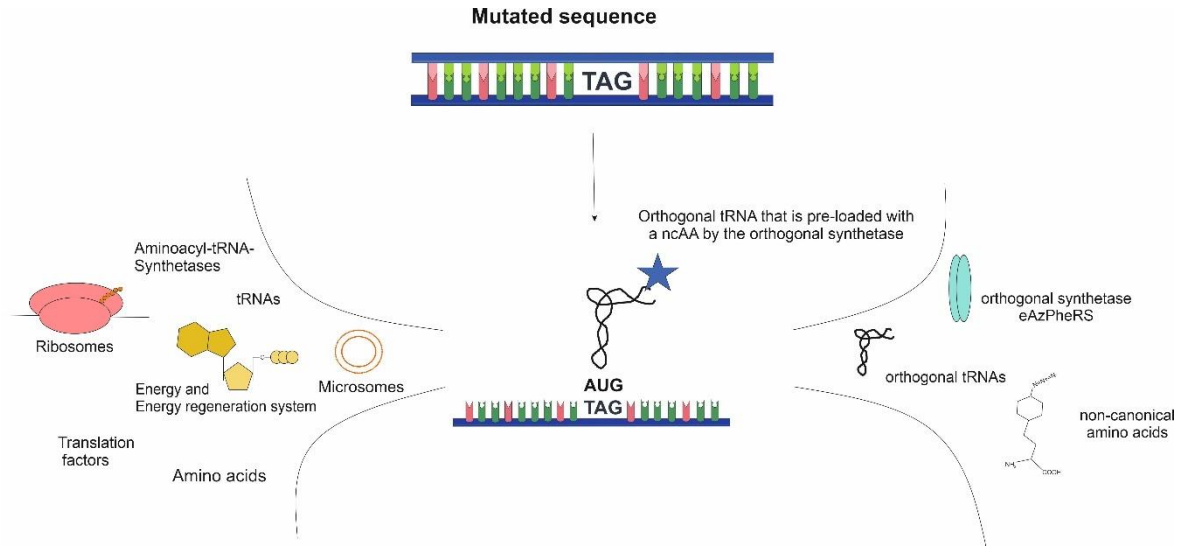

Figure 3: Schematic overview of orthogonal cell-free system.

A new field of application for CFPS are so-called biosensors that trace a signal on the basis of a biological component. Such sensors could be based on array formats. Using CFPS for microarray development has been studied using the example of enzyme screenings or even protein-protein interactions by manifesting techniques such as the protein *in situ* array method and the DNA array to protein array method[61–63]. These studies proved that cell-free systems are capable of keeping up with conventional systems. Latest studies have even shown that cell-free systems can be used to detect biomarkers of infectious diseases, such as *Pseudomonas aeruginosa* infections in cystic fibrosis patients[64] and therefore validating CFPS for diagnostic applications.

Taken together CFPS offers a fast, efficient and cost-effective way for the synthesis and characterization of proteins, screening of relevant protein inhibitors and modification of proteins.

1.2.1.3 Cell-free synthesis of toxic proteins

Since the development of CFPS different kinds of proteins have been synthesized and functionally characterized using this methodology. Difficult-to-express proteins such as membrane proteins or toxins can be synthesized in cell-free systems as neither the cell's viability is harmed during protein translation nor do cellular barriers limit the translation of complex proteins[26,53]. With the help of CFPS quite a number of toxins have been synthesized over the past decades (Table 1). Unfortunately, not all studies have additionally functionally characterized the respective toxin. First studies synthesizing toxins in a cell-free manner just used CFPS in order to analyze mRNA that was isolated from venoms[65,66]. Some studies even stated that the synthesis of a toxin in a cell-free system was not possible such as the synthesis of the U_2-sicaritoxin-Sdo1a from the venom of the six-eyed sand spider *Hexophthalma dolichocephala* in *Sf*21 lysate[67]. This

protein is an inhibitory cysteine knot motif containing complex disulfide structures. Some pitfalls might have been that commercially available cell-free systems were not optimized to the toxins need such as by using a redox system. In studies where intensive optimizations were performed the total protein yield as well as specific activity of the cell-free synthesized toxin could be increased. Such an example is the synthesis of the venom protein kallikrein where the yield was increased from 0.13 to 0.74 mg/mL. The specific protease activity of this toxin was determined to be 1.3 U/mg as compared to crude venom extracts at 1.74 U/mg which was explained by a missing sugar chain in the wheat germ cell-free synthesized protein[68]. Nevertheless, when synthesizing toxins the mechanism of action should be kept in mind. Toxins that target the translation machinery could also inhibit cell-free systems without the use of optimized techniques as shown for the plant derived protein Dianthin[69,70].

Another difficulty when synthesizing a protein is to maintain its functionality. A study expressing the pore-forming protein thermostable direct hemolysin (TDH) showed that the addition of a tag could influence the toxins activity. The position and size of the tag determined whether the toxin was as active as the wild type (WT) protein[26]. Apart from the characterization of toxins, CFPS has already been used to synthesize immunotoxins, so-called targeted toxins. As a first study for cell-free synthesized immunotoxins, fragments of the diphtheria toxin (DT) and pseudomonas exotoxin (PE) were fused with an antibody fragment and synthesized in the rabbit reticulocyte cell-free system. Cell-based toxicity assessment and the adenosine diphosphate (ADP) transferase activity showed that the PE immunotoxin was more potent than the DT immunotoxin[71].

All in all, these studies have shown the potential benefits of CFPS for the synthesis of toxins. Nevertheless, further optimization strategies and more intense testing is necessary to validate cell-free systems for that matter. Until today, few studies have compared the functionality of diverse cell-free synthesized toxins in one study.

Table 1: Cell-free synthesized toxins
List of cell-free synthesized toxins including publications that originated from this doctoral thesis.

Toxin	**Cell-free system**	**Functionality assessment/ Application**	**Year**	**Citation**
α-Hemolysin	*E. coli*	Fluorescence microscopy, pore formation in bilayers	2011	[72]
Cholera toxin	CHO, *Sf*21	Cell-based toxicity, mutational analysis, fluorescent labelling	2022	[73]

DT	*E. coli*	ADP-Transferase Activity	1974	[74]
	Rabbit reticulocyte	Cell-based toxicity, immunotoxin	1993	[71]
Heat-labile enterotoxin	CHO, *Sf*21	Cell-based toxicity, fluorescent labelling	2022	[73]
Heat-stable enterotoxin	*E. coli*	Protein analysis	1980	[75]
Hemolysin BL	CHO	Cell-based toxicity, hemolytic activity	2021	[76]
Kallikrein	Wheat germ	Enzymatic substrate hydrolysis	2012	[68]
Leukocidin	*E. coli*	Electrophysiology, hemolytic activity	2001	[77]
Melittin	Wheat germ	Protein analysis	1977	[66]
			1978	[78]
Non-hemolytic enterotoxin	CHO	Cell-based toxicity, electrophysiology, Hemolytic activity	2020	[79]
Pierisin	*Sf*21	Cell-based toxicity	2011	[54]
		In vitro DNA-ADP-ribosylation	2016	[80]
PE	Rabbit reticulocyte	Cell-based toxicity, immunotoxin	1993	[71]
South African puff adder venom	Wheat germ Rabbit reticulocyte	mRNA analysis	1985	[81]
Tetanus toxin fragment	*E. coli*	Anti-tumor responses in mouse model, ELISA, immunotoxin	2011	[82]
TDH	*E. coli*	Hemolysis analysis	2013	[26]
			2015	[83]
		Electrophysiology	2018	[84]
U_2-sicaritoxin-Sdo1a	*Sf*21 (no translation) *E. coli* (no translation) *E. coli* PURE	Cell-based toxicity	2021	[67]
Queen-bee venom	Wheat germ	mRNA analysis	1984	[65]

1.2.1.4 Cell-free synthesis of viral proteins

In comparison to classical toxic proteins, the cell-free synthesis of viral proteins has been investigated more thoroughly. Diverse studies have shown the synthesis of single viral proteins in *E. coli*[85], HeLa[86], wheat germ[45], hybridoma[87], rabbit reticulocyte[88], *S. cerevisiae*[89] and tobacco[90] cell-free systems. Initial studies demonstrated that isolated viral genetic information can be translated into proteins in cell-free systems[45,91], but no further intense characterization of these proteins was performed. After the first known cell-free synthesis of a viral protein in 1963[91], CFPS has helped to gain detailed information on viral proteins and was applied for the development of new diagnostic and therapeutic technologies. Diverse proteins such as viral proteases[92], non-structural polyproteins[93], viral membrane proteins[94] and even multimeric antigens for potential vaccine development[95] were synthesized and characterized. In 2004, Klein and colleagues showed, that two cell-free systems were able to demonstrate the assembly of the capsid protein of the hepatitis C virus core protein which could not be detected in primate cell culture systems[96]. These optimizations of cell-free systems allowed for new leaps in protein synthesis technologies. Selected proteins from bacteriophages and even complete phages have been synthesized. The ΦX174 lysis toxin could be synthesized and assembled into a complex that inserted itself into membranous structures[97]. In an *E. coli* cell-free system the T7 bacteriophage could be assembled[98], showing that CFPS can be used for a variety of purposes not only limited to single proteins. A field that has gained attention over the last few decades are virus-like particles (VLP) which are viral particles that do not contain the genetic information of the virus itself and are therefore of interest for vaccine developments. Several studies have shown that cell-free systems are able to form stable VLPs. Norovirus VLPs[99], hepatitis B VLPs[100–103], MS2 VLPs[101,102] and Qβ-phage VLPs[101,104] were synthesized in *E. coli* based systems. VLPs from the human papillomavirus[89] or hepatitis B virus[105] were synthesized and assembled in *S. cerevisiae* and *P. pastoris*, respectively. A latest approach has developed MS2 and Qβ VLPs that were modified by click chemistry in order to harbour different ligands[106]. Such modified VLPs might be interesting for drug delivery or vaccine developments in the future.

Strikingly, prokaryotic cell-free systems were mainly used for the synthesis of viral proteins and particles. Eukaryotic systems have been more frequently used in recent years. While single studies have investigated mammalian systems, yeast based lysates were the cell-free systems of choice. Hence, further optimized mammalian cell-free systems are needed, especially considering VLPs that require PTMs.

1.3 Toxins in diagnostics

As a first response after an intoxication or viral infection an antidote, antibiotic or antiviral compound is given. Diagnostic steps are necessary to specifically react to a certain toxic effect and to prevent an illness. The type of infection, the underlying toxin and its mechanism of action have to be identified in order to properly block the toxin and inhibit its causes. Biological, biochemical or chemical methods are used to detect the toxin in diverse samples, but in order to develop these techniques, the toxin itself has to be present[107–109]. Therefore, stable methods for the production and isolation of these proteins have to be available in order to generate detection molecules such as antibodies against the toxin[108]. Another difficulty in the diagnosis of toxins is the versatility and the growing number of contaminants, pollutants, venoms and other causes of toxicity. One major cause of toxicities are bacterial infections. A large number of bacteria encode toxins, so-called bacterial toxins, which can cause a wide range of effects[2]. They can cause mild symptoms such as vomiting or diarrhea triggered by bacterial enterotoxins as for example emitted by *Bacillus cereus* (*B. cereus*)[110] or *Vibrio cholerae*[2]. Other bacterial strains produce toxins that cause serious diseases such as whopping cough (Pertussis toxin by *Bordetella pertussis*) or botulism (Botulinum toxin by *Clostridium botulinum*)[2]. Hence, the correct diagnosis and characterization of the involved toxin is of utmost importance.

1.3.1 Mechanism of action analysis

The characterization of the mechanism of action is the description of biological events caused by the toxin. It defines the detailed steps at a molecular level[111]. Therefore, the analysis of the mechanism of action provides detailed information on the possible ways to inhibit the toxin itself or block certain pathways that are activated by the toxin of interest.

As stated before, a variety of bacterial strains produce toxins. One of these bacteria is *B. cereus* which is a gram-positive, spore-forming bacterium that can survive harsh stress conditions such as acidic conditions[112,113]. The *B. cereus* group comprises a variety of different strains such as the *B. cereus* strain itself, *Bacillus anthracis* or *Bacillus cytotoxicus*[114] and thus encodes a large number of different toxins with different mechanisms of action. These toxins include proteases, phospholipases, enterotoxins such as hemolysins or even the severely dangerous anthrax toxin[112,113]. Some toxins such as the anthrax toxin are well studied whilst a tremendous amount of questions still remains for others. An infection with *B. cereus* can occur after the consumption of food that was contaminated with spores. As a consequence toxins are produced in the human gut. Non-gastrointestinal as well as gastrointestinal diseases can be triggered after an infection depending on the type of toxin[112]. Food-borne gastrointestinal diseases can be categorized into two different types, namely the emetic and diarrhoeal type[115]. The emetic

type is mainly caused by cereulide which is produced by bacterial cells on contaminated food. As cereulide is stress resistant to heat, acids and proteases, cooking does not neutralize this toxin and it passes through the gastrointestinal tract without being degraded[116]. It ultimately binds to the serotonin receptor and stimulates the nervous system leading to emesis[117]. The diarrhoeal type is caused by enterotoxins that are synthesized by bacterial cells inside the intestines and further released into the human gut. Subsequently, these toxins attack the gastrointestinal cells causing diarrhoea and abdominal distress[112,113]. A major class of enterotoxins produced by *B. cereus* are pore-forming toxins (PFTs), that penetrate the cell membrane and cause apoptosis. PFTs are homo- or heteromeric proteins that multimerize and assemble into a cylindrical or conical form and embed into a lipid bilayer such as cell membranes. Such an assembly either takes place directly within the membrane or the pore can pre-assemble and subsequently embed into the membrane[118]. Unfortunately, the detailed mechanisms of action of the individual enterotoxins still have to be elucidated.

1.3.1.1 Tripartite enterotoxins as model proteins

To date numerous PFTs have been identified in *B. cereus*. Three of these enterotoxins have been linked to be major causes for toxicity. The first one is the single protein Cytotoxin K (CytK) while the other two are tripartite toxins, namely the Non-hemolytic enterotoxin (Nhe) and Hemolysin BL (Hbl)[115]. These tripartite toxins consist of three individual domains that form a multicomponent structure that acts as a PFT. Whilst *B. cereus* strains generally produce multiple toxins simultaneously, Nhe is present in most strains[119]. After its discovery in 1996, it was shown that all three subunits, NheA, NheB and NheC, are required for the complex formation and the pore-forming character and at first no hemolytic activity was reported[120,121]. Intense research has led to the further characterization of Nhe and showed that Nhe does possess hemolytic activity that can be linked to the formation of pores[122]. The toxic nature of the multicomponent structure is caused by a pre-assembly of NheB and NheC before binding to NheA[123], while maintaining a molar subunit ratio of 10:10:1 (NheA:NheB:NheC)[121].

In contrast to Nhe, the second tripartite enterotoxin Hbl directly confirmed a strong characteristic ring-shaped hemolytic zone when all three subunits were present[124,125]. The three subunits are encoded by the *hblCDA* operon. HblA encodes the B binding component while hblC and hblD encode the two lytic components L_2 and L_1, respectively[125,126]. The mechanism of action of Hbl was widely discussed. Initial studies suggested an independent binding of all subunits to erythrocytes and thereby causing hemolysis[124], but later studies showed that the binding of the B subunit to the erythrocytes followed by binding the lytic components is necessary for functional activity[127]. Soluble pre-complexes for B and L_1, L_1 and L_2 or even an oligomerization of the B component into

heptamers was proposed[128,129]. This shows the versatility in which PFTs can evolve their toxicity and the need of a fast and efficient method to characterize these proteins. As these multicomponent PFTs are major pathogenicity factor after *B. cereus* intoxications and their mechanisms of action remain to be elucidated, Nhe and Hbl were chosen as model proteins for the synthesis and characterization of multicomponent PTFs.

1.3.2 Biological nanopores

Studying the mechanism of action is the first step in understanding the individual toxin. When the toxin of interest is fully characterized, it can be used for various applications not only for detecting the toxin itself in patient as well as environmental samples. An application for toxins, PFTs in particular, are so-called biological nanopores. A nanopore is a small and well-defined structure that allows for sensing of ion flow based on planar lipid bilayer measurements. Such nanopores are used for the detection of biomolecules, sequencing of nucleic acids, studying enzymatic processes or even investigating protein folding[130,131]. As described in 1.3.1 PFTs assemble into multimers and embed into a lipid bilayer und thus form a whole within the bilayer. The stability of the multimeric assembly and the stable and characteristic flow of ions in electrophysiological measurements enable PFTs as the best biological nanopores[130,132]. Using proteins that form pores with different geometries, diverse molecules can be analyzed and characterized. Very small molecules will directly go through the pore without any interaction of the ion flow while slightly larger molecules will bounce off of the inner wall of the pore and the ions will partially be repressed. A pore will be blocked by molecules that are as large as the pore itself. The time the molecule lingers within the pore is called dwell time[130]. The detection of molecules of different sizes is represented in Figure 4. These characteristics enabled the development of specified nanopores that allowed for the differentiation of proteins that only differed in a point mutation / an amino acid such as microcystins[133,134]. The precise discrimination of molecules or enantiomers based on small changes such as secondary structures depends on using a well-characterized nanopore. The most well-known and well-characterized PFT that is used as a nanopore is α-Hemolyin (aHL). The differentiation of microcystins was performed by analyzing the dwell times and the amplitudes of the blockages in an aHL nanopore[133]. Hence, most studies featuring biological nanopores include aHL and newly developed nanopores are either based on their similarity to aHL or compare the nanopore to it. The identification of nanopores is essential as they can be used as biosensors for diverse applications.

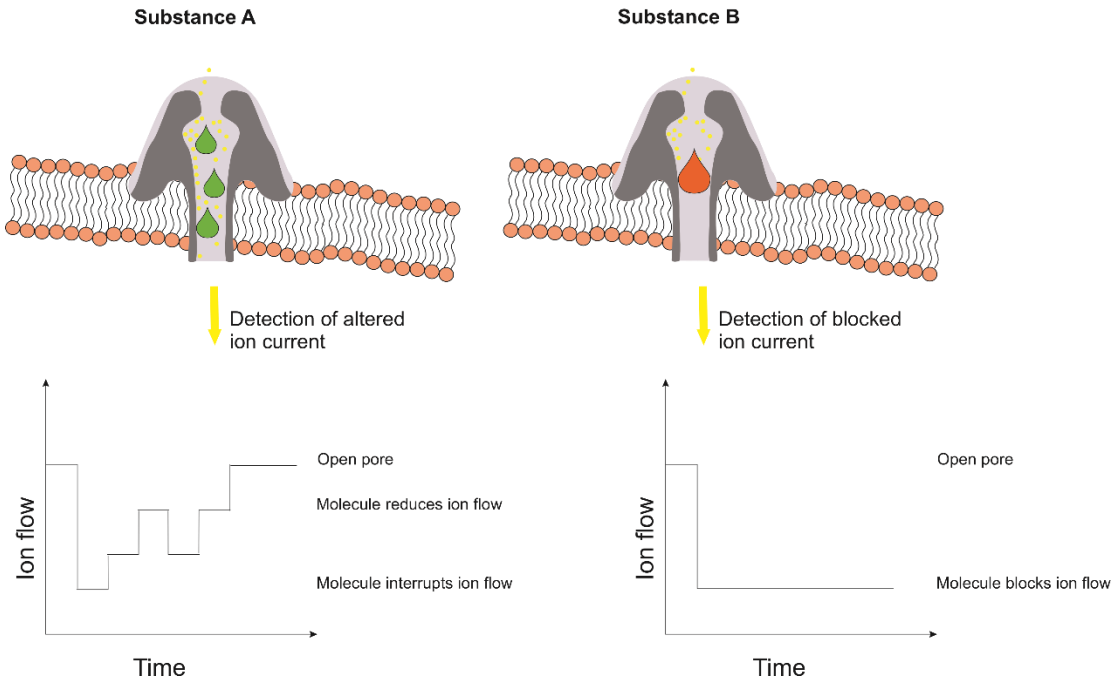

Figure 4: Schematic explanation of a nanopore.

1.3.2.1 Model protein: Cytotoxin K

As described in 1.3.1.1, the *B. cereus* group encodes three enterotoxins that are possibly the major causes for pathogenicity. One of these toxins is Cytotoxin K (CytK) which is a classical beta-barrel, mono-heptameric, pore-forming protein[135]. In 2000, Lund and colleagues first isolated this toxin from *B. cereus* strains[136]. Later studies have identified the *B. cytotoxicus* strain to be the specific strain expressing CytK[135]. Initial studies have demonstrated that CytK forms stable pores in bilayers, its multimers are resistant to detergents but not to boiling and CytK is cytotoxic in cell-based assays[137], indicating the link between a *B. cytotoxicus* intoxication with typical symptoms of a diarrhoea and vomiting after food-poisoning. Interestingly, recent studies have shown that the presence of the *cytk* gene in the bacterial strain does not define the strains cytotoxic effect, as this enterotoxin is only produced at low levels and in some strains the gene is present but not expressed at all[138]. Until today, two variants, CytK1 and CytK2, have been identified that share 89% sequence identity. Even though both variants are fairly similar, it was shown that CytK2 is less toxic than CytK1 as represented by hemolytic analysis and cell-based toxicity assessments[139]. Few studies clearly depicted the toxic effects of both CytK variants and it is still unclear in which manner both variants differ in terms of functionality. Fagerlund *et al.* tried to analyze the pore that is formed by both CytK variants. CytK1 formed pores that showed a conductance value of more than 100 pS while CytK2 predominantly induced conductance values of less than 100 pS[139]. These data indicate that even small amino acid changes lead to different pore formations. Moreover, a 30% sequence identity and 64% sequence similarity was found between CytK and aHL[136].

Therefore, in this thesis it was investigated whether CytK is a suitable candidate for the development of a potential biological nanopore.

1.3.3 Tracking systems

As discussed, bacterial toxins comprise a highly versatile group of proteins that vary in their origin, structure and functionality. In some cases the mechanism of action is difficult to analyze. Biomonitoring of toxins generally starts with samples of hair, blood or urine[140]. This is routinely done for pollutants but is rather difficult for proteinaceous toxins such as bacterial toxins after infections. Food-borne intoxications are usually detected by challenging techniques from contaminated samples or patients' stool samples. PCRs or immunological assays can detect toxins[109,141], but these methods rarely reflect on the mechanism of action and intracellular pathway of the toxin. In order to localize the toxin in the cell und characterize its intracellular trafficking, recent studies have fluorescently labelled toxins[142–144]. Fluorescent labelling of toxins might enhance the rapidity of the characterization of the toxin and therefore will be a useful tool for future applications.

1.3.3.1 AB_5 toxins as model proteins

A diverse group of bacterial toxins is the class of AB_5 toxins which are present in various pathogenic bacteria. This led to a sub-classification to the Pertussis family, the Cholera family, the Shiga family and the lastly added Subtilase family[145]. The Subtilase cytotoxin was detected in the late 1990s and led to the newest AB_5 toxin family[146], showing that there is a high need in fast, sensitive and efficient detection and characterization methods for AB_5 toxins. Apart from the latest addition to the AB_5 toxin family, well-known representatives of this group are the Cholera toxin (Ctx), the Pertussis toxin, the Shiga toxin and the Heat-labile enterotoxin (LT). Each toxin reflects a characteristic multicomponent structure consisting of an A subunit and a B subunit that multimerizes into a pentameric ring structure. The only exception is reflected by the Pertussis toxin where the B subunit consists of 4 different proteins[145]. The A subunit contains the enzymatic centre of the toxin and is therefore the catalytic subunit which induces the toxic effect. Further, this subunit can be separated into two fragments by a furin cleavage site. The so-called A1 fragment harbours the catalytic domain and is once again linked to the A2 fragment by a disulfide bridge after both fragments were cleaved[147]. The A2 fragment is the anchor of this multicomponent structure, as it also connects the A subunit to the B ring. The B subunit, especially the pentameric form, acts as the receptor binding domain and directly targets the cell surface[145,148].

The Cholera family comprises the Ctx from *Vibrio cholerae* and LT I and LT II from *E. coli*, all of whom are well-studied. The A subunit of these toxins are highly homologous, whilst the B subunits of LT I and II reflect differences in their cell binding properties. The B

subunit of Ctx and LT I share a homology of more than 80% and present similar cell binding properties[148]. Therefore, Ctx and LT I have been used to establish different techniques to fluorescently label toxins in this thesis.

After an intoxication with these toxins, mild or even severe symptoms can occur. The most well-known description of such intoxications is the term travellers' disease. Symptoms include dehydration, vomiting, watery stool or severe diarrhoea[145,149]. Both toxins have a similar mechanism of action as both target the monosialoganglioside GM1 receptor that can be found on jejunal intestinal cells[150,151]. Unfortunately, later studies have shown that these toxins can bind to the cell surface by cross-reactivity to other glycoproteins on the cell surface and thus inducing toxicity in the absence of GM1[152,153]. The symptoms associated with an intoxication with Ctx and LT are caused by the secretion of chloride ions and water into the intestinal lumen. As both toxins trigger the ADP-ribosylation of the Gs alpha subunit of the heterotrimeric G protein, the adenylate cyclase is continuously activated and produces cyclic adenosine monophosphate (cAMP) initiating the described ion loss[145,154]. In addition to the secretion of ions, cell-based assays revealed that CHO cells undergo characteristic morphological changes after the application of these toxins such as elongated cell bodies[154]. The exact mechanism of action and uptake of the toxins themselves are not yet fully understood. Studies suggest a toxin uptake by clathrin coated vesicles and caveolae resulting in a transportation by early endosomes to the Golgi apparatus and leading to the ER[145]. Even though, the KDEL/RDEL motif on the A2 subunits of Ctx and LT supports this theory[145,155], other studies have shown that the Golgi apparatus is not necessarily needed for the toxin transport[156]. This shows that even with such well-studied toxins many questions still arise and new methods for the elucidation of those mechanisms are needed.

1.4 Therapeutic use of toxins

The harmful nature of a toxin is the first characteristic that comes to mind when discussing toxins. Interestingly, the use of toxins as therapeutic entities has emerged after decades of research. The therapeutic use of the Botulinum neurotoxin is one of the best-known examples. This may be due to its cosmetic use for facelifting, but other indications such as chronic pain or neurological disorders can be tackled by this neurotoxin as well[157]. Not only bacterial toxins are used as therapeutics but also components of animal venoms have been widely evaluated and progressed for therapeutic uses. Other examples are components of snake venoms that are used for cardiovascular diseases such as Captopril that is used for the treatment of hypertension and is based on a peptide from the venomous viper *Bothrops jararaca*[158].

A different approach in using toxins is the development of vaccines, but generally non-toxic mutants or non-toxic fragments are used for such matters. Mutated toxin fragments are either directly used for vaccination as for example for Diphtheria and Tetanus vaccines or used as an adjuvant such as CtxB and LTB which are co-administered with vaccines and stimulate the immune response[159–161].

A growing field of research are toxin-conjugates that are targeted against a certain cell type. Such so-called targeted toxins are of major interest for malignant diseases[162].

1.4.1 Targeted toxins

The basic concept of a targeted toxin combines the toxic moiety of the toxin itself with a targeting moiety. The target specific fragment can consist of an antibody or antibody-fragment, growth factor, interleukin or cytokine. Whenever an antibody or antibody-fragment is used the more specified term of an immunotoxin is used[162,163]. A wide variety of targeted toxins have been investigated, tested and even approved for medical use. In 1999, Denileukin diftitox was the first targeted toxin that was approved by the U.S. Food and Drug Administration for the treatment of cutaneous T-cell lymphoma. The transmembrane domain of the Diphtheria toxin (DT) was fused to interleukin 2 as a targeting moiety, but due to major side effects this drug was discontinued in 2014[164]. In general, the toxin has to translocate into the cell and surpass cell degradation processes[165,166]. To circumvent such limitations endosomal escape enhancers can be used to enable the retrograde transport to the ER. These enhancers can either be chemical, bacterial or plant derived compounds[167]. Furthermore, the specificity of the targeting moiety has to be exceptional so that non-cancerous cells are not targeted by the toxin-conjugate[162,163]. As antibodies are rather large, other targeting moieties gained more importance regarding the development of these therapeutics. Smaller antibody fragments or growth factors can offer valuable alternatives. For example, interleukins as already used for Denileukin diftitox were studied. The combination of interleukin 3 with DT led to another approved targeted toxin in 2018, while the combinations of interleukin 2, 4, 6 and 13 were also studied in combination with PE[162,168]. Various cancers are known to overexpress the EGFR, which makes it a suitable target for targeted toxins[169]. Initial studies reported the binding of the transforming growth factor (TGF) to the EGFR when fused to DT[170] or PE[171]. Later studies evaluated the binding of the epidermal growth factor (EGF) to the EGFR when bound to PE[172]. Bacterial toxins have been explored the most for the generation of targeted toxins. Apart from them, plant derived toxins have come into focus for novel targeted toxins[162,163].

1.4.1.1 Model protein: Dianthin

Plant derived ribosome inactivating proteins (RIP) have emerged as promising toxin moieties for the development of therapeutics. RIPs inactivate eukaryotic ribosomes as they possess an N-glycosidase activity which means that the N-glycosidic bond at an adenosine on the 28S unit of the ribose is cleaved[173]. Ultimately, this leads to the inhibition of protein synthesis and cell death of the invaded cell. There are two major types of RIPs, where type I proteins only present the toxic domain and type 2 proteins also harbor a cell binding domain[173].

One example of a type I RIP is the plant toxin Dianthin which was originally found in the *Dianthus caryophyllus L.* ornamental plant[174,175]. Previous studies have demonstrated an anti-viral effect of Dianthin[175], emphasizing the use of Dianthin for therapeutic applications. Since then Dianthin was fused to transferrin[176], antibodies[177–179] and EGF[180–183] in order to develop a potent targeted toxin. Some of these studies showed that the use of an endosomal escape enhancer increased the cytotoxic effect of the Dianthin conjugate[179,180,183]. Taken together, Dianthin has been studied extensively as a targeted toxin, but as it inactivates eukaryotic ribosomes its synthesis in eukaryotic systems is rather limited and therefore previous studies have focused on prokaryotic systems. In this study, Dianthin was used as a model protein for the synthesis and development of a targeted toxin. Using a unique method it was shown that a potent RIP-based targeted toxin can be synthesized in a eukaryotic cell-free system.

1.5 Rapid response to novel zoonotic diseases

In comparison to typical proteinaceous toxins such as CytK, LT or Dianthin, viral proteins are not initially associated with toxicities. Unfortunately, the individual viral proteins induce immune responses and trigger disease progression[3] and thus identifying viral proteins as potential cytotoxic proteins. In recent years CFPS has generally been used to synthesize single viral proteins or VLPs (see 1.2.1.4). Nonetheless, rapid, stable and safe techniques for the characterization of diverse viral proteins are needed as novel pathogens continuously arise worldwide and have the potential to cause infectious diseases[184]. Different types of pathogens can trigger epi- or pandemics, but a major health issue generally comes from zoonotic diseases[184]. A zoonosis is an infectious disease that was originally transferred from an animal to a human being. Over the centuries the world population has been faced with several once animal borne diseases such as the plague, avian borne influenza infections or coronavirus transmissions[184,185]. As the interaction with animals, either in livestock or with domesticated animals, is rapidly rising, the risk of novel zoonotic diseases is rising. The rapid detection, characterization and inhibition of such a pathogen are essential in preventing larger outbreaks.

1.5.1 Model proteins: SARS-CoV2 cytotoxic proteins

The latest pandemic caused by the severe acute respiratory syndrome coronavirus type 2 (SARS-CoV2), or shortly the novel coronavirus, has shown to what extent global health and economic systems suffer during a pandemic, even today. Hence, the versatile set of viral proteins expressed by SARS-CoV2 was used to establish CFPS as a rapid response platform for future infectious diseases that could lead to epidemics or even pandemics.

Recent history has shown that corona viruses are able to cross from animals to humans and become zoonotic as was not only shown for SARS-CoV2 but also for its predecessors severe acute respiratory syndrome coronavirus (SARS-CoV) and Middle East respiratory syndrome coronavirus (MERS-CoV)[184]. SARS-CoV2 is a single-stranded, positive-sense ribonucleic acid (RNA) virus and it expresses ten different open reading frames (ORFs) which encode the set of cytotoxic viral proteins[186,187] as represented by the schematic overview in Figure 5.

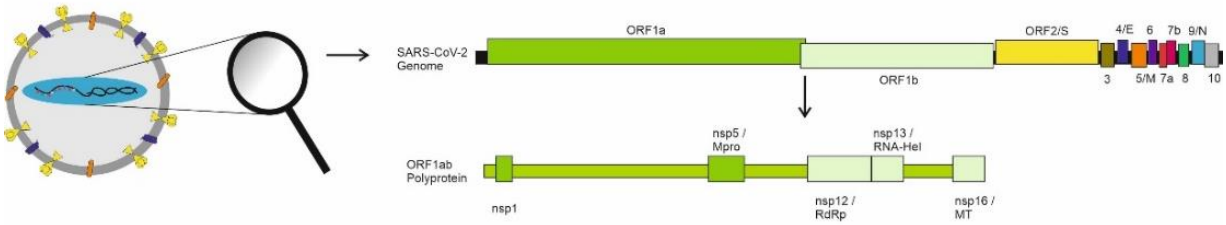

ORF	Protein	Short form	Function
1ab	nsp1	-	Inhibition of protein translation
	nsp5	m^{Pro}	Protease
	nsp12	RdRp	RNA-dependent RNA polymerase
	nsp13	RNA-Hel	RNA-helicase
	nsp16	MT	Methyltransferase
2	Surface glycoprotein	Spike / S	Binding of host cells
3	ORF3	-	Ion channel
4	Envelope	E	Facilitates assembly
5	Membrane protein	M	Interacts with E, S and N to form stable assembly
6	ORF6	-	Immune invasion
7	ORF7a	-	Virus-host interaction
	ORF7b	-	Virus-host interaction
8	ORF8	-	Immune invasion
9	Nucleocapsid protein	N	Genome packaging
10	ORF10	-	Unclear

Figure 5: SARS-CoV2 proteins and their individual functions.
Modified from Ramm *et al*., 2022.

ORF1ab is a polyprotein encoding 16 different non-structural proteins (nsp). These proteins are expressed as a single polyprotein and subsequently cleaved by its own proteases[187]. Apart from the proteases nsp3 and nsp5, ORF1ab mainly encodes proteins that are responsible for viral replication such as a RNA-helicase (nsp13)[188] and a RNA-dependent RNA-polymerase (RdRp, nsp12)[189]. The other ORFs generally encode single

proteins that are divided into classes of viral proteins. The first class are structural proteins that assemble to the viral capsid. In SARS-CoV2 four proteins make up this core structure of the virus, namely the ORF2 surface glycoprotein which is known as the Spike protein, the ORF4 envelope protein, the ORF5 membrane glycoprotein and the ORF9 nucleocapsid protein[187]. The second class of viral proteins are the accessory proteins which help the virus to invade the host. The accessory proteins of SARS-CoV2 are very diverse. ORF3 encodes a possible ion channel in order to regulate the ion flux inside the cell[190]. ORF6 and ORF8 are small proteins that play a role in the immune invasion of the host and regulate interferon signaling[191,192]. ORF7 is divided into two proteins, ORF7a and ORF7b, which are membrane proteins responsible for virus-host interactions[193,194]. The last ORF, ORF10 is not expressed during all infections as a read through of this protein can occur[195,196]. Together these three classes of proteins invade the host organism, replicate the viral genetic information and induce the disease progression.

1.6 Scope of the work

Cell-free protein synthesis has established itself as a manner to synthesize recombinant proteins for research applications as well as for the development of therapeutically relevant proteins. The combination of a cell lysate rather than living cells with the open system that is used for CFPS enables various opportunities for the synthesis and characterization of toxic proteins. Numerous studies on cell-free synthesized toxins have been performed, but CFPS has not yet been established as a platform technology for proteinaceous toxins. This study focusses on the synthesis, functional characterization and application of diverse proteinaceous toxins in order to evolve cell-free protein synthesis as such a platform technology and tool box for the fast response to pathogens, for its use in diagnostics as well as for the application of toxins as therapeutic agents.

This thesis is divided into three sections:

In the first part, model toxins with an unmet diagnostic need were evaluated. Cell-free protein synthesis was used to evaluate the eligibility of eukaryotic cell-free systems to synthesize multimeric proteins while remaining their functional activity such as the tripartite enterotoxins Nhe and Hbl from *B. cereus* or AB_5 toxins such as Ctx and LT. In a next step, cell-free protein synthesis was adapted to further understand the mechanisms of action and molecular signalling of these bacterial enterotoxins. Ctx and LT were modified to fluorescently label individual subunits as a proof-of-concept for intracellular trafficking or future coupling of payloads for drug delivery. At last, it was investigated whether CytK is a potential candidate for the development of a nanopore for the diagnostic use.

In the second part, the therapeutic relevance of cell-free synthesized modified toxins was evaluated. Therefore, a targeted toxin for the directed response against tumour growth was investigated. The toxicity of the targeted toxin combining the plant-derived Dianthin as a toxic moiety and EGF as a targeting moiety was studied in cell-based assays. Further, a so-called soft-agar assay using squamous cell carcinoma samples was established for cell-free synthesized toxins. This assay allowed for the validation of the clinical relevance of the cell-free synthesized Dianthin-EGF.

In the third and last part, the potential of eukaryotic cell-free systems as a rapid response platform against novel viral pathogens was demonstrated. Viral pathogens, especially air-borne pathogens, can cause epidemic or even pandemic outbreaks. Using the SARS-CoV2 viral proteins, cell-free synthesis was used to rapidly synthesize and characterize the proteins as well as to set up a rapid detection system for viral proteins.

All in all, this thesis develops a platform technology for the cell-free synthesis and functional characterization of toxic proteins with clinical and diagnostic relevance using eukaryotic cell-free systems. The synthesis of diverse toxic proteins has not yet been performed in one study, hence the comparison of CFPS for toxic and viral proteins is limited to speculations concerning the compatibility of single studies. This thesis studied different types of toxins allowing to enhance CFPS as a multipurpose instrument for the standardized and comparable synthesis and application of proteinaceous toxins.

2 Materials and methods

2.1 Materials

2.1.1 Instruments

Agarose gel imager (Gel iX Imager)	Intas Science Imaging Instruments GmbH
Agarose gel system (PerfectBlue Gelsystem)	Peqlab Biotechnologie GmbH
Amersham Typhoon RGB	GE Healthcare
Azure c600 Gel Imaging System	Azure Biosystems
Balances BP41005 and BP211D	Sartorius Stedim Biotech GmbH
Biometra Trio PCR cylcer	Analytik Jena
CCD-Camera	Nikon
Cell culture incubator	Binder
Cell freezing container	Nalgene
Centrifuges 5415R, 5424 and miniSpinPlus	Eppendorf
Centrifuge Avanti J-25	Beckman Coulter GmbH
Confocal laser scanning microscope LSM-510	Carl Zeiss
Enhancer Dot Blot System	G-Bioscience
Gel dryer (Unigeldryer 3545 D)	UniEquip Laborgerätebau- und Vertriebs GmbH
Gel UV-detection system	Biometra
Gene Pulser Xcell Electroporation System	Bio-Rad Laboratories GmbH
GFL heating bath	GFL Gesellschaft für Labortechnik
HEKA, single channel amplifier EPC-10	HEKA Electronic Dr. Schulze GmbH
iBlot Gel Transfer System	Invitrogen
Image Eraser	GE Healthcare
Incubator BD23	BINDER GmbH
Incubator shaker Innova40	New Brunswick Scientific
Inverted microscope including 10X lens / phase contrast	Leica
Laboratory platform shaker	Heidolph Instruments GmbH & Co. KG
Magnetic separator	Promega Corporation

Microwave	Siemens
Millipore system Ariium (611 VF)	Sartorius
Mithras^2 LB 943 microplate reader	Berthold Technologies GmbH & Co. KG
Olympus IX83 Inverted Microscope	Olympus
Orbit 16	Nanion Technologies
Orbit Mini	Nanion Technologies
Orbital shaker Unimax 1010	Heidolph Instruments GmbH & Co.KG
PCR thermocycler (DNA Engine, PTC-200)	Bio-Rad Laboratories GmbH
pH electrode Orion 8220BNWP	Thermo Fisher Scientific, Inc.
Phosphor screen	GE-Healthcare
Rotator	neoLab Migge GmbH
Scintillation counter Hidex 600 SL	Hidex
Scintillation counter LS 6500	Beckman Coulter GmbH
Spectrophotometer (NanoDrop ND2000c)	Thermo Fisher Scientific, Inc.
Sterile working bench Biowizard Standard (Cell-culture)	Kojair
Sterile working bench HERAsafe HS (Toxin laboratory)	Thermo Fisher Scientific, Inc.
SureCast Gel Handcast System	Thermo Fisher Scientific, Inc.
ThermoMixer comfort (batch) and C (CECF)	Eppendorf
Thoma counting chamber	Carl Roth GmbH und CO. KG
Vacuum filtration system (FH225V)	Hoefer, Inc.
Vibrax (VXR basic)	IKA Werke GmbH & Co. KG
Vortex Genie 2	Scientific industries

2.1.2 Consumables and lab supplies

µ-slide, 18 well	Ibidi GmbH
24-well cell culture plate	Sarstedt
48-well cell culture plate	Sarstedt
96-well cell culture plate	Sarstedt
Amicon Centrifugal Filter Devices (10 kDa cut off)	Amicon
Blood agar plates	VWR International GmbH

Cell culture flask, 25 cm²	Sarstedt
Cell culture flask, 75 cm²	Sarstedt
Costar 96-well microtiter plate (flat bottom, clear)	Sigma-Aldrich GmbH
Dialysis chambers (50 µL and 1 mL)	Biotechrabbit GmbH
Dot blot sample tubes	G-Bioscience
Electroporation cuvettes (1 mm)	Bio-Rad Laboratories GmbH
Filter tips SafeSeal Professional	Biozym Scientific GmbH
Forceps (disposable, sterile)	VWR International GmbH
Glass fiber papers	VWR International GmbH
Gravity Flow StrepTactin Superflow Column (0.2 mL)	IBA GmbH
iBlot® Transfer Stack, PVDF, regular size	Thermo Fisher Scientific Inc.
Multi-Electrode Cavity Array (MECA) Chips	Ionera Technologies GmbH
MECA4 chips	Ionera Technologies GmbH
Nitrocellulose membrane	GE Healthcare
Nunc 96-well microtiter plate (flat bottom, black)	Thermo Fisher Scientific
NuPAGE 10% Bis-Tris gels	Life technologies GmbH
Petri dish (12 x 12 cm)	Greiner Bio-One International AG
Petri dish TC 35 (3 cm, with and without grid)	Sarstedt
PIPETBOY	Starlab
Pipette (2.5, 10, 100, 200, 1000 and 5000 µL, multichannel pipettes 10-100 and 30-300 µL)	Eppendorf
Pipette tips	Starlab
PluriStrainer (cell strainer, 400 µm)	pluriSelect Life Science
Rotilabo Blotting paper (1.0 mm)	Carl Roth GmbH und CO. KG
Scintillation vials	Zinsser Analytic GmbH
Serological pipettes	Sarstedt
Sheep blood agar plates (5%, precast)	VWR International GmbH
Surgical scalpel (disposable, sterile)	B. Braun
Thoma cell counting chamber (0.1 mm deep, C-Square: 0.0025 mm²)	Marienfeld Superior
Zeba™ Micro Spin Desalting Columns (cut off of 7 kDa)	Thermo Fisher Scientific Inc.

2.1.3 Chemicals, biochemicals and reagents

1,2-diphytanoyl-sn-glycero-3-phosphocholine (DPhPC)	Avanti Polar Lipids
^{14}C-Leucine	Perkin Elmer, Inc.
3-((3-cholamidopropyl)-dimethylammonio)-1-propanesulfonate (CHAPS)	Amresco
5´ Cap analogue (m^7G)	Warsaw University, Prof. Darzynkiewicz Thermo Fisher Scientific, Inc.
Acetone, analytical grade	VWR International GmbH
Acetone, technical grade	VWR International GmbH
Acrylamide (40% v/v)	Thermo Fisher Scientific, Inc.
Amino acids	Merck KGaA
ATP	Roche Deutschland Holding GmbH
Atto 488-Biotin	Thermo Fisher Scientific, Inc.
Ampicillin (Amp)	Sigma-Aldrich GmbH
BODIPY-TMR-Lysin-tRNAGAA	Biotech Rabbit GmbH
Bovine serum albumin (BSA)	Sigma-Aldrich GmbH
Braunol (Povidone-iodine)	B. Braun
Calcium chloride ($CaCl_2$)	Carl Roth GmbH und CO. KG
Casein hydrolysate	Carl Roth GmbH und CO. KG
Caspase inhibitor AC-DEVD-CMK	Santa Cruz Biotechnology
Caspase inhibitor Z-VAD-FMK	Promega Corporation
Chloroform	Carl Roth GmbH und CO. KG
Cholesterol (Cho)	Avanti Polar Lipids
Copper(II) sulfate pentahydrate ($CuSO_4$ $5H_2O$)	Sigma-Aldrich GmbH
Creatine phosphate	Roche Deutschland Holding GmbH
Culture supernatant containing Nhe (*Bacillus cereus* (s.l.)-strain BfR-BA-00963)	Unit Bacterial Toxins, Department Biological Safety, Bundesinstitut für Risikobewertung (BfR)
Cycloheximide	Alfa Aesar
Cytidine triphosphate (CTP)	Roche Deutschland Holding GmbH
Difco agar, technical	Becton, Dickinson & Company by Th. Geyer
Dimethyl sulfoxide (DMSO)	Sigma-Aldrich GmbH

Dodecyl -D-maltoside (DDM)	Qiagen GmbH
Dithiothreitol (DTT, cell-free reaction supplement)	Life technologies GmbH
DTT (SDS-PAGE)	Applichem GmbH
DY-632 phosphine	Dyomics GmbH
Erythromycin	Alfa Aesar
Ethanol	Biomol GmbH
Ethylene diamine tetraacetic acid (EDTA)	Biomol GmbH
Ethylene glycol tetra acetic acid (EGTA)	Biomol GmbH
Formaldehyde	Kallies Feinchemie AG
Fromamide, deionized	Fluka Analytical
Glycerine	Carl Roth GmbH und CO. KG
Glucose	Merck KGaA
Guanosine triphosphate (GTP)	Roche Deutschland Holding GmbH
Hydroxyethyl-piperazineethane sulfonic acid (HEPES) (cell-free synthesis)	Carl Roth GmbH und CO. KG
HEPES (electrophysiology)	Sigma-Aldrich GmbH
His-Dianthin-EGF (recombinant protein from *E. coli*)	AG Fuchs; Charité-Universitätsmedizin Berlin
Hydrochloric acid (HCl)	Carl Roth GmbH und CO. KG
Imidazole	Merck KGaA
Isopropanol, analytical grade	VWR International GmbH
Isopropyl-β-D-thiogalactopyranoside (IPTG)	Sigma-Aldrich GmbH
Lysogeny broth (LB)	Carl Roth GmbH und CO. KG
Magnesium acetate ($Mg(OAc)_2$)	Merck KGaA
Magnesium chloride ($MgCl_2$)	Merck KGaA
Magnesium sulfate ($MgSO_4$)	Sigma-Aldrich GmbH
Methanol	Carl Roth GmbH und CO. KG
Ni-NTA Magnetic Agarose Beads	Qiagen
Octane	Sigma-Aldrich GmbH
p-Azido-L-Phenylalanine (AzF)	Iris Biotech GmbH
Peptone	Carl Roth GmbH und CO. KG
PeqGold Universal Agarose	PeqLab VWR International GmbH

Phosphate-buffered saline (PBS)	VWR International GmbH
PBS without calcium and magnesium	Merck, Biochrome GmbH
Poly-dispersed poly-ethylene glycol (polyPEG)	Sigma-Aldrich GmbH
Poly guanin (PolyG)	IBA
Potassium acetate (KOAc)	Carl Roth GmbH und CO. KG
Potassium chloride (KCl) (for cell-free synthesis)	Merck KGaA
KCl (for electrophysiology)	Sigma-Aldrich GmbH
Potassium hydroxide (KOH)	Merck KGaA
p-propargyloxy-L-Phenylalanine (pPa)	Iris Biotech GmbH
Propidium iodide	MP Biomedicals
RNasin Ribonuclease Inhibitor	Promega Corporation
SO1861 (a saponin isolated from *Saponaria officinalis L*.)	AG Fuchs; Charité-Universitätsmedizin Berlin
Sodium acetate (NaOAc)	Merck KGaA
Sodium ascorbate (NaAsc)	Carl Roth GmbH und CO. KG
Sodium azide (NaN_3)	Merck KGaA
Sodium chloride (NaCl)	Merck KGaA
Sodium dihydrogen phosphate (NaH_2PO_4)	Carl Roth GmbH und CO. KG
Sodium dodecyl sulphate (SDS)	Serva Electrophoresis GmbH
Spermidine	Sigma-Aldrich GmbH
Sulfo-Cy5-Azide	Lumiprobe GmbH
Sulfuric acid (H_2SO_4)	Carl Roth GmbH und CO. KG
SureCast ammonium persulfate (APS)	Thermo Fisher Scientific, Inc.
SureCast tetramethylethylenediamine (TEMED)	Thermo Fisher Scientific, Inc.
Trichloroacetic acid (TCA)	Carl Roth GmbH und CO. KG
Tris(hydroxymethyl)-aminomethane (Tris)	Carl Roth GmbH und CO. KG
Tris(3-hydroxypropyltriazolylmethyl)amine (THPTA)	Iris Biotech GmbH
Triton-X 100	Sigma-Aldrich GmbH
TRIzol	Thermo Fisher Scientific, Inc.
tRNATyrCUA	Self-prepared
Trypan blue	Sigma-Aldrich GmbH

Tween-20	Sigma-Aldrich GmbH
Uridine triphosphate (UTP)	Roche Deutschland Holding GmbH
Western Bright ECL HRP substrate	Advanstra
Yeast extract	Carl Roth GmbH und CO. KG

2.1.4 Buffers, solutions and standards

All buffers and solutions were prepared using ultrapure water derived by ion exchange and reverse osmosis (Arium 611V laboratory water system), further called bidestilled water (ddH_2O).

Electrophysiological measurement

Stock solution potassium buffer	10 mM HEPES
	1 M KCl
	pH 7.45
Stock solution sodium buffer	10 mM HEPES
	1 M NaCl
	pH 7.45
HEPES solution for dilution	10 mM HEPES
	pH 7.45

Hot TCA precipitation and liquid scintillation

TCA/ casein hydrolysate	10% (v/v) TCA
	2% (w/v) casein hydrolysate
TCA for preparation for scintillation measurement	5% (v/v) TCA
Scintillation solution	
Quicksafe A scintillation cocktail	Zinsser Analytic GmbH

Preparation of Aminoacyl-tRNA Synthetases

Synthetase storing buffer	50 mM HEPES pH 7.6
	10 mM KOAc
	1 mM MgCl2
	4 mM DTT

Strep-Tag purification	
Strep-Tag washing buffer (10x)	IBA GmbH
Strep-Tag elution buffer (10x)	IBA GmbH
Strep-Tag regeneration buffer (10x)	IBA GmbH

SDS-PAGE

General components

SeeBlue Pre-Stained Standard	Life technologies GmbH
SeeBlue Plus2 Pre-Stained Standard	Life technologies GmbH
SimplyBlue Safe Stain	Life technologies GmbH

Precast gels

Sample Buffer:	
NuPAGE LDS Sample Buffer (4 x)	Life technologies GmbH
DTT (if not stated otherwise)	50 mM
NuPAGE MES SDS Running Buffer (20 x)	Life technologies GmbH

Self-cast gels

10% SDS-Resolving gel:	10% (w/v) acrylamide
	25% (w/v) SureCast resolving buffer, Thermo Fisher Scientific, Inc
	1% (v/v) APS
	0.1 % TEMED
14% SDS-Resolving gel:	14% (w/v) acrylamide
	25% (w/v) SureCast resolving buffer, Thermo Fisher Scientific, Inc
	1% (v/v) APS
	0.1% TEMED
10% SDS-stacking gel:	10% (w/v) acrylamide
	25% (w/v) SureCast stacking buffer, Thermo Fisher Scientific, Inc
	1% (v/v) APS
	0.1% TEMED
Tris-Glycine running buffer (10x)	Life technologies GmbH

Western Blotting and Dot Blotting

Protein sample buffer (Dot Blot)	G-Bioscience
Tris-buffered saline (TBS, 10 x)	200 mM tris base, 1.5 M NaCl
	pH 7.6 with HCl
TBS-Tween (TBST)	1x TBS
	0.1% (v/v) Tween-20
	pH 7.6 with HCl
Blocking solution	2% (w/v) BSA in TBST
Washing solution	TBST
Antibody dilution	1% (w/v) BSA in TBST
Detection:	
ECL-Western Blotting reagent	Biozym Scientific GmbH

In-solution ELISA

Binding buffer	PBS
Washing solution	50 mM NaH_2PO_4
	300 mM NaCl
	20 mM Imidazol
	0.05% Tween 20, pH 8.0
Antibody dilution	PBS
Detection Tetramethylbenzidine (TMB)	Life Technologies GmbH
Stopping solution	0.5 M H_2SO_4 in ddH_20

2.1.5 DNA / RNA analytics

2-Log DNA ladder 0.1 - 10.0 kb	New England Biolabs GmbH
DNA quantification standard (100 ng/µL; 1000 bp & 500 bp)	Gensura
DNA Stain Clear G	Serva Electrophoresis GmbH
Gel loading dye (6x)	New England Biolabs GmbH
Tris base borate EDTA (TBE) (10 x)	Carl Roth GmbH und CO. KG
ssRNA ladder	New England Biolabs GmbH

Restriction digestion

CutSmart Buffer (10x)	New England Biolabs GmbH
Fast Digest Green Buffer (10x)	Thermo Fisher Scientific, Inc.

2.1.6 PCR

HotStar HiFidelity PCR Puffer (5X)	Qiagen GmbH
dNTPs	Qiagen GmbH
$MgCl_2$	Thermo Fisher Scientific, Inc.
Taq buffer (10x)	Thermo Fisher Scientific, Inc.

2.1.7 Glycosidase Assay

Peptide-N-Glycosidase F (PNGase F) *digestion*

Glycoprotein denaturing buffer (10x)	New England Biolabs GmbH
G7 reaction buffer (10x)	New England Biolabs GmbH
NP-40 (10%)	New England Biolabs GmbH

Endoglycosidase H (Endo H) digestion

Glycoprotein denaturing buffer (10x)	New England Biolabs GmbH
G5 reaction buffer (10x)	New England Biolabs GmbH

2.1.8 Enzymes

Calf intestinal alkaline phosphatase (CIP)	New England Biolabs GmbH
Creatine kinase	Roche Deutschland Holding GmbH
DNAseI	New England Biolabs GmbH
Endo H	New England Biolabs GmbH
Fast digest restriction nucleases	Thermo Fisher Scientific, Inc.
HotStart HiFidelity DNA Polymerase (Hifi)	Qiagen GmbH
PNGaseF	New England Biolabs GmbH
Taq-DNA polymerase	Thermo Fisher Scientific, Inc.
T7 RNA polymerase	Agilent Technologies, Inc.

2.1.9 Plasmids

The plasmids listed in Table 2 encoding toxic proteins were purchased from BioCat GmbH as a plasmid preparation or lyophilized stock.

Table 2: Toxin coding plasmid templates

Plasmid name	Sequence origin	Sequence design for CFPS
pcDNA3.1-NCM-His-Dianthin	AG Fuchs, Charité	Fraunhofer IZI-BB
pcDNA3.1-NCM-His-Dianthin-EGF		
pUC57-1.8k-NC-CytK1-C0	BfR-BA00399 (NVH 391-98; DSM 22905), *Bacillus cytotoxicus*	Fraunhofer IZI-BB
pUC57-1.8k-NC-CytK1-A196P-C0		Franziska Ramm & Danny Kaser, IZI-BB
pUC57-1.8k-NC-CytK1-Q13S-C0		
pUC57-1.8k-NC-CytK1-D191del-C0		
pUC57-1.8k-NC-CytK1-I91F-C0		
pUC57-1.8k-NC-CytK1-I91G-C0		
pUC57-1.8k-NC-CytK2-C0	BfR-BA00010 (ATCC 14579; DSM 31), *Bacillus cereus*	Fraunhofer IZI-BB
pUC57-1.8k-NC-CytK1-S196P-C0		Franziska Ramm & Danny Kaser, IZI-BB
pUC57-1.8k-NC-CytK1-Q13S-C0		
pUC57-1.8k-NC-CytK1-D191del-C0		
pUC57-1.8k-NC-CytK1-V91F-C0		
pUC57-1.8k-NC-CytK1-V91G-C0		
pUC57-1.8k-NC-HblA-C0	BfR-BA00010	Fraunhofer IZI-BB
pUC57-1.8k-NC-HblC-C0		
pUC57-1.8k-NC-HblD-C0		
pUC57-1.8k-NC-NheA-C0		
pUC57-1.8k-NC-NheB-C0		
pUC57-1.8k-NC-NheC-C0		
pUC57-1.8k-NCM-CtxA-C0	UniProtKB - P01555	Franziska Ramm, IZI-BB
pUC57-1.8k-NCM-CtxA1-C0		
pUC57-1.8k-NCM-CtxA2-C0		
pUC57-1.8k-NCM-CtxA-AmbE110-C0		
pUC57-1.8k-NCM-CtxA-AmbE112-C0		
pUC57-1.8k-NCM-CtxB-C0	UniProtKB - P01556	

pUC57-1.8k-NCM-LTA-TwinStrep-C0	UniProtKB - P06717	
pUC57-1.8k-NCM-LTB-C0	UniProtKB - P32890	
pUC57-1.8k-NCM-LTB-Strep-C0	UniProtKB - P32890 and P22629	

Table 3 lists plasmid DNA templates encoding viral proteins, which were purchased from BioCat GmbH as a lyophilizate and amplified in house:

Table 3: Plasmid DNA templates encoding viral proteins

Plasmid name	**Sequence origin**	**Sequence design for CFPS**
pUC57-1.8k-NCM-CoV-2-nsp1-C0	GenBank: MN908947.3	Franziska Ramm, IZI-BB
pUC57-1.8k-NC-CoV-2-Mpro-C0		
pUC57-1.8k-NC-CoV-2-RdRp-C0		
pUC57-1.8k-NC-CoV-2-Helicase-C0		
pCII-NCM-SARS-CoV-2-Spike-C0		
pUC57-1.8k-NCM-CoV-2-Spike-S1-C0		
pUC57-1.8k-NCM-CoV-2-Spike-S2-C0		
pUC57-1.8k-NC-CoV-2-ORF3-C0		
pUC57-1.8k-NC-CoV-2-Envelope Protein-C0		
pUC57-1.8k-NCM-CoV-2-Envelope Protein-C0		
pUC57-1.8k-NCM-CoV-2-Membrane-Glycoprotein-C0		
pUC57-1.8k-NC-CoV-2-ORF6-C0		
pUC57-1.8k-NCM-CoV-2-ORF6-C0		
pUC57-1.8k-NC-CoV-2-Nat-SP-ORF7a-C0		
pUC57-1.8k-NCM-CoV-2-ORF7a-C0		
pUC57-1.8k-NC-CoV-2-ORF7b-C0		
pUC57-1.8k-NCM-CoV-2-ORF7b-C0		

pUC57-1.8k-NC-CoV-2-ORF8-C0		
pUC57-1.8k-NCM-CoV-2-ORF8-C0		
pUC57-1.8k-NC-CoV-2-Nucleocapsid-Protein-C0		
pUC57-1.8k-NC-CoV-2-Nucleocapsid-Protein-SER343-C0	GenBank: MT123290.1	
pUC57-1.8k-NC-CoV-2-Nucleocapsid-Protein-ASN202-C0		
pUC57-1.8k-NC-CoV-2-ORF10-C0	GenBank: MN908947.3	
pUC57-1.8k-NCM-CoV-2-ORF10-C0		

The following plasmids encoded non-toxic proteins that were used as model proteins and a tRNA used for the orthogonal system. All plasmids were in stock at the Fraunhofer IZI-BB beforehand.

pIX3.0-CrPV-Luc-C0	Fraunhofer IZI-BB
pIX3.0-CrPV-Mel-eYFP-SII-C0	Fraunhofer IZI-BB
pIX3.0-CrPV-Mel-Flag-hEGF-C0	Fraunhofer IZI-BB
pIX3.0-CrPV-Luc-C0	Fraunhofer IZI-BB
pIX4.0-eYFP-C0	Fraunhofer IZI-BB
pQE2-eAzFRS-SII	Fraunhofer IZI-BB
ptTyr Klon3	Biotechrabbit GmbH

2.1.10 DNA Primers

The following oligonucleotides used in this study were purchased from IBA GmbH and purified by high performance liquid chromatography. The following sequences are represented from 5’ → 3’ end (Table 4).

Table 4: PCR-Primers

Primer name	Sequence	Sequence design
NCM-oe-Strep-F	TAC ATT TCT TAC ATC TAT GCG GAC GAC CCC TCC AAG GAC TCG AA	Franziska Ramm, IZI-BB
oe-EXFP-F	TGT CTA GAG GTG AGC AAG GGC GA	Fraunhofer IZI-BB

tCUATyrEc-R (2´O-Me)	TGG TGG TGG GGG AAG GAT TCG	
tCUATyr-Ec-F	CGA GCT CGC CCA CCG GAA TTC	
X-LTA1-oe-C0-R	CTT GGT TAG TTA GTT ATT AGA TTG TTC TTG ATG AAT T	Franziska Ramm, IZI-BB
X-LTB-oe-eYFP-R	CTT GCT CAC CTC TAG ACA GTT TTC CAT ACT GAT TGC CGC	
X-NCM-oe-LTA2-F	TAC ATT TCT TAC ATC TAT GCG GAC ACA GGT GAT ACT TGT AAT	
XF-Bio	Biotin-ATG ATA TCT CGA GCG GCC GCT AGC TAA TAC GAC TCA CTA TAG	Fraunhofer IZI-BB
XR-Bio	Biotin–ATG ATA TCA CCG GTG AAT TCG GAT CCA AAA AAC CCC TCA AGA C	

The following oligonucleotides used in this study were generated at the Fraunhofer IZI-BB.

The following sequences are represented from 5’ → 3’ end.

C0	Biotin-ATG ATA TCA CCG GTG AAT TCG GAT CCA AAA AAC CCC TCA AGA CCC GTT TAG AGG CCC CAA GGG GTA CAG ATC TTG GTT AGT TAG TTA TTA
N0	Biotin-ATG ATA TCT CGA GCG GCC GCT AGC TAA TAC GAC TCA CTA TAG GGA GAC CAC AAC GGT TTC CCT CTA GAA ATA ATT TTG TTT AAC TTT AAG AAG GAG ATA AAC AAT G
NCM-F	ATG ATA TCT CGA GCG GCC GCT AGC TAA TAC GAC TCA CTA TAG GGA GAC CAC AAC GGT TTC CCT CTA GAA ATA ATT TTG TTT AAC TTT AAG AAG GAG ATA AAC AAA AGC AAA AAT GTG ATC TTG CTT GTA AAT ACA ATT TTG AGA GGT TAA TAA ATT ACA AGT AGT GCT ATT TTT GTA TTT AGG TTA GCT ATT TAG CTT TAC GTT CCA GGA TGC CTA GTG GCA GCC CCA CAA TAT CCA GGA AGC CCT CTC TGC GGT TTT TCA GAT TAG GTA GTC GAA AAA CCT AAG AAA TTT ACC TGC TAA ATT CTT AGT CAA CGT TGC CCT TGT TTT TAT GGT CGT ATA CAT TTC TTA CAT CTA TGC GGA C

2.1.11 Antibodies

Anti-mouse IgG HRP-linked mAb	Cell Signaling Technologies
Anti-rabbit IgG HRP-linked mAb	Cell Signaling Technologies
SARS NC antibody (sc58193)	Santa Cruz Biotechnology
SARS-CoV-2 Nucleocapsid antibody (ABIN6953059)	Antibodies online

2.1.12 Cell lines and biopsy samples

The following cell lines were used in the course of this thesis:

Caco2 (human colorectal adenocarcinoma cells)	DSMZ
CHO-K1	DSMZ
E. coli strain K12 JM109	New England Biolabs GmbH
Epithelial squamous cell carcinoma biopsy samples	Charité-Universitätsmedizin Berlin, Campus Benjamin Franklin, Campus Virchow Klinikum
HEK293	DSMZ
K562	DSMZ
PC-9	ECACC
*Sf*21	ECACC

2.1.13 Cell cultivation

Dulbecco Modified Eagle Medium (DMEM)	Merck, Biochrome GmbH
Ham's F12	Merck, Biochrome GmbH
Fetal bovine serum (FBS)	Merck, Biochrome GmbH
L-Glutamine, stabilized	Merck, Biochrome GmbH
Minimum Essential Medium (MEM)	Merck, Biochrome GmbH
MEM-Vitamins	VWR International GmbH
Non-essential amino acids (NEAAs)	Merck, Biochrome GmbH
Penicillium/Streptomycin (Pen/Strep)	Merck, Biochrome GmbH
Penicillium/Streptomycin/Amphotericin B (Pen/Strep/Ampho)	VWR International GmbH
PBS without calcium and magnesium	Merck, Biochrome GmbH
RPMI 1640 media	Merck, Biochrome GmbH
Sodium pyruvate	Merck, Biochrome GmbH
Trypsin with EDTA; 0.25% (w/v) with 0.02%	Merck, Biochrome GmbH

2.1.14 Media

E. coli cultivation

LB medium	20g/L LB
LB agar plates	20 g/L LB medium
	15 g/L agar powder

Super optimal broth with catabolite repression (SOC) medium	20 g/L peptone
	5 g/L yeast extract
	10 mM NaCl
	2.5 mM KCl
	10 mM $MgCl_2$
	10 mM $MgSO_4$
	20 mM glucose
	pH 7.0
Caco2 cultivation	78% MEM
	20% FBS
	1% NEAA
	1% Pen/Strep
CHO-K1 cultivation	96% DMEM
	1% FBS
	2% L-Glut
	1% Pen/Strep
HEK293 cultivation	87% DMEM
	10% FBS
	2% L-Glut
	1& Pen/Strep
PC-9 cultivation	89% RPMI
	10% FBS
	1% Pen/Strep
Tumor-Medium	84% MEM
	10% FBS
	2% L-Glut
	1% NEAA
	1% Sodium pyruvate
	1% MEM vitamins
	1% Pen/Strep/Ampho

2.1.15 Kits

Booster MTT Assay	VWR International GmbH
CellTox Green Cytotoxicity Assay	Promega
DyeEx 2.0 SpinKit	Qiagen GmbH
EasyXpress *E. coli* kit	Biotech Rabbit GmbH
Hotstart HiFidelity PCR kit	Qiagen GmbH
PCR Purification Kit	Qiagen GmbH
PureLink™ HiPure Plasmid Midiprep Kit	Thermo Fisher Scientific, Inc.
RTS 500 HY *E. coli* Kit	Biotech Rabbit GmbH

2.1.16 Software

BioDoc Analyze (Agarose Gel Imager)	Biometra
CellSens Imaging Software	Olympus
Clampfit 10.7	Molecular Devices
Clone Manager 8	Scientific & Educational Software, Sci-Ed
CorelDRAW Graphics Suite	Corel Corporation
Elements data reader 3	Elements s.r.l.
ImageJ	National Institutes of Health
ImageQuantTL	GE-Healthcare
Mikrowin 2000	Berthold Technologies GmbH & Co. KG
NanoDrop 2000c Software	Thermo Fisher Scientific, Inc.
Origin 2021	OriginLab Corporation
Patchmaster	HEKA Elektronik
Python 3.10	Python Software Foundation
Visual Studio Code	Microsoft
Zen 2009 (microscopy)	Carl Zeiss

2.2 Methods

2.2.1 Template design

The gene templates were designed according to Brödel *et al*. including CrPV IRES to allow for a cap-independent translation initiation[40]. Whenever a protein was known to harbor a post-translational modification or a protein was toxic to eukaryotic ribosomes, the protein of interest had to be co-translationally translocated into the ER-based vesicles.

The sequence for the Mel signal peptide was used for that purpose. Gene templates encoding proteins that natively contained signal peptides either harbored the gene sequence for the native or the Mel signal peptide. All templates contained regulatory sequences necessary for transcription and translation including a T7 promotor and terminator.

2.2.2 Generation of linear DNA templates by expression PCR

A major advantage of cell-free protein synthesis is that a diverse range of templates can be used (see 1.2.1). Hence, DNA sequences can be altered using a PCR allowing for the insertion of mutations as well as purification tags. This linear DNA template can be directly used for CFPS without cloning processes and without the generation of genetically modified organisms.

PCR using Taq polymerase

The generation of suppression-tRNA used for labelling of toxins was performed by the amplification of the coding sequence using a Taq PCR scheme as described in Table 5. Therefore, the gene-specific forward primer (tCUATyr-Ec-F) and gene-specific, methylated reverse primer (tCUATyrEc-R (2´O-Me)) were used.

Table 5: Standard PCR components for the PCR using the Taq polymerase

Component	**Stock-concentration**	**Final concentration (f.c.)**
Plasmid template	variable	0.01 ng/µL
Taq buffer	10x	1x
dNTPs	10 mM	0.2 mM
$MgCl_2$	25 mM	2.5 mM
Forward primer	3 µM	0.5 µM
Reverse primer	3 µM	0.5 µM
Taq polymerase	5 U/µL	0.04 U/µL
ddH_2O		variable

PCR using Hifi polymerase

Templates coding for proteins synthesized in a cell-free reaction were amplified using the Hifi polymerase as this polymerase has a high proof-reading rate. A standard Hifi PCR was pipetted according to the manufacturer (Table 6).

Table 6: Standard PCR components for the PCR using the Hifi polymerase.

Component	**Stock-concentration**	**Final concentration (f.c.)**
Plasmid template	2.5 ng/µL	0.2 ng/µL
or PCR template		8 ng/µL

HiFi-buffer	5x	1x
Forward primer	3 µM	0.3 µM
Reverse primer	3 µM	0.3 µM
Hifi polymerase	2.5 U/µL	0.05 U/µL
ddH_2O		variable

AB_5 toxins are versatile tools for research and in this thesis these model proteins have been varied. The plasmids NCM-CtxA-AmbE110-C0, NCM-CtxA-AmbE112-C0 and NCM-LTB-Strep-C0 were obtained as lyophilizates from BioCat GmbH and were amplified in a Hifi PCR using the forward primer XF and the reverse primer XR. In order to equally synthesize the other components of the AB_5 toxin as well as to compare the synthesis to unmodified WT constructs, NCM-CtxA-C0, NCM-CtxB-C0, NCM-LTA-TwinStrep-C0 and NCM-LTB-C0 were amplified in the same manner.

The CytK1 and CytK2 sequences were modified *in silico* in collaboration with Danny Kaser (IZI-BB) to assess the possibility of a nanopore construction. The plasmids for the CytK mutants were obtained by *de novo* gene synthesis from BioCat GmbH and also amplified using the XF and XR primers in a Hifi polymerase scheme. To assure a similar transcription/translation rate of mutants and WT, CytK1 and CytK2 WT constructs were additionally amplified in the same manner.

Plasmids coding for the full-length surface glycoprotein of SARS-CoV2 could not be amplified using plasmid preparations as cloning procedures were not efficient, neither by BioCat GmbH nor by in house techniques. Hence, linear DNA templates, that were amplified using XF and XR primers in a Hifi polymerase scheme, were used for CFPS.

Standard PCR parameters

The standard protocol was adjusted based on the used template gene (Table 7). The annealing temperature was calculated based on the primer hybridization according to the following formula:

$$Annealing\ temperature = Melting\ temperature\ T_m - 5°C$$

$$T_m = 2°C * (number\ of\ adenines\ and\ thymines) + 4°C * (number\ of\ guanines\ and\ cytosines)$$

The elongation time was calculated based on the length of the gene of interest (1 min/1 kb) for PCR products that contained less than 2 kb. The resulting PCR products were analyzed using agarose gel electrophoresis and compared to the theoretical sizes of the DNA fragments.

Table 7: Standard PCR-scheme for the generation of linear constructs.
Time was measured in minutes (‘) and seconds (‘’), temperature was measured in degrees Celsius (°C).

Phase	Time	Temperature	Cycles
Initiation	5’	95°C	
Denaturation	15’’	94°C	
Annealing	1’	variable	29-45x
Elongation	1’/1 kb	72°C (<2 kb)	
Final extension	10’	72°C	
Cooling	∞	16°C	

2.2.3 2-Step EPCR

The modification of templates and the generation of new fusion constructs was performed by two subsequent PCR schemes. In the first step, the template of interest was amplified using a gene-specific primer that contained an overhang sequence to either regulatory sequences or to another protein. In the second PCR step, the template from the first step was fused to the regulatory sequence or protein of interest as represented by Figure 6. Both PCRs were performed using the Hifi polymerase and the standard Hifi protocol (see 2.2.1), if not stated otherwise.

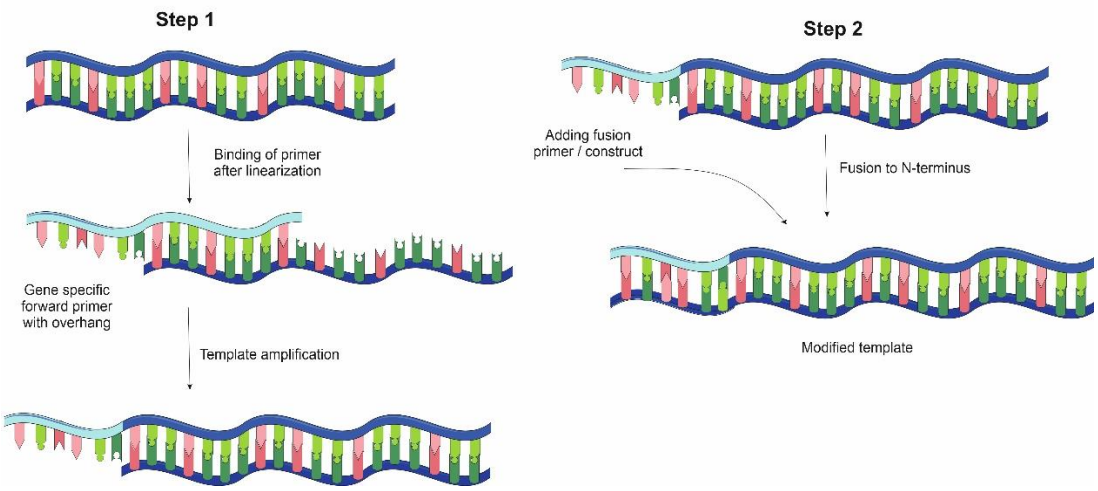

Figure 6: Schematic overview of a 2-step EPCR.

LTA1 and LTA2

To assess the holotoxin formation of the AB_5 toxins, the A and B subunit were co-expressed. As an additional step, the co-expression of the already cleaved A1 and A2 fragments with the B subunits was studied. For LT toxin synthesis, the templates for A1 and A2 fragments were generated using a 2-step EPCR.

For the generation of the LTA1 template, a first PCR step was performed using the N0 forward and the gene-specific X-LTA1-oe-C0-R reverse primer. This primer included an overhang to the C0 primer. The C0 primer included all relevant regulatory sequences in the 3'-end for CFPS. The amplified PCR template from step 1 was fused to the C0 primer in the presence of the N0 primer in a second PCR step.

To generate the LTA2 template, a first PCR step with the gene-specific X-NCM-oe-LTA2-F forward and C0 reverse primer was undertaken. The forward primer contained an overhang to the Mel signal sequence. In the second step, the NCM-F primer, which harbored the regulatory sequences including CrPV IRES and the Mel signal peptide in the 5'-end, was fused to the PCR template from the first step in the presence of N0 and C0. The templates from the first PCR step and the NCM-F primer were applied in an equal molar template ratio of 12.5 nM.

LTB-eYFP

A fusion construct of the LTB sequence with the enhanced yellow fluorescent protein (eYFP) was generated to assess the co-translational translocation into the microsomal vesicles. In a first step the N0 forward primer and the gene-specific reverse primer with an overhang to the eYFP construct (X-LTB-oe-eYFP-R) were used with LTB as a template. In parallel to this PCR, the eYFP template was modified by using the gene-specific forward primer oe-EXFP-F with the corresponding overhang and C0 reverse primer. In a second

step, the templates of LTB and eYFP with their respective overhangs were fused together by mixing them in a 1:1 molar ratio and amplifying them using N0 and C0 primers.

Strep monomer construct

The *in silico* generated LTB-Strep fusion construct was used for further labelling of biotin-conjugated fluorophores. As a further control, the streptavidin (Strep) monomer without any fusion was used. The Strep monomer template was constructed based on the LTB-Strep plasmid. The gene specific forward primer NCM-oe-Strep-F with an overhang to the Mel signal peptide and the C0 reverse primer were used in the standard PCR reaction. The second PCR was performed by using the first PCR product as a template and fusing the NCM-F primer to the construct. Both templates were used in an equal molar concentration of 12.5 nM. The constructs were amplified with N0 and C0.

2.2.4 Qualification and quantification of nucleic acids

Agarose gel electrophoresis

DNA samples derived from PCRs or digested plasmids were separated on an agarose gel. Therefore, a 1% (w/v) agarose gel was cast by dissolving the agarose in 1x TBE buffer by heating the mixture in the microwave. After a short cooling process DNA Stain Clear G (3 µL per 100 mL agarose gel) was supplemented. The liquid solution was poured into the agarose gel electrophoresis chamber, a sample crest was placed into the slide of the agarose chamber and the gel was allowed to polymerize. Subsequently, the chamber was filled with 1x TBE buffer and, hence, the agarose gel was covered with buffer so that the crest could be removed. PCR samples were prepared by using 1 µL of the sample, 9 µL ddH_2O and 2 µL of gel loading dye. DNA samples derived from restriction digestion were directly loaded onto the gel. A DNA ladder (0.4 µL 2-log DNA ladder, 9.6 µL ddH_2O and 2 µL of gel loading dye) and a 1,000 or 500 base pairs (bp) standard (f.c. 100 ng/µL, 1 µL standard, 9 µL ddH_2O and 2 µL loading dye) were additionally used in order to validate the approximate number of bps and the approximate concentrations of the products. At last, the gel electrophoresis was performed for about 60 min at 80 V to separate the DNA fragments. The gel was analyzed using an UV-transilluminator by stimulating the gel with UV light at 305 nm.

Quantification of nucleic acids

DNA concentrations of amplified plasmid DNA and purified PCR templates were quantified by absorbance measurements using the spectrophotometer at an optical density of 260 nm according to the following formula:

$$Absorption\ (260\ nm) = 1 = 50\ \frac{\mu g}{mL}$$

The purity of the corresponding sample was analyzed by the absorbance ratio of 260 nm/280 nm.

2.2.5 Preparation of plasmid DNA

Transformation of plasmid DNA

Plasmids encoding single viral proteins and non-toxic proteins were amplified for cell-free protein synthesis. Therefore, a transformation by electroporation of the expression vectors into *E. coli* JM109 cell was performed. 25 ng of plasmid DNA were incubated in 20 µL of the *E. coli* cell stock for at least 1 min on ice. The mixture was transferred to a precooled electroporation cuvette. Subsequently, a standard protocol of applying 1.8 kV at a 5-6 ms pulsation was used. 1 mL of SOC medium, preheated to 37°C, was added to the transformed cells and incubated at 37°C for 30-60 min. 150 µL of the suspension was platted onto LB agar plates (f.c 100 µg/mL Amp) and incubated over night at 37°C. For long term storage, the LB agar plates were kept at 4°C.

Amplification of plasmid DNA

Single bacterial colonies were picked from the LB agar plate and transferred into 50 mL of LB medium containing Amp (f.c. 1 µg/mL) in a shake flask. Shake flasks containing the bacterial colony and culture medium were incubated at 37°C over night at a constant agitation of about 120 revolutions per minute (rpm). Glycerine cryo-stocks were prepared by mixing 600 µL of overnight culture with 200 µL 80% (v/v) glycerine. Stocks were kept at -80°C for future plasmid amplifications. Plasmid preparation was performed using the PureLink™ HiPure Plasmid Midiprep Kit according to the standard protocol provided by the manufacturer. The following changes were performed: Harvested *E. coli* cells were pelleted at 5,000xg for 10 min at 18°C. The resuspension buffer was used without the supplementation of RNAse A and to allow for a more efficient RNA-precipitation an increased volume of 4.4 mL precipitation buffer was used. After the addition of 3.5 mL isopropanol, a centrifugation at 15,000xg and 4°C for 30 min was performed. At last, pellets were air dried, resuspended in 50-100 µL ddH_2O and incubated at 37°C for 5 min. A final centrifugation for 5 min at 15,000xg was performed to isolate the DNA. The DNA was quantitatively analyzed using the spectrophotometer and qualitatively analyzed by restriction digestion on an agarose gel.

Restriction digestion

As a quality control amplified plasmid DNA was digested by suitable restriction enzymes. 250 ng of the plasmid DNA were incubated with FastDigest restriction enzymes and FastDigest Buffer at 37°C for 15 min. A linearization with one restriction enzyme and a double digestion were performed. The linearized and digested DNA fragments were analyzed on a 1% agarose gel (see 2.2.4).

2.2.6 Preparation of components for protein modification

In order to modify cell-free synthesized proteins in eukaryotic cell-free systems, an aminoacyl-tRNA synthetase and suppression tRNA were needed. These components were prepared individually in advance.

Preparation of the aminoacyl-tRNA synthetase eAzFRS

In this study the *E. coli* tyrosine-tRNA-synthetase (eAzFRS) was used. Therefore, a commercial RTS 500 HY *E. coli* kit was used according to the manufacturer's protocol to synthesize the eAzFRS. The plasmid pQE2-eAzFRS-SII was applied at a final concentration of 100 ng/µL. The reaction was induced by IPTG (100 mM) and the synthesis was performed for 24 h at 30°C in a dialysis chamber. A reaction mixture of 1 mL and a feeding solution of 11 mL was prepared. Subsequently, the soluble protein was separated by a centrifugation at 16,000xg and 4°C for 10 min. The resulting supernatant was separated and the eAzFRS was purified as a C-terminal Strep-Tag was present. StrepTactin Gravity Flow Columns were used according to the manufacturer's standard operating procedure and each fraction was analyzed by sodium dodecyl sulphate polyacrylamide gel electrophoresis (SDS-PAGE). All elution fractions containing the protein were combined. A buffer exchange to the synthetase storing buffer was performed using the Zeba™ Micro Spin Desalting Columns with a cut off of 7 kDa. At last the synthetase was concentrated using 0.5 mL Amicon Centrifugal Filter Devices with a 10 kDa cut off. The total protein concentration was determined by measuring the absorption with the spectrophotometer and calculating the concentration by using the molecular weight of the synthetase (48.5 kDa) and the extinction coefficient (54.3). The final product was frozen in liquid nitrogen and stored at -80°C until further use.

Preparation of suppression-tRNA

The suppression-tRNA used in this study was the tRNA TyrCUA. An in house developed protocol for the production of this suppression-tRNA was used. At first, a PCR template was generated using the gene-specific forward primer and gene-specific, methylated reverse primer using the Taq PCR scheme (see 2.2.2). This PCR template was purified using the Qiagen PCR purification kit according to the manufacturer's protocol. Subsequently, the PCR template was transcribed using the T7 RNA polymerase as described in Table 8. The methylation of the PCR product was necessary in order to prevent an unspecific elongation with nucleotides at the 3’ end of the tRNA resulting in a reduced aminoacylation efficiency. The transcription was incubated over night at 37°C and 500 rpm. The next day, the transcribed RNA was centrifuged for 1 min at 12,000xg. The supernatant was digested using DNAseI (1 U DNAseI/ 1 µg DNA) for 10 min at 37°C and 500 rpm.

Table 8: Components for a transcription.

Component	Stock-concentration	Final concentration (f.c.)
ddH_2O	-	variable
PCR template	variable	8 ng/µL
Transcription buffer	5x	1x
NTP mix	5x	1x
Enzyme mix	20x	1x

Next, the RNA was isolated using a TRIzol/chloroform isolation procedure. TRIzol, three times the volume of the transcription reaction, was added to the RNA mixture and incubated for 5 min at room temperature. 200 µL chloroform per 1 mL TRIzol were added in the next step, mixed and incubated at room temperature for 3 min. Following that, the sample was centrifuged for 15 min at 12,000xg and 4°C. This centrifugation resulted in three phases. The aqueous phase was isolated and incubated over night at 4°C with 500 µL isopropanol per one ml TRIzol mixture. The following day, the mixture was centrifuged at 15,000xg and 4°C for at least one hour and the resulting supernatant was discarded. The pellet was coated with 75% ethanol and subsequently incubated at -20°C for 30 min. After a final centrifugation at 7,500xg for 10 min at 4°C, the pellet was air dried and resolved in ddH_2O. The final concentration of the RNA was determined using the spectrophotometer. The RNA was folded in a slow cooling process using a temperature range from 80°C to 25°C in the PCR cycler. At last, the folded tRNA was frozen in liquid nitrogen and stored at -80°C until further use.

2.2.7 Cell-free protein synthesis

Cell-free protein synthesis was based on translationally active lysates derived from *Sf*21 insect cells, CHO-K1 cells and human K562 cells. The lysate production was performed by the working groups Cell-free Protein synthesis and Eukaryotic Lysates at the Fraunhofer IZI-BB. The commercial EasyXpress *E. coli* kit based system was used for the synthesis of a model protein in the *in vitro* translation inhibition assay (see 2.2.15) according to the manufacturer's guideline.

Cell-free protein synthesis can be performed in versatile modes and formats. A rapid batch-based, one-pot reaction and a prolonged CECF reaction using a two-chamber system have been used during the course of the thesis.

Cell-free protein synthesis in a batch-based eukaryotic system

Coupled batch-based reactions were performed in all mentioned eukaryotic systems in 1.5 mL tubes, incubated for 3 h at 500 rpm. Syntheses using *Sf*21 lysates were incubated at 27°C while syntheses using CHO and K562 lysates were performed at 30°C. Batch-formatted reactions were performed in a volume of 15-80 µL. Larger reaction volumes were needed when experiments contained functionality assessments such as cell-based

toxicity analysis. In general, plasmid DNA with a final concentration of 60 ng/µL, if not stated otherwise, was used as a template. If template optimizations were conducted, the DNA template was a PCR template. The composition of a standard batch-based synthesis for an IRES-dependent reaction is summarized in Table 9.

Table 9: Standard composition of batch-formatted cell-free reactions.

Component	**Final concentration (f.c.)**
ddH_2O	variable
DNA template	variable
Lysate	40% (v/v)
HEPES-KOH (pH 7.6)	30 mM
KOAc	150 mM
$Mg(OAc)_2$	3.9 mM
Amino acids	100 µM
Spermidine	0.25 mM
Creatine phosphate	20 mM
Creatine kinase	100 µg/mL
ATP	1.75 mM
GTP, CTP, UTP	0.3 mM
$m^7G(ppp)G$-Cap	0.1 mM
PolyG	12 µM
DTT	2.5 mM
T7 RNA polymerase	1 U/µL for Plasmid DNA templates
	3 U/µL for PCR templates

DTT was not added when a protein was known to form disulfide bridges. If necessary, ^{14}C-leucine was added at a final concentration of 25-50 µM for quantitative and qualitative analysis as described in 2.2.10 and 2.2.12. All components were directly added to the reaction. ddH_2O was adjusted to fill up the reaction to the desired final volume.

Repetitive cell-free synthesis in a batch-mode

A so-called repetitive synthesis scheme was used in order to enrich the LTB-eYFP variant within the microsomal vesicles for subsequent visualization of co-translationally translocated proteins. Therefore, three cycles of cell-free synthesis were performed in a 20 µL standard batch-based reaction in *Sf*21 lysate for 3 h at 27°C and 500 rpm. After the first cycle, the reaction mixture was centrifuged (10 min, 16,000xg, 4°C) and the microsomal vesicles containing the LTB-eYFP were separated from the soluble reaction components. These vesicles were used for the second reaction cycle and added to a new reaction mixture. This new reaction mixture was identical to the first cycle with the

exception that the lysate used was depleted of the microsomes by centrifugation. Hence, the vesicles from the first cycle were further enriched with target protein in the second cycle. This procedure was repeated for the third synthesis cycle.

Cell-free synthesis of labelled proteins using precharged tRNA

In a first step to fluorescently label a toxic protein, the precharged tRNA was used. In this case a commercially available construct was used where the BODIPY-Tetramethylrhodamine-(TMR) dye was coupled to the tRNA. The tRNA used in this thesis addressed the phenylalanine-codon UUC, hence harboring a GAA anticodon. When this precharged tRNA was used, the cell-free synthesized protein was statistically labelled by addressing each phenylalanine-codon and incorporating a lysine with the fluorescent dye into the polypeptide chain. The model protein used was the Nhe tripartite toxin. The precharged tRNA BODIPY-TMR-Lysine was added to the cell-free reaction at a final concentration of 2 µM. All other reaction components remained as described in Table 9.

Cell-free protein synthesis of modified proteins through the incorporation of non-canonical amino acids in batch-based reactions

The CtxA subunit was used as a model protein for the incorporation of a ncAA using amber-suppression. Two newly designed templates, namely NCM-CtxA-AmbE110-C0 and NCM-CtxA-AmbE112-C0, were amplified using the Hifi PCR protocol (see 2.2.2). A standard batch-based synthesis as described above was performed. Additionally, the eAzFRS synthetase (f.c. 1 µM), tRNA TyrCUA (f.c. 5 µM) and either pPa or AzF as a non-canonical amino acid (f.c. 2 mM) were added to the cell-free synthesis. After optimization experiments, a modified CHO lysate designed by Jeffrey Schloßhauer[197] (IZI-BB) containing a stably transfected eAzFRS was used and no additional eAzFRS had to be added to the cell-free synthesis. All other components were equally administered to the reaction as stated before. The reaction with this modified CHO lysate was incubated for 3 h at 30°C and 500 rpm.

Cell-free protein synthesis using a CECF format

A continuous exchange cell-free system (CECF) can be used to prolong the synthesis time and thus also increase the total protein yield. When using the CECF format, a dialysis chamber is used where the reaction mix is separated from a feeding mixture by a 10 kDa cut off semipermeable membrane. Small-scale dialysis chambers comprising a reaction chamber with 50 µL and a feeding chamber with 1000 µL were used. The reaction and feeding mix were prepared separately from one another containing the standard compositions as described in Table 10. In general, plasmid DNA with a final concentration of 60 ng/µL, if not stated otherwise, was used as a template. In comparison to a batch-formatted synthesis, sodium azide was added to suppress microbial growth. In

order to prevent protein degradation, the caspase inhibitor Z-VAD-FMK was added in *Sf*21 reactions while the caspase inhibitor AC-DEVD-CMK was supplemented for CHO and K562 reactions.

Table 10: Standard composition of a CECF reaction.

Component	Final concentration (f.c.)	Reaction	Feed
ddH_2O	variable	X	X
DNA template	variable	X	
Lysate	40% (v/v)	X	
HEPES-KOH (pH 7.6)	30 mM	X	X
KOAc	150 mM	X	X
$Mg(OAc)_2$	3.9 mM		X
	22 mM	X	
Amino acids	100 µM	X	X
Spermidine	0.25 mM	X	X
Creatine phosphate	18.5 mM	X	X
Creatine kinase	100 µg/mL	X	X
ATP	1.75 mM	X	X
GTP, CTP, UTP	0.3 mM	X	X
PolyG	10 µM	X	
DTT	2.5 mM	X	X
Sodium azide	0.02%	X	X
Caspase inhibitor	30 µM	X	X
T7 RNA polymerase	1 U/µL	X	

Again, DTT was not added for disulfide bridge containing proteins. If necessary, ^{14}C-leucine was added at a final concentration of 11 µM for quantitative and qualitative analysis as described in 2.2.10 and 2.2.12. All components were directly added to the reaction or feeding mixture. ddH_2O was adjusted to fill up the reaction to the desired final volume. First, the feeding mixture was added to the chamber and at last the reaction mixture was filled into the reaction chamber. CECF reactions were incubated for 24-48 h at 600 rpm and at 27°C when using *Sf*21 lysate and at 30°C when using CHO and K562 lysates.

General aspects for cell-free protein synthesis

Cell-free protein synthesis was performed using different templates, in particular plasmids encoding proteins or linear DNA fragments derived from PCRs. Further, multicomponent proteins were synthesized in various parts of this thesis. The synthesis of each individual subunit was performed as a control experiment, but in order to synthesize the complete

protein complex templates encoding each individual subunit were either synthesized individually and mixed together after the synthesis or co-expressed as represented for Hbl in Figure 7 A and B, respectively.

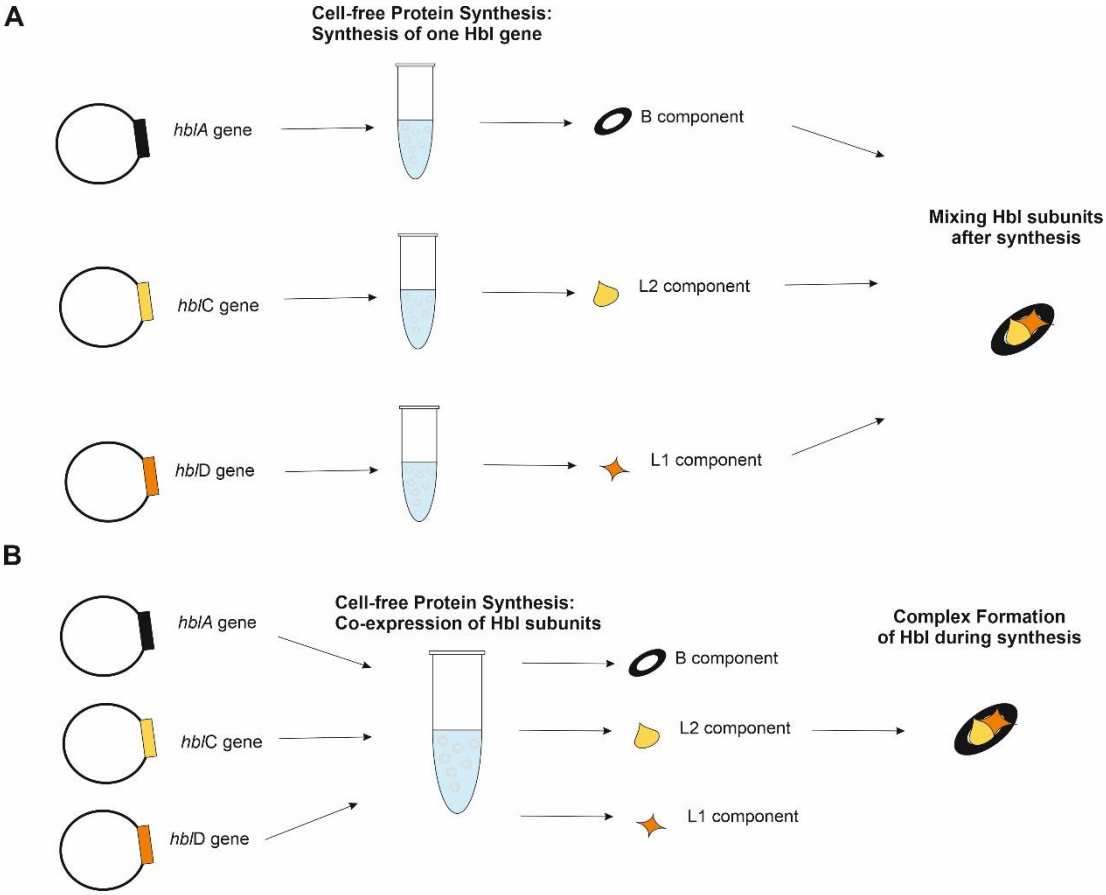

Figure 7: Schematic overview of Hbl cell-free synthesis.
(A) Synthesis of single Hbl subunits and mixing after the synthesis. (B) Co-expression of all three Hbl subunits and complex formation.

In a co-expression, the templates were added in molar ratios. The tripartite toxins Nhe and Hbl, consisting of 3 individual subunits were co-expressed in varying molar plasmid ratios as further stated in 3.2.1. Subunits of AB_5 toxins were synthesized individually or were co-expressed with the template for the B subunit 5-times the molar ratio of the A subunit. As the A subunit can further be split into the A_1 and the A_2 fragment, a co-expression of the A_1, A_2 and B subunit templates was performed in a 0.5:0.5:5 molar ratio (Figure 8).

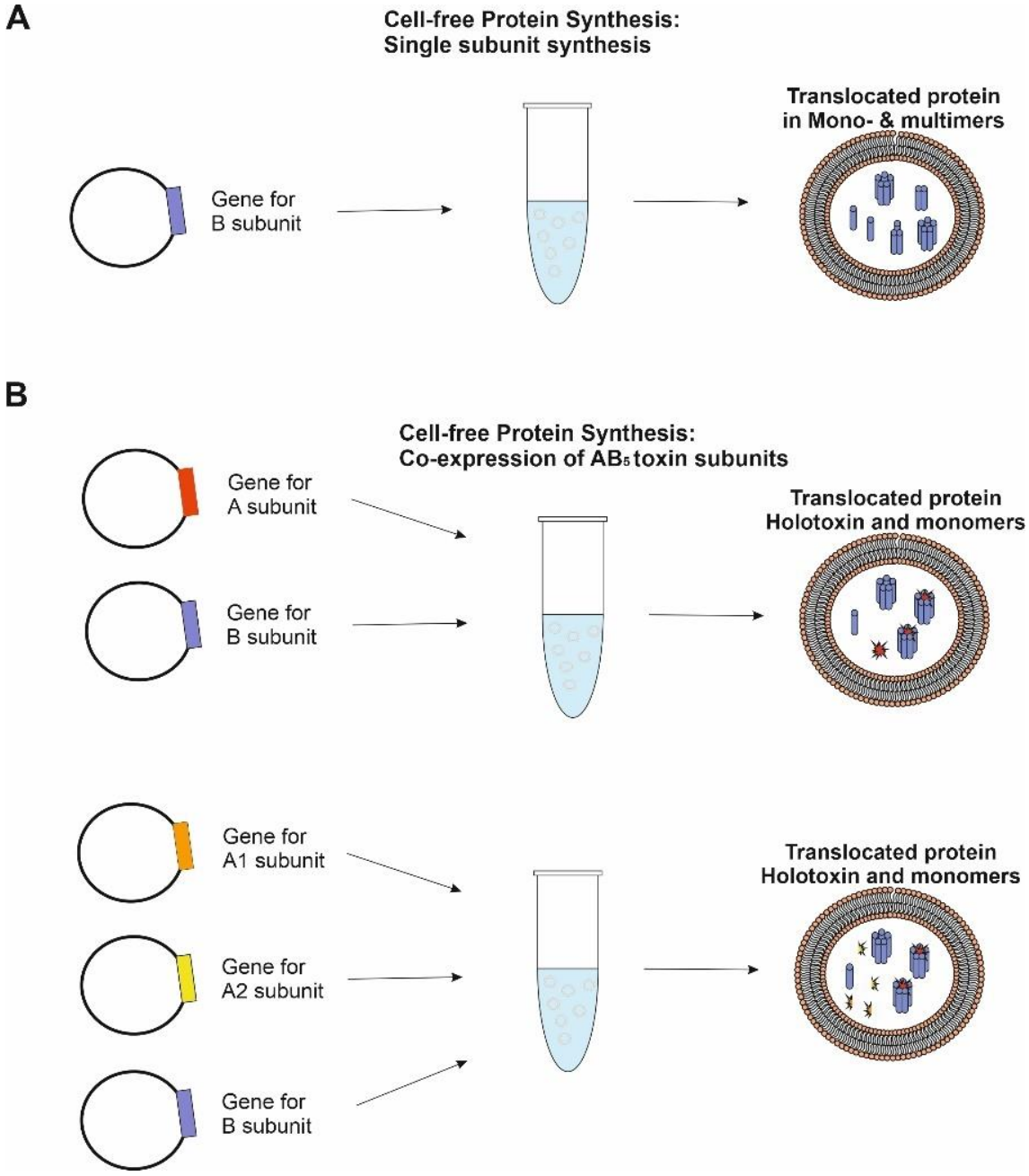

Figure 8: Schematic overview of AB_5 toxin synthesis.
(A) Synthesis of single subunits as an example of the B subunit. (B) Co-expression of the individual subunits

For functionality assessments of all proteins, a synthesis containing ^{14}C-leucine was prepared in parallel to a non-labelled synthesis. Total protein concentrations of the radio-labelled fractions were measured by TCA-precipitation (see 2.2.10) and, consequently, assumed for non-labelled fractions as both reactions were prepared simultaneously.

2.2.8 Fractionation of translation mixtures

After the translation reaction a crude translation mixture (TM) was present. In order to separate soluble proteins, membrane proteins as well as proteins translocated into the microsomal vesicles the following fractionation procedures were performed.

Soluble and membrane proteins

The crude TM was centrifuged for 10 min at 16,000xg and 4°C. The resulting supernatant (SN) containing soluble proteins was quantitatively removed from pelleted microsomal vesicles. These vesicles were resuspended in the same volume of PBS as the SN that was removed. The resuspended pellet, the so-called microsomal fraction (MF), contained membrane proteins and translocated proteins.

Translocated proteins

If a protein was post-translationally modified or a protein was toxic to eukaryotic ribosomes, the protein was synthesized in the presence of a MeI signal peptide. Proteins that natively contained signal peptides either harbored the native or MeI signal peptide. These proteins were also translocated into the ER-based vesicles during translation. Such proteins had to be harvested from the microsomal vesicles after the cell-free synthesis. Therefore, the reaction was centrifuged for 10 min at 16,000xg and 4°C. This first supernatant (SN) was quantitatively removed and the pellet was resuspended with an equal volume of a mild detergent-PBS solution to perforate the microsomal membranes. The proteins were further released under intense agitation for at least 30 min. At last, in order to separate aggregated microsomal debris from the translocated proteins the mixture was centrifuged for 10 min at 16,000xg and 4°C. This second supernatant (SN2) containing the soluble proteins was removed and analyzed.

2.2.9 Selective modification of reactive groups

Fluorescent labelling using biotinylated fluorophores

After the synthesis of the LTB-Strep fusion protein and the respective controls, the biotinylated fluorophore Atto 488-Biotin (f.c. 1 µM) was incubated with the protein for 90 min at room temperature. 90 min were chosen to compare the reaction to Staudinger ligation labelling reactions.

Staudinger ligation

After the incorporation of the ncAA AzF, an reactive azido group is present in the protein which can react with a phosphine. Hence, a direct labelling with DyLight-632 phosphine was carried out. The SN2 fractions of the modified CtxA subunits were incubated for 90 min at room temperature with 5 µM DyLight-632 phosphine.

Copper(I)-catalyzed click chemistry

After the incorporation of the ncAA pPa, a copper(I) catalyzed click reaction was used to label the SN2 of the modified CtxA subunit. CtxA was incubated with the catalysator $CuSO_4$ $5H_2O$ (f.c. 200 µM), THPTA for copper(I) ion stabilization (f.c. 600 µM), the

reducing reagent NaAsc (f.c. 5 mM) and the fluorescent label Sulfo-Cy5-Azide (f.c. 5 µM). This mixture was incubated at room temperature for 90 min.

2.2.10 Quantitative protein analysis by TCA precipitation

The total protein yield of cell-free synthesized proteins that were labelled with ^{14}C-leucine was quantified by hot TCA precipitation and successive liquid scintillation measurement. A sample of each fraction of interest (TM, SN, MF, SN2) was transferred into glass vials. Each analysis was undertaken in triplicates while using 5 µL samples in batch-based reactions and 3 µL samples in CECF reactions. 3 mL of 10% (v/v) TCA mixed with 2% (v/v) casein hydrolysate were added onto each sample. After 15 min incubation in an 80°C water bath, the test tubes were precipitated on ice for at least 30 min. The samples were separated from free ^{14}C-leucine using a vacuum filtration system as ^{14}C-labelled proteins retained on the glass fibre filter paper. Filters were washed twice with 5% (v/v) TCA, dried with acetone and placed into scintillation vials. The filter paper was covered with 3 mL scintillation cocktail, and placed on an orbital shaker for at least 1 h. The HIDEX 600 SL was used to detect the scintillation counts which could be used to calculate the total protein concentration based on the following formula:

$$Protein\ yield\ \left[\frac{\mu g}{mL}\right] = \frac{scintillation\ counts\left[\frac{dpm}{mL}\right] * molecular\ weight\left[\frac{\mu g}{pmol}\right]}{specific\ radioactivity\ (A_{spec})\left[\frac{dpm}{pmol}\right] * number\ of\ leucines}$$

$$A_{spec}\ \left[\frac{dpm}{pmol}\right] = \frac{stock\ concentration\ of\ ^{14}C\ leucine\ [\mu M] * A_{spec}\ of\ ^{14}C\ leucine\ stock\ [\frac{dpm}{pmol}]}{Total\ concentration\ of\ leucine\ [\mu M]}$$

The specific radioactivity was calculated for batch and CECF reactions with the following concentrations:

Batch:

Concentration of ^{12}C-leucine = 100 µM

Specific radioactivity of ^{14}C-leucine stock = 200 dpm/pmol

Concentration of ^{14}C-leucine = 50 µM

Total concentration of leucine = 150 µM

Specific radioactivity in batch reactions = 66.66 dpm/pmol

CECF:

Concentration of ^{12}C-leucine =100 µM

Specific radioactivity of ^{14}C-leucine stock = 100 dpm/pmol

Concentration of ^{14}C-leucine = 11 µM

Total concentration of leucine = 111 µM
Specific radioactivity in CECF reactions = 9.9 dpm/pmol

Protein yields in each experiment were obtained from triplicate analysis and the experiments in this thesis were performed in three independent experiments if not stated otherwise. Therefore, the arithmetic mean ($x_{arithmetic}$) and the standard deviation (SD) were calculated according to the following:

$$x_{arithmetic} = \frac{1}{n}\sum_{i=1}^{n} x_i = \frac{1}{a} * (x_1 + x_2 + x_a)$$

$$SD = \sqrt{\frac{\sum_{i=1}^{n}(x_i - x_{arithmetic})^2}{n}}$$

2.2.11 Glycosylation analysis

Protein N-glycosylation was investigated using PNGaseF or EndoH digestion according to the manufacturer's protocol. The ORF8 protein from SARS-CoV2 was synthesized in a cell-free *Sf*21 system in the presence of ^{14}C-leucine. Subsequently, 5 µL of the protein sample were used for the deglycosylation assay and were mixed with 0.7 µL of denaturing buffer. After an incubation of 10 min at 95°C, 0.7 µL endoglycosidase was added. For EndoH reactions, 0.7 µL G5 reaction buffer was further added. 0.7 µL G7 reaction buffer and 0.7 µL NP-40 were added for PNGaseF reactions. The protein samples were digested for 1 h at 37°C. Subsequently, samples were precipitated in acetone for SDS-PAGE analysis as described in 2.2.12.

2.2.12 Qualitative protein analysis by SDS-PAGE, in-gel fluorescence and autoradiography

Proteins synthesized in the presence of ^{14}C-leucine were separated on an SDS-PAGE. Therefore, 3-5 µL of the cell-free synthesized protein sample were mixed with ddH_2O (final volume of sample and ddH_2O of 50 µL) and 150 µL ice-cold acetone were added. The mixture was incubated for at least 15 min on ice. Subsequently, the precipitated protein was separated from the acetone by centrifugation (16,000xg, 10 min, 4°C). After the acetone supernatant was removed, the protein pellet was dried for at least 30 min at 45°C on a thermomixer. The dried pellet was resuspended in 20 µL LDS sample buffer and agitated for at least 15 min. LDS sample buffer contained 50 mM of DTT whenever proteins did not contain disulfide bridges. Before samples were loaded onto the SDS-PAGE, samples were heated at 70°C for 10 min, if soluble proteins were used. Two types of gels were used during the course of this thesis. Precast NuPAGE 10% Bis-Tris gels were run at 185 V for 35 min using the NuPAGE MES SDS running buffer (1x) for

qualitative analysis of small proteins (<20 kDa) or to analyze multicomponent complexes. Self-prepared gels were cast according to the manufacturer`s protocol and run at 150 V for 55 min using Tris-Glycine running buffer (1x). After the separation of the protein samples, gels were washed three times with dH_2O in a microwave (600 W, 1.5 min). The SDS-PAGE was stained for 10 min using Simply blue safe stain solution on an orbital shaker and de-stained for at least 30 min in dH_2O. At last, gels were dried onto Whatman paper at 70°C for 70 min and for later detection of the standard marker its bands were marked with ink containing ^{14}C-leucine. The dried gel was placed on a phosphor screen for at least 3 days to allow for the detection by autoradiography and were visualized with the phosphor-imager system.

Fluorescently labelled proteins were separated on an SDS-PAGE as described above. Subsequently, gels were placed into dH_2O and analyzed with the Amersham Typhoon RGB imager with a fluorescence detector (DyLight-632 phosphine and Sulfo-Cy5-Azide: excitation 633 nm, emission 670 nm; BODIPY-TMR-dye: excitation 530 nm, emission 580 nm; Atto 488-Biotin dye, excitation 488 nm, emission 520 nm). Afterwards, gels were washed, stained, dried and autoradiographs were detected as explained above.

2.2.13 Fluorescence analysis

The LTB-eYFP fusion protein was used to identify whether the protein was co-translationally translocated. After three cycles of a repetitive synthesis 5 µL of the reaction mixture were diluted in 20 µL PBS. Using a µ-IBIDI slide, a fluorescence scan with the Cy2 laser was performed using the Amersham Typhoon RGB imager. Subsequently, the translocation of the protein was studied by confocal laser scanning microscopy (CLSM). The eYFP containing protein samples were excited with the argon laser at 488 nm. The emitted light was captured with a photomultiplier after passing a long pass filter at 505 nm. The Zen 2009 software was used for image processing.

2.2.14 Protein detection

In order to validate the binding of commercial antibodies against the nucleocapsid protein, Western Blots, a Dot Blot and in-solution ELISAs were performed.

Western Blot

The SN fractions of the nucleocapsid WT protein and the two mutants were analyzed. Therefore, samples synthesized in a cell-free manner and precipitated with ice cold acetone and run on a self-cast SDS-PAGEs as described in 2.2.12. The SeeBlue Plus 2 Pre-Stained marker was used as a weight measurement. Afterwards, western blotting was performed and proteins were blotted onto a PVDF membrane with 20 V for 10 min. The membranes were washed with TBS/T for 5 min. The membranes were incubated

overnight at 4°C with blocking buffer (2% BSA in TBS/T) under constant agitation. The next day, the membranes were washed three times in TBS/T before incubating the membrane with a primary antibody solution (1:1,000, 1% BSA in TBS/T) for 3 h at room temperature on an orbital shaker at 60 rpm. Two primary antibodies were used, namely the anti-SARS NC sc58193 and anti-SARS-Cov-2 N protein ABIN6953059. Afterwards, the membranes were washed again with TBS/T three times for 5 min. At last the membranes were incubated for 2 h with the secondary HRP-linked anti-mouse or anti-rabbit IgG antibody solution (1:3000, 1% BSA in TBS/T) for anti-SARS NC sc58193 and anti-SARS-Cov-2 N protein ABIN6953059, respectively. The binding was visualized with chemiluminescent Western Bright ECL HRP substrate and detected with the Azure c600 Gel Imaging System.

Dot Blot

The SARS-CoV2 nucleocapsid protein was synthesized in a CHO cell-free system and its total protein yield was determined by hot TCA precipitation as described in 2.2.10. Defined yields of 15, 10, 5, 1 ng protein were precipitated in ice cold acetone and the dried pellet was solubilized in 4 µL LDS buffer and 1 µL protein binding buffer. Subsequently, the Enhancer Dot Blot System was used to spot the protein samples onto a nitrocellulose membrane. The same washing, blocking and antibody incubation procedures as for the Western Blot analysis were performed. The primary antibody against the SARS-Cov-2 N protein ABIN6953059 was used and the HRP-linked anti-mouse secondary antibody was used for detection. Again, the binding was visualized with chemiluminescent Western Bright ECL HRP substrate and detected with the Azure c600 Gel Imaging System.

In-solution ELISA

Cell-free synthesized nucleocapsid proteins were mixed with Ni-NTA Magnetic Agarose Beads according to the manufacturer's protocol. Protein samples were diluted with PBS. Shortly, samples were incubated with beads over night at 4°C on a rotator. All following steps were performed on ice and a magnetic separator was used to collect the beads with the bound protein. On the next day, beads were washed three times with 200 µL washing solution and 200 µL of primary antibody (anit-SARS-Cov-2 N protein ABIN6953059, 1:1,000 in binding buffer) were added to the beads and incubated at 4°C on a rotator for 2 h. Subsequently, the samples was washed again three times with 200 µL washing buffer. The secondary HRP-linked anti-rabbit antibody (1:3,000 in binding buffer) was added to the beads and the solution was incubated for 2 h at 4°C on a rotator. After a final washing procedure, 100 µL TMB were added to the beads and incubated on ice for 1 min. The TMB solution was separated from the beads and mixed with 100 µL H_2SO_4 detection

solution and pipetted into wells of a flat bottom clear 96-well plate. The absorbance at 450 and 620 nm was measured using the Mithras Tristar^2 LB 943.

2.2.15 *In vitro* translation inhibition assay

Dianthin

As described in 1.4.1.1 the plant derived toxin Dianthin inhibits protein translation in eukaryotes[174]. In previous work an *in vitro* translation inhibition assay was developed in order to test whether cell-free synthesized Dianthin inhibits the *in vitro* translation of a model protein[70]. This assay was optimized and modified in this thesis. Shortly, Dianthin or Dianthin-EGF was synthesized in a batch-based CHO reaction. A defined concentration of 1.5 and 3 nM of the SN2 fraction were added to the cell-free synthesis of the model protein Luciferase (LUC). LUC was synthesized in the eukaryotic CHO und prokaryotic *E. coli* system. Reaction mixtures containing the LUC with ddH_2O, PBS, 0.5% CHAPS/PBS or the NTC were used as controls. An NTC without the addition of the template for LUC was used as an overall control. After the synthesis, the total protein yield of LUC was determined as described in 2.2.10 and LUC was qualitatively analyzed by autoradiography as described in 2.2.12.

SARS-CoV2 nsp1

The leader protein nsp1 from SARS-CoV2 induces a host protein translation inhibition[198].
The nsp1 protein was pre-synthesized in a CHO-based cell-free system and subsequently administered to the synthesis of a non-viral model protein, in this case eYFP. Defined concentrations of 25 and 90 nM nsp1 were administered to the cell-free synthesis of eYFP. The NTC was administered as a volume equivalent to 90 nM nsp1. A 50 µl reaction of the eYFP was pipetted into a black 96-well plate. A continuous recording of the fluorescence intensity of the eYFP was performed over a 3 h synthesis time. The fluorescence was measured every 10 min using the Mithras^2 LB 943. An eYFP control synthesis was used as a standard control. The fluorescence signal of eYFP without the supplementation of nsp1 was defined as a baseline value of 100%. The fluorescence intensity of eYFP supplemented with nsp1 was normalized to the baseline value.

2.2.16 Hemolytic activity testing on blood agar plates

Pore-forming proteins can induce lytic activity. In order to assess the hemolytic activity of cell-free synthesized PFTs from *B. cereus* precast blood agar plates containing 5% sheep blood were used. A total volume of 10 µL *de novo* synthesized toxin were directly spotted onto the blood agar plate. To suppress microbial growth, erythromycin and gentamycin (f.c. 50 µg/mL) were added to each sample. As a positive control, 10 µL of 0.25% Triton-X 100 detergent solution were used. After 24 h of incubation at 37°C, hemolytic zones were visualized and documented with a CCD camera.

To sample defined toxin concentrations, protein yields were determined by hot TCA-precipitation (see 2.2.10) and concentrations were calculated. The protein samples were diluted with PBS to a 10 µL mixture containing the protein of interest in a defined concentration and then the mixture was spotted on the blood agar plate.

In order to compare different hemolytic zones, a defined length of 1 cm was additionally photographed. The pixels within the photograph of this 1 cm length as well as the lytic areas on the blood agar plates were measured using ImageJ. The measured pixels for the hemolytic areas were translated to a defined length in cm according to the following calculation:

$$Length\ (cm) = \frac{Measured\ pixels}{Measured\ pixels\ of\ 1\ cm\ defined\ length}$$

2.2.17 Cell cultivation

Cell-based toxicity assays were performed using Caco2, CHO-K1, PC-9 and HEK293 cells. Caco2 cells were cultured in MEM supplemented with 20% (w/v) FBS and 1% (w/v) NEAA. CHO-K1 and HEK293 cells were cultured in DMEM supplemented with 2% stabilized L-glutamine and with 1 and 10% (w/v) FBS, respectively. PC-9 cells were cultured in RPMI 1640 media supplemented with 2% stabilized L-glutamine and 10% (w/v) FBS. When cell-free synthesized proteins were added to seeded cells, 1% (w/v) Pen/Strep was supplemented to the medium.

Cells were split every 5-7 days according to standard protocol using 0.25% trypsin/ 0.02% EDTA. Cell cultures were maintained in a cell culture incubator at 37°C and 5% carbon dioxide (CO_2) atmosphere. Before cells were seeded for cell cultivation or for toxicity assessment, the viable cell number was determined. 50 µL cell suspension were mixed with 50 µL trypan blue which stains dead cells. The cell number was determined using the Thoma cell counting chamber.

2.2.18 Morphological analysis of cells

All morphological changes were documented using a light microscope where phase contrast micrographs were captured with a CCD camera. Image processing was performed with ImageJ.

Hbl

The effect of Hbl on Caco2 cells was analyzed to assess the toxicity on cells from the gastrointestinal tract. Cells were seeded into 48-well plates in a cell suspension of 15,000 cells per well and incubated for 24 h at 37°C and 5% CO_2 airflow to allow for adhesion. Afterwards, the CHO-based cell-free synthesized tripartite toxin, two co-expressed

subunits or the individual subunit was diluted in cell culture medium to a concentration of 2.5 nM for SN and 0.25 nM for MF fractions. A volume equivalent NTC sample was applied. The samples were added to the individual wells and after 4 h incubation at 37°C and 5% CO_2 airflow morphological changes were documented.

Ctx and LT

The effect of the AB_5 multicomponent structures and individual subunits was assessed on CHO-K1 cells. 24-well plates were used and 25,000 cells/well were added to each well. Cells were seeded shortly before adding the toxin. Modified Ctx multimers were synthesized in a CHO batch-based reaction while LT multimers and LT single subunits were synthesized in *Sf*21 lysate. The SN2 fractions were used for functionality assessment. 4 nM of Ctx samples and 5 nM of LT samples were supplemented to the cells. In order to allow for the same detergent concentration of the final sample that was added to the cells, all samples were diluted and filled up to the same volume of 0.5% CHAPS/PBS. The toxin / detergent solution, 0.5% CHAPS/PBS or medium was added to individual wells. An NTC was added by using a volume equivalent to the toxin fragment. Morphological changes were documented after 48 h, if not stated otherwise.

Dianthin

The apoptotic effect of the Dianthin-EGF targeted toxin was studied on the EGFR expressing human lung adenocarcinoma cell line PC-9[199]. HEK293 cells were used as a control cell line as a lower EGFR expression rate is detected[200]. Cells were seeded into 24-well plates at 50,000 and 25,000 cells per well in 500 µL for PC-9 and HEK293 cells, respectively, and allowed to adhere for 24 h in a cell incubator at 37°C and with 5% CO_2 airflow. HEK293 cells had a faster reproduction rate and were therefore seeded at lower cell numbers as determined in prior experiments. The next day, 125 µL of cell culture medium with or without the addition of the endosomal escape enhancer SO1861 (f.c. 1 µg/mL) was added. At last, 125 µL containing cell-free synthesized toxin, EGF control or a volume equivalent NTC (all SN2 fraction) diluted in 0.5% CHAPS/PBS were added. Three different concentrations were evaluated, namely 0.0000001 nM (= 0.1 fM), 0.00001 nM (= 10 fM) and 0.001 nM (= 1000 fM). The NTC was diluted and treated in the same manner as the protein with the lowest overall protein yield used in the assay and applied in a volume equivalent. Medium and 0.5% CHAPS/PBS detergent solution were used as untreated and buffer controls, respectively. After 48 h in a cell incubator at 37°C with 5% CO_2 changes were documented.

2.2.19 MTT-Assay

In order to quantify the effects of Nhe and Dianthin the MTT viability assay was chosen. In this colorimetric assay the NAD(P)H-dependent cellular oxidoreductase in mitochondria

reduce the yellow 3-(4,5-dimethylthiazol-2-yl)-2,5-diphenyltetrazolium bromide (MTT) to the insoluble, purple formazan. When the absorbance was measured at 570 nm and 630 nm using the Mithras^2 LB 943, the cell viability can be quantified as the degree of absorption, indicated by the purple color. This depends on the insoluble formazan that is accumulated in viable cells. Therefore, the cell viability can be calculated by

$$Cell\ viability\ [\%] = \frac{OD\ 570 - OD\ 630\ of\ test\ substance}{OD\ 570 - OD\ 630\ of\ 0\ nM\ test\ substance} * 100$$

Nhe

For the analysis of the cytotoxic effect of cell-free synthesized Nhe on Caco2 cells, 100 µL of 100,000 cells/mL cell suspension were seeded into a 96-well plate (f.c. 10,000 cells/well). After 24 h of incubation at 37°C and 5% CO_2 airflow in order for cells to adhere, 10 µL of the SN fraction of the cell-free synthesized toxin, a volume equivalent NTC or medium (untreated cells) were added to the wells. The NTC was diluted and treated in the same manner as the tripartite toxin used in the assay and applied in a volume equivalent to the toxin. Serial dilutions of cell-free synthesized Nhe toxin ranging from 0.01 to 0.1 nM (steps of 0.01 nM) and a second dilution of 0.1 to 1 nM (steps of 0.1 nM) were tested. Toxin samples were diluted in medium. Cells exposed to the toxin were incubated for 24 h in a cell incubator at 37°C with 5% CO_2.

Dianthin

100 µL of PC-9 cell suspension were seeded into each well of a 96-well plate (80,000 cells/mL, f.c. 8,000 cells/well) and cells were allowed to adhere for 24 h at 37°C and 5% CO_2 airflow. 50 µL of medium was removed and replaced by 50 µL fresh medium with or without the addition of SO1861 (f.c. 1 µg/mL in each well). 10 µL SN2 fraction of Dianthin, the Dianthin-EGF targeted toxin, EGF as a control or a volume equivalent NTC were added to each well. A concentration gradient of each sample was pipetted by diluting the stock solution of the protein with the 0.5% CHAPS/PBS detergent solution with final concentrations of 0.1 fM, 1 fM, 0.01 pM, 0.1 pM, 1 pM, 0.01 nM, 0.1 nM and 1 nM. The NTC was diluted and treated in the same manner as the protein with the lowest overall protein yield used in the assay and applied in a volume equivalent. Medium and 0.5% CHAPS/PBS detergent solution were used as untreated and buffer controls, respectively. Cells were incubated for an additional 48 h in a cell culture incubator at 37°C with a 5% CO_2 flow rate.

After the respective cells were incubated with the toxin, the MTT assay was performed according to the manufacture's protocol. Shortly, 10 µL MTT were added to each well and incubated for 4 h. For solubilizing the formazan, 100 µL solubilizing solution were added to

each well and incubated for a minimum of 4 h. The absorbance was measured and the cell viability calculated as explained above. Each sample was analyzed in technical triplicates in three independent experiments (three biological replicates).

2.2.20 Membrane integrity assay using propidium iodide

The potential of the pore-forming protein Hbl to perforate the cell membrane was assessed using the propidium iodide uptake assay. Therefore, 10,000 Caco2 cells in 150 µL medium per well were seeded into a 96-well plate. Cells were allowed to adhere for 24 h at 37°C and 5% CO_2 airflow. 20 µL of cell-free synthesized toxin fraction were added to each well. Concentrations of 0.5, 1.5 and 2.5 nM were studied for the SN fraction while 0.05, 0.15 and 0.25 nM were studied for the MF fraction. Untreated cells and an NTC were used as controls. The latter was diluted to a volume equivalent of the protein of interest. Each sample was analyzed in triplicates, if not stated otherwise. Subsequently, 30 µL of propidium iodide (f.c. 10 µg/mL) were added to each well. Cells exposed to samples were incubated for 4 h at standard conditions. Propidium iodide could only enter the cell when the cell membrane was disrupted by the toxin. Within the cell, propidium iodide bound to the DNA, resulting in a change in the emission of the propidium iodide. The emission of the propidium iodide was measured in relative light units (RLU) at 616 nm using the Mithras^2 LB 943 . The mean of each triplicate measurement was calculated and subtracted by the mean triplicate measurement of medium treated cells. Each sample was analyzed in technical triplicates in two independent experiments.

2.2.21 Cytotoxicity assessment

The cytotoxic effect of the AB_5 toxins LT and Ctx was quantified using the CellTox Green Cytotoxicity Assay according to the manufacturer's protocol in a 96-well plate. CHO-K1 target cells were seeded at a concentration of 4,000 cells/well in 90 µL directly before adding the toxins. Modified and non-modified LT holotoxin as well as individual subunits were synthesized in *Sf*21 lysate and 6 nM of the SN2 fractions were added to the cells. Ctx WT multimer as well as the modified multimer were synthesized in CHO lysate. 4 nM of the SN2 fractions were supplemented to the cells. All multimers and subunits were diluted in 0.5% CHAPS/PBS and medium in order to ensure the same detergent concentration within the experiment. The NTC was administered in a volume equivalent to the toxin fragment that was diluted the least. A medium control as well as a 0.5% CHAPS/PBS detergent control and a 1% Triton-X 100 control were additionally used. Subsequently, CHO-K1 cells were incubated for 48 h at 37°C and 5% CO_2 airflow. After the incubation, 100 µL 2x reagent were added to each well and the microplate was agitated on an orbital shaker at 800 rpm for 1 min. Following that, the plate was incubated for 15 min shielded from light. The fluorescence intensity (excitation 485 nm, emission

520 nm) was measured with the Mithras^2 LB 943. A high fluorescence identified non-viable cells as the reagent could only enter the cell when the membrane was disrupted. Then, the cyanine dye within the reagent could bind to the available DNA[201]. Again, the individual samples were analyzed in technical triplicates in three independent experiments (three biological replicates).

2.2.22 Soft-Agar Assay

In order to validate the targeted toxin Dianthin-EGF for a potential clinical application, an assay based on primary tumor cells from human patients was established. Therefore, epithelial squamous cell carcinoma biopsy samples, later called tumor samples, were provided by the Charité - Universitätsmedizin Berlin (Campus Benjamin Franklin and Campus Virchow Klinikum). The ethical approval of this study was obtained from the Ethikkommission, Ethikausschuss am Campus Virchow-Klinikum, approval number EA2I239/17. As no personalized data were stored during this process no declarations of consent from the patients were required. This decision was based on § 25, 1 no. 4 of the State Hospital Act and § 40 of the Federal Data Protection Act.

The assay was performed in petri dishes with a diameter of 3 cm. As a first step, a difco agar solution was prepared with a final concentration of 2.5%. 0.2 mL agar were mixed with 0.8 mL tumor medium and a layer of agar was slowly cast in the petri dish. The agar was allowed to solidify. Next, the tumor samples were washed three times in Braunol in order to disinfect the patient sample from any kind of pathogen. The tumor sample was cut into small pieces using forceps and a surgical scalpel to simplify the single cell separation using a cell strainer. The optimized cell strainer pore size was identified as 500 µm. Subsequently, the shredded tumor sample was washed in medium and centrifuged for 10 min at 800xg. This was repeated 3 times. The pellet containing the single tumor cells was resuspended in fresh medium. The number of viable single cells was determined using trypan blue and a Thoma counting chamber. 100,000 tumor cells were mixed with either Dianthin, Dianthin-EGF, EGF, NTC or tumor medium in the presence and absence of the endosomal escape enhancer SO1861 (f.c. 1 µg/mL). Final protein concentrations of 0.1 and 1 nM were evaluated. The NTC was used in a volume equivalent to Dianthin-EGF. At last, a mixture of 0.8 mL containing the tumor cell suspension, analyte sample (Dianthin, Dianthin-EGF) or control (Medium, EGF, NTC) and, optionally, SO1861 was mixed with 0.2 mL difco agar. This mixture was cast on top of the solidified first agar layer. Soft-agar plates were incubated for 8-11 days in a cell culture incubator at 37°C with a 5% CO_2 flow rate. After the incubation time, an overview image of the complete petri dish containing the embedded tumor cells was taken with the

MIA stage configuration (cellSens software) with a 4x magnification of the Olympus IX83 inverted microscope. Tumor colonies were counted using ImageJ.

2.2.23 Planar lipid bilayer measurements

The electrophysiological measurements of Nhe and the SARS-CoV2 envelope protein were proceeded by Dr. Srujan Kumar Dondapati (IZI-BB). Proteins were provided by me. The data analysis was performed in collaboration with him. The electrophysiological measurements of CytK were undertaken by me and Danny Kaser (IZI-BB). The data analysis for CytK was done by me.

Nhe

Nhe was synthesized in a batch synthesis in CHO lysate. For functional analysis the SN fraction was used in order to assess the pore-formation in lipid membranes based on ion currents. For the electrophysiological measurements the Orbit 16 system using 16 MECA chips with a 50 µm cavity were used. A single channel amplifier (EPC-10, HEKA Electronic Dr. Schulze GmbH) was connected to the multiplexer electronics port of the Orbit16 system. A 1 M KCl, 10 mM HEPES salt solution buffered at a pH of 7.45 was used as an electrolyte. To allow for an ion current, 200 µL of this buffered salt solution were added to the chamber. Prior to measurements a lipid bilayer was formed across the 50 µm cavity using 1,2-diphytanoyl-sn-glycero-3-phosphocholine (DPhPC) and cholesterol (Cho) in a ratio of 90:10 (DPhPC:Cho). Lipids were dissolved in octane at a concentration of 10 mg/mL. After a stable bilayer was formed, the protein sample or an NTC was added to the chamber and recordings of activity were performed at a sampling rate of 50 kHz with a 10 kHz Bessel filter using the Patchmaster software. The continuous recording was performed at +60 mV. Up to 5 µL of the SN fraction of Nhe or the NTC were added. In order to identify and characterize the pore, polyPEG-1500 (Mw = 1400–1600 g/mol) was dissolved in the electrolyte solution to a concentration of 10 mg/mL, 2 µL of this solution were added to the electrolyte solution in the measurement chamber for recordings.

CytK

CytK proteins were synthesized in CHO lysate. Testing was performed using the Orbit mini system. This device was used as the Meca4 chip contains four individually addressable chambers allowing a parallel analysis of multiple pores. The Orbit mini was calibrated according to the manufacturer's protocol. The four cavities were calibrated so that the derivate from zero was less than 2 pA during the calibration. 150 µL of 1 M KCl, 10 mM HEPES buffer solution were added to the chip. DPhPC (10 mg/mL) was used to form a bilayer in each of the four chip cavities. Subsequently, the CytK sample or NTC (1 µL) was added to the chamber. Measurements were recorded with sampling rates of 10 kHz and a voltage of -20 mV. The Elements data reader 3 software recorded the data.

The maximum resolution was set to 200 pA. The SN and MF samples were initially tested and as the MF showed more stable recordings reproducibility of data was performed with the MF. Further recordings comparing the WT proteins with the mutants were performed using the Orbit mini under equal conditions.

SARS-CoV2 envelope protein

The SARS-CoV2 envelope protein was synthesized in CHO lysate. Measurements were performed with the Orbit 16 system using a 16 MECA chip with a 50 µm cavity. Lipid bilayers were formed from DPhPC dissolved in octane at a concentration of 10 mg/mL. A buffer solution of 150 mM sodium chloride with 10 mM HEPES buffered at pH 7.0 was used as an electrolyte. The single channel amplifier EPC-10 from HEKA Electronic Dr. Schulze GmbH was connected to the multiplexer electronics port of the Orbit 16 system. Recordings were performed at a sampling rate of 50 kHz with a 10 kHz Bessel at +100 mV. 5 µL MF of the cell-free synthesized envelope protein were added into the chamber containing 180 µL of the buffer and mixed gently by pipetting for a better fusion of microsomes with the underlying lipid bilayer. After waiting for 20 min electrophysiological measurements were started and recorded using the Patchmaster software.

2.2.23.1 Electrophysiological analysis

Data sets from electrophysiological recordings were analyzed with the Clampfit software. Traces were filtered with a lowpass Gaussian filter using default values configured by Clampfit. Histograms of traces were generated and pA values for the individual peaks were identified. Single channel activity analysis was performed. The pore insertions and single channel activity were visualized and graphs were exported.

CytK

Data of CytK WT and mutant proteins were analyzed in more detail in order to assess the possibility of a nanopore development. As described the traces were filtered and histograms were used to identify signal intensity peaks for the individual samples and individual recordings. CytK WT and mutant proteins were measured in 10 different recordings and for all recordings peaks were analyzed. These records were converted into conductivity (σ). This value defined the change of the conductivity that occurred after a pore insertion. The conductivity was calculated according to the following formula:

$$\sigma\,[nS] = \frac{I\,[pA]}{U\,[mV]}$$

With:
I - Amperage
U - Voltage

In order to analyze the average conductivity level of each individual CytK sample, the calculated values were analyzed in a python data script programmed by Danny Kaser (IZI-BB) based on the knowledge gathered during this thesis. The python code can be found in the supplementary material (8.1.1). The calculation of the average conductivity was based on a gaussian distribution so that a mean value was calculated. Therefore, data of all measurements for each individual protein were pooled. As observed during the recordings, multiple pore insertions occurred. In order to include all levels of inserted pores the mathematical model included in the python script consisted of two steps.
In the first step, the average conductivity of a single pore was calculated. Therefore, all data values were screened for the reference value of either 1000 or 627 pS. 1000 pS reflected the mean conductance in KCl buffer as evaluated during this thesis. 627 pS served as a reference value from the literature and was based on measurements in NaCl buffer as described by Hardy *et al.*[137]. When 627 pS were used for the calculation an offset value of 1.26 were integrated in the computation in order to efficiently compare the data gathered here in KCl buffer with the literature value. A deviation of ± 25% of the reference value was included. The mean value and the standard deviation were calculated, which was further used for the second step. The second step focussed on the analysis of the conductivity of levels consisting of multiple pores. Up to 9 pore levels were assessed based on the following interval:

$$Interval\ (n) = [n \times reference\ value - deviation\ ;\ n \times reference\ value + deviation]$$

With:
n - Pore level
Reference value - Calculated mean conductivity for one pore
Deviation - 25% of the mean reference value

All data points for the individual samples were evaluated. Data points that did not meet the criteria for an interval between 1 and 9 were not included in the final calculation. Values that met the interval criteria were divided by the interval level n in order to normalize the data set to the conductivity of one pore level. The mean conductivity value of all normalized data points was determined. This value now differed from the reference value used in the first step and was used for the further analysis. A limit calculation with 100 iterations was performed to approximate the conductance value of a single pore insertion. At last, a final conductivity and the standard deviation were presented.

At last, the dimensions of the individual pores were calculated which was based on prior work of Hardy *et al.*[137] as described by the following formula:

$$\frac{G}{\sigma} = \frac{(\pi r^2)}{l}$$

With:

G - Conductance of the pore as calculated by the python script

σ - Conductivity of the buffer

r - Radius of the pore

l - Length of the pore

The formula was solved for pore radius r and calculated. The length l was assumed based on the calculation from Hardy *et al.*[137] where l equalled 100 Å as it was set equal to the length of aHL[202].

2.2.24 Statistical analysis

2.2.24.1 Statistical significance

An univariate analysis of variance (ANOVA) was used to assess the significant changes in the *in vitro* translation inhibition assays for Dianthin proteins. Further, an ANOVA was performed to assess the statistical significance of the cytotoxicity of modified LT and Ctx proteins. The Origin 2021 software was used to performed the ANOVA. Significance was tested according to both Bonferroni and Tuckey. Three thresholds for the probability of an error (p-value) were used to define the statistically significant change. A significantly different change (*) was defined at $p < 0.05$, a very significantly different change (**) at $p < 0.01$ and a highly significantly different change (***) at $p < 0.001$.

2.2.24.2 IC_{50} determination

The half maximal inhibitory effect (IC_{50}) was determined for Nhe on Caco2 cells and Dianthin as well as Dianthin-EGF on PC-9 cells. Therefore, a non-linear, logistic fit was performed and the IC_{50} was calculated using Origin 2021.

2.2.25 Figures

Schematic figures were designed with CorelDRAW Graphics Suite. Schematic figures for CFPS, orthogonal cell-free systems and the soft-agar assay partially included graphics from Servier Medical Art.

3 Results

3.1 Identification of toxin classes

Proteinaceous toxins comprise a variety of protein classes with different characteristics, mechanisms of action and binding properties. In order to validate cell-free protein synthesis as a platform technology for the synthesis, characterization and application of proteinaceous toxins, a multifaceted set of model proteins had to be identified. Model proteins were chosen based on the following characteristics:

- Different biological taxonomic domains
- Versatile mechanisms of action
- Limited data on functionality
- Possibility for future applications

At last, prokaryotic as well as eukaryotic model proteins displaying different functionalities were chosen as represented in Figure 9.

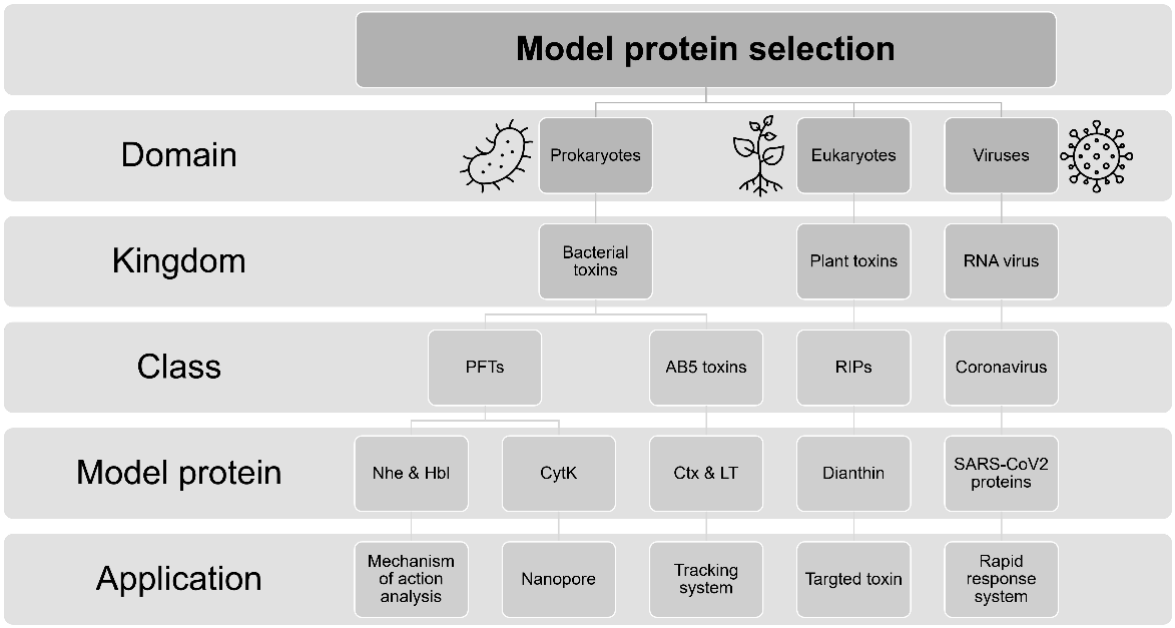

Figure 9: Model protein selection.

3.2 Diagnostic use of toxins

When a novel toxin producing pathogen is detected, the underlying toxins have to be analyzed in terms of their pathogenicity towards a living organism. Whenever such a pathogenic protein is well characterized, it might be used to identify a potential underlying cause of disease or develop novel detection applications using these toxins. This first part of the thesis focusses on the validation of cell-free protein synthesis for such matters.

3.2.1 Mechanism of action analysis

Pore-forming proteins are responsible for the perforation of cells[118]. Homo-multimeric PFTs such as aHL have been widely discussed but the characterization of hetero-multimeric PFTs is more difficult. The pathogenic bacterial strain *B. cereus* produces two tripartite PTFs, namely the Non-hemolytic enterotoxin (Nhe) and the hemolytic enterotoxin Hemolysin BL (Hbl) [120,124]. The mechanisms of action in which the pore of Nhe and Hbl are formed and how these pores function are not yet fully understood. As an initial step, the capacity of CFPS to synthesize a functionally active tripartite protein was investigated.

3.2.1.1 Hemolysin BL

The tripartite pore-forming enterotoxin Hbl has been characterized as a stable multimeric toxin with hemolytic and cytotoxic activity[124,203]. Therefore, this protein was chosen to analyze the assembly of the three subunits in the CHO-based eukaryotic cell-free system. The three individual subunits were synthesized either separately or in a co-expression of two or three different subunits. In a co-expression, the plasmids were added in a 1:1:1 molar plasmid ratio for the subunits B:L_2:L_1. Quantitative analysis using liquid scintillation depicted that higher amounts of protein were detected in the SN fraction as compared to the MF fraction indicating a higher amount of soluble protein (Figure 10 A). These data were validated by qualitative analysis via autoradiography. Intense protein bands could be detected for the single subunits in the TM and SN whilst less intense protein bands were detected in the MF. When B and L_1 were co-expressed only one intense protein band was visual in the autoradiograph as both proteins have a similar molecular weight (38.41 kDa and 40.71 kDa for B and L_1, respectively; (Figure 10 B)). The hemolytic activity of the protein was assessed by spotting cell-free synthesized tripartite Hbl, two co-expressed subunits or single subunits onto 5% sheep blood agar plates. Single subunits and two co-expressed subunits did not show any lytic activity while the tripartite Hbl demonstrated an intense ring shaped lytic area when the TM and SN were spotted. The MF showed a less prominent lytic area (Figure 10 C, uncropped blood agar plates Supplementary Figure 1 A). When single subunits and two co-expressed subunits were spotted in close proximity to each other on one agar plate, crescent shaped areas occurred at zones between spots. When the L_1 component and co-expressed B-L_2 components were spotted close to each other, an intense crescent shaped lytic area was visible. When co-expressed B-L_2 components were spotted close to B-L_1 a less intense crescent ring was detectable (Figure 10 D, uncropped blood agar plate Supplementary Figure 1 B).

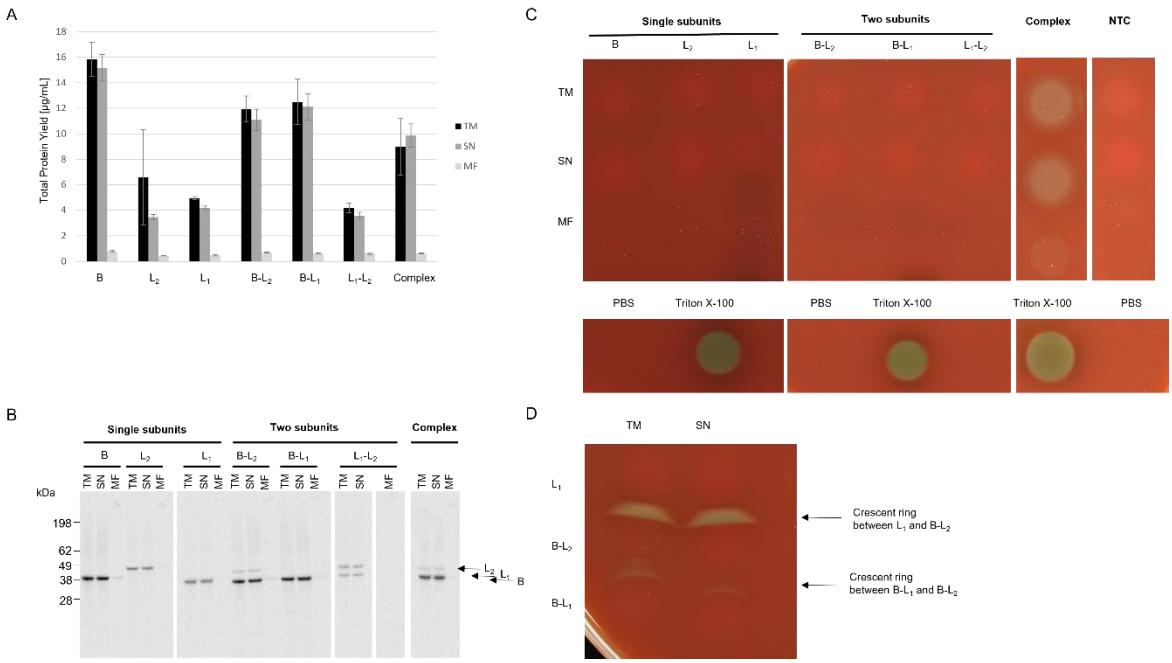

Figure 10: Establishing CFPS for the Hbl enterotoxin.

Hbl subunits were synthesized in CHO lysate either separately or in a co-expression of either two or three subunits. (A) Quantitative analysis of cell-free synthesized Hbl and subunits as performed by liquid scintillation counting. Standard deviations were calculated from triplicate analysis. (B) Autoradiograph showing ^{14}C-leucine labelled Hbl single subunits and co-expressed subunits using a molar plasmid ratio of 1:1 for two subunits or a ratio of 1:1:1 for three subunits. (C) Hemolytic activity was assessed on 5% sheep blood agar plates by spotting 10 µl of the single subunits, two co-expressed subunits and the Hbl complex for TM, SN and MF. A no template control (NTC) and PBS were used as negative controls. Triton-X 100 as a positive control. (D) Crescent formation on 5% sheep blood agar plates of L_1 and B-L_2 as well as B-L_2 and B-L_1 spots in close proximity to each other in TM and SN. Modified from Ramm *et al*., 2021.

Different ratios were used when subunits were either co-expressed or when subunits were mixed together after the synthesis in order to identify optimal parameters for the complex formation. Defined molar plasmid ratios of 1:1:1, 2:1:1, 1:2:1, 1:1:2, 10:10:1, 10:1:1, 1:10:1, 1:1:10, 10:1:10 and 1:10:10 [B:L_2:L_1] were used. Co-expressed Hbl complexes induced hemolytic activity at each individual plasmid combination (Supplementary Figure 2 A). When subunits were mixed together after the synthesis, an over-representation of the L_2 and L_1 subunit in a 10-fold manner inhibited the hemolytic activity (Supplementary Figure 2 B). These data indicated the stability of the complex. The co-expressed complex was used for further functional characterization.

For the characterization of the functionality of PFTs, an assay has to be chosen that identifies perforated cells as the outer membrane is damaged after the cell is attacked. A propidium iodide uptake assay was used to study the effects on a cell layer of Caco2 cells representing cells from the gastrointestinal tract. The perforating effect of the co-expressed Hbl tripartite complex was assessed on 10,000 Caco2 cells. Various concentrations were tested to obtain the concentration rage for the active complex. Toxic

effects could be detected starting at 0.1 nM (Ramm *et al.,* 2021, Supplementary Figure 3). To further validate toxic effects of the complex as well as the effect of the individual subunits, the Hbl complex, the individual subunits as well as two co-expressed subunits were administered to the cells. The NTC was analyzed in parallel and administered as a volume equivalent to the tripartite complex. Three different concentrations for the SN and the MF fraction were chosen based on previous results (Supplementary Figure 3). When performing the assay using the SN fraction, the Hbl complex showed membrane perforating activity at 0.5 nM while single subunits and two co-expressed subunits did not. Unfortunately, with rising concentrations the fluorescence intensity of L_2 reached the same intensity as the complex. When co-expressed subunits L_1 and L_2 were administered to the cells an even higher fluorescence intensity was measured at 2.5 nM as compared to the Hbl complex (Figure 11 A). When the MF fraction was used in the assay, increases in the fluorescence intensity could already be detected at concentrations of 0.05 nM. The application of the Hbl complex resulted in the highest fluorescence intensity at all concentrations, namely 0.05 nM, 0.15 nM and 0.25 nM. Nonetheless, co-expressed B and L_2 as well as L_1 and L_2 also resulted in an increased fluorescence intensity (Figure 11 B).

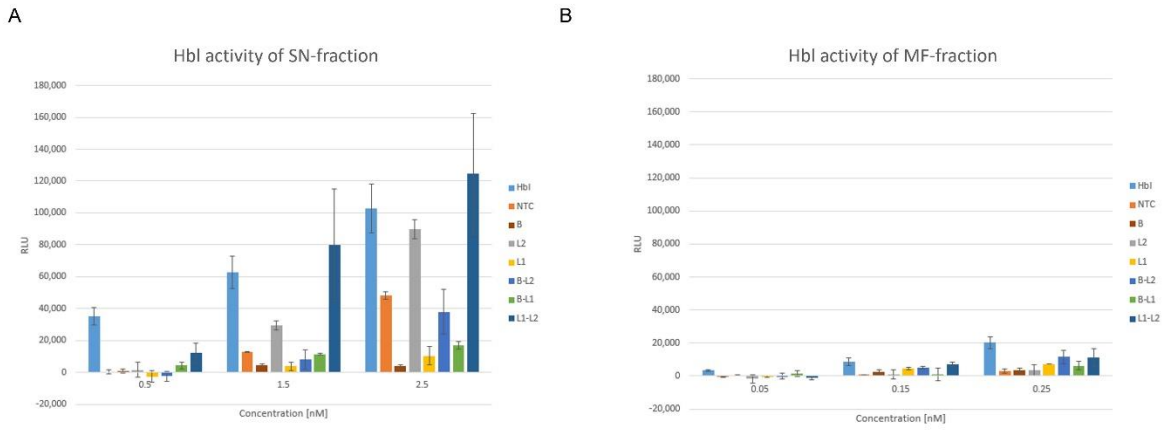

Figure 11: Membrane perforation of the Hbl complex and the individual subunits.
Hbl subunits were synthesized in CHO lysate either separately or in a co-expression of either two or three subunits. Subsequently, proteins or protein complexes were administered to Caco2 cells and assessed for their cytotoxic effects using the DNA intercalating PI. Both the SN (A) and the MF (B) fraction were analyzed. NTC, single subunits and two co-expressed subunits were used as controls. Standard deviations were calculated from triplicate samples of two independent experiments (n=6). Modified from Ramm *et al.*, 2021.

A morphological analysis of Caco2 cells subjected to the complex, two co-expressed subunits as well as the single subunits was performed with the aim to prove the cytotoxic effect of the Hbl complex. The cells were incubated with the samples at a final concentration of 2.5 nM and 0.25 nM for the SN and MF, respectively, for 4 h in accordance to the membrane perforation assay. The tripartite complex resulted in cell death. Strikingly, the SN fraction of co-expressed L_1:L_2 subunits showed a reduced cell

confluency (Figure 12) suggesting a potential pre-pore formation. All other single subunits and two co-expressed subunits did not induce morphological changes (Supplementary Figure 4). Summarizing the data on the Hbl enterotoxin, a stable complex formation could be shown and a putative pre-pore complex was detected. These data were subsequently published in 2021[76].

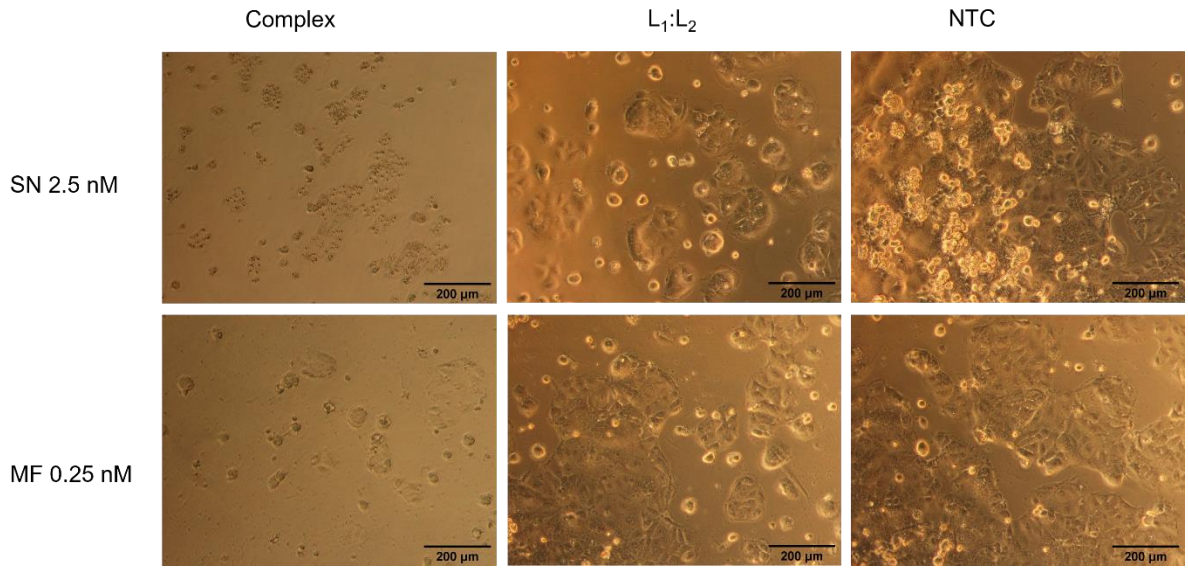

Figure 12: Morphological assessment of Caco2 cells after Hbl exposure.
Hbl subunits were synthesized in CHO lysate either separately or in a co-expression of either two or three subunits. Subsequently, proteins or protein complexes were administered to Caco2 cells (15,000 cells/well) and assessed for their cytotoxic effects. The NTC was applied as an volume equivalent. Scale bar indicated 200 µm.

3.2.1.2 Non-hemolytic Enterotoxin

In comparison to Hbl, Nhe is known to multimerize in a more defined manner as compared to Hbl. Prior work suggested that a defined molar ratio of 10:10:1 for the individual subunits A:B:C resulted in the highest functional activity[121]. Therefore, Nhe was chosen to assess the possibility to synthesize a multimeric toxin with defined prerequisites. Adding each subunit individually to a cell-free synthesis as well as adding all three subunits together in a molar plasmid ratio of 10:10:1 and 1:1:1 resulted in defined protein bands for each individual subunits visualized by autoradiography (Figure 13 A). Hemolytic activity on 5% sheep blood agar plates could be detected for the tripartite enterotoxin synthesized in a 10:10:1 molar plasmid ratio, but not when synthesized in a 1:1:1 ratio. As Hbl was active after co-expression of all three subunits and when mixing the subunits together after their individual syntheses, the same was tested for Nhe. Both ratios, 10:10:1 as well as 1:1:1, showed a spot on the 5% sheep blood agar plate, but no intense hemolytic activity could be detected (Figure 13 B, uncropped blood agar plates Supplementary Figure 5 A). Single subunits did not show hemolytic activity neither

(Supplementary Figure 5 B). When further plasmid ratios were tested, it could be shown that NheA and NheB had to be synthesized in excess over NheC to be functionally active. As soon as Nhe was synthesized in a molar plasmid ratio of 10:10:2.1 [A:B:C] the tripartite complex did not display hemolytic activity anymore (Supplementary Figure 6, Ramm *et al.,* 2020). Thus, all latter syntheses were conducted in a molar plasmid ratio of 10:10:1 [A:B:C].

The detection of proteins is the foundation for scientific research and development in protein characterization. Not all laboratories offer isotopic labelling facilities, thus fluorescent labels had to be validated as an alternative. As CFPS is an open system, statistical labelling with a fluorescently labelled dye was evaluated for Nhe. Bodipy-TMR-Lysine was added to the cell-free synthesis of Nhe. Two intensely labelled protein bands, corresponding to NheA and NheB, could be detected by in-gel fluorescence whilst no detectable protein bands could be visualized for non-labelled Nhe or the labelled and unlabelled NTC. Moreover, the fluorescently labelled tripartite enterotoxin was still hemolytic active on a 5% sheep blood agar plate (Figure 13 C, uncropped blood agar plate Supplementary Figure 5 C). These data indicate the multimerization of the labelled tripartite Nhe toxin.

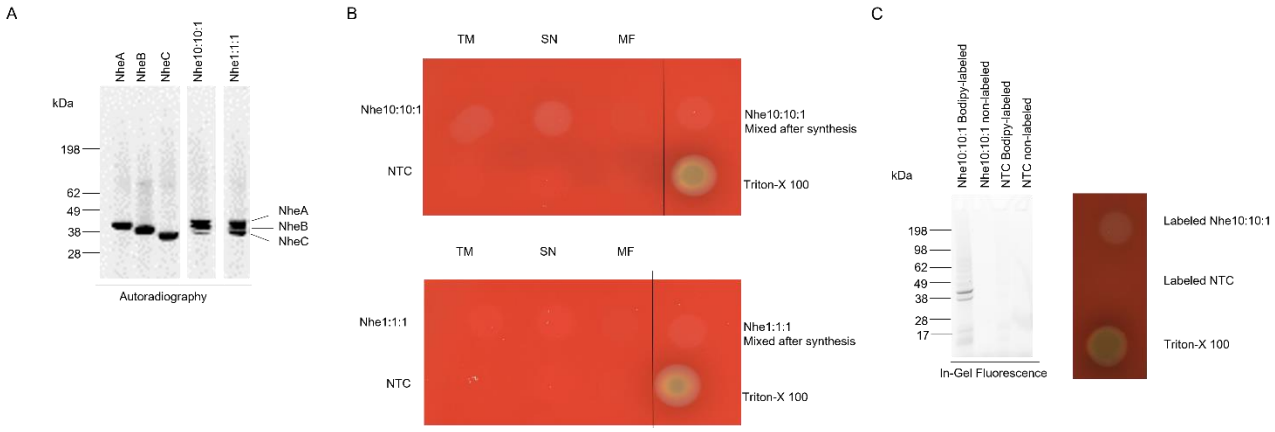

Figure 13: Establishing CFPS for Nhe.

Nhe subunits A, B and C were synthesized in CHO lysate either separately or were co-expressed to form the tripartite toxin using molar plasmid concentrations of 10:10:1 and 1:1:1 ratios. (A) Autoradiograph showing ^{14}C-leucine labelled Nhe subunits and Nhe tripartite toxin when synthesized using molar plasmid concentrations of 10:10:1 and 1:1:1 ratios. (B) Hemolytic activity of the Nhe tripartite toxins was assessed on 5% sheep blood agar plates in TM, SN, MF fractions. (C) Bodipy-labelled Nhe toxin was assessed by in-gel fluorescence and functional activity was assessed by 5% sheep blood agar plates. Figure modified from Ramm *et al.*, 2020.

In order to show that CFPS can produce toxins that can be used for diagnostic applications, the hemolytic activity on 5% sheep blood agar plates of cell-free synthesized Nhe was compared to Nhe expressed in *B. cereus*. These data showed that a

concentration of 10 µg/mL of cell-free synthesized Nhe resulted in a similar lytic zone as about 7 µL of culture supernatant (Supplementary Figure 7). Furthermore, a standardized technique to verify *B. cereus* strains containing Nhe, is the Duopath lateral flow assay. A detection of the cell-free synthesized Nhe subunits was successful (Ramm *et al.*, 2020).

The data acquired to this point showed the lytic character of Nhe, but in native surroundings *B. cereus* pores target cells within the gastro-intestinal tract[119]. In order to assess the targeting of cells and the stability of the pore, the MTT viability assay and planar lipid bilayer recordings were performed. A serial dilution of Nhe was subjected to the human colorectal cancer cell line Caco2. The tripartite Nhe synthesized in a batch and CECF manner showed an increasing cytotoxic effect with an increasing Nhe concentration. In initial experiments a concentration range from 0.01 nM to 0.1 nM did not induce stable cytotoxic activity by Nhe synthesized in both batch and CECF format. At a concentration of 0.09 nM first cytotoxic effects were suspected (Figure 14 A and B for batch and CECF format, respectively). Further experiments exposing Caco2 cells to Nhe at a concentration range from 0.1 to 1 nM showed a reduced cell viability in both reaction formats. Non-viable cells could be measured at 0.7 nM and 0.6 nM for Nhe synthesized in a batch and CECF manner, respectively (Figure 14 C and D). Using the second data set measuring the cytotoxicity between 0.1 and 1 nM, the IC_{50} was determined using a non-linear regression stating the value at which Nhe inhibited 50% of the biological processes in the assay. Nhe synthesized in a CECF format resulted in an IC_{50} value of 0.32 nM whilst Nhe from a batch-formatted synthesis resulted in a value of 0.48 nM. As the regression for the batch-based synthesis resulted in a correlation coefficient of 0.93, a second calculation starting at 0.3 nM resulted in a correlation coefficient of 0.98 and an IC_{50} value of 0.46 nM (Supplementary Figure 8). This indicated that the baseline value at which a toxic measurement started was 0.3 nM when Nhe from a batch synthesis was administered. Nonetheless, Nhe derived from a CECF synthesis resulted in a lower IC_{50} value suggesting a higher toxicity.

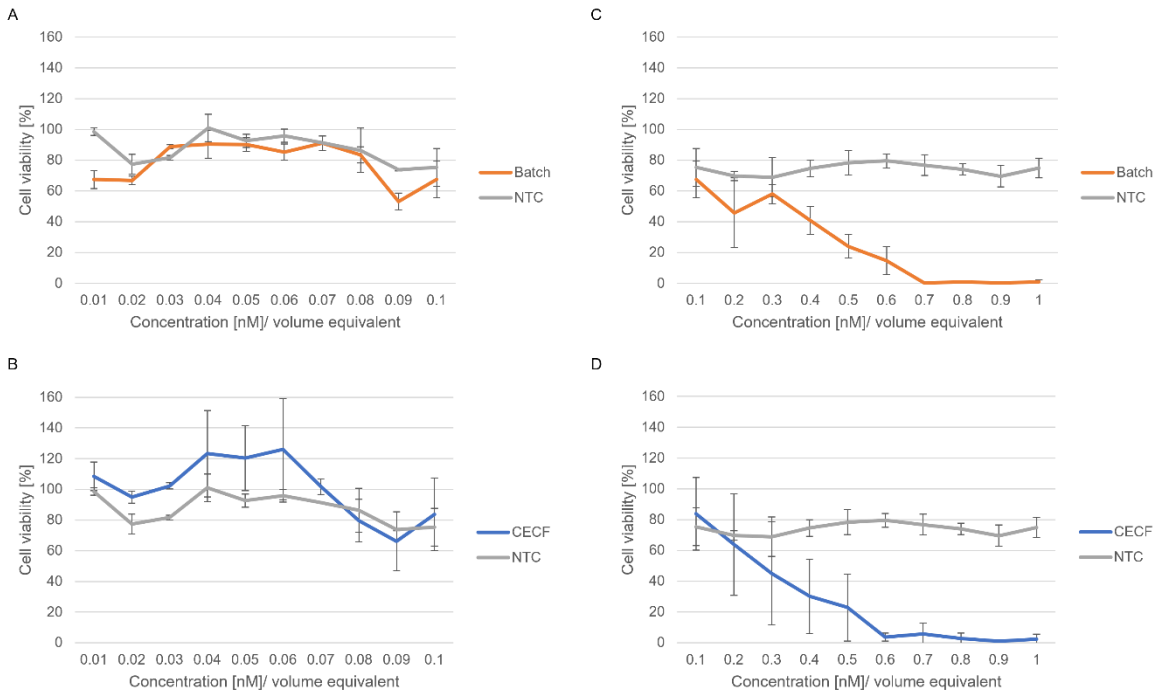

Figure 14: MTT cytotoxicty induced by Nhe.
The Nhe tripartite toxin was synthesized in batch (A, C) and CECF mode. (B, D) An NTC was used as a negative control and used as a volume equivalent. A serial dilution of Nhe ranging from 0.01 to 0.1 nM (A, B) and a second serial dilution ranging from 0.1 to 1 nM (C, D) were tested for both synthesis modes. Standard deviations were calculated from triplicate samples of three independent experiments. Figure modified from Ramm *et al.,* 2020.

The pore-forming character and the stability of the pore were assessed by planar lipid bilayer electrophysiological recordings. A stable current could be detected resembling the open state of the pore when a recorded trace was magnified. The all-time histogram of the representative trace showed a broad single peak that corresponds to the single current activity of almost 880 pA (Figure 15 A). PolyPEG1500 was added to the recording in order to certify the stability of the pore and allow for single channel activity blockings. A baseline level decrease from 880 pA to 690 pA was detected after the application of PolyPEG. Transitions of the single channel activity between the two current levels of 630 and 690 pA were seen. A histogram of the representative current trace depicted two peaks with a similar intensity that correspond to the two current levels (Figure 15 B). These data showed that Nhe synthesized in a cell-free manner forms a stable characteristic pore with lytic and cytotoxic activity.

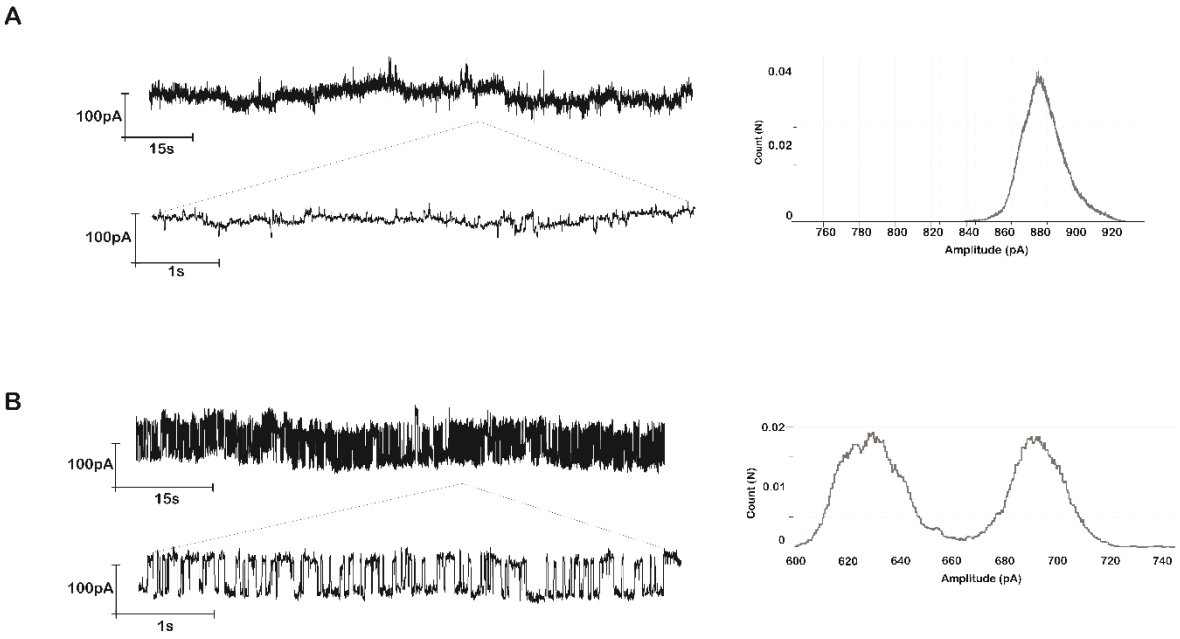

Figure 15: Planar lipid bilayer recordings of Nhe.

Nhe subunits A, B and C were synthesized in a CHO lysate at a molar plasmid ratio of 10:10:1 and applied for planar lipid bilayer recordings using the Orbit 16. Recording buffer composition was 10 mM HEPES and 1 M KCl at a pH of 7.45. The planar lipid bilayer was formed from 10 mg/mL DPhPC: cholesterol (90:10) in octane. (A) Continuous recordings of current response at +60mV in the presence of Nhe10:10:1. Magnification of a small portion of the pore current. Histogram of the current response measured at +60mV. (B) Continuous recordings of Nhe10:10:1 and its current response in the presence of PEG 1500 at +60mV. Magnification of a small portion of the response. Histogram of the current response measured at +60mV. Figure modified from Ramm *et al.,* 2020.

The data on the Nhe tripartite enterotoxin presented here resulted in a publication accepted in 2020[79]. Taken together, the data on Hbl and Nhe showed that hetero-multimeric toxins can be synthesized in a cell-free manner while maintaining their functional activity. Hence, enabling the further characterization of the toxin's cytotoxic mechanism of action.

3.2.2 Nanopore identification

In comparison to the tripartite toxins Nhe and Hbl, the mono-heptameric CytK from *B. cereus* is a classical beta-barrel PFT[137]. Such classical PFTs form stable pores that are of interest for nanopore applications[130]. Because of its similarity to aHL[136], which is the best studied biological nanopore[133], CytK might be a potential candidate for a nanopore development. Hence, the cell-free synthesis of CytK was established and the potential for a nanopore application was identified. Initial syntheses were performed in a CHO-based cell-free system using standard conditions (3 h synthesis at 30°C). The determination of the total protein yield after liquid scintillation counting showed that a high amount of protein could be detected in the microsomal vesicles (Figure 16 A), indicating an insertion

of CytK into the microsomes. Interestingly, this embedding of CytK into the microsomal vesicles was possible without a prior signal peptide used for directed translational processes. Autoradiography depicted the monomeric protein band for CytK1 and CytK2 and showed clotted high molecular weight bands (Figure 16 B). These data indicated the presence of SDS-stable multimers. The functional activity as assessed by the hemolytic activity on 5% sheep blood agar plates demonstrated lytic activity for both CytK variants (Figure 16 C). Hemolytic assessment of each individual fraction showed that all fractions (TM, SN and MF) were functionally active (Supplementary Figure 9).

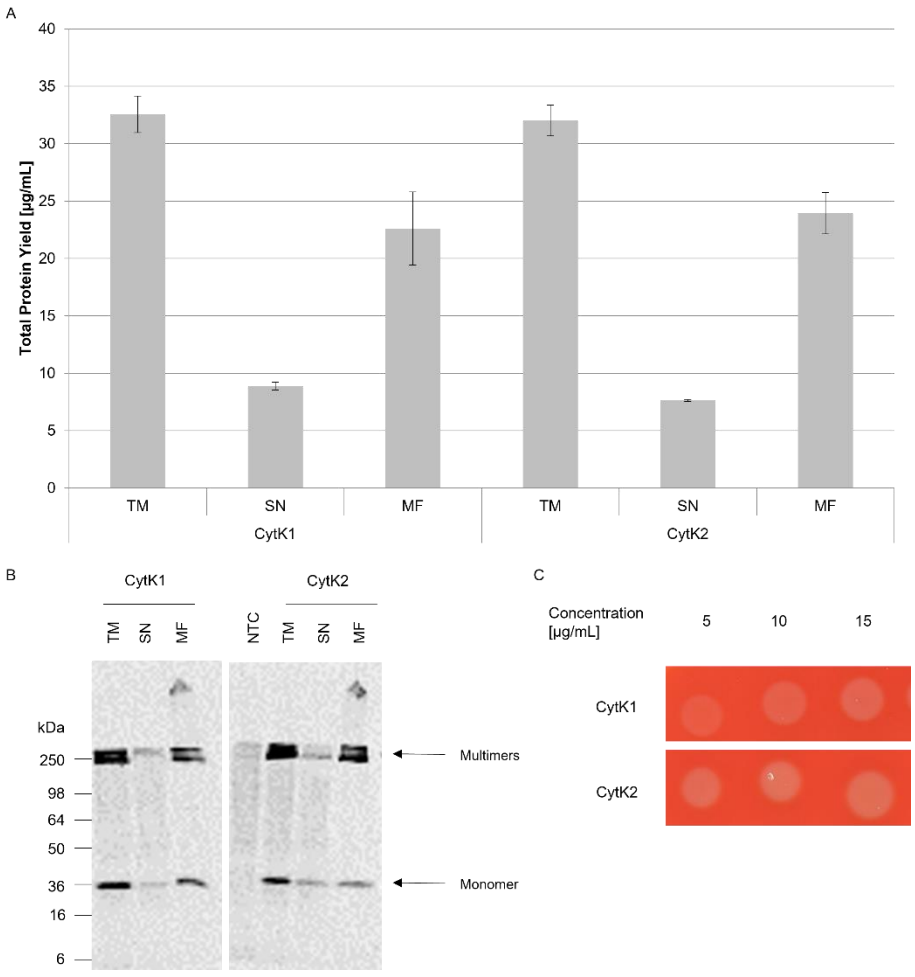

Figure 16: Cell-free synthesis of CytK.
CytK1 and CytK2 were synthesized in CHO lysate. After the synthesis the crude translation mixture (TM) was fractionated into the soluble components in the supernatant (SN) and the microsomal fraction (MF). (A) Quantitative analysis of CytK1 and CytK2 was performed by liquid scintillation counting. Standard deviations were calculated from triplicate analysis. (B) Autoradiograph showing ^{14}C-leucine labelled CytK 1 and CytK2. A no template control (NTC) was used as a negative control. Hemolytic activity of the TM of CytK1 and 2 was assessed on 5% sheep blood agar plates.

After synthesis optimizations such as template concentrations and temperature variations (data not shown), the functionality of CytK in planar lipid bilayer measurements was

assessed as a stable ion current is the basis for a nanopore. A pore insertion could be detected by current jumps from the baseline (0 pA). As representatively shown for CytK1, the pore inserted into the lipid bilayer and a stepwise insertion of multiple pores was possible as shown by the voltage clamp and by the all-time histogram of a selected trace (Figure 17). Initial pore insertions could generally be seen at -20 to -30 pA. Over a short period of time, as an example shown for 2 min (Figure 17 A), current jumps to around -80, -100, -115, -125 and -160 pA could be detected for the depicted trace.

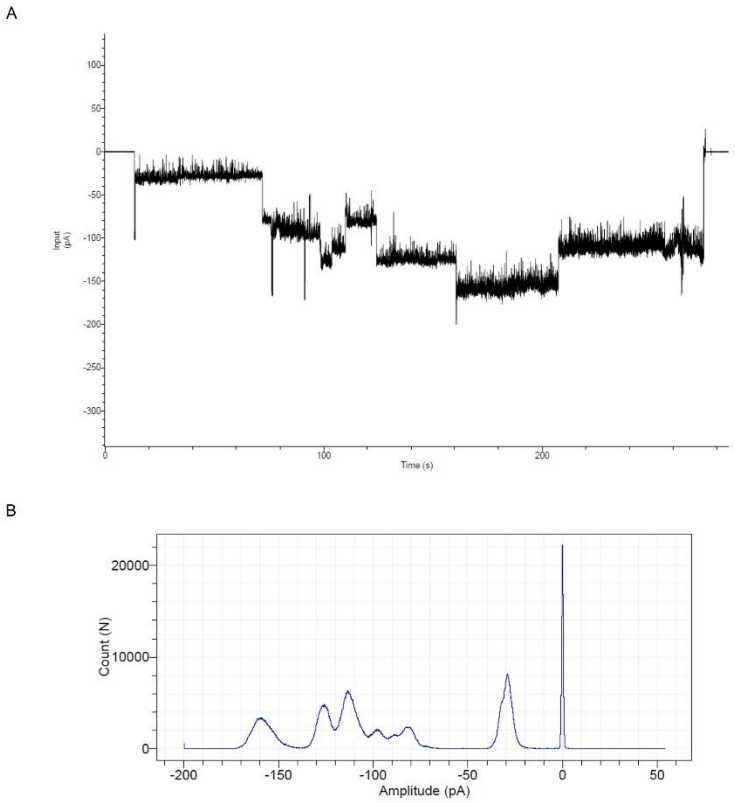

Figure 17: Pore-forming character of CytK1.
CytK1 was synthesized in a CHO cell-free system and the MF was applied for planar lipid bilayer recordings. Recording buffer composition was 10 mM HEPES and 1 M KCl at a pH of 7.45. The planar lipid bilayer was formed from 10 mg/mL DPhPC in octane. (A) Continuous recordings of current response at -20 mV in the presence of CytK1. (B) All-time histogram identifying multiple pore insertions.

CytK2 showed a similar response patterns. The trace as well as the all-time histogram indicated various current jumps as already seen for CytK1. A representative trace of 2 min shows current jumps of about -50, -90, -140, and -190 pA (Figure 18). These current jumps also indicated multiple pore insertions.

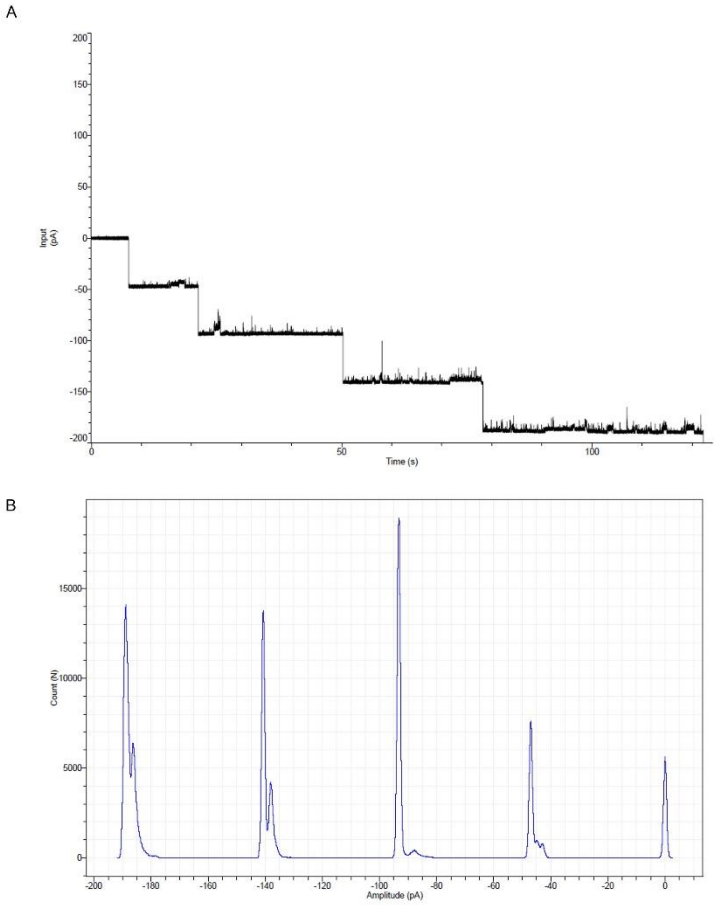

Figure 18: Pore-forming character of CytK2.
CytK2 was synthesized in a CHO cell-free system and the MF was tested in planar lipid bilayer recordings. Recording buffer consisted of 10 mM HEPES and 1 M KCl at a pH of 7.45. The planar lipid bilayer was formed from 10 mg/mL DPhPC in octane. (A) Continuous recordings of current response at -20 mV in the presence of CytK2. (B) Respective all-time histogram identifying multiple pore insertions.

Thus, these data indicated that CytK1 and CytK2 formed stable pores which could be analyzed using lipid bilayer techniques and suggested a potential nanopore development. Danny Kaser continued the work on CytK during a research internship and a subsequent master thesis. Based on his data optimized CHO and *Sf*21 systems were available for the synthesis of functionally active CytK, the pH sensitivity and cell-based toxicity could be assessed and the visualization of the individual multimers which allowed for a possible identification of mono-, tri-, penta- and heptamers was addressed[204]. Relying on these data, five CytK1 and CytK2 mutants were designed. These mutants were designed based on sequence similarities to aHL and potential sequence patterns that are involved in the multimerization of CytK. The mutations in CytK1 and CytK2 induced the same changes in order to allow for a direct comparison of CytK1 and CytK2 (Supplementary Table 1). The stability of a pore after mutation indicates whether a pore is suitable for a nanopore development. Based on initial experiments from Danny Kaser[205], I analyzed and categorized the synthesis and activity of the mutants (Table 11).

Table 11: CytK mutant behaviour.

Mutant	Characteristics of CFPS	Hemolytic activity	Multimerization	Electrophysiology
CytK1-A196P	Similar to CytK1	Yes	Similar to CytK1	Changed blocking
CytK1-Q13S	Similar to CytK1	Yes	Similar to CytK1	Changed blocking
CytK1-D191del	Reduced MF ratio	Reduced	Loss of 2 bands	Changed blocking
CytK1-I91F	Similar to CytK1	Yes	Similar to CytK1	Changed blocking
CytK1-I91G	Similar to CytK1	Yes	Loss of 2 bands	No blocking
CytK2-S196P	Similar to CytK2	Yes	Similar to CytK2	Changed blocking
CytK2-Q13S	Similar to CytK2	Yes	Similar to CytK2	Changed blocking
CytK2-D191del	Reduced MF ratio	No	Loss of 3 bands	Not measurable
CytK2-V91F	Similar to CytK2	Yes	Loss of 2 bands	Changed blocking
CytK2-V91G	Reduced MF ratio	No	Loss of 3 bands	Not measurable

These data showed that CytK1 was a more promising candidate for an application as a nanopore as it appeared to be more stable. In order to assess the ability of a nanopore application of CytK1, further electrophysiological analyses were performed on CytK1 and its mutants. The in depth analysis of CytK1 WT and CytK1 mutant proteins was performed using electrophysiological measurements. As a first step, the insertion of the pore into the planar lipid bilayer as well as the characteristic pore-like behavior was assessed. Similar to the CytK1 WT protein multiple pore insertions could be detected. Especially CytK1-A196P and CytK1-Q13S showed a similar pattern to the CytK1 WT protein (Figure 19).

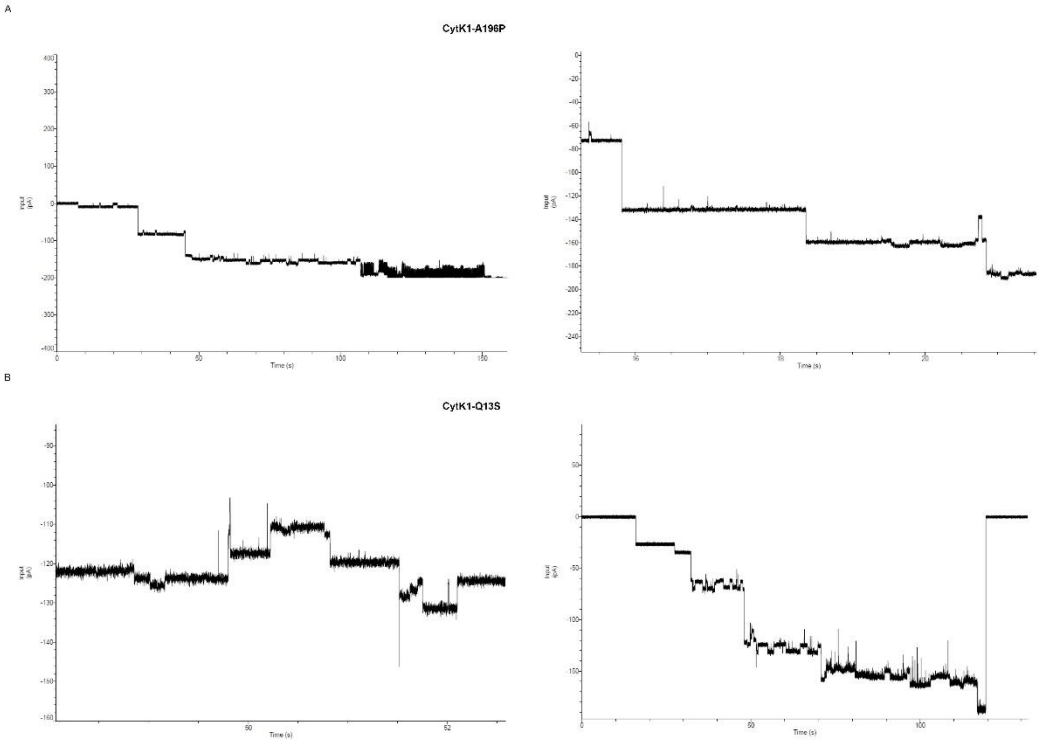

Figure 19: Pore-forming character of CytK1-A196P and CytK1-Q13S.
CytK1-A196P (A) and CytK1-Q13S (B) were synthesized in a CHO cell-free system and the MF was applied for planar lipid bilayer recordings using the Orbit mini. Recording buffer composition was 10 mM HEPES and 1 M KCl at a pH of 7.45. The planar lipid bilayer was formed from 10 mg/mL DPhPC in octane. Continuous recordings of current response at -20 mV.

The pore insertion into the planar lipid bilayer was less frequent in CytK1-D191del and CytK1-I91G and bilayer ruptures occurred more frequently. Hence, more measurements were needed to assess the same number of bilayers. The other three mutants were stable in the recordings. Even though the insertion rate was less frequent for these two mutants, CytK1-D191del also demonstrated a characteristic pore behaviour as shown by opening and closing of the pore (Figure 20 A). The CytK1-I91G mutant could also insert into the bilayer. Before a stable insertion of the pore was possible, an instable current response could be detected (Figure 20 B).

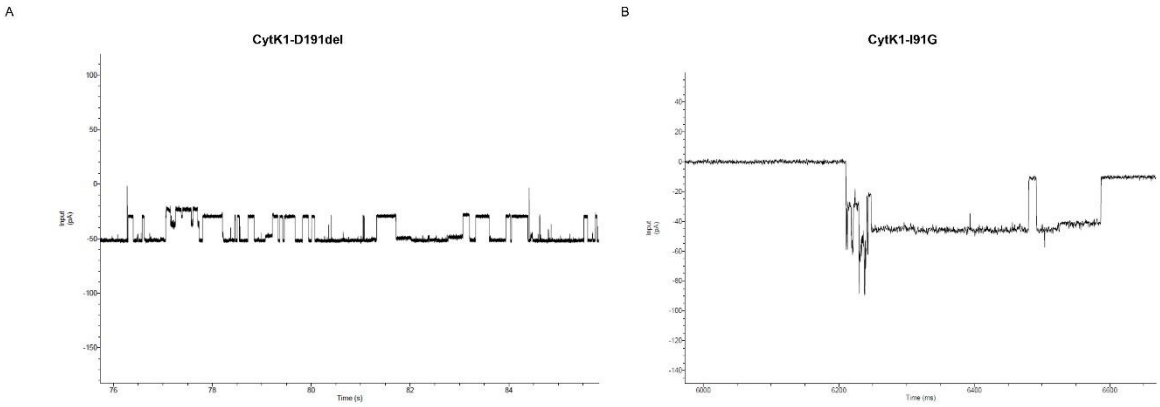

Figure 20: Pore-forming character of CytK1-D191del and CytK1-I91G.
CytK1-D191del (A) and CytK1-I91G (B) were synthesized in a CHO cell-free system and the MF was applied for planar lipid bilayer recordings using the Orbit mini. Recording buffer consisted of 10 mM HEPES and 1 M KCl at a pH of 7.45. The planar lipid bilayer was formed from 10 mg/mL DPhPC in octane. Continuous recordings of the current response at -20 mV. (A) Pore-like behaviour of CytK1-D191del. (B) Pore insertion into the planar lipid bilayer of CytK1-I91G.

In order to precisely analyze the individual mutants and to detect changes in their conductivity, a python script was developed. The script used data from 10 different planar lipid bilayer measurements for each individual protein. It calculated the mean conductivity of a single pore in comparison to a reference value and iterated the values of multiple pore insertions. Two different reference values were chosen. A value of 1000 pS was determined as a first value as the initial data gathered on CytK1 depicted mean conductivity values of 1000 pS. A second value of 627 pS was based on a literature value where CytK measured in NaCl buffer[137]. These calculated conductivity values were used to assess the pore radius based on prior calculations of Hardy *et al*[137]. As depicted in Table 12, the point mutations changed the characteristics of the pore and widened the radius.

Table 12: Conductivity and calculated pore radius of CytK1 WT and mutants.

Mutant	**Reference value 1000 pS**		**Reference value 627 pS**	
	Mean conductivity [pS]	Pore radius [Å]	Mean conductivity [pS]	Pore radius [Å]
CytK1 WT	691.05 ± 70.99	4.56	696.12 ± 37.81	4.58
CytK1-A196P	772.84 ± 64.90	4.82	786.35 ± 58.04	4.86
CytK1-Q13S	760.08 ± 91.46	4.78	713.52 ± 63.98	4.63
CytK1-D191del	1133.30 ± 87.86	5.84	1016.90 ± 66.16	5.53
CytK1-I91F	1116.91 ± 70.66	5.78	679.45 ± 49.37	4.52
CytK1-I91G	1075.99 ± 84.88	5.69	780.57 ± 36.96	4.85

CytK was still stable and presented a pore-forming character after different mutations. Using 1000 pS as a reference value, all mutants showed a widened pore radius in comparison to the wildtype. CytK1-A196P and CytK1-Q13S only showed small changes while the other three induced widenings of more than 1 Å. Looking at the radii determined based on the 627 pS reference value, mutant I91F reflected a similar radius to the wildtype protein, while the other mutants appeared to be slightly enlarged. The CytK1-D191del mutant showed the largest pore widening. The conductivity values of mutants I91F and I91G generally depicted large differences when applying the different reference values. This could hint at the biased python script based on the reference value used for the mathematical calculation which should be further optimized in future modifications of the analytical tool. This could also help to further reduce the high standard deviations. Nonetheless, these data identified CytK1 as potential candidate for a nanopore development based on its stable pore-forming character. This shows the successful establishment of using CFPS for the synthesis, characterization and modification of pore-forming proteins.

3.2.3 AB_5 toxins as tracking systems

Another class of bacterial toxins are AB_5 toxins. The characteristic structure of AB_5 toxins allows for bioengineering of the individual subunits for versatile purposes. The A subunit can be modified in order to silence the toxic effect, whilst the B subunit can be modified to shuttle a molecule into the cell. This thesis focused on the modification of the two model proteins Ctx and LT The reproducible synthesis of the individual subunits and their co-expression was established. Subsequently, the combined work of me and Jack 2020[206] showed that the complete holotoxins, meaning the complete AB_5 constructs, were more functional when both the reaction buffers as well as the cell disruption and reconditioning buffer for lysate preparation did not contain any traces of DTT. When traces of DTT were present, the AB_5 toxin was less active. First apoptotic effects could be detected at 4 nM when Ctx was added while 5 nM led to complete cell death (Supplementary Figure 10). Additionally, concentration ranges in a cell-based toxicity assessment showed that after 24 h of incubation LT induced morphological changes which were represented by elongated CHO-K1 target cells. After 48 h LT induced complete cell death at 6 nM. We could further show that only the co-expressed A and B subunits induced apoptotic effects while a mixture of pre-synthesized single subunits did not induce any effects (Supplementary Figure 11).

In parallel, it was assessed whether the holotoxin formation was detectable by autoradiography. The single subunits as well as the co-expressed subunits were run on SDS-PAGEs either after acetone precipitation or without the degradation process.

Acetone precipitated samples were loaded onto the gels either in the presence or in the absence of DTT. Autoradiography confirmed all individual subunits but no holotoxin formation could be detected after a synthesis in CHO (Figure 21) and *Sf*21 lysate (Supplementary Figure 12). Some multimerization patterns could still be detected as for CtxB (Figure 21 A).

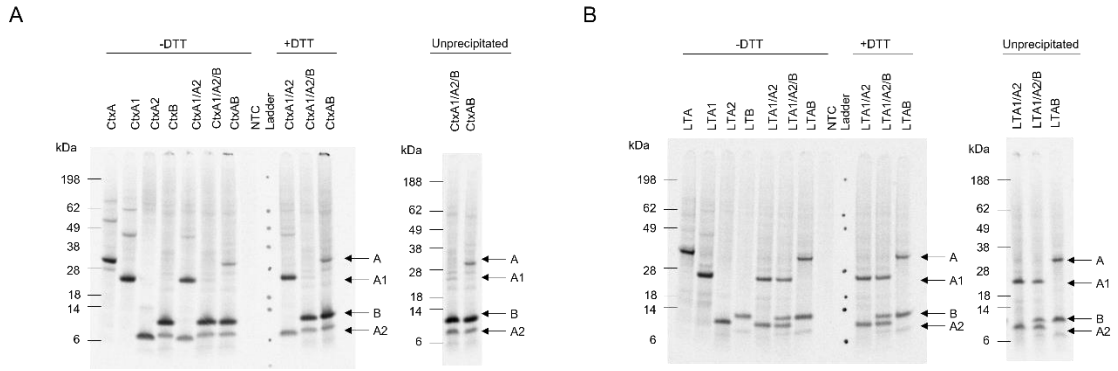

Figure 21: Holotoxin formation of Ctx and LT in CHO lysate.
Single subunits and co-expressed subunits of Ctx (A) and LT (B) were synthesized in a lysate. Autoradiographs depicting the ^{14}C-labelled protein bands after a synthesis. A no template control (NTC) was used as a negative control. Figure modified from Ramm *et al.,* 2022.

The pentameric ring of AB_5 toxins is formed by stable non-covalent binding. Only minor multimerization of the B subunits could be detected and optimizations were attempted. Prior studies have shown that the multimerization is more likely to occur at higher concentrations of 35 µM and low pH values[207]. Hence, CtxB and LTB were loaded onto the SDS-PAGE at a final concentration of 35 µM. Further, the pH value of the TT mix of the reaction as well as changing the pH of the CHAPS/PBS used for reconstituting the AB_5 toxins from the microsomal vesicles was changed. At last, a repetitive synthesis was performed for Ctx and the microsomal vesicles were enriched in 6 steps. In the first step the template for CtxA was added, while in the next 5 steps the CtxB template was added. None of the optimizations led to additional multimerization patterns (data not shown).
Overall, the data on the cell-free synthesis of Ctx and LT gathered here and by Jack 2020[206] as well as the data on complex formation acquired in this work demonstrated that we were able to successfully synthesize individual subunits and co-express the subunits of Ctx and LT using eukaryotic cell-free systems. Multimerization of individual subunits indicated that the assembly of the AB_5 toxin structure was possible. This was further confirmed as the toxins were functionally active. These data thus validated a reproducible synthesis of these multimeric complexes and led to the modification of individual subunits.

3.2.3.1 Modification of LTB

As a first modification step, the B subunit of LT was altered. A fusion construct of LTB and Streptavidin (Strep) was designed. In order to assess whether the synthesis of the modified protein was altered, LTB-Strep was synthesized in comparison to LTB alone in both CHO and *Sf*21 lysate. Both constructs harbored a Mel signal peptide facilitating co-translational translocation and PTMs which allowed for the analysis of translocated soluble proteins within the microsomal vesicles. While the CHO-based system generally resulted in higher total protein yields, the LTB-Strep fusion protein demonstrated higher total protein yields in comparison to LTB alone (Figure 22 A). In the CHO system, 5.3% of the total protein yield of LTB and 4.9% of LTB-Strep were translocated and could be released from the vesicles (SN2 protein yield). 6.1% and 5.9% could be retrieved for LTB and LTB-Strep, respectively, after a synthesis in *Sf*21 lysate. As AB_5 toxins form complexes that are formed in the presence of disulfide bridges[147], the following experiments relied on the translocation efficiency of the cell-free system. Therefore, the *Sf*21 lysate was chosen for further experiments with LT constructs.

Subsequently, an Atto 488-Biotin conjugated fluorophore was incubated with the different LT subunits. All single subunits and co-expressed LTAB, as well as co-expressed LTAB-Strep and a Strep molecule alone were labelled with the fluorophore. Only Strep alone and LTB-Strep containing samples were expected to be coupled to the fluorophore. The in-gel fluorescence showed undefined fluorescent signals in lower molecular weights that over-shadowed signals up to 38 kDa. Nonetheless, defined high molecular weight bands could be detected for Strep, LTB-Strep and LTAB-Strep, which might suggest a multimerization of the Strep molecules. Autoradiography confirmed these protein bands and additionally detected lower molecular weight bands (Figure 22 B). These data indicated a protein specific labelling with the biotin conjugated fluorophore and confirmed the multimerization of the Strep-molecule.

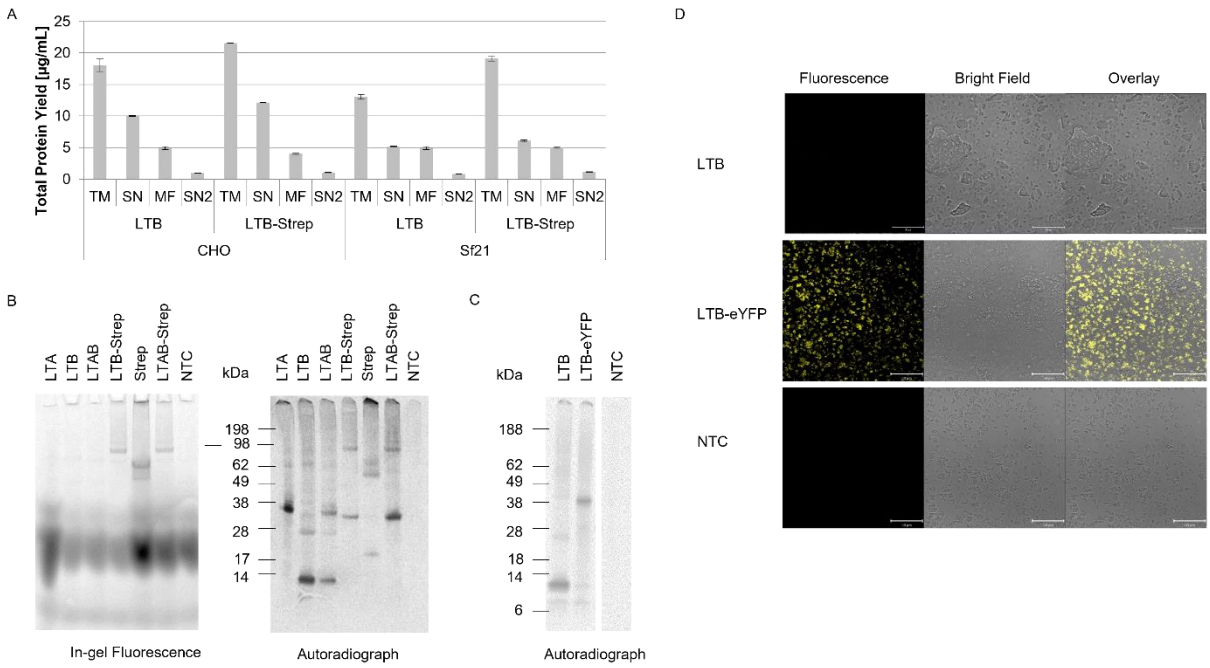

Figure 22: LTB modification.

(A) Determination of total protein yields for LTB and LTB-strep after a synthesis in a CHO and *Sf*21 lysate. Total protein yields of *de novo* synthesized protein were analyzed by liquid scintillation for translation mixture (TM), the first supernatant (SN), the microsomal fraction (MF) and the translocated soluble protein in the second supernatant (SN2). Standard deviations were calculated from triplicate analysis. (B) LTA, LTB, LTAB, LTB-Strep, Strep, LTAB-Strep and the no template control (NTC) were synthesized in the *Sf*21 system and the SN2 fraction was fluorescently labelled with an Atto 488-Biotin dye. In-gel fluorescence showing the Atto 488 labelled protein bands and autoradiograph depicting the ^{14}C-labelled bands. (C) Autoradiograph depicting the ^{14}C-labelled proteins after the ^{3}rd round of synthesis in *Sf*21 lysate for LTB, LTB-eYFP and the NTC. (D) CLSM images for LTB, LTB-eYFP and the NTC after three rounds of synthesis in *Sf*21 lysate. Figure modified from Ramm *et al.,* 2022.

A second fusion protein was used in order to further visualize the co-translational translocation of the protein. LTB fused to the fluorescent protein eYFP was synthesized in a repetitive synthesis reaction mode in order to enhance the translocation efficiency of LTB and LTB-eYFP. After three syntheses the autoradiograph showed specific protein bands for the respective proteins but not the NTC (Figure 22 C). Using CLSM the microsomal vesicles were visualized. The fluorescence signal of the LTB-eYFP fusion protein in comparison to the NTC and LTB WT protein clearly showed a strong difference in the fluorescence of the microsomal vesicles (Figure 22 D). Hence, a clear translocation of the LTB-eYFP into the microsomes was detected.

The B subunit of AB_5 toxins is the binding domain of the complex, thus a modification of this domain might be used for the development of Trojan horse systems. The modified LTB-Strep fusion protein might not only be coupled to the biotinylated fluorophore, but to toxic moieties that are linked to biotin. Therefore, the functional activity of the LTB-Strep

protein was investigated. LTB or LTB-Strep were co-expressed with LTA and added to CHO-K1 target cells at a concentration of 5 nM. These data showed that at a concentration of 5 nM of the LTAB multimer induced minor apoptotic effects after 48 h. As larger cultivation areas and thus higher cell densities were used, the cytotoxic effect of the LT complex was not as intense as seen for LTAB in prior studies[206].The LTAB-Strep complex did not show any apoptotic cells, but CHO-K1 cells were less confluent. Single subunits as well as Strep alone did not induce morphological changes (Figure 23). These data suggest that the modification of the B subunit led to a reduced functionality. It was further attempted to quantify these effects of the individual subunits and the multimers. The CellTox CyGreen assay was used which measures the cytotoxicity based on the binding of nucleic acids after cells are apoptotic. High RLU demonstrate strong toxic effects. High values were detected for the co-expressed LTAB multimer but not the mixed LTA+B multimer. Strikingly, the LTB-Strep sample depicted high fluorescence values as well (Supplementary Figure 13). Visual determination of cells showed that no morphological changes could be detected after the supplementation of LTB-Strep alone (Ramm *et al.,* 2022). This indicated that the high RLU might correspond to background noise from the *Sf*21 lysate, similar to the PI uptake assay performed for Hbl.

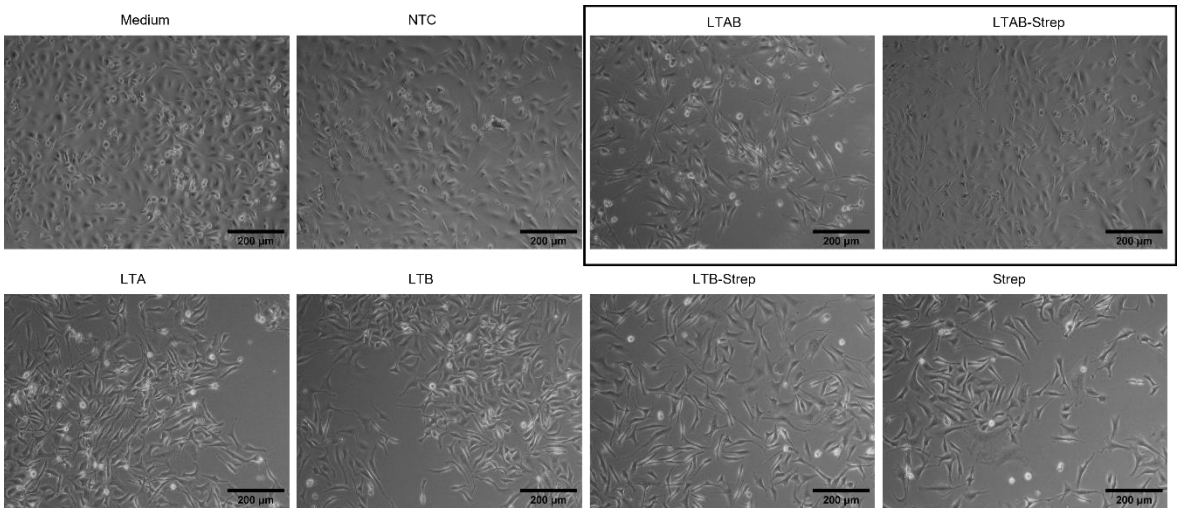

Figure 23: CHO-K1 cells exposed to LTB-Strep variants.
Co-expressed LTAB and LTAB-Strep as well as single subunits were synthesized in *Sf*21 lysate and supplemented to CHO-K1 cells (25,000 cells/well) at 5 nM in a 24-well plate. Phase contrast photographs were taken after 48 h of incubation. Scale bar indicated 200 µm.

Taken together, the LTB-Strep fusion protein could be synthesized in an efficient manner using CFPS while being co-translationally translocated. The functional activity of the LTAB-Strep complex was not as effective as the LTAB complex, suggesting optimization procedures. Nonetheless, it could be shown that LTB fusion proteins could be used to fluorescently label the protein.

3.2.3.2 Modification of CtxA

As a final step in modifying AB_5 toxins, a mutational analysis of the catalytic A subunit was performed. Two mutants of CtxA were designed and the glutamic acid codon at either position 110 or 112 was exchanged for the amber stop codon. These constructs were termed CtxAambE110 and CtxAambE112. The amber stop codon was inserted as diverse ncAAs can be inserted at the desired position. Subsequently, these ncAAs can be addressed for site-specific labelling of the protein. As positions 110 and 112 are within the active center of the A subunit[208], the toxic effect was expected to be silenced. Using a silenced CtxA protein, such labelling techniques would allow for tracking studies within the cell. The proof-of-concept for the incorporation of the ncAAs AzF and pPa into the CtxA subunit was performed in two eukaryotic lysates. The incorporation efficiency was not yet sufficient and therefore the reaction parameters were optimized in both CHO and *Sf*21 based reactions. Different concentrations of orthogonal components were tested using the CtxAambE110 construct. The incorporation efficiency in the CHO system was optimized when using 0.5 µM eAzFRS when incorporating pPa, while the addition of 2.5 µM orthogonal tRNA led to the best incorporation efficiency in an *Sf*21 system when using the ncAA AzF (Figure 24 A and B, respectively). The incorporation efficiency was determined by the presence of a full-length protein band and only a minor termination product.

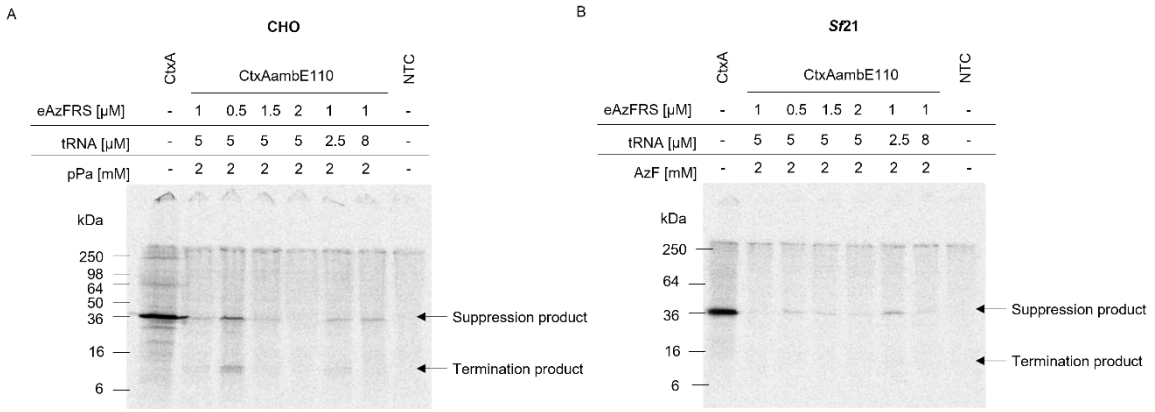

Figure 24: Optimization of the orthogonal system for CtxA.
Optimization of the incorporation of ncAAs to CtxAambE110 using cell-free orthogonal systems. Autoradiograph of ^{14}C-labelled protein bands after the synthesis optimization in (A) CHO and (B) *Sf*21 lysate.

Next, the co-expression of the mutated CtxA fragment with the CtxB fragment was tested in both eukaryotic systems, but neither the in-gel fluorescence nor the autoradiograph depicted any full-length proteins (Supplementary Figure 14). The supplementation of the PCR templates for both CtxA and CtxB as well as the components for the orthogonal system was necessary for the cell-free synthesis reaction. This led to a reduced amount of each individual PCR template within the reaction mixture which might have led to insufficient protein concentrations. A novel CHO lysate with an integrated aminoacyl-tRNA

synthetase eAzFRS[197] was used, which eliminated the need for supplementation of the synthetase. Fluorescently labelled protein bands for the CtxA mutants were detected when orthogonal tRNA and a ncAA was added. No fluorescently labelled band could be detected when one component was missing. This was demonstrated for both mutated constructs (CtxAambE110 and CtxAambE112) when the ncAA AzF was incorporated and the proteins were subsequently labelled with DyLight-632 phosphine by Staudinger ligation (Figure 25 A). Constructs that incorporated pPa were subsequently labelled in a copper-catalyzed click reaction. Labelled CtxA subunits were detected (Supplementary Figure 15). Copper-catalyzed click reactions might be disadvantageous in cell-based assays, as copper might harm the cells[209]. Therefore, the incorporation of AzF was further applied. The in-gel fluorescence of both modified CtxA mutants when co-expressed with CtxB in the presence of AzF showed intensely labelled protein bands. No fluorescence signal was detected when AzF was missing from synthesis and when the control reactions of wild type CtxA or the NTC were labelled. The respective autoradiograph depicted intense protein bands for the CtxA wild type. The CtxA full-length protein based on the CtxAambE110 construct showed an intense full-length protein band. The CtxAambE112 construct only presented a minor full-length band in the presence of AzF. The termination products were not detectable as they were about the same size as the CtxB monomer (Figure 25 B).

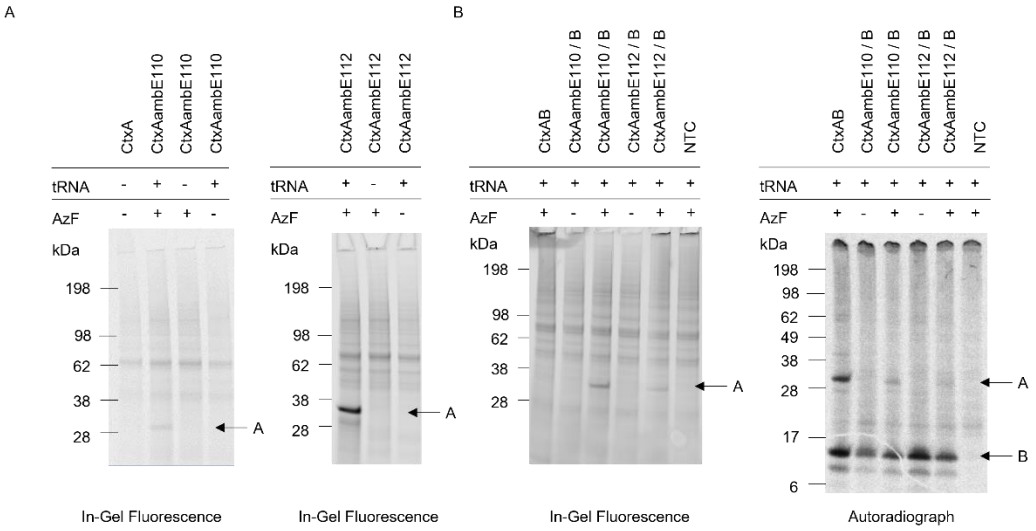

Figure 25: Synthesis of CtxAamb mutants and labelling in a modified CHO system.
Cell-free synthesis of CtxAamb mutants in the modified CHO system. (A) In-gel fluorescence of CtxAamb mutants labelled with DyLight-632 phosphine. (B) In-gel fluorescence and autoradiography of co-expressed multimer after labelling with DyLight-632 phosphine. Figure modified from Ramm *et al.,* 2022.

These data indicated that the modified CHO system was necessary for the labelling of co-expressed AB_5 toxin complexes, but the translation efficiency was unfortunately reduced compared to the wild type CtxA fragment.

As a last step, the effect of an AB_5 complex including the modified CtxA mutants on CHO-K1 target cells was studied. The CtxB subunit was co-expressed with the CtxA WT or one of the mutants using the modified CHO lysate in the presence of AzF and orthogonal tRNA. A co-expression with the CtxA WT and an NTC synthesis reaction were performed in the presence of AzF and orthogonal tRNA as well. Negative controls of the co-expression of CtxAamb mutants and the CtxB subunit without AzF were additionally performed. All multimers were added at a concentration of 4 nM. Untreated cells were highly confluent after 48 h, while the NTC induced a reduced cell confluence. As expected, CtxAB showed apoptotic cells. Cells that were supplemented with a complex containing a mutated A subunit were as confluent as the non-treated cells. No differences could be detected in samples where AzF was added to the synthesis reaction and where AzF was missing from the mixture. Few apoptotic cells could be detected in wells where the amber-suppressed CtxAambE112 mutant was used, but due to the high cell confluence this effect cannot be traced to the Ctx complex (Figure 26 A). In order to quantify the apoptotic effects a cytotoxicity assay was performed. Using the CellTox CyGreen assay initial apoptotic effects from the CtxAB WT multimer could be detected. Multimers containing a modified CtxA subunit did not induce toxic effects. In comparison to the NTC lysate control, the CtxAB multimer and the positive control Triton-X 100 induced statistically significant changes (Figure 26 B). As expected, these data suggest that the incorporation of a ncAA in the enzymatic center of the toxin inhibited the functionality of the toxin. Such a silencing of a toxin of interest will be beneficial for future studies tracking the toxin within the target cell. Nonetheless, future studies should use higher toxin concentrations and therefore use plasmid DNA templates. This would consequently result in more prominent toxicity results of the CtxAB WT sample.

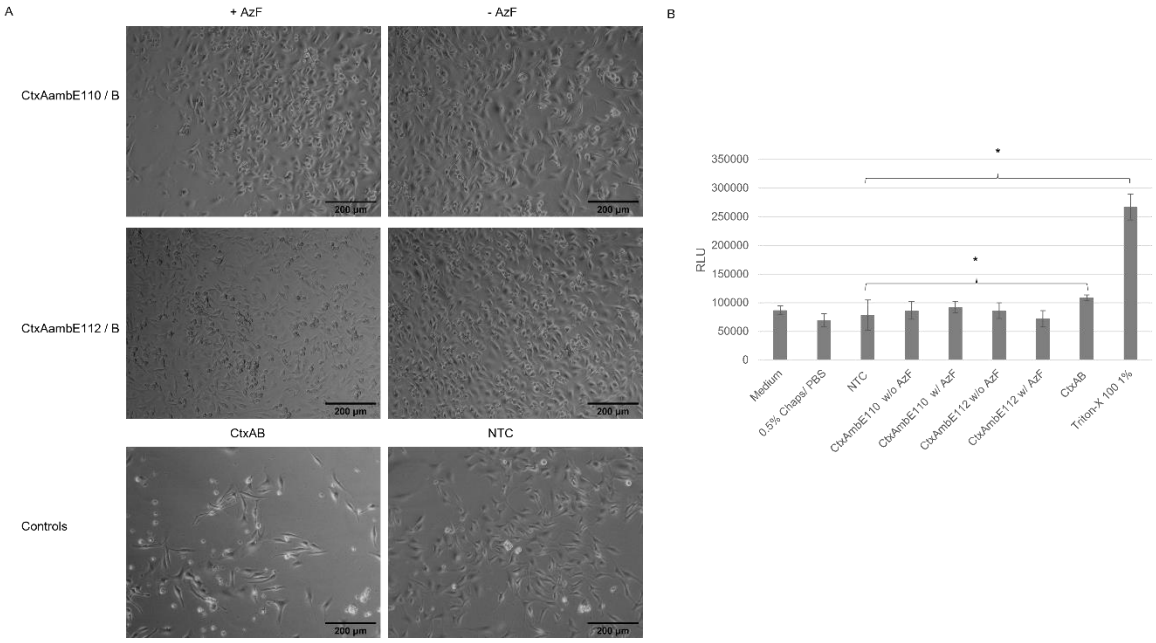

Figure 26: Morphological analysis of CHO-K1 cells supplemented with Ctx toxin with a modified A subunit. Ctx subunits were co-expressed in a modified CHO lysate and supplemented to CHO-K1 cells. Cells supplemented with a volume equivalent NTC served as control. (A) CHO-K1 cell were seeded in a 24-well plate (25,000 cells/well). Phase contrast photographs were taken after 48 h of incubation. Scale bar indicated 200 µm. (B) CHO-K1 cell were seeded in a 96-well plate (10,000 cells/well). Cytotoxicity was anaylzed using the CellTox CyGreen assay after 48 h. Relative light units (RLU) detected apoptotic effects. Cells supplemented with medium, 0.5% CHAPS/PBS, an NTC in an volume equivalent served as controls. 1% Triton-X 100 was a positive control. Standard deviation derived from three assays with triplicate analysis (n=9). Statistical significance indicated by *. Figure from Ramm *et al.,* 2022.

Taken together, the data represented for the modification of AB_5 toxins demonstrated that versatile methods such as fusion proteins and site-specific labelling by Staudinger ligation can be used for fluorescent labelling of toxins. Further, diverse modifications can be performed to study the individual toxin subunits. These data led to a publication in a special issue on “Novel Aspects of Bacterial AB5-Toxins” in 2022[73]. These technologies will allow for future diagnostic and medical applications such as Trojan horses, targeted toxins and intracellular trafficking.

3.3 Therapeutic use of toxins

At a first glance toxins are associated with a negative effect. Nonetheless, a toxic effect on a cell can be used for targeting specific cells such as tumor cells. Experimental strategies to combine a toxin with a targeting moiety in order to attack specific tumor cells has been developed in the past[170,173]. The second part of this thesis aimed to investigate the feasibility of cell-free protein synthesis for the development of targeted toxins and their clinical use.

3.3.1 Targeted toxin Dianthin-EGF

Toxins specifically inhibiting protein translation have been widely considered as an ideal basis for the development of targeted toxins[173]. Hence, in this thesis the plant derived ribosome inactivating toxin Dianthin and its targeted toxin variant Dianthin-EGF were analyzed. The cell-free synthesis and initial functionality assessments of both toxin variants have been established in prior work[69,70]. As Dianthin inactivates eukaryotic ribosomes, different CHO lysates were tested to assess the efficiency of the translocation of Dianthin into the microsomal vesicles. The analysis of the SN2 fraction demonstrated that Dianthin was only partially translocated into the microsomal vesicles (as represented for three CHO lysates in Supplementary Figure 16). The inefficient translocation of Dianthin resulted in low overall total protein yields. Thus, lysates with a high translocation efficiency were chosen for experiments focusing on. In this thesis the specific functional activity and clinical relevance of cell-free synthesized Dianthin and Dianthin-EGF were investigated. It was further assessed whether the low protein yields derived from the synthesis in the eukaryotic system were sufficient for the functional characterization.

As a first step, the ribosome inactivating potential of Dianthin and Dianthin-EGF was investigated. Therefore, an *in vitro* translation inhibition assay using the model protein luciferase (LUC) was performed in the eukaryotic CHO and prokaryotic *E. coli* cell-free system. Dianthin and Dianthin-EGF were pre-synthesized using the CHO cell-free system and the total protein yield was determined. A defined concentration of 1.5 and 3 nM non-radioactively labelled SN2 fraction of Dianthin and Dianthin-EGF were supplemented to the cell-free synthesis of LUC. Control reactions in the presence of LUC template were supplemented with PBS, CHAPS/PBS or an NTC equivalent to the volume of Dianthin-EGF. A synthesis reaction of LUC supplemented with an equivalent volume of ddH_2O was used as a standard reaction and benchmark. An NTC reaction without LUC template was used to monitor the lysate background. As expected, in the eukaryotic cell-free system a reduction in the total protein yield of LUC was detected in the presence of Dianthin and Dianthin-EGF. Minor reductions in the total protein yields were detected in the presence of control supplements PBS, CHAPS/PBS or the NTC volume equivalent by reducing the LUC yield from about 30 µg/mL to 20-25 µg/mL. As Dianthin and Dianthin-EGF samples were diluted with CHAPS/PBS, the statistical analysis of the reduction of the total protein yield after the addition of Dianthin samples was analyzed in comparison to the LUC + CHAPS/PBS sample. All Dianthin samples reduced the total protein yield of cell-free synthesized LUC in a statistically significant manner (Figure 27 A). The total percentage of inhibited LUC protein synthesis was calculated based on the LUC reaction which was supplemented with CHAPS/PBS. This calculation showed that Dianthin inhibited the LUC synthesis by up to 88% and 93% at 1.5 and 3 nM, respectively. Dianthin-EGF inhibited the

synthesis by up to 86% at 1.5 nM and 92% at 3 nM. The autoradiograph depicted intense protein bands for LUC supplemented with control substances. Conversely, almost no protein bands were detected when Dianthin was added, while Dianthin-EGF supplemented reactions resulted in very faint bands in comparison to the control reactions (Figure 27 B).

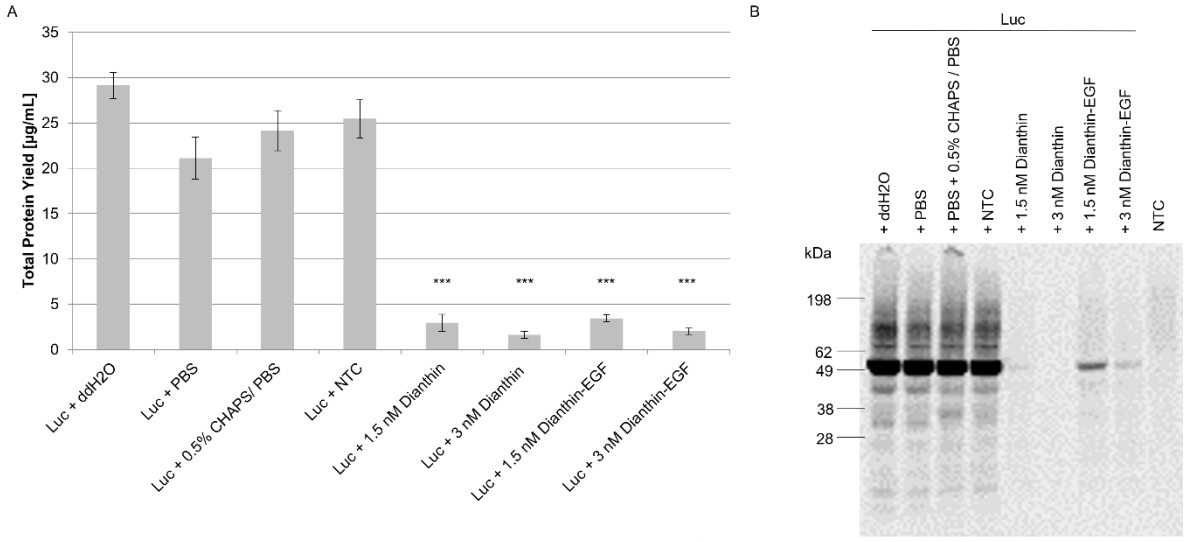

Figure 27: *In vitro* inhibition of LUC synthesis by cell-free synthesized Dianthin and Dianthin-EGF.
Dianthin and Dianthin-EGF were pre-synthesized in CHO lysate and added to the CHO-based cell-free synthesis of LUC. (A) Quantitative analysis of cell-free synthesized LUC in the presence of Dianthin and Dinathin-EGF or control supplements by liquid scintillation counting. Standard deviations were calculated from duplicate analysis of three individual experiments. Statistical analysis using an ANOVA based on Bonferroni. (B) Exemplary autoradiograph showing ^{14}C-leucine labelled TM fraction of LUC after the supplementation of Dianthin and Dianthin-EGF as well as control supplements.

No statistically relevant reduction in LUC total protein yield could be detected in a prokaryotic system, neither in the presence of Dianthin and Dianthin-EGF nor in the presence of control substances. The autoradiograph confirmed these results by showing intense protein bands for all samples (Supplementary Figure 17). Taken together, these data show a ribosome-inactivating effect of Dianthin and Dianthin-EGF specific to eukaryotic ribosomes.

As a next step, the cytotoxic effect of Dianthin and Dianthin-EGF on cells was determined by morphological assessment of cells and by using the MTT cell viability assay. For both assays, PC-9 cells naturally expressing EGFR were used, and HEK293 cells served as a control cell line[199,200]. In order to assess initial toxic effects three different concentrations were tested, namely 0.1 fM, 10 fM and 1000 fM. Further, cells were exposed to EGF alone in the same final concentrations as the toxins to monitor effects triggered by ligand cell-binding. The NTC was applied in a volume equivalent to Dianthin-EGF in order to detect

background effects originating from the cell-free reaction. All samples originated from the SN2 fraction after cell-free synthesis. The effects of each sample as well as a medium and CHAPS/PBS control were analyzed in the presence and absence of the endosomal escape enhancer SO1861, which is a saponin isolated from *Saponaria officinalis L.*.

Phase contrast images showed that PC-9 cells subjected to Dianthin-EGF and SO1861 became apoptotic, while cells treated with Dianthin-EGF alone showed a decreased confluency. In the presence of SO1861, Dianthin-EGF induced toxic effects starting at a concentration as little as 0.1 fM (Figure 28). Instead, without its supplementation, Dianthin-EGF induced initial apoptotic effects at a concentration of 1000 fM (Supplementary Figure 18). Thus, the endosomal escape enhancer increased the toxicity of Dianthin-EGF by factor 10,000. Dianthin alone as well as the control supplements EGF, NTC and CHAPS/PBS did not induce apoptotic changes. However, EGF and Dianthin treated cells showed a minor decrease in cell confluency at 1000 fM.

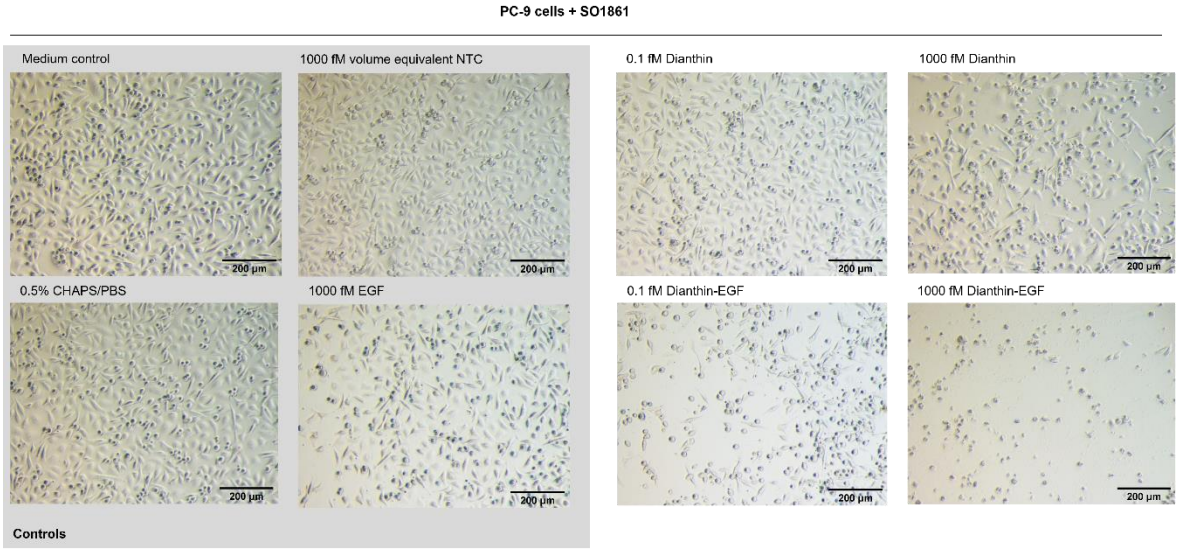

Figure 28: PC-9 cells supplemented with Dianthin and Dianthin-EGF in the presence of SO1861.
Cell-free synthesized Dianthin and Dianthin-EGF supplemented to PC-9 cells in a 24-well plate. Morphological changes of PC-9 cells after supplementation of Dianthin and Dianthin-EGF in concentrations of 0.1 fM and 1000 fM in the presence of SO1861 were investigated. Untreated cells, cells supplemented with CHAPS/PBS, cells supplemented with an NTC and cells supplemented with cell-free synthesized EGF were used as controls. Scale bar indicated 200 µm.

While in PC-9 cells the effects of Dianthin-EGF were already obvious at concentrations as little as 0.1 fM, for HEK239 cells much higher toxin concentrations were needed to detect similar effects. Dianthin-EGF induced apoptotic effects at 1000 fM in the presence of SO1861 demonstrating that a concentration 10,000 times higher was necessary to induce effects on HEK293 cells. In comparison to the medium control the cells' confluency was reduced by Dianthin, EGF and the NTC sample but these samples did not induce

apoptosis (Figure 29). No effects on HEK293 cells could be detected without the supplementation of SO1861 (Supplementary Figure 19).

To summarize, Dianthin-EGF showed a stronger toxic effect compared to Dianthin alone, while PC-9 cells reacted much more sensitive to Dianthin-EGF as compared to HEK293 cells. Taken together, these data indicated a targeted effect of Dianthin-EGF on a cellular basis.

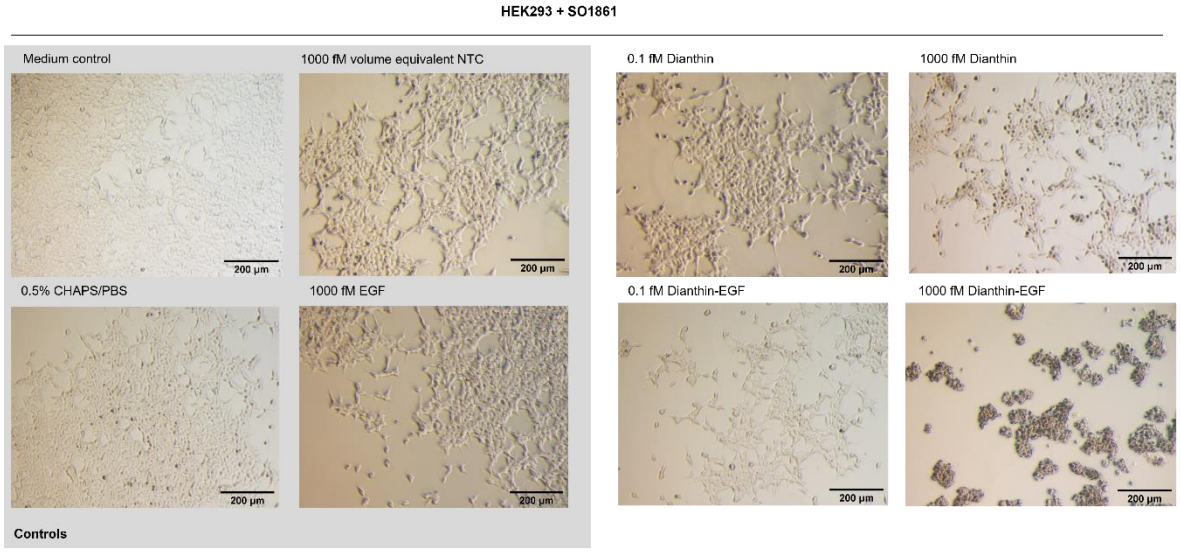

Figure 29: HEK293 cells supplemented with Dianthin and Dianthin-EGF in the presence of SO1861.
Cell-free synthesized Dianthin and Dianthin-EGF supplemented to HEK293 cells in a 24-well plate. Morphological changes of HEK293 cells after supplementation of Dianthin and Dianthin-EGF concentrations of 0.1 fM and 1000 fM with SO1861 were investigated. Untreated cells, cells supplemented with CHAPS/PBS, cells supplemented with an NTC and cells supplemented with cell-free synthesized EGF were used as controls. Scale bar indicated 200 µm.

In order to confirm the toxic effects seen for Dianthin-EGF in the morphological analysis of cells, the MTT viability assay was performed based on PC-9 cells. Prior work has investigated the effect of cell-free Dianthin and Dianthin-EGF on HeLa and HEK293 cells[70], but not on PC-9 cells. Thus, a concentration gradient of each sample with a concentration of 0.1 fM, 1 fM, 0.01 pM, 0.1 pM, 1 pM, 0.01 nM, 0.1 nM and 1 nM was applied. Further, the assay was performed in the presence and absence of the endosomal escape enhancer SO1861. The obtained data depicted that without the addition of SO1861 neither Dianthin nor Dianthin-EGF induced a reduced cell viability. In contrast, in the presence of SO18618, the cell viability was reduced by Dianthin starting at 0.001 nM resulting in a reduction of cell viability of almost 90% at a concentration of 1 nM (Figure 30 A). Remarkably, the targeted toxin Dianthin-EGF started to induce a reduction in cell viability at 1 fM while only approximately 12% viable cells were present at 0.001 nM (Figure 30 B). The ligand EGF and the NTC did not influence the cell viability (Figure 30 C

and D, respectively). Based on these data, the IC_{50} value of Dianthin-EGF was determined using a logistic fit. An IC_{50} value of $1.82*10^4$ fM ($\pm 1*10^4$ fM) was determined for the co-administration of Dianthin and SO1816 when including data point between 0.0001 and 1 nM Dianthin. Concentrations below 0.0001 nM could not be included as no reduction in the cell viability was observed and no fit was possible. In contrast, an IC_{50} of 2.86 fM (±1.3 fM) was calculated when Dianthin-EGF was co-administered with SO1861. Accordingly, no fit could be calculated for the supplementation of Dianthin and Dianthin-EGF without a co-administration of SO1816 as all tested concentrations did not reduce the cell viability.

All in all these data reflected the findings from the morphological cell analysis of PC-9 cells and suggest that Dianthin-EGF is a potent targeted toxin.

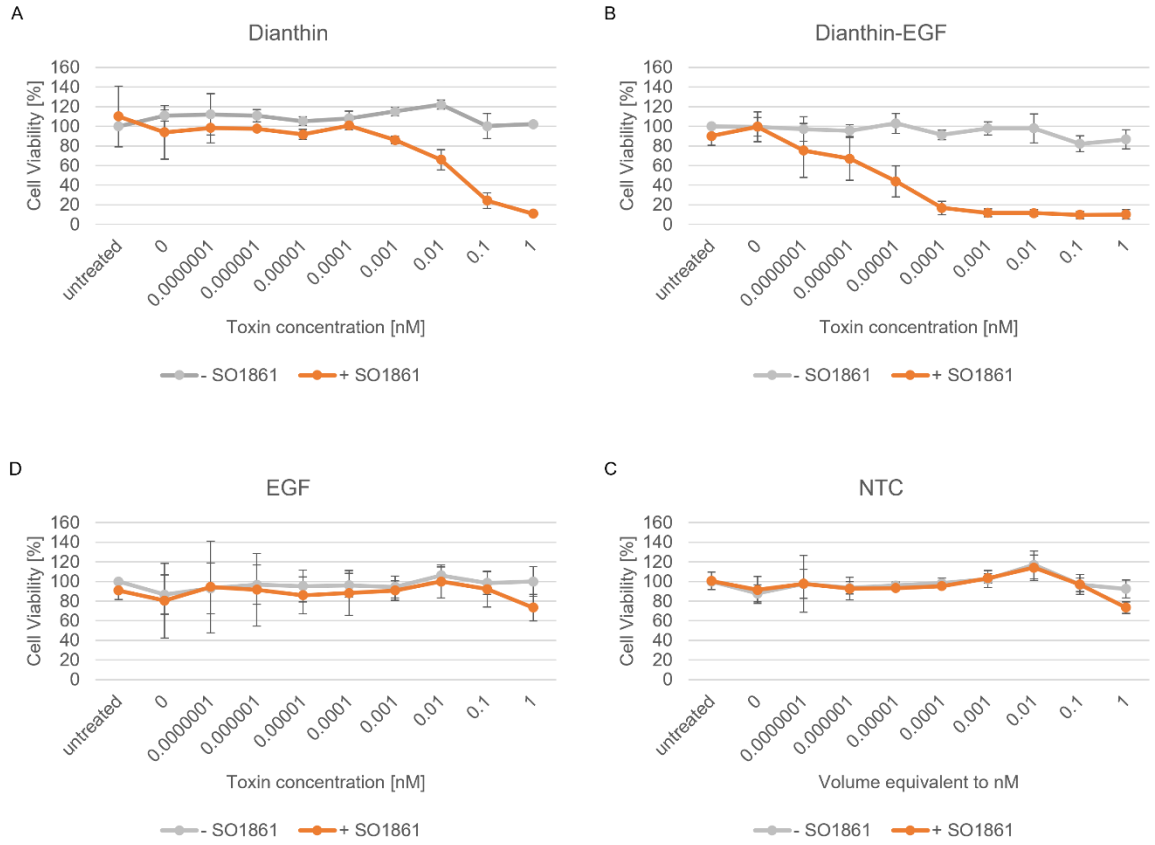

Figure 30: MTT viability assay of PC-9 cells supplemented with Dianthin and Dianthin-EGF.
Dianthin, Dianthin-EGF, EGF and an NTC were pre-synthesized in CHO lysate and supplemented to PC-9 cells. The MTT cell viability assays was used to assess the effect of Dianthin (A) and Dianthin-EGF (B), EGF (C) and NTC (D) on PC-9 cells with and without SO1861. A serial dilution of each analyte ranging from 0.1 fM to 1 nM was tested. The NTC was applied at an equivalent volume as used for Dianthin-EGF. Untreated cells reflected medium control while 0 nM indicated 0.5% CHAPS/PBS. Standard deviations were calculated from triplicate samples of three independent experiments.

As a final step, the clinical relevance of the targeted toxin was evaluated using primary tumor samples from patients. For this purpose, the so-called soft-agar assay[210] was

established within the frame of this thesis. Cells were separated and embedded in a soft-agar layer for 8-11 days until spherical cell colonies were obtained (Figure 31). The assay was based on the investigation of the growth behavior of these embedded cells upon treatment with Dianthin and Dianthin-EGF in the presence or absence of SO1816. An inhibitory effect of Dianthin and Dianthin-EGF on the growth of the tumor colonies was expected.

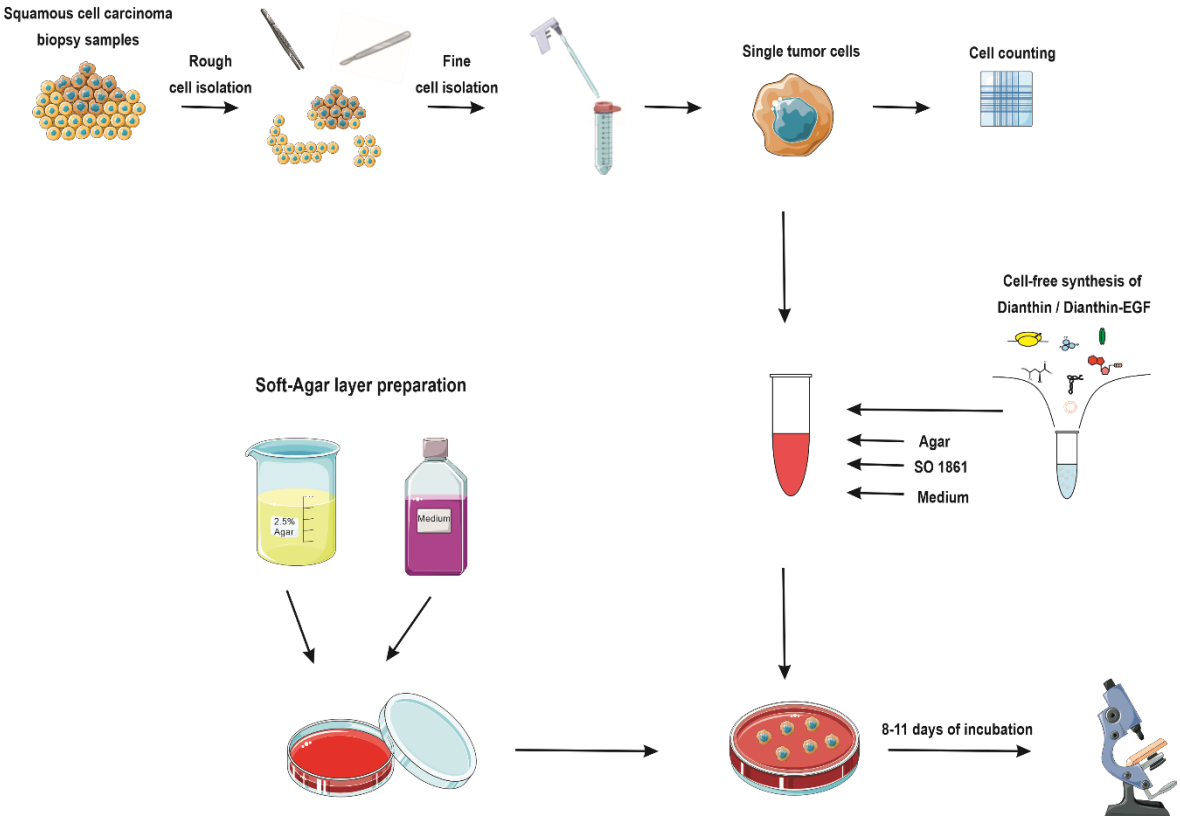

Figure 31: Schematic overview of the soft-agar assay.

To set up this method, PC-9 cells were used as an initial step. A medium control and Dianthin-EGF concentrations with and without SO1861 were analyzed on the cells that were embedded within the soft-agar. After 10 days of incubation large PC-9 cell colonies were detected within the soft-agar layer of the medium control regardless of the presence of SO1861 (Supplementary Figure 20). Treatment of PC-9 cells with Dianthin-EGF in the absence of SO1861 did not have a negative effect on cell colony growth. On the contrary, when PC-9 cells were incubated with Dianthin-EGF and SO1861 the cells within the agar were widely spread and cells did not form colonies (Supplementary Figure 20). In order to transfer the method to primary tumor cells (epithelial squamous cell carcinoma biopsy samples) cell strainers with diverse pore diameters as well as different tumor cell counts were tested to allow for an optimal tumor colony growth (data not shown). During these initial experiments, a cell number of 100,000 tumor cells per petri dish and a cell strainer of 500 µm was identified. Further, a defined concentration range of Dianthin-EGF was

detected by supplementing recombinant Dianthin-EGF from cell-based *E. coli* expression provided by the AG Fuchs. It could be shown that a concentration between 0.1 and 10 nM Dianthin-EGF inhibited the tumor colony growth (data not shown). Strikingly, each tumor sample formed unique tumor colonies with different sizes and clusters (Figure 32).

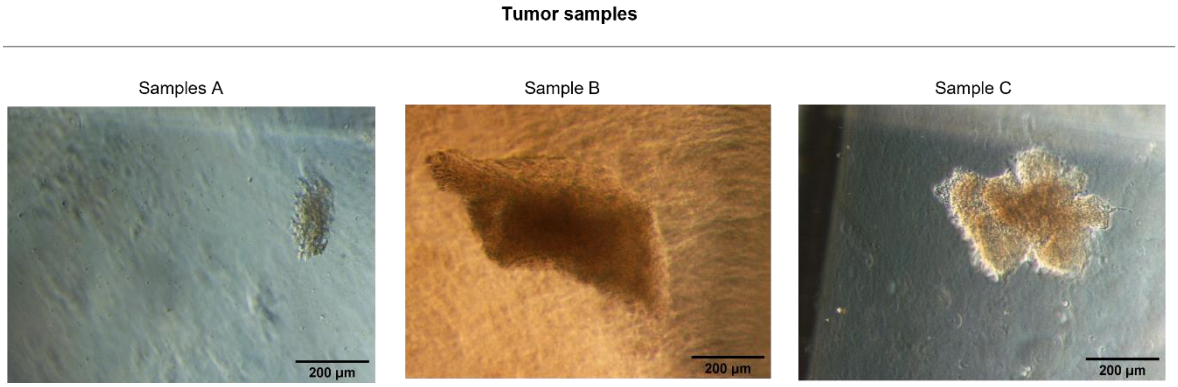

Figure 32: Tumor colonies.
Cell-free synthesized Dianthin-EGF supplemented to tumor samples in the soft-agar assay. Photographed after 8-11 days using a light microscope and CCD camera. Scale bar indicated 200 µm. Samples were numbered independently from the experiment for this thesis in order to prevent a tracking of potential patient data.

Thus, for the following experiments colonies of treated cells were always evaluated in relation to the size of the colonies of untreated samples (medium control). In fact, this meant that colonies smaller than the tumor colonies in the medium control were not counted. As a next step, cell-free synthesized Dianthin-EGF was applied to the tumor samples at different concentrations in the presence of SO1861 in order to identify whether cell-free synthesized samples were active in the same concentration range as the recombinant Dianthin-EGF produced in *E. coli* cells. The experiment was repeated three times (Table 13). A concentration of 0.1 nM Dianthin-EGF reduced the number of tumor colonies to 53.84% ± 7.08 the number of colonies in the untreated samples. As a consequence, 0.1 and 1 nM were chosen as effective concentrations of Dianthin-EGF for the next experiments. The data also showed that the individual tumor samples reacted in different intensities to the NTC samples. This indicated that the lysate background and the CHAPS/PBS detergent mixture also had an effect on some tissue samples.

In the next step, each tumor sample was treated with Dianthin, Dianthin-EGF, EGF and a volume equivalent NTC with and without the supplementation of SO1861. All samples should be analyzed in duplicates from each tumor sample. In order to perform a statistical analysis a large set of patient samples is necessary accounting for the variability of patient samples due to genetic and phenotypic factors.

Table 13: Concentration gradient of Dianthin-EGF on Tumor samples.
Cell-free synthesized Dianthin-EGF was supplemented to tumor cells embedded in the soft-agar assay and incubated for 8-11 days. Samples were numbered independently from the experiment in order to prevent a potential tracking of patient data.

Sample	Concentration [nM]	Replicate	Number of colonies		
			Sample D	Sample E	Sample F
Medium	/	1	87	97	75
	/	2	84	88	74
Dianthin-EGF	0.01	1	58	57	54
		2	56	71	47
	0.05	1	44	72	48
		2	42	64	60
	0.1	1	37	59	44
		2	/	/	40
	0.5	1	34	33	31
		2	/	/	36
	1	1	24	29	32
		2	/	/	29
NTC	0.1	1	63	68	50
	1	1	73	46	39

Up until the writing of this thesis a total of 11 samples have been studied for this set of experiments (data not shown) and the experiments are still ongoing. Unfortunately, 4 samples could not be analyzed due to contaminations. Further limiting factors for experiments were the size and nature of the tumor sample. The size of the patient's tumor sample varied in each experiment and in some cases the sample contained blood vessels which had to be cut from the sample and thus reduced the available tumor cells. Hence, a thorough statistical analysis was not yet possible as more tumor samples are needed. Nonetheless, setting up the soft-agar assay showed that cell-free synthesized Dianthin-EGF induced toxic effects on patient's tumor samples and thus enabling CFPS for clinical screening applications.

3.4 Rapid response to novel zoonotic diseases

Viral pathogens such as SARS-CoV2 induce cytotoxic effects and inflict disease progressions. An interplay of a variety of proteins that are encoded by the virus is responsible for such effects. A rapid system to synthesize and characterize accessory, structural as well as non-structural proteins is necessary to understand the mechanism of action of the virus. In order to validate CFPS as a rapid response system for viral

pathogens, especially those that can induce zoonotic diseases, SARS-CoV2 viral proteins were synthesized in eukaryotic cell-free systems.

3.4.1 Cell-free synthesis of SARS-CoV2 proteins

In an initial step, all structural and accessory proteins as well as five non-structural proteins (nsp1, nsp5, nsp12, nsp13 and nsp16) were synthesized in a CHO-based system. Qualitative analysis by autoradiography showed that all proteins tested could be synthesized as depicted by defined proteins bands. Multimerizations of membrane proteins ORF3 and ORF7a as well as of unclassified proteins ORF8 and ORF10 could be detected. The autoradiograph also showed cleavage products as seen for Spike full-length protein, for the S1 and S2 domain of the Spike protein and for nucleocapsid protein (Figure 33).

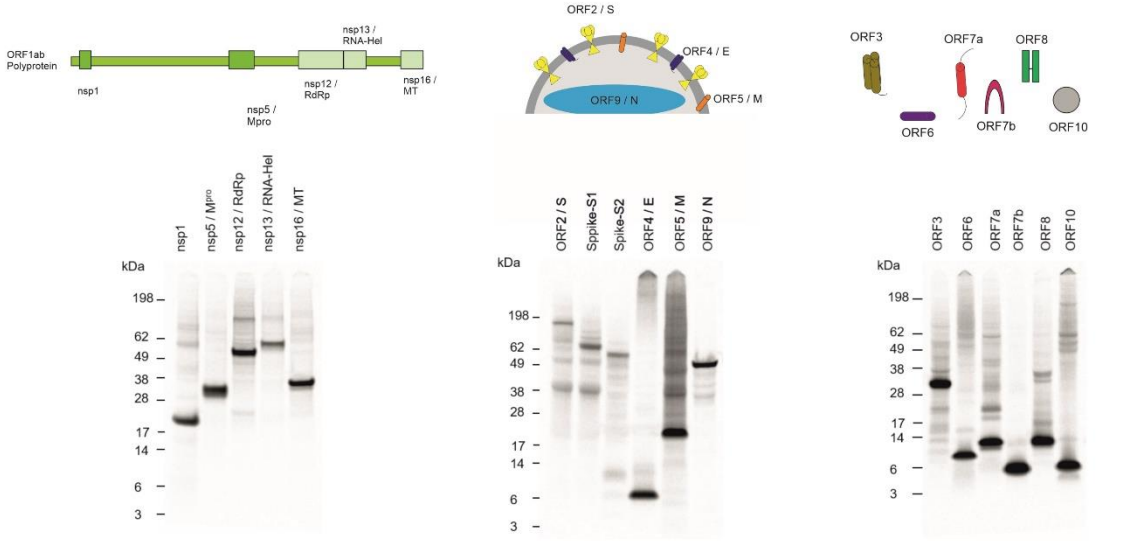

ORF	Protein	Molecular weight [kDa]
1ab	nsp1	22.17
	nsp5/m^{Pro}	33.87
	nsp12 / RdRp	61.18
	nsp13 / RNA-Hel	66.92
	nsp16 / MT	33.33

ORF	Protein	Molecular weight [kDa]
2	Surface glycoprotein / Spike / S Full-length protein	139.60
	S1 subunit	75.11
	S2 subunit	64.50
4	Envelope / E	8.30
5	Membrane glycoprotein / M	25.03
9	Nucleocapsid protein / N	45.56

ORF	Protein	Molecular weight [kDa]
3	ORF3	31.06
6	ORF6	7.21
7	ORF7a	12.10
	ORF7b	5.12
8	ORF8	13.77
10	ORF10	4.06

Figure 33: Cell-free synthesis of SARS-CoV2 proteins.
SARS-CoV2 proteins were synthesized in a batch-based CHO reaction. Qualitative analysis by autoradiography. Autoradiograph showing ^{14}C-leucine labelled proteins derived from the translation mixture (TM). Modified from Ramm *et al*., 2022.

Next, a quantitative analysis of the whole reaction mixture as well as the soluble and microsomal proteins was performed. These data demonstrated that the non-structural proteins were mainly present in a soluble form as higher protein yields were detected in the SN as compared to the MF. The structural proteins M and the S1 and S2 domains of the Spike protein could be synthesized in higher yields as compared to full-length Spike, E and N. The cell-free protein synthesis of the full-length Spike protein was performed using

a PCR template as the cloning into a vector could not be performed, neither in house nor by the gene synthesis supplier. This could have resulted in a lower template concentration and thus in a lower total protein yield. Nonetheless, the high molecular weight Spike protein could be synthesized in an equal amount to the comparably small E protein. The initial data for the synthesis of the accessory proteins showed that all proteins could be synthesized as well. The putative ion channel ORF3 was synthesized at the highest protein amounts while the immunomodulatory protein ORF6 showed the overall lowest protein yield (Figure 34).

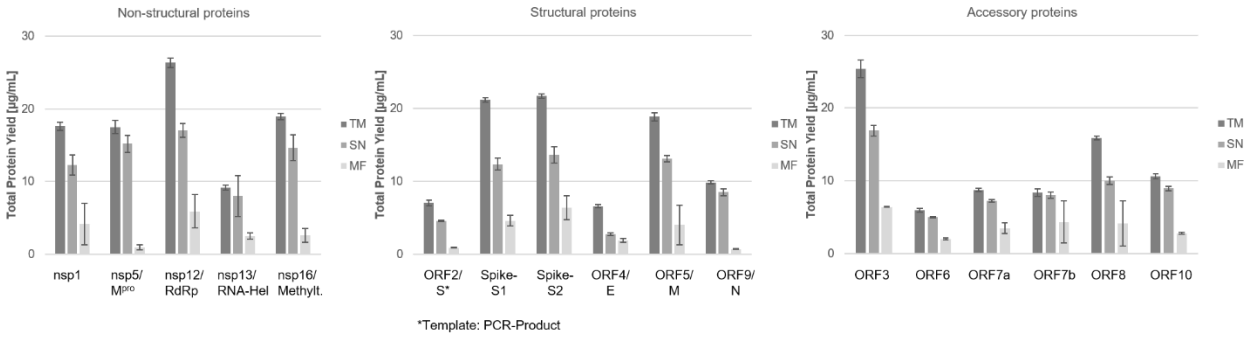

Figure 34: Quantitative analysis of SARS-CoV2 proteins.
SARS-CoV2 proteins were synthesized in a batch-based CHO reaction. Quantitative analysis of ^{14}C-labelled proteins was performed by liquid scintillation counting. Standard deviations were calculated from triplicate analysis. The translation mixture (TM) was separated into the soluble proteins in the supernatant (SN) and the microsomal fraction (MF). Template for the full-length Spike protein was based on a PCR-template as indicated by *. Modified from Ramm *et al*., 2022.

After these initial syntheses, it was studied which eukaryotic cell-free system showed the most promising results. As a rapid response system has to be versatile and flexible, the use of different lysates might result in the faster characterization of proteins as each lysate has its own advantages and drawbacks. Therefore, the individual proteins were synthesized in *Sf*21, CHO and K562 lysates. These data demonstrated that all proteins could be synthesized in all three eukaryotic lysates (represented for nsp5 and ORF5 / M protein in Supplementary Figure 21 and represented for ORF4 / E protein in Supplementary Figure 22).

A representative protein from each viral protein class was chosen and a CECF reaction in each lysate was performed in order to test the high yield production of viral proteins. This is especially important if CFPS would be used for providing antigens for downstream applications. Nsp12, the M protein and ORF3 were chosen. The CECF reactions were performed for 24 h. In general, the CHO system resulted in the highest protein yields after 24 h. The *Sf*21 and K562 lysate depicted lower overall protein yields, which suggested

that further synthesis optimizations were necessary (Figure 35). A prolonged reaction time of 48 h did not significantly increase the protein yields (data not shown).

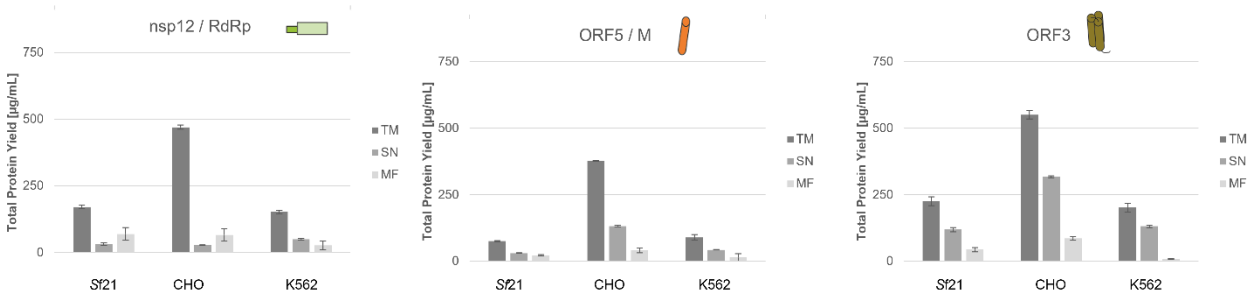

Figure 35: CECF reactions of nsp12, M protein and ORF3.
Nsp12, the M protein and ORF3 were synthesized in CECF reactions with *Sf*21, CHO and K562 lysate for 24 h. Quantitative analysis of ^{14}C-labelled proteins as performed by liquid scintillation counting. Standard deviations were calculated from triplicate analysis. The translation mixture (TM) was separated into the soluble proteins in the supernatant (SN) and the microsomal fraction (MF). Modified from Ramm *et al*., 2022.

When combining the data from the various protein syntheses and their optimizations, the CHO lysate showed the highest protein yields for most proteins. Hence, the following experiments were performed in the CHO system, if not stated otherwise. To test whether cell-free systems can be widely used for the characterization of viral pathogens, the different protein groups were analyzed.

3.4.2 Analysis of nsp1's inhibitory effect

Non-structural viral proteins are generally involved in the viral replication[187]. Nsp1 is known to inhibit host cell protein translation[198,211]. An *in vitro* translation inhibition assay was performed. Nsp1 was pre-synthesized in CHO lysate and added to the synthesis of the model protein enhanced yellow fluorescent protein (eYFP). A continuous recording of the eYFP fluorescence was performed during the 3 h synthesis time (Figure 36 A). As a control, an eYFP synthesis without the supplementation of any protein was executed. This value was established as a baseline value of 100%. All other measurements were normalized to this fluorescence intensity. After further optimizations (data not shown), nsp1 protein was added to the eYFP synthesis at two concentrations, namely 25 and 90 nM. A control reaction containing the eYFP synthesis that was supplemented with a volume equivalent NTC was assessed. The normalized fluorescence intensity of eYFP started to decrease after 20 min when nsp1 was supplemented. A concentration dependent effect could be detected. Interestingly, the inhibitory effect of nsp1 decreased and the eYFP fluorescence increased again (Figure 36 B). No effect was seen after the supplementation of an NTC control. Nonetheless, an inhibitory effect on the protein translation of eYFP could be determined after the nsp1 supplementation.

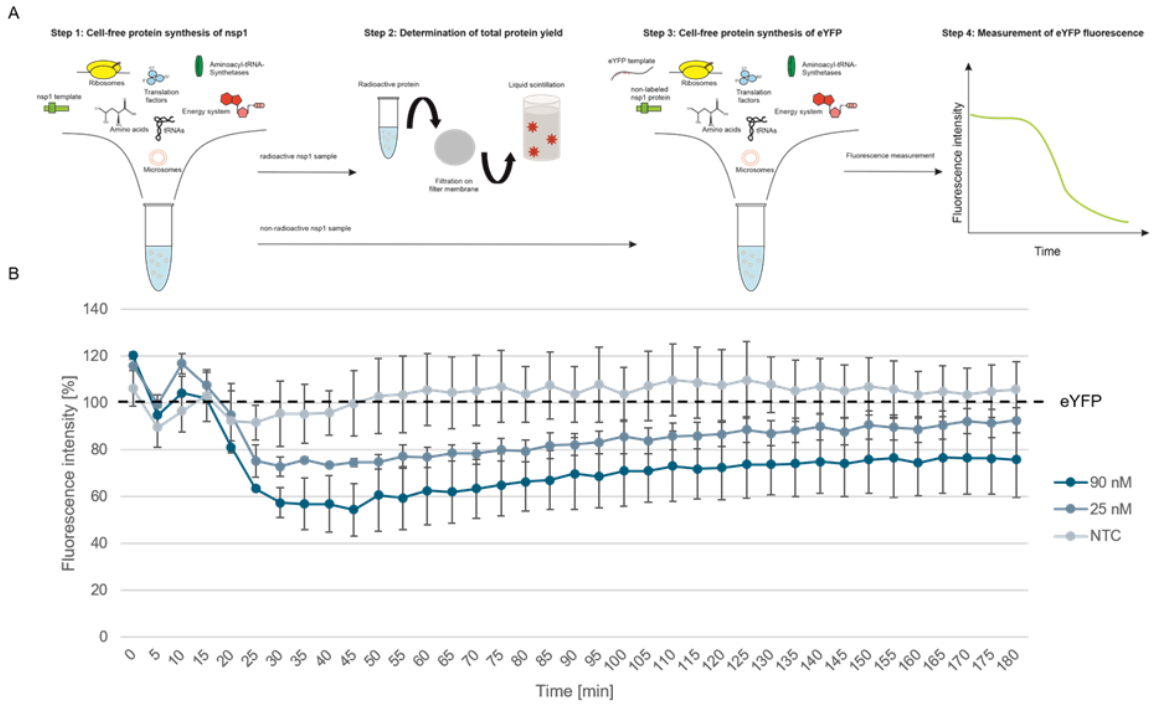

Figure 36: Inhibitory effect of nsp1.

(A) Schematic overview of nsp1 functionality assay. (B) Supplementation of cell-free synthesized nsp1 at 90 and 25 nM to the cell-free protein synthesis of the model protein eYFP. Data were normalized to eYFP fluorescence signal. Standard deviation was calculated from two experiments. Figure from Ramm *et al*., 2022.

3.4.3 Characterization of accessory proteins

In the next steps, several proteins were analyzed more thoroughly. The accessory proteins of viral pathogens are known to be needed to attack the host[187]. These proteins carry out different tasks within the host organism and as the structural proteins are generally the first proteins to be analyzed, the defined characteristics of accessory proteins often remain unresolved for a longer time. The accessory proteins ORF3, ORF6, ORF7b, ORF8 and ORF10 were synthesized with and without a Mel signal peptide which allows for the co-translational translocation of proteins. This comparison depicted that all ORFs were more stably expressed in the presence of a signal peptide (Figure 37 A). The NCM-ORF3 construct was based on a PCR template, which might have resulted in a lower overall translation efficiency due to a lower template concentration. This was the only protein with a lower protein yield after a synthesis based on the NCM template. Strikingly, ORF10 could not be synthesized without a signal peptide (Figure 37 A, red box). This demonstrated a better translation initiation in the presence of the Mel signal peptide. The type I transmembrane protein encodes a native signal peptide (Nat-SP)[193]. The Nat-SP and Mel signal peptide were compared concerning their translation efficiency and translocation to the microsomal vesicles. The template of ORF7a containing the Nat-SP resulted in a higher total amount of protein and a higher protein yield in the MF as

compared to the template containing the Mel signal peptide. Qualitative analysis showed potential multimerization when both signal peptides were used. Autoradiography showed protein bands of the monomer (~12 kDa), a dimer (~24 kDa), a trimer (~36 kDa) and a pentamer (~60 kDa) (Figure 37 B). The ORF8 protein showed stable protein yields with and without a Mel signal peptide. Unfortunately, recent studies have shown that ORF8 contains a sequence homology to the SARS CoV ORF8ab native signal peptide[212], which indicated that the NCM-ORF8 construct contained two signal peptides. Thus, later experiments only focused on the ORF8 template without the Mel signal peptide but containing its potential Nat-SP. The analysis of the ORF8 protein depicted that possible multimerization could be detected even in the presence of DTT. The autoradiograph also depicted a protein band with a higher molecular weight of about 15 kDa in the TM and MF fraction, but not in the SN fraction indicating a glycosylated ORF8 (Figure 37 C)

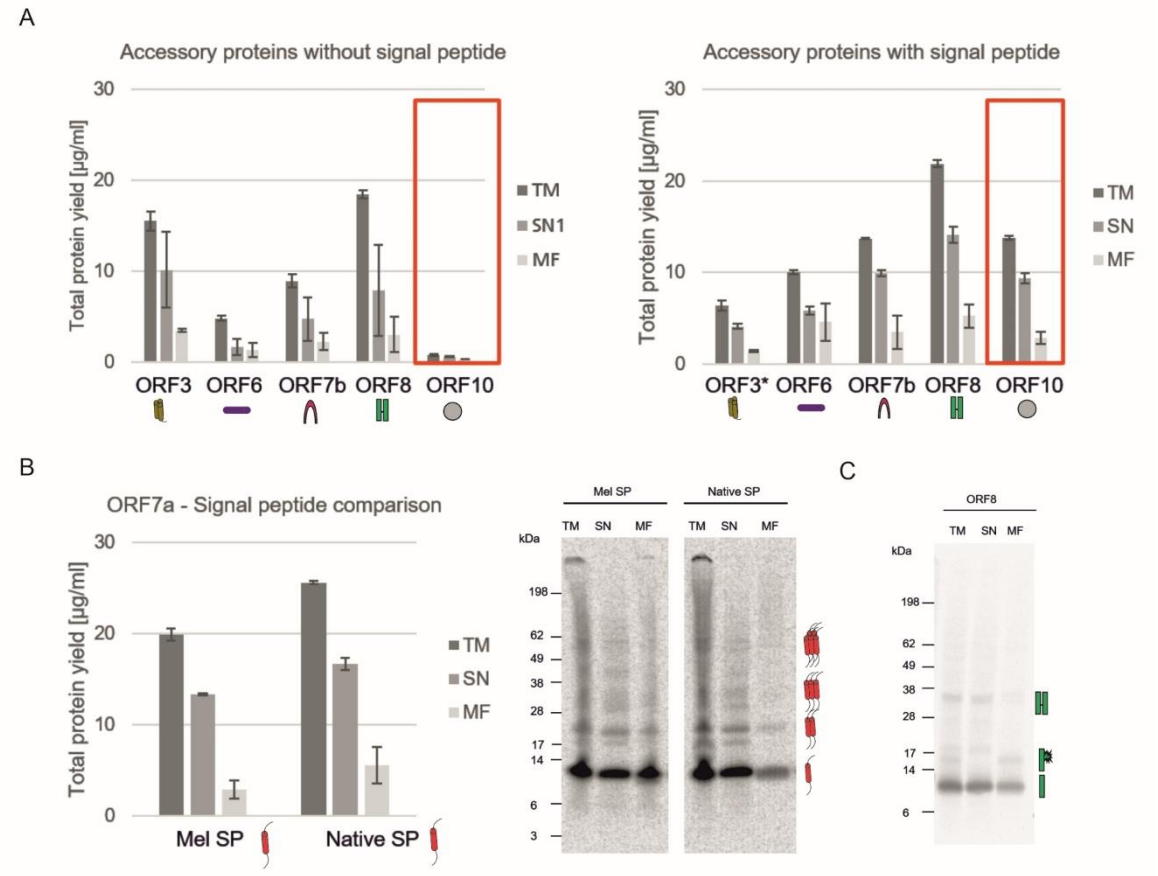

Figure 37: Analysis of SARS-CoV2 accessory proteins.

(A) Accessory proteins ORF3, ORF6, ORF7b, ORF8 and ORF10 were synthesized in a CHO batch-based reaction with and without a Mel signal peptide. Quantitative analysis of ^{14}C-labelled proteins was performed by liquid scintillation counting. Standard deviations were calculated from triplicate analysis. Template for ORF3 with a Mel signal peptide was based on a PCR-template as indicated by *. (B) ORF7a was synthesized in a CHO batch-based cell-free system with Mel and a native signal peptide. Quantitative analysis of cell-free synthesized proteins as performed by liquid scintillation counting. Standard deviations were calculated from triplicate analysis. Qualitative analysis by autoradiography including potential multimers as indicated by the

star. (C) Autoradiograph showing ORF8 synthesized in a CHO cell-free system. In all experiments, the translation mixture (TM) was separated into the soluble proteins in the supernatant (SN) and the microsomal fraction (MF). Figure taken from Ramm *et al.,* 2022.

3.4.4 Glycosylation analysis

The glycosylation of the ORF8 protein was only slightly visible in the autoradiograph after a synthesis in the CHO system. The *Sf*21 system is known for its high capacity to form N-glycosylation[34]. Therefore, the Spike protein and the ORF8 were additionally synthesized in *Sf*21 to analyze the glycosylation of these proteins. The glycosylation of the full-length Spike protein was not detectable after a CHO synthesis, but an intense additional protein band could be detected in the *Sf*21 system (Figure 38 A). The additional protein band of ORF8 could also be confirmed in the *Sf*21 system. A further glycosidase digestion with PNGaseF and EndoH confirmed this glycosylation (Figure 38 B).

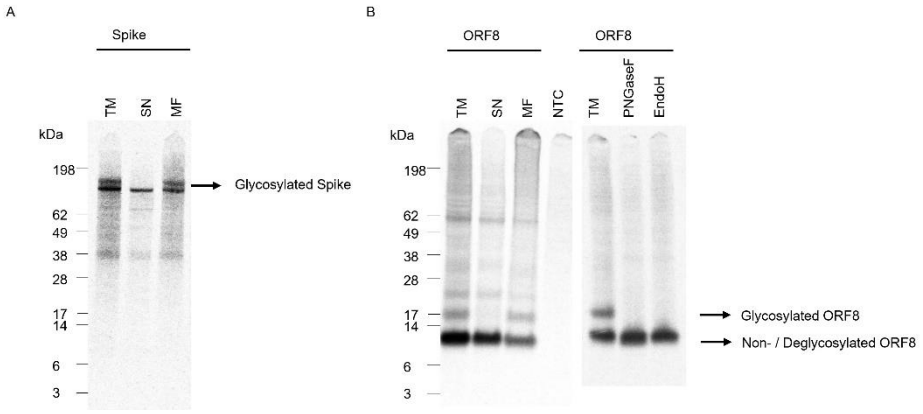

Figure 38: Glycosylation of full-length Spike and ORF8.
SARS-CoV2 Spike and ORF8 were synthesized in a batch-based *Sf*21 reaction. The translation mixture (TM) was separated into the soluble proteins in the supernatant (SN) and the microsomal fraction (MF). Qualitative analysis by autoradiography showing ^{14}C-leucine labelled proteins for (A) Spike protein and (B) ORF8.

3.4.5 Nucleocapsid protein for diagnostic used

The structural proteins are responsible for host cell targeting[213] and are main structures for diagnostic purposes[214]. Therefore, these proteins are generally used for first response mechanisms. The N protein was chosen to validate CFPS for the rapid detection of novel antigens, for testing antibodies and thus for providing cell-free synthesized antigens for diagnostic uses. The N protein as well as two early onset mutants (SER343, ASN202) were investigated. In a first step, an in-solution ELISA was performed. Therefore, the N protein was immobilized on Ni-NTA Magnetic Agarose Beads via the his tag. The N proteins were synthesized in a batch and in a 24 h CECF reaction based on CHO lysate. The ELISA showed that the WT and the mutants could be detected, but the mutant N proteins showed a higher detection after a CECF reaction (Figure 39 A). A further in-solution ELISA was performed where the three N proteins were synthesized in a CECF

reaction in the three eukaryotic lysates and two different concentrations were tested. These data showed that the detection worked very well for *Sf*21 and CHO synthesized N proteins, but was less efficient in K562 synthesized proteins (Supplementary Figure 23 A). In the second step, a quantitative dot blot analysis was performed. The N WT protein synthesized in a CHO lysate was blotted onto a nitrocellulose membrane at four different concentrations (15, 10, 5, 1 ng). These data showed that proteins at a concentration of 1 ng could already be detected (Figure 39 B). As SARS-CoV2 is a beta-coronavirus, it shares major similarities to SARS-CoV and MERS[215]. When a novel pathogen arises, established antibodies and antivirals against similar viral strains are tested for their efficacy. The detection of the N protein with an anti-SARS-CoV-2 N antibody (ABIN6953059) was compared to an anti-SARS N antibody (sc58193). A Western Blot analysis showed that the N proteins were detected by both antibodies. Further, cleavage products could be detected and a protein band at about 30 kDa in the WT and SER343 mutant but not in the ASN202 mutant was identified (Figure 39 C). The binding of the anti-SARS-CoV-2 N antibody (ABIN6953059) was further tested on the N protein synthesized in the three eukaryotic cell-free systems. No differences in the detection of the N protein could be detected between the different lysates (Supplementary Figure 23 B). These data highlight the efficiency of cell-free protein synthesis for the validation of antibodies detecting viral proteins.

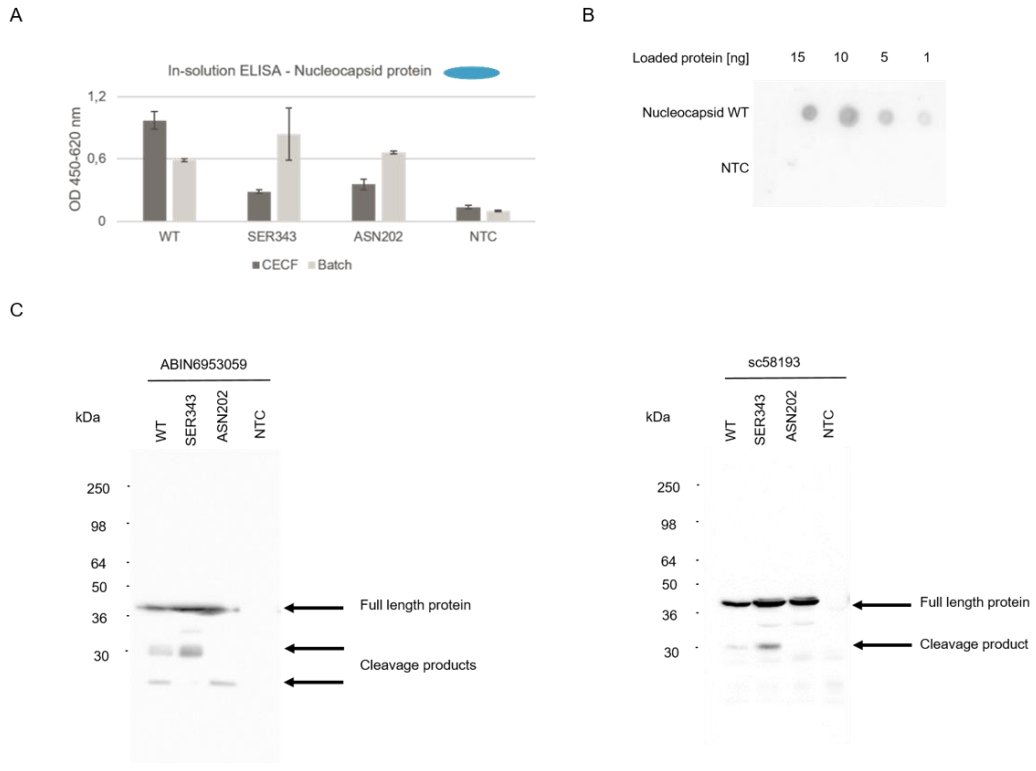

Figure 39: Detection of SARS-CoV2 N protein.

The N WT protein as well as both mutants (SER343 & ASN202) were synthesized in a CHO cell-free system. Detection of cell-free synthesized nucleocapsid protein in an in-solution ELISA (A), a Dot Blot (B) and Western Blots (C). Figure taken from Ramm *et al.,* 2022.

3.4.6 Cytotoxic behaviour of the envelope protein

Due to the similarity of the ORF4 / E from SARS-CoV2 to MERS and SARS-Cov, it can be assumed that the envelope protein is an ion channel[216]. Such ion channels can inflict toxic effects in the host. In cooperation with Dr. Srujan Dondapati (IZI-BB) the ORF4 / E was analyzed in planar lipid bilayer measurements. In order to allow for the stability of the pentameric assembly as well as to differentiate measured signals from endogenous proteins in the microsomal vesicles, a physiological buffer of 150 mM NaCl was chosen. Different types of signals could be detected. Cytotoxic events with large current levels of more than 50 pA were identified. Single channel activity could be detected in which the channel switched from open (5-7 pA) to closed states (Figure 40).

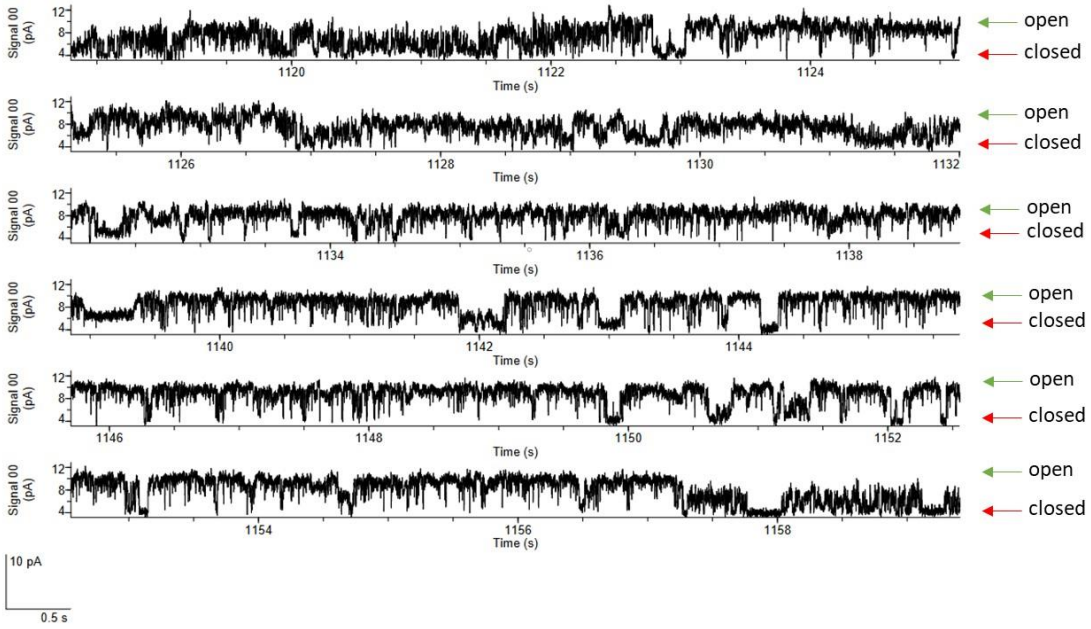

Figure 40: Single channel activity of ORF4 envelope protein.
Current recordings at +100 mV of the ORF4 envelope protein reconstituted into DPhPC bilayer. All measurements were done in the presence of 150 mM NaCl, 10 mM HEPES, pH 7.0 buffer (n = 5). Figure taken from Ramm *et al.,* 2022.

This single channel like activity could further develop to pore-like response with a stable current flow at 12-13 pA which was determined by the histogram (Figure 41). These data highlight the possibility to analyze functionally active channel-like viral proteins. This combination of CFPS with planar lipid bilayer techniques could be used to identify blockers as potential pharmaceuticals in future projects.

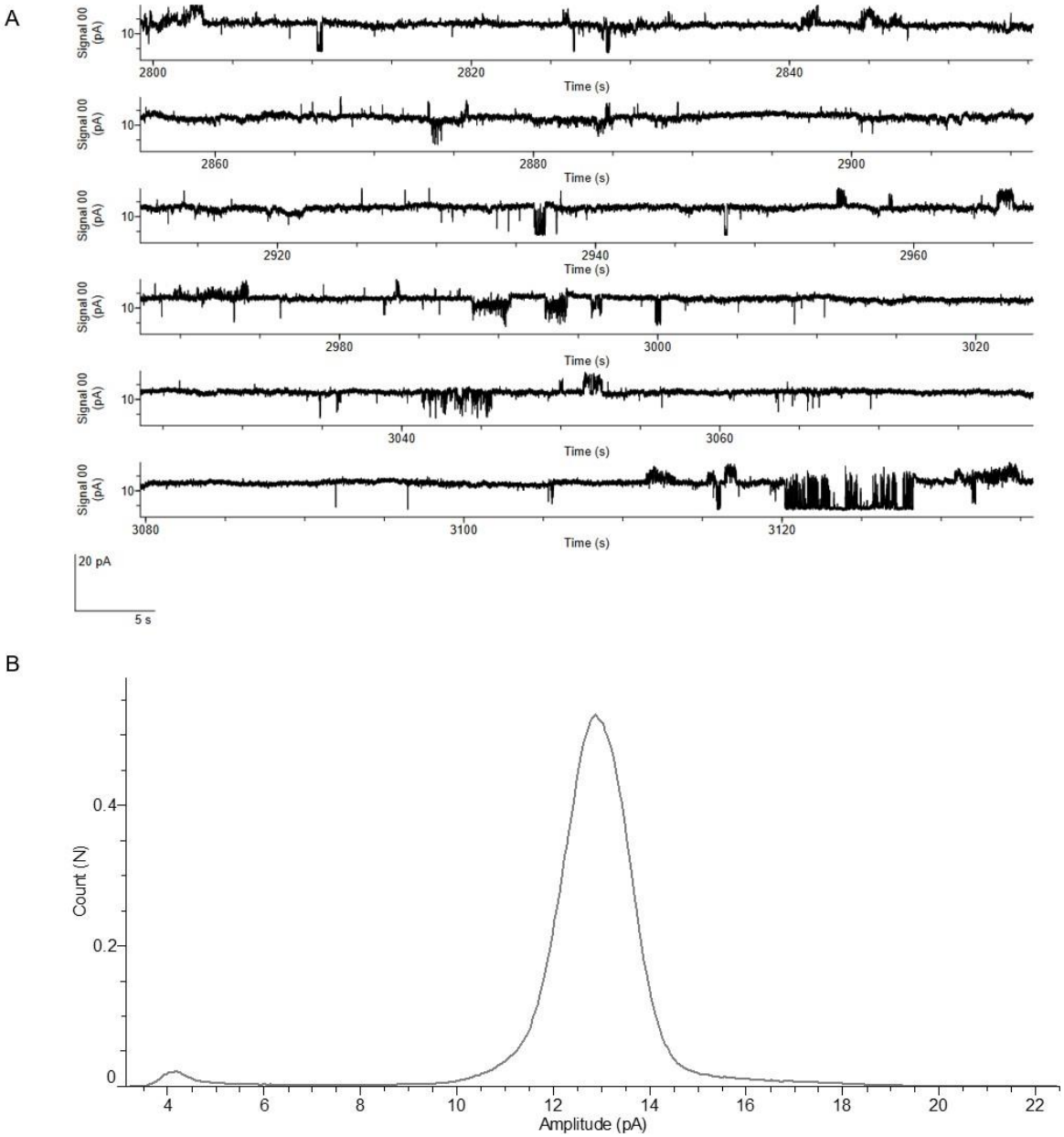

Figure 41: Pore-forming character of ORF4 envelope protein.
(A) Current recordings at +100 mV from the ORF4 reconstituted into DPhPC bilayer. (B) Histogram plotted from the current recordings showing the large peak at 13 pA indicating a stable pore. All measurements of ORF4 were done in the presence of 150 mM NaCl, 10 mM HEPES, pH 7.0 buffer (n = 5). Figure taken from Ramm *et al.,* 2022.

Taken together these data clearly show the necessity of cell-free protein synthesis for the in depth analysis of viral proteins. It was further demonstrated that cell-free synthesized viral proteins can be applied in diagnostic uses such as the validation of antibodies leading to a publication in 2022[217].

3.5 Summary

Summarizing the data acquired in this thesis, it can be said that a versatile set of toxins and cytotoxic viral proteins could be synthesized and functionally characterized. Three different eukaryotic cell-free systems, *Sf*21, CHO and K562, were used, indicating the diversity of eukaryotic cell-free systems that can be applied. Each system had its advantages and drawbacks. Multiple functionality assays were established for the cell-free synthesized proteins. Taken together the data gathered over the course of this thesis presented the synthesis, characterization, modification and application of PFTs, AB_5 toxins, RIPs and viral cytotoxins.

4 Discussion

In the field of toxicology, research and development is mainly focused on the identification of toxic substances and eventually counteracting them. Numerous toxic effects that have to be tackled are known to be caused by naturally occurring compounds from bacteria or even animals[2,25,160]. The mechanism of action of such proteins always triggers a toxic effect in the host. As toxins might be misused, the handling of toxins underlies strict regulations[6,218,219]. Nevertheless, in order to characterize the toxin and identify a potential inhibitor, the toxin itself has to be synthesized or extracted. In some cases modified toxins or only toxin fragments are used as the full-length toxic proteins cannot be expressed in living cells. This is mainly due to the damage to living cells but also due to high laboratory safety standards[1,13,18].

The aim of this thesis was to establish CFPS as an alternative to circumvent the toxic effects on the production system as well as to set up CFPS as a screening platform for toxins, in order to efficiently characterize them by identifying their mechanism of action as well as applying toxins for future developments in the field of diagnostics and therapeutics. Therefore, relevant classes of toxins as model proteins were identified, their cell-free protein synthesis was established, mechanisms of action were analyzed and proteins were functionally characterized. At last, the most promising candidates were used to identify potential applications for toxins. First results in this field of work were gathered since the early 1970s (see Table 1). Based on these findings the cell-free synthesis of hetero-multimeric toxins was established, a nanopore was identified, toxins were fluorescently labelled, a plant-derived targeted toxin was validated for its clinical relevance and cell-free protein synthesis was established as a rapid response system for viral pathogens.

4.1 Cell-free protein synthesis

Cell-free systems were originally developed in the early 1960s based on an idea by Matthaei and Nirenberg[19]. Until today CFPS has been established as a well acknowledged method for protein synthesis. Different lysates ranging from prokaryotic over fungal to mammalian systems have been set up[34,220]. These developments have led to the synthesis of versatile proteins such as antibodies[48,221], VLPS[102,104], membrane proteins[33,40,41,53] and glycoproteins[40,59]. Meanwhile, cell-free protein synthesis has even been used for the modification of proteins such as fluorescent proteins[222], glycoproteins[59,223], VLPs[106] and antibodies[60,224].

4.1.1 Cell-free synthesis of toxins

CFPS has come into focus for studying toxic and viral proteins in 1974[74] and 1963[91], respectively. Since then diverse toxic and viral proteins have been synthesized (see Table 1 and 1.2.1.4), but no general platform has been set up. As a result, one study even demonstrated that the toxin of interest, the U_2-sicaritoxin-Sdo1a from a snake venom, could not be synthesized[67]. As commercially available systems were used, this set up might not be focused on individual proteins but rather is a broad spectrum system. These data demonstrated the necessity of a robust and reproducible set up. This thesis has shown that a diversity of toxic proteins could be synthesized in an active form in eukaryotic cell-free systems. The synthesis of PFTs that perforate the membrane, AB_5 toxins targeting eukaryotic cellular pathways as well as ribosome inactivating proteins (RIPs) were synthesized and functionally characterized. Until this thesis, no study published the synthesis of a RIP which was synthesized in a cell-free system. Initial studies have been performed on subunits of the DT toxin which interacts with the translation elongation factor eEF2 and thus inhibiting protein translation, as well. Further, the diphtheria toxin (DT) consists of an A and B subunit similar to AB_5 toxins[225]. Murphy *et al.* could not detect an active protein[74] and Nicholls *et al.* demonstrated that a DT targeted toxin was not active, as well[71]. These data demonstrate that up until now a synthesis of a functional AB toxin or the synthesis of a translation inhibiting toxin was not possible in cell-free systems.

Several studies have successfully synthesized and characterized PFTs[26,72,77,83]. While the PFTs TDH and aHL only consist of one domain, leucocidin is a bicomponent toxin. A tripartite PFT has not been synthesized in a cell-free manner until this thesis. This clearly further demonstrates the need for a defined system to synthesize toxins in a cell-free manner.

4.1.2 Cell-free protein synthesis of viral proteins

In comparison to classical proteinaceous toxins, a larger amount of viral proteins has been synthesized in a cell-free manner. In general, studies have focused on the synthesis of single proteins such as viral proteases[92], non-structural polyproteins[93] or viral membrane proteins[94]. Newer studies concentrated on the synthesis of VLPs[99,100,103]. No study used CFPS to synthesize and characterize the proteins encoded in a complete virus gene. Two studies have used the wheat germ cell-free system to synthesize SARS-CoV2 proteins. In a preprint Fogeron *et al.* showed the synthesis of ORF7b and its multimerization[226]. Comparing the data acquired here in a CHO based system (Figure 37) with the wheat germ based findings, it can be said that both systems could synthesize the ORF7b in a reproducible manner and SDS stable multimers could be formed. A large study synthesized ORF3, ORF6, ORF7b, ORF8, ORF9, the E and M protein in a wheat germ

cell-free system. The data acquired in this thesis (see 3.4) further expanded the data gathered by Altincekic and colleagues who further purified the proteins and used them for NMR spectroscopy[227]. This thesis showed that the individual viral protein classes, namely structural as well as non-structural and accessory proteins, can be synthesized and functionally characterized using the same lysate.

Combining these facts, this thesis showed that eukaryotic cell-free systems can be applied to synthesize a variety of different proteinaceous toxins and viral cytotoxins by adjusting the synthesis parameters to the protein's individual need.

4.1.3 Functional characterization of cell-free synthesized toxins

A bottleneck in protein production is to ensure a high amount of active protein. A major challenge after *in vivo* protein production is the necessity to extract and purify the proteins from the cells. Over the course of this thesis diverse assays have been set up and it could be shown that the cell-free synthesized toxins can directly be used for downstream applications.

Toxins generally target specific cellular pathways and induce apoptosis[228]. A dose response of the toxin to the particular cell type can be initially evaluated when studying the morphology of the cells after supplementing the toxin of interest. Within this thesis, the response of cells to defined concentrations of Hbl (see 3.2.1), Ctx, LT (see 3.2.3) and Dianthin (see 3.3.1) has been studied. All four toxins induced characteristic morphological changes and apoptosis. Nonetheless, it was necessary to apply buffer and lysate controls in order to compare the cell confluency and the cell viability. A prior study by Orth *et al.* has already shown the feasibility of this assay for the apoptosis inducing toxin pierisin[54]. This assay thus allows for the identification of the incubation time needed for the toxin's effect on the cell and a potential concentration range can be defined. The cells can be observed over a large time frame. As this assay is just a qualitative manner of analysis, a quantification of the cells' viability had to be performed. The MTT assay is one of the most classical cell viability assays. A defined assay kit or just the chemical itself can be used to quantitatively define the toxic effect on the cell. Various parameters can be optimized. The cell number per well has to be defined, the incubation time within the certain steps and even the concentration of the MTT itself can be optimized[228]. Conditions such as the cell number have been optimized for the individual cell lines throughout this thesis (data not shown). Such a quantitative assay can be used for the screening of different concentrations as well as different toxin fragments or controls as was performed for Dianthin and its targeted variant Dianthin-EGF (see 3.3.1). The data acquired in this thesis also showed the compatibility of cell-free synthesized toxins with the MTT assay as low background values were observed. In future settings other assays detecting specific pathways such as ATP, protease or cAMP assays should be considered. In comparison to

the MTT assay the PI uptake assays showed interaction with the crude cell extract after Hbl synthesis (Figure 11). PI can bind DNA which results in a change in its excitation and emission. As it cannot passively cross the membrane, only perforated cells can be stained which facilitated PI as a staining and quantification tool for dead cells[229]. The interaction of PI with the cell-free mixture might be caused by endogenous nucleic acids within the lysate and untranslated template from the reaction. The CellTox CyGreen assay kit is based upon a similar reaction mode as the PI assay. Instead of the propidium iodide, a cyanine dye is used. Unfortunately, high background signals were detected when assessing the cytotoxic effect of the AB_5 toxin LT. When the modified LTB-Strep protein that was synthesized in *Sf*21 lysate was administered to CHO-K1 target cells, a high fluorescence signal was detected. That signal was even higher than the toxic multimer (Supplementary Figure 13). Interestingly, a better signal to noise ratio was present when using the modified CHO lysate that integrated the eAzFRS synthetase. Less background activity was monitored and an increased cytotoxicity could be detected for the Ctx holotoxin (Figure 26). A lower background noise might have also been derived as less template was used in these reactions. In general, a protein purification might be needed to accurately quantify the toxin's effect on the cells using the PI uptake assay and the CellTox CyGreen assay.

PFTs have been widely studied and therefore various techniques for their functional assessment are possible. A fast and easy alternative to the PI assay are blood agar plates. Most PFTs are able to induce hemolytic activity which can be visualized in these blood agar plates after the erythrocytes have been lysed[230]. A quantification of the toxin's activity cannot be undertaken, but the initial testing for toxicity might indicate a pore-forming character of the protein. After this preliminary testing, a precise characterization of the pore-formation can be performed using planar lipid bilayer measurements as was done for Nhe and CytK (Figure 15 and Figure 17). The opened and closed state as well as the identification of blockings in the presence of PEG molecules for example is possible which allows the precise characterization of the pore[231]. Data on Nhe, CytK and the SARS-CoV2 envelope protein showed that PFTs and cytotoxic viral proteins can be characterized by electrophysiological measurements. Prior studies have assessed cell-free synthesized ion channels and pore-forming proteins[84,232]. Hence, the data gained in this thesis underlined the combination of CFPS with planar lipid bilayer measurements which could allow for screening of pharmaceuticals in future studies.

In general, no prior purification of the protein is needed when using eukaryotic cell-free systems, but if an assay such as PI uptake assay is used, a purification might be useful. Bechlars *et al.* demonstrated that the position of a purification tag can alter the toxins

activity[26] suggesting that a tag has to be tested for each individual toxic protein. During a purification various buffers are used and final elution steps might need the use of chemicals such as imidazole or boiling such as for polyhistidine tags[233]. These factors might lead to a reduced functionality of the proteins of interest. No purification steps were performed in this thesis and the only assay type interacting with reaction components of CFPS was the class of membrane integrity assays such as the PI uptake assay. In prior studies a PURE system for the prokaryotic cell-free system has been established[35]. This system uses purified and modified components in order to reduce the background noise. The PI and CellTox CyGreen assay could be tested in the presence of proteins synthesized in such a PURE system which could improve the overall assay results. Nonetheless, these data demonstrated that, in general, toxic proteins synthesized in eukaryotic cell-free systems can directly be applied for functionality assays thereby facilitating the use of CFPS for the further application of toxins.

4.2 Diagnostic use of toxins

Potential applications of CFPS might be identified in the field of diagnostics. As a first step, the toxin of interest has to be detected. A variety of methods, such as biological and immunological assays as well as mass spectrometry, is used for the detection and quantification of toxins in various samples[109,234,235]. Samples such as hair, blood, urine or stool are used for the determination of pollutants and food-borne intoxications by using diverse immunological assays[140,109,141]. Intoxications with marine toxins after seafood consumption and intoxications with venoms from e.g. spiders or snakes still cause major health care and diagnostic challenges. A fast and efficient response with an antitoxin is necessary but the diagnosis can be time consuming[236–238]. In some cases the proteinaceous toxin is well characterized and studied. Commercially available detection kits are present for such well-known and well-characterized pathogens and their underlying toxins such as the Duopath™ assay for *B. cereus* used in this thesis, as well. It was shown that the Duopath™ assay could detect Nhe[79] and Hbl (data not shown) indicating the possibility of CFPS for providing antigens in the production pipeline of detection assays. This assay is a typical lateral flow assay for the detection of pathogens in food. The L_2 subunit of Hbl and the NheB subunit are detected by monoclonal antibodies[239]. As the cell-free synthesized proteins induced a positive result on the assays, this indicates a correct folding of the applied toxins. Thus, these data validate CFPS for the synthesis of toxins for diagnostic applications.

A prerequisite for such assays are molecules that recognize the toxin[108], and therefore, the toxin itself or fragments of it, have to be available in the production pipeline. The data gathered in this thesis demonstrate that a versatile set of toxins and viral proteins from

diverse pathogens could be synthesized in a reproducible manner. Therefore, cell-free synthesized proteins might be used as antigens for the generation of antibodies. In case of highly toxic proteins, non-toxic mutants could be generated for such a cause in order to prevent the host animal from dying after an immunization. The growing number of pathogens including bacteria and viruses as well as growing numbers of mutants impairs the availability of suitable detection assays. In such cases the detection of pathogens is performed by PCR technologies as also used during the SARS-CoV2 pandemic[240,241]. Novel systems to produce and characterize the individual toxins are necessary to develop new detection and characterization technologies.

4.2.1 Mechanism of action analysis

A further step in characterizing the toxin is the precise analysis of the mechanism of action of the respective toxin and whether variants might be able to act differently[111].

The exact number of bacterial species and strains is unclear, but it is estimated that there are about 30,000 different species[242]. Various bacterial strains encode toxin classes such as AB toxins, heat-stable toxins, superantigens or PFTs[2,243]. All of these individual bacterial toxins have different mechanisms of action, which makes it more difficult to analyze them in one specific system. Cell-free systems allow for the syntheses of versatile toxin classes which speeds up the production pipeline. In order to analyze whether cell-free synthesized multicomponent bacterial toxins are functional and can be studied in detail, the two tripartite toxins Hbl and Nhe from *B. cereus* were chosen. The *B. cereus* group itself encodes various toxins such as hemolysins, phospholipases or the anthrax toxin. A major class of toxins from *B. cereus* are PFTs that penetrate the cell membrane and trigger cell death[112,113]. The general mechanism how the multimeric structure of PFTs are formed is understood, but the detailed processes including pre-pore formation are not yet fully described. The synthesis and characterization of the bacterial toxins Hbl and Nhe has been performed in eukaryotic cell-free systems. In case of PFTs the accessibility of endogenous membranous structures[34,59] might additionally be favorable for the embedding and multimerization of the toxin. The data presented here show the reproducible synthesis of Hbl and Nhe in eukaryotic cell-free systems. Both toxins consist of three individual subunits. This offers a wide range of analyses such as toxicity assessments in its complex form as well as by using its individual subunits.

Looking at the soluble Hbl enterotoxin, the cell-free synthesized subunits were mainly found in the SN fraction (Figure 10), which indicates that the binding receptors of Hbl are not present in the microsomal vesicles. The initial testing of hemolytic activity on 5% sheep blood agar plates showed that the MF still harboured functionally active Hbl protein (Figure 10 C). Prior studies have demonstrated that the B component targets cell

surfaces[125,126]. It is also suggested that Hbl targets LPS-Induced TNF-α Factor and the cell death inducing p53 target 1[244]. A proteinase K digestion, which digests the fragments on the outside of the membrane, showed that the B component interacts with the microsomal vesicles in the cell-free system (Ramm *et al.,* 2021). The Human protein Atlas does not clearly indicate that Hbl's cell targets are present in the ER thus indicating a wider targeting range of Hbl than suspected before. As these cell targeting structures might be missing from the microsomal vesicles, an enrichment on the vesicular surface might not be possible which would explain the lower protein yields in the MF (Figure 10).

When individual subunits were spotted onto the agar plate no hemolytic effects could be detected. Strikingly, when the L_1 component was in close proximity to the co-expressed B-L_2 components, a crescent shaped zone occurred (Figure 10 D). This phenomenon has been shown before by Beecher and colleagues in 1990[245]. A diffusion of the individual subunits towards each other might be a potential explanation for this phenomenon. These findings implied an unknown subunit interaction. Due to the open character of CFPS the individual subunit concentrations could individually be adapted and thus a comparison of the molar plasmid ratio with the molar protein ratio, when subunits were individually synthesized and mixed afterwards, could be performed. Various concentration ratios were chosen and each individual subunit was overexpressed in order to investigate the influence of the single subunits on the whole Hbl complex (Supplementary Figure 6). After a co-expression of all subunits, less intense hemolytic activity was confirmed for ratios of 1:10:10, 1:10:1 and 1:1:10 ($B:L_2:L_1$). When subunits were mixed together after the synthesis protein ratios of 1:10:1 and 1:1:10 resulted in no activity. These data indicated that an excess of the soluble subunits can inhibit the functional activity. As blood agar plates are only a qualitative analytical method, quantitative analyses should further be performed by using precise numbers of soluble erythrocytes. Prior studies have already confirmed that an excess of L_1 inhibits the hemolytic activity of the complex[124] and slows the pore-forming process[203]. Unfortunately, Beecher and colleagues also showed that an excess of the B component hinders the activity of the L_1 component[124]. Such findings were not obtained in this thesis, which further implies the use of other hemolysis assays. Beecher *et al*. as well as other studies determining hemolytic effects on toxins perform quantitative hemolysis assays with defined numbers of erythrocytes[124]. Thus, the 50% hemolytic units can be calculated[246]. Using a defined concentration of red blood cells might also allow real time measurements of hemolytic effects. Future studies evaluating hemolytic toxins should focus on establishing such an assay for cell-free synthesized proteins.

The subunit interactions of Hbl have been widely discussed in the past. Initially, it was shown that the addition of the B component to erythrocytes after the soluble lytic

components did not induce hemolysis[245]. Hence, a sequential binding order of B followed by L_1 and L_2 at last was presented in 2013[127]. Later on, pre-complex formation was identified for B and L_1 as well as for both lytic components[129]. This thesis attempted to add information on these previous finding. It could be shown that the complex formations was not hindered when the subunits were mixed together after the synthesis in several steps by incubation steps on ice (Ramm *et al.,* 2021). This suggested that a sequential binding order might only be valid, if a targeting surface is available. In a next step, the membrane integrity of the pore was studied on Caco2 target cells. The PI uptake assay and morphological analysis indicated cytotoxic effects of the Hbl complex (Supplementary Figure 3 and Figure 12). Jessberger *et al.* showed cytotoxic effects of the Hbl complex on Vero cells[203] that are in line with the findings presented here. They further detected a concentration dependent activity and 50% inhibition at 0.3 nM[203]. An IC_{50} was not calculated as the viability of cells was not determined, but the data gathered here showed toxic effects at 0.25 nM (Supplementary Figure 3). This might suggest a similar activity pattern of cell-free synthesized Hbl, especially considering that 2.5 nM of the SN and 0.25 nM of the MF complex led to complete cell death after 4 h (Figure 12). In contrast to Jessberger and colleagues the data from this thesis showed that individual subunits and particularly two co-expressed subunits, led to an increase in RLU (Figure 11). With increasing protein concentrations applied in the assay, higher background values were detected as described above (see 4.1.3) Thus, the PI uptake assay showed that it is only applicable at lower concentrations of cell-free synthesized proteins, or otherwise purified samples should be applied. Nonetheless, the L_1-L_2 co-expressed sample did not only show higher RLU values, but also induced a reduced cell confluence in comparison to NTC and untreated samples (Figure 11 and Figure 12). This indicates an interaction with the target cells and a possible pre-pore formation of the lytic compounds which are comparable to finding from Tausch and colleagues[129]. Pre-pore formations are frequently observed in PFT as an enrichment of the protein at the target site leads to multimerization and pre-pore complexes[118]. A pre-pore assembly has already been detected for Perfringolysin, CylA and even Nhe[118,247,248], hence a pre-pore complex of Hbl is likely and should be further characterized as by structural analyses.

The pore-forming character and its pre-pore complex of Nhe has been widely discussed as Nhe is the most prominent enterotoxin in *B. cereus*[119]. Initial reports have implied that all subunits are necessary for the formation of the Nhe complex. Interestingly, early studies could not show hemolytic activity[120,121]. Hemolytic activity could be seen on 5% sheep blood agar plates in this thesis (Figure 13), but the lytic activity was not comparable to Hbl which induced intense lytic rings. In 2008, Fagerlund *et al.* also demonstrated Nhe's lytic activity and linked this to the formation of pores[122]. To further show the pore-

formation, planar lipid bilayer measurements were conducted here. Current responses of 800 pA could be detected for the complex. Single channel activity was seen with transitions between two current levels (Figure 15), which is typical for cytolysin-like pores and has been observed for Nhe before[122,248]. Current jumps after the insertion of the tripartite complex were determined[79,139]. Smaller conductance values could indicate partially formed pores. It was shown that an interaction of NheB and NheC takes place before NheA is recruited[123,249] and the presence of partially formed pores was described[247,248]. Thus, the data acquired in this thesis underline the potential pre-pore complex of the *B. cereus* protein.

In 2004, Lindbäck and colleagues also identified that a molar subunit ratio of 10:10:1 (NheA:NheB:NheC) induced the maximum toxicity on Vero cells[121]. In cell-free systems the supplementation of Nhe at molar plasmid ratios of 10:10:2.1 resulted in inactive complexes. A molar plasmid ratio for NheC of 2 was determined as a threshold to induce toxic effects (Supplementary Figure 6). It could also be detected that Nhe did not induce lytic effects in the MF (Figure 13), which suggests that Nhe did not bind to the microsomal vesicles as the needed receptors are not present. It is still unclear which specific receptor on the plasma membrane is targeted by Nhe, but it could be shown that death receptors in the Fas-mediated apoptosis were triggered by Nhe and were dependent on p38-MAP kinase[250].

In prior studies, toxic effects of Nhe were generally assessed based on bacterial culture supernatants or purified single subunits, therefore limited data on initial toxic concentrations and IC_{50} values of Nhe are available. Nhe's hemolytic activity was assessed by comparing culture supernatants containing Nhe with cell-free synthesized Nhe. It was shown that cell-free synthesized Nhe at a concentration of 10 µg/mL was equally active to 7 µL culture supernatant (Supplementary Figure 7). As the blood agar plates are only a qualitative activity measure and as the concentration of Nhe in the culture supernatant could not be determined, it can only be said that the cell-free synthesized protein is comparable to bacterial expressions. Prior studies have studied the effect of Nhe by PI cell staining and potential PI influx[122,250]. Lindbäck and colleagues further suggested that 1 nM Nhe was the minimal concentration needed for the toxicity and thus inhibited 69% of protein synthesis in Vero cells[121]. In their study, the rate of protein synthesis was measured as the ability of the Vero cells to incorporate radioactively labelled leucine for protein synthesis analyzed by subsequent TCA precipitation. The data gathered in this thesis focused on the detection of the cell viability as detected by the MTT assay in order to assess the toxic concentrations of Nhe. Sometimes limited data on the toxicity of a toxin itself are available. Using cell-free systems it was possible to determine that even 0.32 nM of Nhe induced 50% cell death, identifying a toxicity range of Nhe for

the first time. IC_{50} values between 0.32 and 0.46 nM could be calculated for CECF and batch-based reactions, respectively. These data indicate that measuring the cell viability is a more sensitive tool to assess the lethal toxicity while determining the protein synthesis rate might be a tool to identify initial toxic effects before cell death occurs. Interestingly, Nhe synthesized in a CECF reaction resulted in higher toxicities. This might indicate that the assembly of the individual subunits was potentially more stable than in a batch reaction. These data indicate that a longer synthesis time is required for the assembly of the complex. In a prior study it was shown that a CECF reaction resulted in an 31 fold higher amount of an active single chain fragment variable antibody fragment[42] which underlines the possibility of a prolonged assembly time. Further multicomponent structures should be analyzed in both batch and CECF reactions.

The findings on these two tripartite PFTs showed that it is possible to synthesize multicomponent PFTs and analyze their characteristics, but it is essential to identify the ideal synthesis and assay conditions. Diverse activity assays could be performed and showed that cell-free synthesized Hbl was as active as Hbl expressed in bacterial cultures. In this thesis an IC_{50} value for the activity of Nhe could be determined and identified the toxicity on the cell viability rather than on the protein synthesis within the cell. Combining CFPS with defined analytical procedures can be used to establish a stepwise approach for studying the mechanisms of toxins. As the receptor binding domains on the plasma membrane are still fully identified, cell-free synthesized toxins could be used for the in depth analysis of the toxin's cell target. As seen in this thesis, only low amounts of protein are necessary to trigger initial toxic effects. This will allow to assess the targets without killing the cells and offers a fast and cost-efficient alternative to *in vivo* expressed toxin subunits.

4.2.2 Tracking systems

The precise mechanism of action could help to tackle the toxic effect of the pathogen early on. Biomonitoring of pollutants is done with samples of hair, blood or urine[140], but as proteinaceous toxins and viral cytotoxins trigger diverse mechanisms in the human body and might be further processed, such routine testing is not possible. In several cases the localization of the toxin within the cell and its intracellular pathways are unclear. Fluorescently labelled toxins are useful for that matter and speed up the characterization of the toxin's pathway. Several studies have tested fluorescently labelled toxins by using fusion proteins with fluorescent proteins[251], enzymatic labelling[144] and chemical labelling[142]. In a first attempt in this thesis, Nhe was statistically labelled with BODIPY-TMR-Lysine (Figure 13 D). Prior studies have used this approach to label antibody fragments[252], membrane proteins[253] and even the cytotoxic protein pierisin[80]. Random

labelling always faces the fact that the preloaded amino acid is in competition with the natural amino acid. Hence, it is not known how many positions are labelled which could result in varying fluorescence signals. Therefore, random labelling is suitable for initial testing of fluorescent labels but site-specific labels should be used for further applications.

4.2.2.1 Cell-free synthesis of AB_5 toxins

The two AB_5 toxins Ctx and LT were used as model proteins for applying different labelling techniques. The cell-free synthesis and modification of these two complexes and their individual subunits has been established. These two toxins are prokaryotic toxins and thus prior studies have focused on their synthesis in prokaryotic cell-based systems[147,154,254]. Eukaryotic cell-free systems were chosen because the formation of disulfide bridges is essential for the toxins' functionalities as the A subunit is cleaved to A1 and A2 fragments which are linked via disulfide bridge afterwards[147]. *Sf*21 and CHO based cell-free systems are known to provide PTMs such as disulfide bridges[42,220], while the supplementation of a redox system is necessary in prokaryotic cell-free systems[34,220,255,256]. Only single studies have presented the complete holotoxin formation in SDS-PAGEs. Jobling and colleagues could show an AB_5 formation. The toxins were overexpressed in *E. coli* and purified by various chromatographic purification steps[257]. At last, an anion exchange was performed. Here, a complete holotoxin formation could not be detected in the autoradiograph but few multimerizations such as for CtxB were seen (Figure 21). The multimerization of the B subunits has been studied intensively in the past and studies demonstrated that the pentameric ring formation was observed at concentrations of up to 35 µM and it was further shown that the pH influences the multimerization of the B subunit with a complete pentamer at a pH of 6[207]. Unfortunately, loading higher reaction volumes onto the gel showed an overcrowded SDS-PAGE while changing the pH of the reaction buffer did not result in any changes of the multimerization pattern (data not shown). These data suggest that future studies on multimeric proteins should analyze the complex formation after intensive purification steps and buffer exchanges as demonstrated by Jobling and colleagues. Before modifying the individual subunits, the functionality of the individual toxins had to be confirmed as the holotoxin formation could not be detected via autoradiography. This was performed here and by Jack 2020[206] and indicated that after 24 h characteristic elongated CHO-K1 target cells could be detected which aligns with previous studies[154,258]. Concentration dependent apoptotic effects of the cell-free synthesized toxins could be detected after 48 h when subunits were co-expressed, but not when they were synthesized individually and mixed afterwards (Ramm *et al.*, 2022). These findings underlined the necessity of the disulfide bridging for the presence of a functional AB_5 toxin. As disulfide bridging takes place within the ER derived vesicles in the cell-free system, a signal peptide that translocated the proteins was necessary. It was

shown that the Mel signal peptide increases the amount of secreted proteins[259] and also increases the protein yield in cell-free systems[252]. Therefore, the Mel signal peptide was used for these proteins and proved to efficiently translocate the toxins into the microsomal vesicles. As the Mel signal peptide derives from the honey bee venom[259], it can be assumed that signal peptides from toxic proteins are very efficient for protein translocation. Future studies should therefore also study other signal peptides from toxins and their compatibility with CFPS.

4.2.2.2 Fluorescent labelling of fusion proteins

The presence of functionally active AB_5 toxins allowed for the modification of the individual subunits. Prior studies have focused on fusion-toxins that harbor a fluorescent tag such as an eYFP. Such a fluorescent tag enlarges the protein immensely. Even though the eYFP was twice the size of LTB a co-translational translocation was still possible (Figure 22). Ctx and LT fusion proteins and conjugated subunits have already been studied and did neither impair subunit assembly nor impair the ability to target the cells[251,260]. In order to show a conjugation approach, a fusion protein of the LTB subunit with streptavidin was used to couple the subunit with a biotin labelled fluorophore (Figure 22). Major side bands could be detected which implied that a further purification might be needed to reduce the background signal in the in-gel fluorescence and specifically identify labelled proteins. Streptavidin-biotin linkages are strong and no further supplementation of chemicals are necessary, which accelerates the coupling process[261]. A major advantage of a streptavidin-biotin system is the versatility of the fluorophores or payloads that could be applied. Diverse conjugates can be coupled to a single underlying protein. The LTB-Strep molecule used here might not only be clicked to a biotin labelled fluorophore but also to a toxic payload and could therefore be used as Trojan horse application. Trojan horse application have been studied in various combinations and are generally used as drug delivery applications. A typical approach of drug delivery targets are used for a potential treatment of cancerous cells. The tetanus toxin C fragment was conjugated to nanoparticles that were used to target neurons and selectively targeted neuroblastoma cells[262]. There has been extensive research of AB_5 proteins as carrier molecules. The LTB subunit has been analyzed to deliver protein cargos. Subunits containing shortened A2 subunits as a linker were identified and even linked to fluorescent proteins. This study even showed the internalization of the cargo into CHO-K1 target cells[263]. Thus, using a cell-free synthesized LTB as a drug-delivery molecule will be the next step in protein engineering of cell-free synthesized toxins, but such fusion proteins are only addressable at the N- or C-terminus of a target protein. The assembly of multicomponent toxins might be hindered by modifying the N- or C-terminus. Bechlars *et al.* have shown that the addition of tags could alter the toxicity of the PFT TDH[26]. As discussed, the fusion of Ctx

and LT to fluorescent proteins has been studied before and no negative effects on the proteins' functionalities could be seen[251,260]. In 2005, the C-terminal fragment of the tetanus toxin was fused to the green fluorescent protein and even tracked within the target cell[264], suggesting the potential intracellular trafficking of labelled toxins. In this study, subunits of the Ctx and LT toxins were modified and labelled. Before modifying the CtxA and LTB subunit only minor differences between the functional activity of Ctx and LT could be detected. 5 nM Ctx induced complete cell death of CHO-K1 target cells, while 6 nM of LT induced similar results as shown here and by Jack 2020[206]. Studies comparing both toxins have shown that Ctx is more potent than LT and forms more stable holotoxins[155,265,266]. Strikingly, the multimeric B ring of LT was more resistant to external factors[207]. The data gathered here, showed that cell-free synthesized LT with the modified LTB-Strep molecule reduced the holotoxins toxicity (Figure 23). This might indicate that the modified holotoxin was not as stable as the WT holotoxin. As five B subunits multimerize, five individual Strep molecules will be present in the in the holotoxin. This modification of the LTB subunit might have led to a less stable B subunit multimerization. As LTA is already less potent than CtxA, the reduced holotoxin will have led to a further decrease in the toxicity.

4.2.2.3 Site-directed labelling of toxic proteins

A possible alternative to fusion proteins are site-specifically modified proteins when using bio-orthogonal systems. Orthogonal systems have been widely applied in diverse scientific fields. Prior studies have shown that full-length antibodies as well as antibody fragments were coupled with radiolabels and injected into mice for tracing tumors in xenograft models[267]. Apart from such diagnostic applications, orthogonal systems can be helpful to modify biomolecules. Such an approach was already shown for glycoengineering of erythropoietin using cell-free systems. Zemella *et al.* showed that cell-free synthesized erythropoietin that incorporated either AzF or pPa could be chemo-selectively labeled and modified[59]. As this study showed, CFPS has become a major field for the development and application of orthogonal systems in the fields of glycoproteins[59], membrane proteins[41] or antibody-drug conjugates[60]. Zimmermann *et al.* further showed that the cell-free synthesized antibody Trastuzumab conjugated to monomethyl auristatin, which is a drug for tumor therapy, was functionally active at effective concentrations of 50% inhibition of cells between 0.043 to 0.071 nM[60]. This potency was similar to prior studies using random labelling. Thus, the activity of constructs modified by orthogonal systems was not reduced.

The basis for an efficient orthogonal system is a high incorporation efficiency of the ncAA. The codon sequence surrounding the amber stop codon plays a major role in that matter. The highest incorporation efficiency in human 293 cell tissue culture was achieved when a

cytosine was present at a +4 position to the amber codon[268]. Apart from that, synthesis optimizations as also performed during this thesis, can also increase the incorporation of ncAAs. Schloßhauer and colleagues also showed that novel cell-free systems which partially integrate the orthogonal system can be developed using CRISPR/Cas technology. This technique allowed for the stable integration of the eAzFRS into the CHO lysate and the subsequent synthesis and modification of the adenosine A2a receptor[197]. Combining the CRISPR/Cas technology with the open system used in cell-free protein synthesis will additionally help to develop and screen pharmaceutically relevant proteins such as the adenosine A2a receptor. In order to effectively apply an orthogonal system, the systems advantages and drawbacks have to be taken into account. Even though copper-catalyzed click reactions have been used for almost 20 years now[269], the formation of copper(I) ions can lead to toxic effects in cell-based downstream applications. The formation of reactive oxygen species could eventually lead to cell death[209]. Thus, alternative strategies such as Staudinger ligation need to considered in case a cell-based assay is needed to validate the modified protein of interest.

The modification of toxins by orthogonal systems and their potential applications have already been presented. A study showed the incorporation of ncAAs into microcystins which were labelled using copper-catalyzed click reactions. These labelled microcystins were clicked in living cells and further detected[142]. Hence, implementing orthogonal system for toxin research is a promising step for future research including intracellular trafficking studies. In another study the B subunit of the Shiga toxin, another AB_5 toxin, was linked to the chemotherapeutic substances doxorubicin and monomethyl auristatin F using a bifunctional linker in a copper-free azide click-reaction. This study further assessed the cytotoxic activity of these potential cancer therapeutics on colorectal cancer cells. The Shiga B subunit in combination with doxorubicin led to an IC_{50} of 22.5 nM as compared to an IC_{50} of 84.8 nM when administering doxorubicin alone[270]. This shows that a targeted effect could be detected and orthogonal systems allowed for a reduction in the critical concentration of the drug needed to inhibit the colorectal cancer cell line. If such an approach could be further developed for clinical studies, patients would benefit from a lower treatment concentration. Thus, the modification of toxins using orthogonal systems should further be evaluated and applied for toxin modifications as well as the development of targeted therapies. CFPS could favor these developments.

This thesis assessed the possibility for the application of orthogonal systems on cell-free synthesized toxins using CtxA as a model protein. It could be shown that both pPa and AzF could be incorporated and later on the protein was fluorescently labelled using copper catalyzed click reaction as well as the copper-free Staudinger ligation (Figure 25). After the successful establishment of the site-directed modification of CtxA, the functional

activity of the modified subunit was investigated. As expected, the CtxA amber mutants did not induce any toxic effects on the CHO-K1 target cells because the amber codon was situated within the catalytic center of the subunit (Figure 26). The E112 position has already been studied and modified in the past. Mutations at this site demonstrated non-toxic variants which could be used for further applications such as adjuvant therapies[271]. The data gathered here proved that a single mutation in the active center impaired the toxicity of Ctx.

The data gathered here identified CFPS as a promising methodological approach for the modification and fluorescent labelling of AB_5 toxin subunits. The findings presented here imply that these set ups cannot only be transferred to each individual AB_5 toxin but also to any other proteinaceous toxin. Mutational studies as presented for the CtxA subunit might be applied for screening and identifying potential toxic domains because the amber stop codon can be inserted at any desired position in the gene. Labelling of toxins using bio-orthogonal systems, fusion proteins or biotin-streptavidin bindings will help to further investigate the mechanisms of action of the toxin of interest and facilitate intracellular trafficking in the future, especially by using pH sensitive dyes. A further downstream application of these modified toxins will be the development of Trojan horses and targeted toxins for the therapeutic use. Implementing CFPS will be a driving force for development of these products.

4.2.3 Nanopore development

An application where a toxin itself is used as a downstream product for diagnostic purposes, is the biological nanopore. PFTs and their characteristic structure are the basis of biological nanopores which are used for various applications such as sequencing, detection of molecules or studying enzymatic processes[130,131,272,273]. The best-studied nanopore is aHL. It has been studied as a nanopore for the last decades and nucleic acid sequencing, immunodetection using antibodies or aptamers as well as biomolecule discriminations have been performed[133,274,275].

Various studies have shown the similarity of CytK to aHL[136], which suggested that CytK could be a candidate for the development of a biological nanopore. The two variants CytK1 and CytK2 share a sequence identity of about 89%, but CytK1 is said to be more toxic and to induce higher conductance values in planar lipid bilayer measurements[139]. This already indicated that even small changes in the underlying amino acid sequence of the protein can alter its functionality. CytK is a classical beta-barrel, mono-heptameric, pore-forming protein[135]. Some studies have attempted to visualize the multimers in SDS-PAGEs. Hardy *et al.* has detected the multimers and showed that they are SDS stable but are not present after boiling for 5 min[137]. A further study showed that the multimers were

present in the bacterial isolate but not after further purification steps[139]. A defined set up of diverse SDS-PAGEs could separate the different multimers on the gels and could assign the potential multimers[204], which suggested the multimer formation was possible in using eukaryotic cell-free system. Thus, the higher molecular weight bands shown in Figure 16 can be declared as multimers. A more detailed analysis would be beneficial to determine the individual protein bands in the SDS-PAGEs. Individual protein bands should be isolated from the gels and analyzed using native mass spectrometry. As this has not been done before with CytK, an ideal set up had to be identified where the multimers remain stable. This process would further help to elucidate the structure of CytK. In 2000, Lund and colleagues predicted that hexamers and heptamers are the membrane-damaging units in similar PFTs like Leucocidin and aHL. Due to CytK's high similarity to aHL, the heptameric form could be essential for the pore-forming character[136]. The pore-forming character is best-described in planar lipid bilayer studies. In prior studies it could already be shown that stable pores were formed in planar lipid bilayers and higher conductance was detected when using KCl buffers compared to NaCl buffers[137]. Fagerlund *et al.* studied the difference between CytK1 and CytK2 and found that 75% of CytK1 pores had a higher conductance than 100 pS while CytK2 generally showed a conductance of less than 100 pS in a 250 mM NaCl buffer containing 5 mM HEPES[139].

Studies on nanopores have shown that the pore's shape and size determine the further use of the nanopore. Conical shaped pores were found to be more sensitive for DNA sequencing in comparison to cylindrical shaped pores[276]. In order to modify the diameter of the pore, point mutations are generally used[277,278]. A position of the mutation has to be chosen carefully so that no loss of function occurs. In 2019, aHL was used as a nanopore to discriminate between microcystins. Point mutations in the pore facilitated the analysis of the molecule's dwell time within the pore and the blocking of the ion current[133]. Therefore, CytK mutants were designed to potentially develop altered pores. The CytK mutants were generally designed to target secondary structures that could be responsible for multimerization based on similarities to aHL[204]. The data acquired here and in the work by Danny Kaser showed that no loss of hemolytic activity could be detected and electrophysiological recordings were possible for CytK1 (Table 11 and Figure 19). Walker *et al.* modified aHL and indicated that mutations which led to a lack of multimerization ultimately resulted in a lower activity of the protein[279]. In aHL this was particularly shown for N-terminal regions[279,280]. Due to the high similarity of CytK to aHL, the Q13S mutant was expected to show a reduced hemolytic activity and potentially a reduced pore-forming character. This study could not detect such a phenomenon for the CytK1-Q13S and CytK2-Q13S mutant. Generally, CytK2 mutants induced stronger effects on the protein's functionality. Especially CytK2 variants D191del and V91G presented a reduced hemolytic

activity which further showed a decreased activity in planar lipid bilayers (Table 11). Therefore, the mutations in CytK2 might have hindered the formation of the multimer. These results suggested a higher stability of the CytK1 heptamer in comparison to the CytK2 variant. Hence, CytK1 and its variants were further analyzed.

Initially, the mutant CytK1-I91G showed lower conductance values, which could either indicate a smaller pore size or an unfinished multimerization and potential pre-states. A pre-pore formation was implied for aHL that also showed low conductance values[280]. It was suggested that the stem of the aHL mutant pore differed from the WT and ultimately showed no hemolytic activity. If a structure of the CytK1 mutants would be determined, an effect on the stem of the CytK1-I91G protein could also be verified even though hemolytic activity was still present for this CytK mutant. The CytK1-I91G mutant further showed a changed band pattern in the autoradiograph (Table 11 and Kaser 2020 & 2021[204,205]), which supported the theory of a pore that is not fully formed. In early studies after the identification of CytK, it was demonstrated that non-toxic bacterial isolates produced lower conductance values than toxic isolates[139]. Therefore, it might be suggested that the lower conductance in the I91G mutant could also be linked to a lower toxicity. Unfortunately, results obtained by Kaser 2021 showed that the CytK1 WT protein induced no cytotoxic effect on Caco2 cells[205], but a high conductance level was measured throughout this thesis. In prior studies CytK was cytotoxic in cell-based assays[137], but other studies have shown that the activity was dependent on the chosen strain analyzed[281,282]. The pore-forming character and its affinity to artificial bilayers could be based on other mechanisms than cell targeting. The cytotoxic effect on cells could also be linked to an interplay with other toxins present in the *B. cereus* group. Hence, the pore-formation and cytotoxic behaviour should be assessed individually. The evaluation of the suitability of CytK as a nanopore was based on the electrophysiological measurements alone. The CytK1 mutants were compared to the CytK1 WT protein. The data derived from the python script is an attempt to calculate multiple pore insertions and are limited to the range of ± 200 pA as this is the range of the Orbit mini measuring device. Two reference values were chosen, namely 627 and 1000 pS. The conductivity of the individual pores as calculated by the python script varied depending on the chosen reference value. The calculated conductivity for the CytK1 WT and the A196 mutant was fairly similar when both reference values were applied. The calculated conductivity of the other mutants was higher when 1000 pS was chosen. Mutants CytK1-I91F and CytK1-I91G showed the highest differences in the calculated conductivity values. This might be caused by instable pore insertions and consequently resulting in a more diverse data set. Further, the python script uses a reference value chosen by the experimenter which could lead to biased data analysis which should be optimized in further steps. As the reference value of 627 pS was

based on a literature value, the conductivity values based on a calculation with 627 pS is more reliable at this moment. The conductivity value for the CytK1 WT protein was calculated at about 700 pS. This value is higher than the approximately 100 pS suggested by Fagerlund *et al.*[139]. As different ions and molarities were used for the measurement buffers, a comparison of these data is not possible. Further on in some cases, multiple pores were directly measurable in the bilayer as the pores were pre-formed in the microsomes. This could lead to large current jumps. Next, the calculation of the radii were based on a proposed model. These facts indicate that the calculations and the python script are model-related and exemplary for the setup used in this thesis. In prior work a potential pore diameter of 6.6 Å for CytK was calculated[137]. The radius of the individual pore used in this thesis was calculated based on the same equation as used by Hardy and colleagues. Using 627 pS as a reference value, the CytK1 WT protein presented a radius of 4.58 Å. The mutations within the gene sequence and thus its effects on the protein showed that the radius of the pore enlarged in four mutants (CytK1-Q13S, CytK1-A196P, CytK1-D191del and CytK1-I91G) from approximately 4.56 (CytK1 WT) to up to 5.53 Å (CytK1-D191Del). The data gained here suggest a smaller pore than previously described. Different set ups and different buffer conditions were used. As a potassium buffer showed higher conductance values and more stable pore insertions, the potassium buffer was chosen. Other studies mainly focused on sodium chloride buffers[137,139]. Further, as already seen for cytotoxicity a strain dependence could occur. The precise characteristics of the pore have to be assessed in extensive measurements including blocking experiments with for example PEG molecules of different sizes. A further analytical step would be to apply different voltages and assess the behaviour of the pores in so-called voltage ramps. This would be the next step in the characterization of a nanopore. This worked aimed to assess the potential of CytK as a nanopore based on the stable ion current in planar lipid bilayer.

As discussed, a point mutation can alter the characteristics of the pore and might even hinder the toxin's functionality. Novel techniques to alter the pore diameter are needed to develop new nanopores. Future studies could also address labelling technologies such as bio-orthogonal systems. Using the amber stop codon and therefore site-specifically incorporating a ncAA could alter the shape and diameter of the pore. The addition of a fluorescent label might further change the pore and will combine electrophysiological analyses with monitoring of the pore using the fluorophore. This will open up diverse applications of novel nanopores such as DNA or RNA sequencing and molecule detection[272,273].

This study has shown that PFTs can be synthesized by CFPS and characterized in various ways. The modification of CytK showed that even the alteration of two similar

variants can inflict different outcomes. CytK1 proved to be the more favorable target for a nanopore development as no loss of function of the pore-forming character was detected (Table 11). All mutated pores showed characteristic pore-like behavior and inserted into the planar lipid bilayer even though the radius was changed (Figure 19 and Figure 20). The variation of the pore radius has shown that CytK1 is a potential candidate for nanopore development that could be used for diverse applications as the radius of the pore can be altered by mutating sequence patterns that are involved in the multimerization. Thus, the pore formed by CytK 1 can be adapted for different applications. This study consequently showed the proof-of-concept for the detailed identification of potential biological nanopores in eukaryotic cell-free systems.

Combining the data gathered for the pore-forming enterotoxins from *B. cereus* and the AB_5 toxins Ctx and LT, diverse applications could be established using CFPS. Different functionality assays could be set up to characterize the toxins and help to identify potential mechanisms of action. Labelling of toxins was not only possible with ^{14}C-labelled amino acids as a standard protocol but was also possible with random labelling using Bodipy-TMR-Lysine. Moreover, CtxA could be site-specifically labelled using orthogonal systems and LTB was coupled using the biotin-streptavidin system. On top of that, CytK1 was identified as a putative nanopore. These data showed the diversity of the applications for cell-free synthesized proteins and also showed the proof-of-concept for potential therapeutic uses such as targeted toxins, silenced toxins and Trojan horse applications.

4.3 Therapeutic use of toxins

The medical benefit of toxins has been identified in various fields of medicine. Nowadays, chronic pain that reduces the quality of life can be treated with neurotoxins such as Botulinum toxin[157]. Cardiovascular diseases such as high blood pressure can be treated or thrombotic events can be prevented by therapeutics that are based on peptides originating from snake venoms[158]. Disease outbreaks have been widely reduced by vaccinations that use inactivated fragments from the pathogen of interest. The Diphtheria and Tetanus vaccine are just two examples[160]. A promising approach for using toxins as therapeutics are targeted toxins[162], which are based on Paul Ehrlich's magic bullet concept[5]. The targeted toxins Denileukin diftitox and Tagraxofusp as well as the immunotoxin Moxetumomab pasudotox have been approved by medical agencies in the last two decades[168]. Unfortunately, only Tagraxofusp still has a market authorization[283] as the other two were withdrawn after safety concerns[164,284]. Strikingly, all three therapeutics focused on types of blood cancer and not solid tumors. Other studies have tried to identify other toxic moieties that might trigger fewer safety concerns and might be able to affect

different types of cancerous diseases. A class of proteins come into focus are RIPs which can be found in plants[173].

4.3.1 Dianthin-EGF as a targeted toxin in eukaryotic cell-free systems

Dianthin is a RIP that specifically affects eukaryotic ribosomes, thus in prior studies it was either purified from plant extracts or synthesized in prokaryotic cell-based systems[174,175,179]. As Dianthin is a RIP I protein, it does not contain a targeting domain, but its specific activity and anti-viral properties led to the development of Dianthin based targeted toxins[170,173,178,180]. Prior work in the research group established the cell-free synthesis of Dianthin and targeted Dianthin variants based on eukaryotic systems[69,70]. Dianthin and the targeted variant could have been synthesized in a prokaryotic cell-free system. As discussed before eukaryotic systems contain the ER-based vesicles and PTMs are possible[34]. Targeting moieties such as the EGF or antibodies depend on disulfide bridging. Hence, to set up a eukaryotic system for targeted toxins was more favorable. Further, as CHO cells are largely used for the synthesis of therapeutic proteins[285], a standardized cell-free CHO system for the production of targeted toxins would be beneficial. The feasibility of the synthesis in eukaryotic systems could be shown by using the Mel signal peptide which translocated the protein into the microsomal vesicles. This led to functionally active protein that could not inhibit its own synthesis upon translocation as it was separated from the protein translation machinery by the microsomal membrane. Unfortunately, the protein yield was rather low indicating that Dianthin molecules were not sufficiently translocated into the vesicles and thus inactivated eukaryotic ribosomes. In prior work it was shown that non-translocated Dianthin could be detected in cell-free synthesized samples[69,70]. Hence, the efficiency of the translocation of Dianthin into the microsomal vesicles was of utmost importance. The availability of the signal recognition particle (SRP) is necessary for the this step. Various lysates have been tested throughout this thesis and it could be seen that the amount of protein in the SN2 fraction varied between lysates (Supplementary Figure 16). An in depth analysis of the amount of SRP present in the lysates would allow for a better prediction of the translocation. Other parameters could influence the efficiency of the translocation. A ribosomal stall is necessary for co-translational modification and translocation, but these mechanisms can depend on the sequence context. Further, such a ribosomal pause was also shown to lead to ribosome collisions and co-translational degradation of mRNA. These factors could inhibit the translocation of Dianthin into the microsomes and therefore inhibit its own synthesis[286].

This thesis aimed to characterize the functional activity of Dianthin and the targeted Dianthin-EGF variant in diverse settings. As a first step, an *in vitro* translation inhibition assay was used where Dianthin or its variant was added to the cell-free synthesis of the

model protein LUC. Such a method has been widely used for the assessment of diverse proteins inhibiting protein translation[51,52,287] and was one of the first applications for CFPS. The data acquired here demonstrated that Dianthin and Dianthin-EGF reduced the total protein yield of LUC statistically significant in the CHO based cell-free synthesis but not in an *E. coli* based synthesis (Figure 27 and Supplementary Figure 17). These data showed the specific activity of Dianthin towards eukaryotic ribosomes. In a prior study Dianthin from seed extracts was evaluated for its protein translation inhibition capacity in a rabbit reticulocyte cell-free system. Dianthin and a recombinant Dianthin showed 50% protein translation inhibition at 0.133 and 0.227 nM, respectively. After the conjugation of an monoclonal antibody the recombinant Dianthin showed a 50% protein translation inhibition at 1.054 nM[178]. Another study showed that a Dianthin conjugated to a Fab fragment inhibited 50% of protein translation in a rabbit reticulocyte system at 0.167 nM[288]. This indicates that the conjugation process and the conjugated antibody fragment could change the specific activity of Dianthin.

In this thesis, Dianthin inhibited the protein synthesis of LUC by 88% and 93% at 1.5 and 3 nM, respectively. Dianthin-EGF was less effective and inhibited the synthesis by 86% at 1.5 nM and 92% at 3 nM. As a CHO cell-free system was used in this study, which is a high-yield system[42], higher total protein yields for the model protein can be assumed as compared to the rabbit reticulocyte system.

Another study tested a targeted toxin that combined Saporin, which is also a RIP I protein, with EGF in such an *in vitro* inhibition assay[289]. Chandler *et al*. showed that the cell-free synthesis of LUC in the rabbit reticulocyte system was reduced by both Saporin and Saporin-EGF. Saporin alone inhibited the protein synthesis to 50% at a concentration of 0.007 nM while two Saporin-EGF fusion proteins led to an 50% inhibition at 0.15 and 0.16 nM[289]. The precise amount of ribosomes present in the individual reactions is unclear. As Dianthin directly targeted the eukaryotic ribosomes a defined number of ribosomes as well as a defined number of Dianthin molecules would have been needed for a defined calculation of the activity. Therefore, a comparison of the overall efficiency of cell-free synthesized Dianthin and Dianthin extracted from seeds was rather difficult.

Combining these data with the data acquired during this thesis, it can be assumed that the toxicity of a RIP is reduced when a targeting moiety is fused. Nonetheless, the CHO-based cell-free system was suitable for the synthesis and analysis of a RIP.

The choice of the targeting moiety is crucial to the design of the targeted toxin. As no healthy cells should be affected, the specificity has to be high. Further, larger targeting moieties might be not be able to surpass cellular barriers[162,163,166]. EGF, as chosen for the construct used in this thesis, is a natural growth factor that is only about 6 kDa large. Its natural binding to the EGFR induces dimerization and activates the EGFR[290]. The EGFR

is overexpressed in various cancers such as head and neck squamous cell carcinoma and EGFR mutations might lead to cellular immune responses[169]. These facts show the significance of the EGFR as a cancer target, but unfortunately it is also widely expressed in various healthy non-cancerous cells and tissues. Our study showed that without the supplementation of the endosomal escape enhancer SO1861, Dianthin-EGF did not induce morphological changes on HEK293 cells (Supplementary Figure 19) which are not expressing the EGFR[199,200]. With the supplementation of SO1861 an effect of Dianthin-EGF on HEK293 cells could be detected at 0.001 nM (Figure 29) which showed that an internalization of the targeted toxin can be induced in an unspecific manner by the supplementation of an endosomal escape enhancer. The selection of the cell lines was based on literature research and protein atlas information on the expression level of the EGFR. In order to specify the effects seen on HEK293 cells, the EGFR level in these cells should be determined. In prior experiments during my master thesis a comparison of the EGFR expression of Hela and HEK293 cells was performed by western blotting. These data showed that a low expression of EGFR was detectable on HEK293 cells[70]. Thus, minor activities of the targeted Dianthin was expected. More precise techniques such a quantitative PCRs could be performed to assess the precise expression rate of EGFR in the cells used during this thesis. Saponins as secondary plant metabolites have been studied in the past to increase the toxic effects of such targeted therapies[167,182]. This thesis has shown that SO1861 enhanced the efficacy of Dianthin-EGF on PC-9 cells. In the presence of SO1861 a Dianthin-EGF concentration of 0.001 nM was sufficient to induce complete apoptotic effects (Figure 28), while without the supplementation of SO1861 the same Dianthin-EGF concentration just started to induce apoptotic effects (Supplementary Figure 18). These data demonstrate that endosomal escape enhancer are beneficial but future studies should further focus on the side effects of the supplementation of these enhancer. It should be considered whether the addition of saponins is more beneficial than using higher concentrations of the targeted toxin.

Comparing the activity of cell-free synthesized Dianthin-EGF to other studies using recombinant Dianthin-EGF, the cell-free synthesized fusion was comparable to prior studies. Here an IC_{50} of 2.86 fM on PC-9 cells in the presence of SO1861 was calculated while Weng *et al.* detected an IC_{50} of 0.1 fM on HER14 cells[182] and Bhargava *et al.* calculated a value of 0.17 nM on BxPC-3 and MIA PaCa-2 cells[180]. As different cell lines were used a direct comparison is not possible, but an IC_{50} of 2.86 fM still suggests a very specific targeting.

In order to validate a potential therapeutic, further preclinical testing is necessary before entering human trials. Hence, a tumor assay was developed based on Bachran *et al.*[210]. In their study they showed that a Saporin-EGF fusion construct reduced the colony growth of

the oral squamous cell carcinoma samples of 28 patients to 78% at 10 nM without the addition of the endosomal escape enhancer SO1861. The addition of SO1861 even reduced the colonies to 68%. In this thesis the highest amount of Dianthin-EGF that was supplemented to the tumor samples was 1 nM. As higher concentrations of Dianthin-EGF were not feasible, the protocol from Bachran *et al*. was modified and toxin samples were embedded into the soft agar while Bachran *et al.* pre-incubated the tumor samples for 1 h and subsequently separated the tumor samples from the toxin construct[210]. Hence, a clear comparison cannot be made, but as this thesis showed, cell-free synthesized Dianthin-EGF inhibited the colony formation to 53% at 1 nM in the presence of SO1861 (Table 13). This clearly showed that Dianthin-EGF effectively targeted the tumor cells. No studies are available investigating a Dianthin-fusion construct on human tumor samples, but a Dianthin-EGF toxin chimera was assessed in a xenograft model for pancreatic cancer. Bhargava and colleagues have shown that this therapeutic protein reduced the average tumor size by 51.7% and even led to a regression in 80% when a saponin was co-adminstered[180], showing the efficacy of Dianthin-EGF but also of saponin. Studying the effect of the cell-free synthesized Dianthin-EGF targeted toxin on the epithelial squamous cell carcinoma biopsy samples will be continued to allow for a better characterization of its potential as a therapeutic protein. If the effects of this targeted toxin continue to reduce the number of tumor colonies in a statistically relevant manner, further steps into validating cell-free synthesized targeted toxins should be considered. Next steps should be based on the guidelines from the regulatory agencies for medical compounds. Preclinical safety and efficacy studies, pharmaco- and toxico-kinetic as well as pharmaco- and toxico-dynamic evaluation as well as testing for the immunogenicity of the cell-free synthesized therapeutics should be undertaken[291,292]. Immunogenicity is a critical parameter when studying targeted toxins based on non-human proteins. Strocchi *et al.* identified the immunogenicity of RIPs and showed that Dianthin induced a comparably low antibody titer in comparison to Saporin[293]. Thus, Dianthin is a more promising candidate for the development of a targeted toxin and it should be analyzed if the immunogenicity is different after a cell-free synthesis. Before human trials might be considered, preclinical studies in animal models such as cancer xenograft models have to be performed, as well[294,295].

The results gathered in this thesis showed that eukaryotic cell-free systems are able to produce functionally active targeted toxins. Nonetheless, the next preclinical testing as described above requires large amounts of proteins. Even though Dianthin-EGF was effective at low concentrations, the high yield production of Dianthin and its targeted variant is not possible in a eukaryotic cell-free system. On top of that, the sample was not purified and might lead to immunogenicity. Therefore, the purification of the cell-free

synthesized therapeutic should be considered which would further reduce the total protein yield that can be achieved. Taking this into account cell-free systems are valid to characterize targeted toxins and allow for a preselection of the most effective candidates. Combinations of different targeting and toxic moieties can be rapidly and cost-efficiently analyzed and compared in functionality assays. The most effective candidates can be continued for the analyses on tumor samples. High amounts in the mg range will be needed for further preclinical assessments such as animal models. Such studies will need to perform pharmacological and toxicological screening. Guidelines depict that a sufficient number of animals and at least three different concentrations should be tested[296]. Due to the amount of the required therapeutic protein for the further preclinical steps, the cell-free synthesis would have to be scaled up to liter batches. Such scale ups have already been established before for therapeutically relevant proteins such as antibodies[297]. Unfortunately, if Dianthin was used as a toxic moiety, even such a scale up might not lead to the required amounts of protein. A prokaryotic cell-free system could be tested as Dianthin does not target prokaryotic ribosomes. As the synthesis *in vivo* would be the other choice, toxins interacting with the eukaryotic translations machinery could only be synthesized in prokaryotic cells such as *E. coli* which leads to intensive purification steps once again. CFPS could be used for other toxic moieties that do not inhibit the eukaryotic translation machinery such as the A subunit of AB_5 toxins as these were also used for targeted toxins. Otherwise another production method would have to be identified. Cell-free systems could be used for the screening and identification of potent targeted toxins in the future. Prior studies have already started to establish cell-free systems for automated on chips[80] as well as in microfluidic 96-well format[298]. High-throughput screenings have been established and indicated that CFPS can parallelly test different synthesis conditions as well different mutants as performed for the horseradish peroxidase[299].
One study in 1993 used a eukaryotic cell-free system for the synthesis of targeted toxins. The rabbit reticulocyte system was used to express DT and PE in combination with an antibody fragment against the human transferrin receptor[71]. Therefore, it was a so-called immunotoxin. This study showed a high cell-based toxicity on K562 leukemia cells for the PE immunotoxin but not for the DT immunotoxin. The PE immunotoxin displayed an IC_{50} of 0.1 nM and thus was shown to be more toxic compared to the Dianthin-EGF targeted toxin in our study. Even though different targeting and toxic moieties were used, these data show that cell-free synthesized targeted toxins are very effective.

Taken together, this thesis showed that CFPS in eukaryotic systems is a valid technology for the synthesis, characterization and clinical testing of targeted toxins before entering preclinical studies. Using CFPS as a screening system for targeted toxins would enhance the development of new therapeutic proteins as a variety of candidates could be tested in

parallel to identify the most promising candidates that could be continued for preclinical and human trials. If more candidates and variants can be tested at the same time in a highly parallel manner, a higher likeliness to identify the most potent candidate for the clinic is given.

4.4 Rapid response to novel zoonotic diseases

Diverse types of pathogens can trigger a disease progression in humans. Infectious diseases which are transmitted from animals to humans are so-called zoonoses. In some cases these zoonotic diseases can lead to dreadful health issues all over the world. The most recent example is the beta-coronavirus SARS-CoV2 which has resulted in more than 6 million deaths worldwide as accounted by the WHO[300]. New viral outbreaks are highly possible due to the close interactions with wild and domesticated animals, the increasing consumption of different meats, the intrusion of humans into the natural habitat of animals and climate change[301–303]. Future viral outbreaks are possible and rapid response systems have to be available. Such a system includes the characterization of the pathogen and its individual components, the detection of the pathogen, the counteracting of disease progressions as well as the prevention of its spread by quarantines and vaccines. The third part of this thesis was aimed at the establishment of CFPS as a rapid response system.

4.4.1 Eukaryotic cell-free systems for the synthesis of SARS-CoV2 proteins

As discussed diverse studies have synthesized viral proteins in a cell-free manner which already indicated the possibility of applying CFPS for the intense study of viral proteins. Non-structural proteins[92,84] and viral membrane proteins[94] have been synthesized. One study even demonstrated the use of cell-free synthesized viral antigens for a potential vaccine development[95]. Altincekic and colleagues showed the versatility of cell-free synthesis by using the wheat germ system to synthesize and purify SARS-CoV2 ORF3, ORF6, ORF7b, ORF8, ORF9, the E and M protein[227]. Nonetheless, these studies have not combined the possibilities of cell-free systems with its potential to tackle novel viral pathogens. The data presented here showed that all viral protein classes (non-structural, structural and accessory proteins) could be studied. In comparison to the prior work, two of the viral proteins have been functionally characterized. Further, this is the first time three different eukaryotic lysates were used to assess the cell-free synthesis of viral proteins. Each lysate demonstrated its advantages and disadvantages. Each individual protein appeared to favour individual parameters such as the lysate itself and reaction conditions, but the CHO system was the high-yield system (Figure 35). Prior studies have already established the CHO cell-free system as a high-yield production system, which is why this system is an optimized system for protein production[20,42,304]. These data confer

that the CHO cell-free system could be used for antigen production for further applications and reference material for diagnostic studies. The synthesis of SARS-CoV2 proteins in K562 lysate showed that batch-based syntheses resulted in high total protein yields for individual proteins (Supplementary Figure 21 and Supplementary Figure 22). Unfortunately, the data gathered here showed that further optimizations concerning CECF reactions and compatibility with downstream applications such as an ELISA have to be undertaken in the future. Few studies have used human cell lysates to synthesize and characterize viral proteins. The HeLa cell lysate was in the focus of these studies[86,305]. A lysate derived from human cell lines can be beneficial as it would be a similar surrounding as the viral host. Due to the open system of CFPS, different supplements such as chaperones can be added to the synthesis of a viral protein. Interaction studies could easily be performed as such a lysate would have a similar codon context as the host and a natural folding environment is provided. The *Sf*21 system induced glycosylation of the glycoproteins ORF8 and Spike (Figure 38). In prior studies the *Sf*21 system has been used to synthesize viral proteins that harbour glycosylation sites. Hence, the hepatitis E virus capsid protein[306] and gp120 of the human immunodeficiency virus type-1[307] could be synthesized and the glycosylation was verified. Glycosylation patterns could easily be assessed based on the core glycosylation present in the ER vesicles. The Spike protein is a glycosylated protein and is responsible for cell targeting[308]. The *Sf*21 system with its high potential for core glycosylation could be used to perform binding studies of the Spike protein and its deglycosylated forms.

The accessory protein ORF8 is said to be a co-factor for the immune invasion of the host and structural analyses predicted multimerizations by disulfide bridging and potential glycosylation sites[191,309]. Altincekic and colleagues showed minor multimerization in a wheat germ cell-free system[227]. The CHO-based synthesis presented here demonstrated intense multimerization of ORF8 even in the presence of DTT (Figure 33 and Figure 37) and the potential glycosylation site was verified by glycosidase digestion (Figure 38). In SARS-CoV the corresponding ORF8ab is unstable without the glycosylation[309], but it is still unclear whether this is also the case for SARS-CoV2 ORF8. Further studies should evaluate the effect of ORF8 on the immune system in the presence and absence of glycosylation to define the role of the glycosylation. ORF8 could be co-expressed or added to the synthesis of components of the immune system such as major histocompatibility complexes or T-cell receptors. Afterwards a pull-down assay could be performed by a tag on the ORF8 and assessed whether the other protein is bound the ORF8. This assay could easily detect differences in the binding capacity when using a glycosylated or non-glycosylated ORF8 protein.

SARS-CoV2 ORF10 has been widely discussed and conflicting data on the presence of the gene and protein were presented[195,196]. This thesis showed that ORF10 could only be synthesized in combination with the Mel signal peptide (Figure 37) which suggests a better translation initiation in the presence of the signal peptide. Prior studies have assumed that in a cell-free system the Mel signal sequence stabilized the initiation activity resulting in increased protein yields[252]. Benitez-Cantos and colleagues demonstrated that the codon context immediately following the start codon is essential for the translation initiation[310]. The second amino acid codon of the Mel signal peptide is AAA, which is known to increase the translation efficiency[311]. Nonetheless, a protein translation should be possible at low total protein yields even without a signal peptide, and thus further studies should be performed on the ORF10 translation initiation. Diverse systems including prokaryotic and fungal systems should be used for an in depth analysis in the near future.

Studies have discussed the importance of ORF10 as it was shown that the protein was terminated prematurely or not even synthesized at all in COVID-19 patients[196,312]. A difference in the clinical manifestation could not be detected[196]. In a preprint, Schuster suggested a potential oligomerization of the ORF10 protein, which forms a pore for ion fluctuations[312]. The data on ORF10 gathered here after a synthesis in the CHO system, indicated potential multimerizations (Figure 33). Mena and colleagues showed that ORF10 could bind to an E3 ubiquitin ligase and the N-terminus of the protein was necessary for that matter[313]. Combining these data with the synthesis of ORF10 in the presence of a signal peptide, might indicate that the N-terminus and its codon context are necessary for the successful synthesis of ORF10. Nonetheless, the importance of ORF10 for the pathogenicity of SARS-CoV2 is still not known.

These data demonstrate that in an early response to novel viral pathogens, a diverse set of eukaryotic lysates can be useful to synthesize and characterize the versatile set of viral proteins.

4.4.2 Structural proteins of SARS-CoV2

Structural proteins are generally the first proteins to be analyzed as they target the host cell[213] and proteins such as the Spike protein are used for vaccine development[314]. The N protein is not only a major component of the viral capsid and is a contributor to the humoral response[315], but it is also the viral protein used for rapid antigen tests[214]. Thus, during this thesis it was tested whether eukaryotic cell-free systems can be used to produce viral proteins for the validation of antibodies. This would also imply that cell-free synthesized antigens could be used for downstream applications in the diagnostic field. Furthermore, these data suggest that cell-free synthesized proteins can be used to immunize host organisms to generate antibodies. As the synthesis in cell-free systems is

time efficient, this would allow for a rapid response and development of emergency vaccines. The N protein as well as two early onset mutants were tested in an in-solution ELISA, a dot blot and a western blot (Figure 39). WT and both mutants could be detected in the assays and WT N could even be detected at 1 ng. Various studies have tested the N protein in diverse detection assays. Smits *et al.* even demonstrated that the complete N and N fragments that were used in a dot blot, could identify SARS-CoV2 positive patient samples[315]. These data as well as the data obtained here using an anti-SARS-CoV-2 and anti-SARS antibody for the detection of the N protein, reflected on the possibility of cell-free systems to assist in tackling future pandemics.

4.4.3 Functional analysis of SARS-CoV2 proteins

As a representative for the non-structural proteins, the nsp1 inhibitory protein was characterized. After the virus infects the host cell, host protein synthesis is downregulated in order to allow for the synthesis of the viral proteins. This has been seen for nsp1 leader protein[211]. As already seen for the ribosome inactivating protein Dianthin, cell-free systems allow for the analysis of such proteins. The data presented here showed that a decrease in the eYFP fluorescence could be detected but the inhibitory effect decreased over time. A prior study demonstrated that the nsp1 protein was less efficient in systems where a CrPV IRES site was used for protein translation. When an IRES from the hepatitis C viral genome was used, an increased binding to the ribosomes could be detected[211]. Future experiments could focus on the assessment of cap-dependent and cap-independent / IRES mediated translation initiation pathways. This would allow for a detailed analysis of the mechanism of action of such leader proteins.

As a last step in characterizing individual proteins of SARS-CoV2, the E protein was analyzed. Due to the similarity of SARS-CoV and SARS-CoV2, a similarity of the E proteins is assumed[316,317]. The SARS-CoV E protein is a homo-pentameric cation channel. Channel-like behavior has been described for closely related envelope proteins as from MERS[216] and SARS[318]. Here a multimerization of the E protein could be seen (Figure 33 and Ramm *et al.,* 2022). Mandala and colleagues demonstrated a channel-like structure that assembled a pore of 2.1 Å[319]. Xia *et al.* not only showed its cytotoxic effects on cell lines, but also suggested a selectivity of the channel for potassium, sodium, calcium and magnesium[320]. The ORF4 envelope protein induced different currents in planar lipid bilayer measurements during this thesis. Single channel activity, pore-formation and large undefined cytotoxic currents could be detected (Figure 40 and Figure 41). The pore-forming character could be explained by the formation of the complete pentamer. Smaller current flows could derive from other multimers such as trimers. Thus, these data gathered here and in prior studies indicate that the envelope protein is a cation channel with cytotoxic activity. These characteristics identify the ORF4 envelope protein as a

potential drug target. The pore-forming character of the channel will lead to ion fluctuations in the target cell and will therefore change the pH of the cellular compartment. Blocking the envelope protein might therefore inhibit a pathogenic pathway of SARS-CoV2.

As discussed, this thesis has shown the importance of using versatile eukaryotic cell-free systems as a rapid response mechanism. As we have seen throughout the SARS-CoV2 pandemic, viral mutants might prolong the course of infections[321]. Such variants harbour mutations in the whole genome. Therefore, a rapid response mechanism has to be flexible and should be able to adapt to such variants. In this study two early onset mutations of the SARS-CoV2 N protein have also been investigated as discussed before. A promising characteristic of CFPS is the use of PCR templates. As shown for various proteins throughout this thesis a modification of templates was possible using 2-step PCR techniques. The full-length Spike protein was based on a PCR template and the Mel signal peptide was fused to the ORF3 gene. Prior studies have already established the use of PCR templates in cell-free systems[26,55], and demonstrated the parallel screening of diverse templates. This facilitates CFPS as a promising methodology for the rapid and parallel synthesis of viral proteins and their variants as well as a potential screening of inhibitors. The prevention of viral outbreaks is of highest importance but it is also necessary to identify therapeutic approaches[322]. Future studies should set up further functionality assays for high-throughput screening of functional viral proteins and their inhibitors in cell-free systems. The data gathered here show that CFPS is a versatile technology for the synthesis and characterization of viral proteins. Further, it could be confirmed that the production of antigens for diagnostic uses such as antibody screenings can be performed and thus facilitates CFPS as a rapid response set up for novel viral diseases.

5 Conclusion

The data acquired in this thesis provide a foundation for the usage of CFPS as a platform technology for the synthesis, modification, characterization and application of toxic proteins as presented in Figure 42.

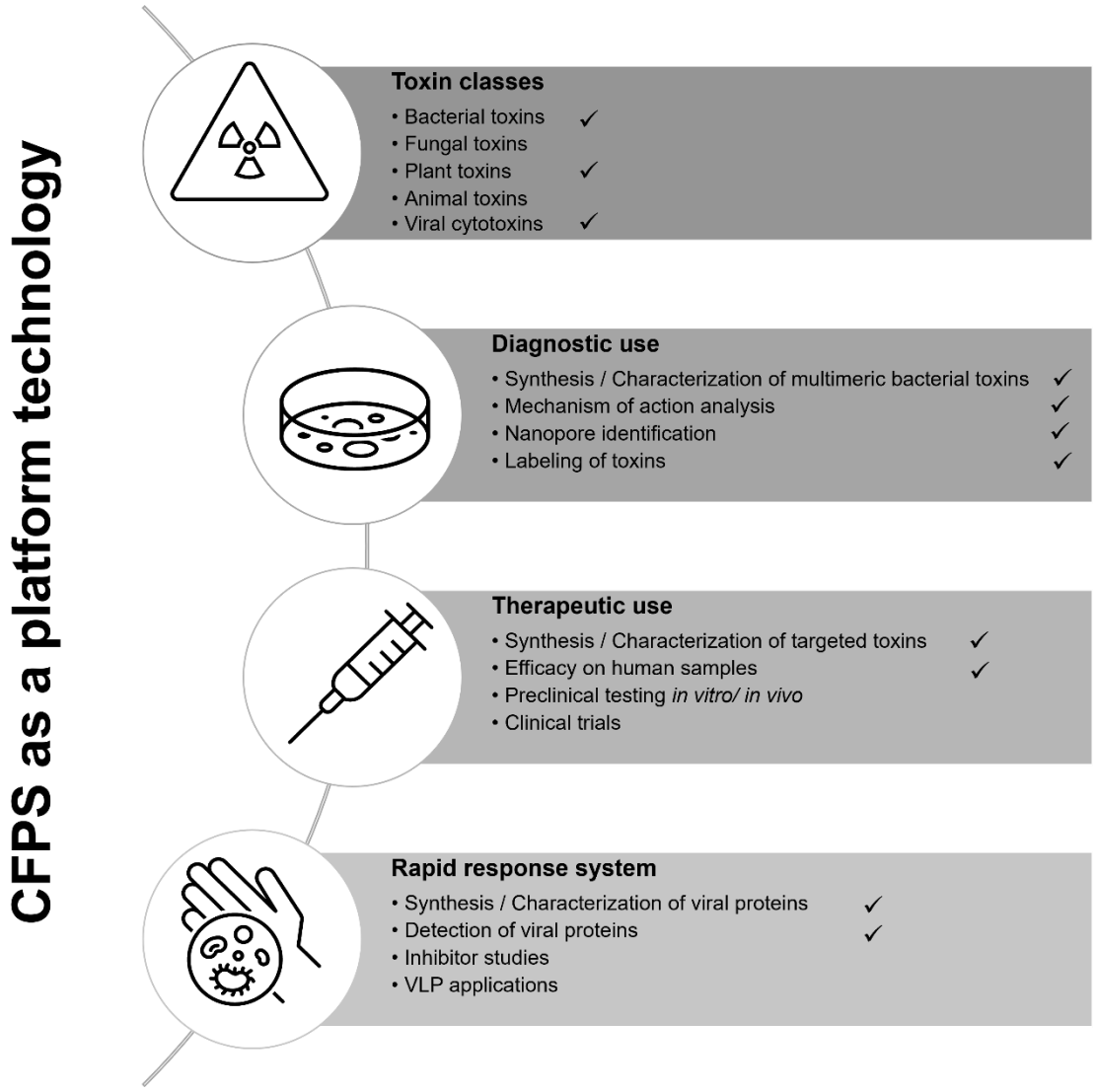

Figure 42: CFPS as a platform technology for toxins.
Overview of CFPS as a platform for the synthesis, characterization and application of cell-free synthesized toxins. Work performed in this thesis indicated by ✓. Parameter was not determined when ✓ was missing and should be performed in the future.

No study has shown the systematic cell-free synthesis and subsequent characterization of diverse toxic proteins, yet. With the knowledge of cell-free systems as well as the detailed analysis of the individual mechanisms of action, this thesis shows that different eukaryotic cell-free systems can be used to study various protein groups. These data can be transferred to other classes of proteinaceous toxins such as toxins from venoms or fungi. Moreover, this thesis proved that CFPS could be used to employ toxins in diagnostic as well as therapeutic applications without major drawbacks. Nonetheless, it is of high importance to know the cell-free system and the toxin of interest in order to adapt the reaction conditions to ensure the toxin's efficient synthesis and functionality. This thesis depicted the possibilities of CFPS in the field of toxicology. Implementing a technology in

the field of medicine takes numerous steps. As this work started on the first step, further preclinical evaluations will have to be undertaken in upcoming experiments. Future studies should also focus on expanding this method to emerging technologies such as drug delivery systems by VLPs and implementing the proof-of-concepts developed here by tracking a silenced toxin within the cell and further developing nanopores.

Taken together, this thesis showed the versatility of CFPS and its relevance in the field of toxicology. By combining different scientific fields such as toxicology, biochemistry, medical research as well as different techniques such as viability assessments and electrophysiology, a toolbox for research and development could be set up.

6 References

1. Aktories, K., Förstermann, U., Starke, K. & Hofmann, F. B. *Allgemeine und spezielle Pharmakologie und Toxikologie. Für Studenten der Medizin, Veterinärmedizin, Pharmazie, Chemie und Biologie sowie für Ärzte, Tierärzte und Apotheker.* 12th ed. (Elsevier, München, 2017).
2. Schmitt, C. K., Meysick, K. C. & O'Brien, A. D. Bacterial toxins: friends or foes? *Emerging infectious diseases* **5,** 224–234; 10.3201/eid0502.990206 (1999).
3. Rai, K. R. *et al.* Acute Infection of Viral Pathogens and Their Innate Immune Escape. *Frontiers in microbiology* **12,** 672026; 10.3389/fmicb.2021.672026 (2021).
4. Schultz-Schultzenstein, K. H. *Die homöobiotische Medizin des Theophrastus Paracelsus. In ihrem Gegensatz gegen die Medizin der Alten, als Wendepunkt für die Entwickelung der neueren medizinischen Systeme und als Quell der Homöopathie* (Hirschwald, 1831).
5. Strebhardt, K. & Ullrich, A. Paul Ehrlich's magic bullet concept: 100 years of progress. *Nat Rev Cancer* **8,** 473–480; 10.1038/nrc2394 (2008).
6. Bundesamt für Wirtschaft und Ausfuhrkontrolle (BAFA). Ausfuhrkontrolle - Veröffentlichung der neuen EU-Dual-Use-Verordnung (VO (EU) 2021/821). Available at https://www.bafa.de/SharedDocs/Kurzmeldungen/DE/Aussenwirtschaft/Ausfuhrkontrolle/20210611_veroeffentlichung_neue-eu-dual-use-vo.html (2021).
7. Ali, Mahmoud Abdu Al-Samie Mohamed. Studies on Bee Venom and Its Medical Uses. *International Journal of Advancements in Research & Technology - IJOART*.
8. Sutar, N. K., Tare, T. G. & Renapurkar, D. M. A study of Snake Venom Yield by different Methods of Venom Extraction. *Amphib Reptilia* **7,** 187–191; 10.1163/156853886X00406 (1986).
9. Burnett, M. J. B. & Burnett, A. C. Therapeutic recombinant protein production in plants: Challenges and opportunities. *Plants People Planet* **2,** 121–132; 10.1002/ppp3.10073 (2020).
10. Bill, R. M. (ed.). *Recombinant Protein Production in Yeast. Methods and Protocols* (Humana Press, Totowa, NJ, 2012).
11. Geisse, S., Jordan, M. & Wurm, F. M. Large-Scale Transient Expression of Therapeutic Proteins in Mammalian Cells. In *Therapeutic Proteins. Methods and*

Protocols, edited by C. M. Smales & D. C. James (Humana Press, Totowa, NJ, 2005), Vol. 308, pp. 87–98.

12. Overton, T. W. Recombinant protein production in bacterial hosts. *Drug discovery today* **19,** 590–601; 10.1016/j.drudis.2013.11.008 (2014).
13. Technischer Arbeitsschutz (inkl. Technische Regeln) - TRBA 466 Einstufung von Prokaryonten (Bacteria und Archaea) in Risikogruppen. Available at https://www.baua.de/DE/Angebote/Rechtstexte-und-Technische-Regeln/Regelwerk/TRBA/TRBA-466.html (2021).
14. Pastan, I., Chaudhary, V. & FitzGerald, D. J. Recombinant toxins as novel therapeutic agents. *Annu. Rev. Biochem.* **61,** 331–354; 10.1146/annurev.bi.61.070192.001555 (1992).
15. Geron, M. Production and Purification of Recombinant Toxins. In *Snake and Spider Toxins. Methods and Protocols,* edited by A. Priel. 1st ed. (Humana, New York, NY, 2020), Vol. 2068, pp. 73–84.
16. Silva, O. N. *et al.* Repurposing a peptide toxin from wasp venom into antiinfectives with dual antimicrobial and immunomodulatory properties. *Proceedings of the National Academy of Sciences of the United States of America* **117,** 26936–26945; 10.1073/pnas.2012379117 (2020).
17. Camperi, S. A. *et al.* Synthetic peptides to produce antivenoms against the Cys-rich toxins of arachnids. *Toxicon: X* **6,** 100038; 10.1016/j.toxcx.2020.100038 (2020).
18. Technischer Arbeitsschutz (inkl. Technische Regeln) - TRBA 462 Einstufung von Viren in Risikogruppen. Available at https://www.baua.de/DE/Angebote/Rechtstexte-und-Technische-Regeln/Regelwerk/TRBA/TRBA-462.html (2021).
19. Matthaei, H. & Nirenberg, M. W. The dependence of cell-free protein synthesis in E.coli upon RNA prepared from ribosomes. *Biochemical and biophysical research communications* **4,** 404–408; 10.1016/0006-291x(61)90298-4 (1961).
20. Brödel, A. K., Sonnabend, A. & Kubick, S. Cell-free protein expression based on extracts from CHO cells. *Biotechnology and bioengineering* **111,** 25–36; 10.1002/bit.25013 (2014).
21. Pelham, H. R. & Jackson, R. J. An efficient mRNA-dependent translation system from reticulocyte lysates. *Eur J Biochem* **67,** 247–256; 10.1111/j.1432-1033.1976.tb10656.x (1976).

22. Carlson, E. D., Gan, R., Hodgman, C. E. & Jewett, M. C. Cell-free protein synthesis: applications come of age. *Biotechnology advances* **30,** 1185–1194; 10.1016/j.biotechadv.2011.09.016 (2012).

23. Madin, K., Sawasaki, T., Ogasawara, T. & Endo, Y. A highly efficient and robust cell-free protein synthesis system prepared from wheat embryos: plants apparently contain a suicide system directed at ribosomes. *Proceedings of the National Academy of Sciences of the United States of America* **97,** 559–564; 10.1073/pnas.97.2.559 (2000).

24. Craig, D., Howell, M. T., Gibbs, C. L., Hunt, T. & Jackson, R. J. Plasmid cDNA-directed protein synthesis in a coupled eukaryotic in vitro transcription-translation system. *Nucleic Acids Research* **20,** 4987–4995; 10.1093/nar/20.19.4987 (1992).

25. Unterholzner, S. J., Poppenberger, B. & Rozhon, W. Toxin-antitoxin systems: Biology, identification, and application. *Mobile genetic elements* **3,** e26219; 10.4161/mge.26219 (2013).

26. Bechlars, S. *et al.* Cell-free synthesis of functional thermostable direct hemolysins of Vibrio parahaemolyticus. *Toxicon : official journal of the International Society on Toxinology* **76,** 132–142; 10.1016/j.toxicon.2013.09.012 (2013).

27. Yabuki, T. *et al.* A robust two-step PCR method of template DNA production for high-throughput cell-free protein synthesis. *J Struct Funct Genomics* **8,** 173–191; 10.1007/s10969-007-9038-z (2007).

28. Kubick, S. *et al.* In Vitro Translation in an Insect-Based Cell-Free System. In *Cell-free protein expression,* edited by J. R. Swartz (Springer, Berlin, Germany, 2003), pp. 209–217.

29. Katzen, F., Chang, G. & Kudlicki, W. The past, present and future of cell-free protein synthesis. *Trends in biotechnology* **23,** 150–156; 10.1016/j.tibtech.2005.01.003 (2005).

30. Kim, D. M. & Swartz, J. R. Prolonging cell-free protein synthesis with a novel ATP regeneration system. *Biotechnology and bioengineering* **66,** 180–188 (1999).

31. Kim, D. M. & Choi, C. Y. A semicontinuous prokaryotic coupled transcription/translation system using a dialysis membrane. *Biotechnology progress* **12,** 645–649; 10.1021/bp960052l (1996).

32. Spirin, A. S., Baranov, V. I., Ryabova, L. A., Ovodov, S. Y. & Alakhov, Y. B. A continuous cell-free translation system capable of producing polypeptides in high yield. *Science (New York, N.Y.)* **242,** 1162–1164; 10.1126/science.3055301 (1988).

33. Ryabova, L. A., Vinokurov, L. M., Shekhovtsova, E. A., Alakhov, Y. B. & Spirin, A. S. Acetyl phosphate as an energy source for bacterial cell-free translation systems. *Analytical biochemistry* **226,** 184–186; 10.1006/abio.1995.1208 (1995).

34. Gregorio, N. E., Levine, M. Z. & Oza, J. P. A User's Guide to Cell-Free Protein Synthesis. *Methods and protocols* **2**; 10.3390/mps2010024 (2019).

35. Shimizu, Y. *et al.* Cell-free translation reconstituted with purified components. *Nature biotechnology* **19,** 751–755; 10.1038/90802 (2001).

36. Junge, F. *et al.* Advances in cell-free protein synthesis for the functional and structural analysis of membrane proteins. *New biotechnology* **28,** 262–271; 10.1016/j.nbt.2010.07.002 (2011).

37. Schweet, R., Lamfrom, H. & Allen, E. THE SYNTHESIS OF HEMOGLOBIN IN A CELL-FREE SYSTEM. *Proceedings of the National Academy of Sciences of the United States of America* **44,** 1029–1035; 10.1073/pnas.44.10.1029 (1958).

38. Anastasina, M., Terenin, I., Butcher, S. J. & Kainov, D. E. A technique to increase protein yield in a rabbit reticulocyte lysate translation system. *BioTechniques* **56,** 36–39; 10.2144/000114125 (2014).

39. Tarui, H. *et al.* Establishment and characterization of cell-free translation/glycosylation in insect cell (Spodoptera frugiperda 21) extract prepared with high pressure treatment. *Appl Microbiol Biotechnol* **55,** 446–453; 10.1007/s002530000534 (2001).

40. Brödel, A. K. *et al.* IRES-mediated translation of membrane proteins and glycoproteins in eukaryotic cell-free systems. *PloS one* **8,** e82234; 10.1371/journal.pone.0082234 (2013).

41. Quast, R. B., Sonnabend, A., Stech, M., Wüstenhagen, D. A. & Kubick, S. High-yield cell-free synthesis of human EGFR by IRES-mediated protein translation in a continuous exchange cell-free reaction format. *Sci Rep* **6,** 30399; 10.1038/srep30399 (2016).

42. Thoring, L., Dondapati, S. K., Stech, M., Wüstenhagen, D. A. & Kubick, S. High-yield production of "difficult-to-express" proteins in a continuous exchange cell-free system based on CHO cell lysates. *Sci Rep* **7,** 11710; 10.1038/s41598-017-12188-8 (2017).

43. Mikami, S., Kobayashi, T., Masutani, M., Yokoyama, S. & Imataka, H. A human cell-derived in vitro coupled transcription/translation system optimized for production of recombinant proteins. *Protein expression and purification* **62,** 190–198; 10.1016/j.pep.2008.09.002 (2008).

44. Bradrick, S. S., Nagyal, S. & Novatt, H. A miRNA-responsive cell-free translation system facilitates isolation of hepatitis C virus miRNP complexes. *RNA (New York, N.Y.)* **19,** 1159–1169; 10.1261/rna.038810.113 (2013).

45. Roberts, B. E. & Paterson, B. M. Efficient translation of tobacco mosaic virus RNA and rabbit globin 9S RNA in a cell-free system from commercial wheat germ. *Proceedings of the National Academy of Sciences of the United States of America* **70,** 2330–2334; 10.1073/pnas.70.8.2330 (1973).

46. Harbers, M. Wheat germ systems for cell-free protein expression. *FEBS letters* **588,** 2762–2773; 10.1016/j.febslet.2014.05.061 (2014).

47. Buntru, M., Vogel, S., Spiegel, H. & Schillberg, S. Tobacco BY-2 cell-free lysate: an alternative and highly-productive plant-based in vitro translation system. *BMC Biotechnol* **14,** 37; 10.1186/1472-6750-14-37 (2014).

48. Buntru, M., Vogel, S., Stoff, K., Spiegel, H. & Schillberg, S. A versatile coupled cell-free transcription-translation system based on tobacco BY-2 cell lysates. *Biotechnology and bioengineering* **112,** 867–878; 10.1002/bit.25502 (2015).

49. Sissons, C. H. Yeast protein synthesis. Preparation and analysis of a highly active cell-free system. *The Biochemical journal* **144,** 131–140; 10.1042/bj1440131 (1974).

50. Zhang, L., Liu, W.-Q. & Li, J. Establishing a Eukaryotic Pichia pastoris Cell-Free Protein Synthesis System. *Front. Bioeng. Biotechnol.* **8,** 536; 10.3389/fbioe.2020.00536 (2020).

51. Ueno, Y., Nakajima, M., Sakai, K., Ishii, K. & Sato, N. Comparative toxicology of trichothec mycotoxins: inhibition of protein synthesis in animal cells. *Journal of biochemistry* **74,** 285–296 (1973).

52. Reyes, A. G. *et al.* The Streptomyces coelicolor genome encodes a type I ribosome-inactivating protein. *Microbiology (Reading, England)* **156,** 3021–3030; 10.1099/mic.0.039073-0 (2010).

53. Klammt, C. *et al.* Cell-free expression as an emerging technique for the large scale production of integral membrane protein. *The FEBS journal* **273,** 4141–4153; 10.1111/j.1742-4658.2006.05432.x (2006).

54. Orth, J. H. C. *et al.* Cell-free synthesis and characterization of a novel cytotoxic pierisin-like protein from the cabbage butterfly Pieris rapae. *Toxicon : official journal of the International Society on Toxinology* **57,** 199–207; 10.1016/j.toxicon.2010.11.011 (2011).

55. Sawasaki, T., Ogasawara, T., Morishita, R. & Endo, Y. A cell-free protein synthesis system for high-throughput proteomics. *Proceedings of the National Academy of Sciences of the United States of America* **99,** 14652–14657; 10.1073/pnas.232580399 (2002).

56. Wang, L., Brock, A., Herberich, B. & Schultz, P. G. Expanding the genetic code of Escherichia coli. *Science (New York, N.Y.)* **292,** 498–500; 10.1126/science.1060077 (2001).

57. Hong, S. H. *et al.* Cell-free protein synthesis from a release factor 1 deficient Escherichia coli activates efficient and multiple site-specific nonstandard amino acid incorporation. *ACS synthetic biology* **3,** 398–409; 10.1021/sb400140t (2014).

58. Quast, R. B., Claussnitzer, I., Merk, H., Kubick, S. & Gerrits, M. Synthesis and site-directed fluorescence labeling of azido proteins using eukaryotic cell-free orthogonal translation systems. *Analytical biochemistry* **451,** 4–9; 10.1016/j.ab.2014.01.013 (2014).

59. Zemella, A. *et al.* Cell-free protein synthesis as a novel tool for directed glycoengineering of active erythropoietin. *Sci Rep* **8,** 8514; 10.1038/s41598-018-26936-x (2018).

60. Zimmerman, E. S. *et al.* Production of site-specific antibody-drug conjugates using optimized non-natural amino acids in a cell-free expression system. *Bioconjugate chemistry* **25,** 351–361; 10.1021/bc400490z (2014).

61. Casado-Vela, J., Fuentes, M. & Franco-Zorrilla, J. M. Screening of protein-protein and protein-DNA interactions using microarrays: applications in biomedicine. *Advances in protein chemistry and structural biology* **95,** 231–281; 10.1016/B978-0-12-800453-1.00008-7 (2014).

62. Zárate, X. & Galbraith, D. W. A cell-free expression platform for production of protein microarrays. *Methods in molecular biology (Clifton, N.J.)* **1118,** 297–307; 10.1007/978-1-62703-782-2_21 (2014).

63. Tinafar, A., Jaenes, K. & Pardee, K. Synthetic Biology Goes Cell-Free. *BMC Biol* **17,** 64; 10.1186/s12915-019-0685-x (2019).

64. K. Y. Wen *et al.* A Cell-Free Biosensor for Detecting Quorum Sensing Molecules in P. aeruginosa-Infected Respiratory Samples. *undefined* (2017).

65. Vlasak, R. & Kreil, G. Nucleotide sequence of cloned cDNAs coding for preprosecapin, a major product of queen-bee venom glands. *Eur J Biochem* **145,** 279–282; 10.1111/j.1432-1033.1984.tb08549.x (1984).

66. Suchanek, G. & Kreil, G. Translation of melittin messenger RNA in vitro yields a product terminating with glutaminylglycine rather than with glutaminamide. *Proceedings of the National Academy of Sciences of the United States of America* **74,** 975–978; 10.1073/pnas.74.3.975 (1977).

67. Lüddecke, T. *et al.* A Spider Toxin Exemplifies the Promises and Pitfalls of Cell-Free Protein Production for Venom Biodiscovery. *Toxins* **13,** 575; 10.3390/toxins13080575 (2021).

68. Wang, Y. *et al.* Establishment and optimization of a wheat germ cell-free protein synthesis system and its application in venom kallikrein. *Protein expression and purification* **84,** 173–180; 10.1016/j.pep.2012.05.006 (2012).

69. Haueis, L. *Forschungsbericht, Zellfreie Synthese und Analyse von Dianthin-eYFP und einem Diantin Immuntoxin in eukaryotischen Lysaten* (2018).

70. Ramm, F. *Master thesis, Synthesis and functional characterization of Apoptin and Dianthin in eukaryotic cell-free systems* (Charité – Universitätsmedizin Berlin; Fraunhofer Institute for Cell Therapy and Immunology (IZI), Branch Bioanalytics and Bioprocesses (IZI-BB), Potsdam-Golm, Germany, 2017).

71. Nicholls, P. J. *et al.* Characterization of single-chain antibody (sFv)-toxin fusion proteins produced in vitro in rabbit reticulocyte lysate. *The Journal of biological chemistry* **268,** 5302–5308 (1993).

72. Chalmeau, J., Monina, N., Shin, J., Vieu, C. & Noireaux, V. α-Hemolysin pore formation into a supported phospholipid bilayer using cell-free expression. *Biochimica et biophysica acta* **1808,** 271–278; 10.1016/j.bbamem.2010.07.027 (2011).

73. Ramm, F. *et al.* Cell-Free Systems Enable the Production of AB5 Toxins for Diagnostic Applications. *Toxins* **14,** 233; 10.3390/toxins14040233 (2022).

74. Murphy, J. R., Pappenheimer, A. M. & Borms, S. T. de. Synthesis of diphtheria tox-gene products in Escherichia coli extracts. *Proceedings of the National Academy of Sciences of the United States of America* **71,** 11–15; 10.1073/pnas.71.1.11 (1974).

75. Lathe, R., Hirth, P., DeWilde, M., Harford, N. & Lecocq, J. P. Cell-free synthesis of enterotoxin of E. coli from a cloned gene. *Nature* **284,** 473–474; 10.1038/284473a0 (1980).

76. Ramm, F., Stech, M., Zemella, A., Frentzel, H. & Kubick, S. The Pore-Forming Hemolysin BL Enterotoxin from Bacillus cereus: Subunit Interactions in Cell-Free Systems. *Toxins* **13,** 807; 10.3390/toxins13110807 (2021).

77. Miles, G., Cheley, S., Braha, O. & Bayley, H. The staphylococcal leukocidin bicomponent toxin forms large ionic channels. *Biochemistry* **40,** 8514–8522; 10.1021/bi010454o (2001).

78. Suchanek, G., Kreil, G. & Hermodson, M. A. Amino acid sequence of honeybee prepromelittin synthesized in vitro. *Proceedings of the National Academy of Sciences of the United States of America* **75,** 701–704; 10.1073/pnas.75.2.701 (1978).

79. Ramm, F. *et al.* Mammalian cell-free protein expression promotes the functional characterization of the tripartite non-hemolytic enterotoxin from Bacillus cereus. *Sci Rep* **10,** 2887; 10.1038/s41598-020-59634-8 (2020).

80. Georgi, V. *et al.* On-chip automation of cell-free protein synthesis: new opportunities due to a novel reaction mode. *Lab on a chip* **16,** 269–281; 10.1039/c5lc00700c (2016).

81. Vandenplas, M. L., Vandenplas, S., Brebner, K., Bester, A. J. & Boyd, C. D. Characterization of the messenger RNA population coding for components of viperid snake venom. *Toxicon* **23,** 289–305; 10.1016/0041-0101(85)90152-7 (1985).

82. Patel, K. G., Ng, P. P., Levy, S., Levy, R. & Swartz, J. R. Escherichia coli-based production of a tumor idiotype antibody fragment--tetanus toxin fragment C fusion protein vaccine for B cell lymphoma. *Protein expression and purification* **75,** 15–20; 10.1016/j.pep.2010.09.005 (2011).

83. Bechlars, S. *et al.* Characterization of trh2 harbouring Vibrio parahaemolyticus strains isolated in Germany. *PloS one* **10,** e0118559; 10.1371/journal.pone.0118559 (2015).

84. Dondapati, S. K., Wüstenhagen, D. A., Strauch, E. & Kubick, S. Cell-free production of pore forming toxins: Functional analysis of thermostable direct hemolysin from Vibrio parahaemolyticus. *Engineering in Life Sciences* **18,** 140–148; 10.1002/elsc.201600259 (2018).

85. Lu, Y., Welsh, J. P. & Swartz, J. R. Production and stabilization of the trimeric influenza hemagglutinin stem domain for potentially broadly protective influenza vaccines. *Proceedings of the National Academy of Sciences of the United States of America* **111,** 125–130; 10.1073/pnas.1308701110 (2014).

86. Kobayashi, T., Machida, K. & Imataka, H. Human cell extract-derived cell-free systems for virus synthesis. *Methods in molecular biology (Clifton, N.J.)* **1118,** 149–156; 10.1007/978-1-62703-782-2_9 (2014).

87. Mikami, S., Kobayashi, T., Yokoyama, S. & Imataka, H. A hybridoma-based in vitro translation system that efficiently synthesizes glycoproteins. *Journal of biotechnology* **127,** 65–78; 10.1016/j.jbiotec.2006.06.018 (2006).

88. Spearman, P. & Ratner, L. Human immunodeficiency virus type 1 capsid formation in reticulocyte lysates. *Journal of virology* **70,** 8187–8194; 10.1128/JVI.70.11.8187-8194.1996 (1996).

89. Wang, X. *et al.* An optimized yeast cell-free system: sufficient for translation of human papillomavirus 58 L1 mRNA and assembly of virus-like particles. *Journal of bioscience and bioengineering* **106,** 8–15; 10.1263/jbb.106.8 (2008).

90. Cooke, R. & Penon, P. In vitro transcription from cauliflower mosaic virus promoters by a cell-free extract from tobacco cells. *Plant molecular biology* **14,** 391–405; 10.1007/BF00028775 (1990).

91. OHTAKA, Y. & SPIEGELMAN, S. TRANSLATIONAL CONTROL OF PROTEIN SYNTHESIS IN A CELL-FREE SYSTEM DIRECTED BY A POLYCISTRONIC VIRAL RNA. *Science (New York, N.Y.)* **142,** 493–497; 10.1126/science.142.3591.493 (1963).

92. Dasmahapatra, B. *et al.* Cell-free expression of the coxsackievirus 3C protease using the translational initiation signal of an insect virus RNA and its characterization. *Virus Research* **20,** 237–249; 10.1016/0168-1702(91)90078-A (1991).

93. Ansari, I. H. *et al.* Cloning, sequencing, and expression of the hepatitis E virus (HEV) nonstructural open reading frame 1 (ORF1). *Journal of medical virology* **60,** 275–283 (2000).

94. Jirasko, V. *et al.* Proton-Detected Solid-State NMR of the Cell-Free Synthesized α-Helical Transmembrane Protein NS4B from Hepatitis C Virus. *Chembiochem : a European journal of chemical biology* **21,** 1453–1460; 10.1002/cbic.201900765 (2020).

95. Welsh, J. P., Lu, Y., He, X.-S., Greenberg, H. B. & Swartz, J. R. Cell-free production of trimeric influenza hemagglutinin head domain proteins as vaccine antigens. *Biotechnology and bioengineering* **109,** 2962–2969; 10.1002/bit.24581 (2012).

96. Klein, K. C., Polyak, S. J. & Lingappa, J. R. Unique features of hepatitis C virus capsid formation revealed by de novo cell-free assembly. *Journal of virology* **78,** 9257–9269; 10.1128/JVI.78.17.9257-9269.2004 (2004).

97. Mezhyrova, J. *et al.* Membrane insertion mechanism and molecular assembly of the bacteriophage lysis toxin ΦX174-E. *The FEBS journal* **288,** 3300–3316; 10.1111/febs.15642 (2021).

98. Shin, J., Jardine, P. & Noireaux, V. Genome replication, synthesis, and assembly of the bacteriophage T7 in a single cell-free reaction. *ACS synthetic biology* **1,** 408–413; 10.1021/sb300049p (2012).

99. Sheng, J., Lei, S., Yuan, L. & Feng, X. Cell-free protein synthesis of norovirus virus-like particles. *RSC Adv.* **7,** 28837–28840; 10.1039/C7RA03742B (2017).

100. Colant, N., Melinek, B., Frank, S., Rosenberg, W. & Bracewell, D. G. Escherichia Coli-Based Cell-Free Protein Synthesis for Iterative Design of Tandem-Core Virus-Like Particles. *Vaccines* **9**; 10.3390/vaccines9030193 (2021).

101. Bundy, B. C. & Swartz, J. R. Efficient disulfide bond formation in virus-like particles. *Journal of biotechnology* **154,** 230–239; 10.1016/j.jbiotec.2011.04.011 (2011).

102. Bundy, B. C., Franciszkowicz, M. J. & Swartz, J. R. Escherichia coli-based cell-free synthesis of virus-like particles. *Biotechnology and bioengineering* **100,** 28–37; 10.1002/bit.21716 (2008).

103. Lu, Y., Chan, W., Ko, B. Y., VanLang, C. C. & Swartz, J. R. Assessing sequence plasticity of a virus-like nanoparticle by evolution toward a versatile scaffold for vaccines and drug delivery. *Proceedings of the National Academy of Sciences of the United States of America* **112,** 12360–12365; 10.1073/pnas.1510533112 (2015).

104. Smith, M. T., Varner, C. T., Bush, D. B. & Bundy, B. C. The incorporation of the A2 protein to produce novel Qβ virus-like particles using cell-free protein synthesis. *Biotechnology progress* **28,** 549–555; 10.1002/btpr.744 (2012).

105. Spice, A. J., Aw, R., Bracewell, D. G. & Polizzi, K. M. Synthesis and Assembly of Hepatitis B Virus-Like Particles in a Pichia pastoris Cell-Free System. *Front. Bioeng. Biotechnol.* **8,** 72; 10.3389/fbioe.2020.00072 (2020).

106. Patel, K. G. & Swartz, J. R. Surface functionalization of virus-like particles by direct conjugation using azide-alkyne click chemistry. *Bioconjugate chemistry* **22,** 376–387; 10.1021/bc100367u (2011).

107. Dillon, M. *et al.* Current Trends and Challenges for Rapid SMART Diagnostics at Point-of-Site Testing for Marine Toxins. *Sensors (Basel, Switzerland)* **21**; 10.3390/s21072499 (2021).

108. Roth, K. D. R. *et al.* Developing Recombinant Antibodies by Phage Display Against Infectious Diseases and Toxins for Diagnostics and Therapy. *Frontiers in cellular and infection microbiology* **11,** 697876; 10.3389/fcimb.2021.697876 (2021).

109. Walper, S. A. *et al.* Detecting Biothreat Agents: From Current Diagnostics to Developing Sensor Technologies. *ACS sensors* **3,** 1894–2024; 10.1021/acssensors.8b00420 (2018).

110. Granum, P. E. Bacillus cereus and its toxins. *Journal of Applied Bacteriology* **76,** 61S-66S; 10.1111/j.1365-2672.1994.tb04358.x (1994).

111. Lambert, J. C. & Lipscomb, J. C. Mode of action as a determining factor in additivity models for chemical mixture risk assessment. *Regulatory Toxicology and Pharmacology* **49,** 183–194; 10.1016/j.yrtph.2007.07.002 (2007).

112. Drobniewski, F. A. Bacillus cereus and related species. *Clinical Microbiology Reviews* **6,** 324–338; 10.1128/CMR.6.4.324 (1993).

113. Senesi, S. & Ghelardi, E. Production, secretion and biological activity of Bacillus cereus enterotoxins. *Toxins* **2,** 1690–1703; 10.3390/toxins2071690 (2010).

114. Rasko, D. A., Altherr, M. R., Han, C. S. & Ravel, J. Genomics of the Bacillus cereus group of organisms. *FEMS microbiology reviews* **29,** 303–329; 10.1016/j.femsre.2004.12.005 (2005).

115. Stenfors Arnesen, L. P., Fagerlund, A. & Granum, P. E. From soil to gut: Bacillus cereus and its food poisoning toxins. *FEMS microbiology reviews* **32,** 579–606; 10.1111/j.1574-6976.2008.00112.x (2008).

116. Rajkovic, A. *et al.* Heat resistance of Bacillus cereus emetic toxin, cereulide. *Letters in applied microbiology* **46,** 536–541; 10.1111/j.1472-765X.2008.02350.x (2008).

117. Agata, N., Ohta, M., Mori, M. & Isobe, M. A novel dodecadepsipeptide, cereulide, is an emetic toxin of. *FEMS microbiology letters* **129,** 17–19; 10.1016/0378-1097(95)00119-P (1995).

118. Dal Peraro, M. & van der Goot, F. G. Pore-forming toxins: ancient, but never really out of fashion. *Nature reviews. Microbiology* **14,** 77–92; 10.1038/nrmicro.2015.3 (2016).

119. Guinebretière, M.-H. *et al.* Ability of Bacillus cereus group strains to cause food poisoning varies according to phylogenetic affiliation (groups I to VII) rather than species affiliation. *Journal of clinical microbiology* **48,** 3388–3391; 10.1128/JCM.00921-10 (2010).

120. Lund, T. & Granum, P. E. Characterisation of a non-haemolytic enterotoxin complex from Bacillus cereus isolated after a foodborne outbreak. *FEMS microbiology letters* **141,** 151–156; 10.1111/j.1574-6968.1996.tb08377.x (1996).

121. Lindbäck, T., Fagerlund, A., Rødland, M. S. & Granum, P. E. Characterization of the Bacillus cereus Nhe enterotoxin. *Microbiology (Reading, England)* **150,** 3959–3967; 10.1099/mic.0.27359-0 (2004).

122. Fagerlund, A., Lindbäck, T., Storset, A. K., Granum, P. E. & Hardy, S. P. Bacillus cereus Nhe is a pore-forming toxin with structural and functional properties similar to the ClyA (HlyE, SheA) family of haemolysins, able to induce osmotic lysis in epithelia. *Microbiology (Reading, England)* **154,** 693–704; 10.1099/mic.0.2007/014134-0 (2008).

123. Lindbäck, T. *et al.* Cytotoxicity of the Bacillus cereus Nhe enterotoxin requires specific binding order of its three exoprotein components. *Infection and immunity* **78,** 3813–3821; 10.1128/IAI.00247-10 (2010).

124. Beecher, D. J. & Wong, A. C. Tripartite hemolysin BL from Bacillus cereus. Hemolytic analysis of component interactions and a model for its characteristic paradoxical zone phenomenon. *The Journal of biological chemistry* **272,** 233–239; 10.1074/jbc.272.1.233 (1997).

125. Beecher, D. J. & Macmillan, J. D. Characterization of the components of hemolysin BL from Bacillus cereus. *Infection and immunity* **59,** 1778–1784; 10.1128/iai.59.5.1778-1784.1991 (1991).

126. Thompson, N. E., Ketterhagen, M. J., Bergdoll, M. S. & Schantz, E. J. Isolation and some properties of an enterotoxin produced by Bacillus cereus. *Infection and immunity* **43,** 887–894; 10.1128/iai.43.3.887-894.1984 (1984).

127. Sastalla, I. *et al.* The Bacillus cereus Hbl and Nhe tripartite enterotoxin components assemble sequentially on the surface of target cells and are not interchangeable. *PloS one* **8,** e76955; 10.1371/journal.pone.0076955 (2013).

128. Madegowda, M., Eswaramoorthy, S., Burley, S. K. & Swaminathan, S. X-ray crystal structure of the B component of Hemolysin BL from Bacillus cereus. *Proteins* **71,** 534–540; 10.1002/prot.21888 (2008).

129. Tausch, F. *et al.* Evidence for Complex Formation of the Bacillus cereus Haemolysin BL Components in Solution. *Toxins* **9**; 10.3390/toxins9090288 (2017).

130. Crnković, A., Srnko, M. & Anderluh, G. Biological Nanopores: Engineering on Demand. *Life (Basel, Switzerland)* **11**; 10.3390/life11010027 (2021).

131. Cao, C. & Long, Y.-T. Biological Nanopores: Confined Spaces for Electrochemical Single-Molecule Analysis. *Accounts of chemical research* **51,** 331–341; 10.1021/acs.accounts.7b00143 (2018).

132. Iacovache, I., Bischofberger, M. & van der Goot, F. G. Structure and assembly of pore-forming proteins. *Current opinion in structural biology* **20,** 241–246; 10.1016/j.sbi.2010.01.013 (2010).

133. Júnior, J. J. S. *et al.* Alpha-hemolysin nanopore allows discrimination of the microcystins variants. *RSC Adv.* **9,** 14683–14691; 10.1039/C8RA10384D (2019).

134. Nivala, J., Mulroney, L., Li, G., Schreiber, J. & Akeson, M. Discrimination among protein variants using an unfoldase-coupled nanopore. *ACS nano* **8,** 12365–12375; 10.1021/nn5049987 (2014).

135. Cairo, J., Gherman, I., Day, A. & Cook, P. E. Bacillus cytotoxicus-A potentially virulent food-associated microbe. *Journal of Applied Bacteriology* **132,** 31–40; 10.1111/jam.15214 (2022).

136. Lund, T., Buyser, M. L. de & Granum, P. E. A new cytotoxin from Bacillus cereus that may cause necrotic enteritis. *Molecular microbiology* **38,** 254–261; 10.1046/j.1365-2958.2000.02147.x (2000).

137. Hardy, S. P., Lund, T. & Granum, P. E. CytK toxin of Bacillus cereus forms pores in planar lipid bilayers and is cytotoxic to intestinal epithelia. *FEMS microbiology letters* **197,** 47–51; 10.1111/j.1574-6968.2001.tb10581.x (2001).

138. Burtscher, J., Etter, D., Biggel, M., Schlaepfer, J. & Johler, S. Further Insights into the Toxicity of Bacillus cytotoxicus Based on Toxin Gene Profiling and Vero Cell Cytotoxicity Assays. *Toxins* **13**; 10.3390/toxins13040234 (2021).

139. Fagerlund, A., Ween, O., Lund, T., Hardy, S. P. & Granum, P. E. Genetic and functional analysis of the cytK family of genes in Bacillus cereus. *Microbiology (Reading, England)* **150,** 2689–2697; 10.1099/mic.0.26975-0 (2004).

140. Murdock, B. S. Tracking toxins. Biomonitoring outshines the indirect assessment of exposure in determining which pollulants enter the body, and whether they cause disease or disability. *EMBO reports* **6,** 701–705; 10.1038/sj.embor.7400493 (2005).

141. Alahi, M. E. E. & Mukhopadhyay, S. C. Detection Methodologies for Pathogen and Toxins: A Review. *Sensors (Basel, Switzerland)* **17**; 10.3390/s17081885 (2017).

142. Kurmayer, R. *et al.* Chemically labeled toxins or bioactive peptides show a heterogeneous intracellular distribution and low spatial overlap with autofluorescence in bloom-forming cyanobacteria. *Sci Rep* **10,** 2781; 10.1038/s41598-020-59381-w (2020).

143. Sinai, N., Meir, A. & Bogin, O. Fluorescently-Labeled Toxins: Novel Tools for Working with Live Cells. *Alomone Labs* (2017).

144. Spolaore, B., Fernández, J., Lomonte, B., Massimino, M. L. & Tonello, F. Enzymatic labelling of snake venom phospholipase A2 toxins. *Toxicon : official journal*

of the International Society on Toxinology **170,** 99–107; 10.1016/j.toxicon.2019.09.019 (2019).

145. Beddoe, T., Paton, A. W., Le Nours, J., Rossjohn, J. & Paton, J. C. Structure, biological functions and applications of the AB5 toxins. *Trends in biochemical sciences* **35,** 411–418; 10.1016/j.tibs.2010.02.003 (2010).

146. Paton, A. W., Srimanote, P., Talbot, U. M., Wang, H. & Paton, J. C. A new family of potent AB(5) cytotoxins produced by Shiga toxigenic Escherichia coli. *The Journal of Experimental Medicine* **200,** 35–46; 10.1084/jem.20040392 (2004).

147. Lencer, W. I. *et al.* Proteolytic activation of cholera toxin and Escherichia coli labile toxin by entry into host epithelial cells. Signal transduction by a protease-resistant toxin variant. *The Journal of biological chemistry* **272,** 15562–15568; 10.1074/jbc.272.24.15562 (1997).

148. Sixma, T. K. *et al.* Crystal structure of a cholera toxin-related heat-labile enterotoxin from E. coli. *Nature* **351,** 371–377; 10.1038/351371a0 (1991).

149. Sack, D. A., Sack, R. B., Nair, G. B. & Siddique, A. K. Cholera. *The Lancet* **363,** 223–233; 10.1016/S0140-6736(03)15328-7 (2004).

150. Wolf, A. A. *et al.* Ganglioside structure dictates signal transduction by cholera toxin and association with caveolae-like membrane domains in polarized epithelia. *The Journal of Cell Biology* **141,** 917–927; 10.1083/jcb.141.4.917 (1998).

151. Chinnapen, D. J.-F., Chinnapen, H., Saslowsky, D. & Lencer, W. I. Rafting with cholera toxin: endocytosis and trafficking from plasma membrane to ER. *FEMS microbiology letters* **266,** 129–137; 10.1111/j.1574-6968.2006.00545.x (2007).

152. Wands, A. M. *et al.* Fucosylation and protein glycosylation create functional receptors for cholera toxin. *eLife* **4,** e09545; 10.7554/eLife.09545 (2015).

153. Yanagisawa, M., Ariga, T. & Yu, R. K. Cholera toxin B subunit binding does not correlate with GM1 expression: a study using mouse embryonic neural precursor cells. *Glycobiology* **16,** 19G-22G; 10.1093/glycob/cwl003 (2006).

154. Guerrant, R. L., Brunton, L. L., Schnaitman, T. C., Rebhun, L. I. & Gilman, A. G. Cyclic adenosine monophosphate and alteration of Chinese hamster ovary cell morphology: a rapid, sensitive in vitro assay for the enterotoxins of Vibrio cholerae and Escherichia coli. *Infection and immunity* **10,** 320–327; 10.1128/iai.10.2.320-327.1974 (1974).

155. Rodighiero, C. *et al.* Structural basis for the differential toxicity of cholera toxin and Escherichia coli heat-labile enterotoxin. Construction of hybrid toxins identifies the A2-

domain as the determinant of differential toxicity. *The Journal of biological chemistry* **274,** 3962–3969; 10.1074/jbc.274.7.3962 (1999).

156. Feng, Y. *et al.* Retrograde transport of cholera toxin from the plasma membrane to the endoplasmic reticulum requires the trans-Golgi network but not the Golgi apparatus in Exo2-treated cells. *EMBO reports* **5,** 596–601; 10.1038/sj.embor.7400152 (2004).

157. Awan, K. H. The therapeutic usage of botulinum toxin (Botox) in non-cosmetic head and neck conditions - An evidence based review. *Saudi Pharmaceutical Journal : SPJ* **25,** 18–24; 10.1016/j.jsps.2016.04.024 (2017).

158. Frangieh, J. *et al.* Snake Venom Components: Tools and Cures to Target Cardiovascular Diseases. *Molecules (Basel, Switzerland)* **26**; 10.3390/molecules26082223 (2021).

159. Fingerut, E., Gutter, B., Meir, R., Eliahoo, D. & Pitcovski, J. Vaccine and adjuvant activity of recombinant subunit B of E. coli enterotoxin produced in yeast. *Vaccine* **23,** 4685–4696; 10.1016/j.vaccine.2005.03.050 (2005).

160. Ghattas, M., Dwivedi, G., Lavertu, M. & Alameh, M.-G. Vaccine Technologies and Platforms for Infectious Diseases: Current Progress, Challenges, and Opportunities. *Vaccines* **9**; 10.3390/vaccines9121490 (2021).

161. Tamura, S.-i. *et al.* Synergistic action of cholera toxin B subunit (and Escherichia coli heat-labile toxin B subunit) and a trace amount of cholera whole toxin as an adjuvant for nasal influenza vaccine. *Vaccine* **12,** 419–426; 10.1016/0264-410X(94)90118-X (1994).

162. Frankel, A. E., Kreitman, R. J. & Sausville, E. A. Targeted toxins. *Clinical cancer research : an official journal of the American Association for Cancer Research* **6,** 326–334 (2000).

163. Kreitman, R. J. Immunotoxins for targeted cancer therapy. *The AAPS journal* **8,** E532-51; 10.1208/aapsj080363 (2006).

164. *LiverTox: Clinical and Research Information on Drug-Induced Liver Injury. Denileukin Diftitox* (Bethesda (MD), 2012).

165. Ravel, S., Colombatti, M. & Casellas, P. Internalization and intracellular fate of anti-CD5 monoclonal antibody and anti-CD5 ricin A-chain immunotoxin in human leukemic T cells. *Blood* **79,** 1511–1517; 10.1182/blood.V79.6.1511.1511 (1992).

166. Olsnes, S., Sandvig, K., Petersen, O. W. & van Deurs, B. Immunotoxins--entry into cells and mechanisms of action. *Immunology today* **10,** 291–295 (1989).

167. Fuchs, H., Weng, A. & Gilabert-Oriol, R. Augmenting the Efficacy of Immunotoxins and Other Targeted Protein Toxins by Endosomal Escape Enhancers. *Toxins* **8**; 10.3390/toxins8070200 (2016).

168. Wolf, P. Targeted Toxins for the Treatment of Prostate Cancer. *Biomedicines* **9**; 10.3390/biomedicines9080986 (2021).

169. Sasada, T., Azuma, K., Ohtake, J. & Fujimoto, Y. Immune Responses to Epidermal Growth Factor Receptor (EGFR) and Their Application for Cancer Treatment. *Frontiers in pharmacology* **7,** 405; 10.3389/fphar.2016.00405 (2016).

170. Bachran, C., Abdelazim, S., Fattah, R. J., Liu, S. & Leppla, S. H. Recombinant expression and purification of a tumor-targeted toxin in Bacillus anthracis. *Biochemical and biophysical research communications* **430,** 150–155; 10.1016/j.bbrc.2012.11.055 (2013).

171. Goldberg, M. R. *et al.* Phase I clinical study of the recombinant oncotoxin TP40 in superficial bladder cancer. *Clinical cancer research : an official journal of the American Association for Cancer Research* **1,** 57–61 (1995).

172. Fischer, A., Wolf, I., Fuchs, H., Masilamani, A. P. & Wolf, P. Pseudomonas Exotoxin A Based Toxins Targeting Epidermal Growth Factor Receptor for the Treatment of Prostate Cancer. *Toxins* **12**; 10.3390/toxins12120753 (2020).

173. Gilabert-Oriol, R. *et al.* Immunotoxins constructed with ribosome-inactivating proteins and their enhancers: a lethal cocktail with tumor specific efficacy. *Current Pharmaceutical Design* **20,** 6584–6643; 10.2174/1381612820666140826153913 (2014).

174. Fermani, S. *et al.* The 1.4 anstroms structure of dianthin 30 indicates a role of surface potential at the active site of type 1 ribosome inactivating proteins. *Journal of structural biology* **149,** 204–212; 10.1016/j.jsb.2004.11.007 (2005).

175. Stirpe, F., Williams, D. G., Onyon, L. J., Legg, R. F. & Stevens, W. A. Dianthins, ribosome-damaging proteins with anti-viral properties from Dianthus caryophyllus L. (carnation). *The Biochemical journal* **195,** 399–405; 10.1042/bj1950399 (1981).

176. Lorenzetti, I. *et al.* Genetic grafting of membrane-acting peptides to the cytotoxin dianthin augments its ability to de-stabilize lipid bilayers and enhances its cytotoxic potential as the component of transferrin-toxin conjugates. *Int. J. Cancer* **86,** 582–589; 10.1002/(SICI)1097-0215(20000515)86:4<582::AID-IJC22>3.0.CO;2-I (2000).

177. Barbieri, L. *et al.* Polynucleotide: adenosine glycosidase activity of immunotoxins containing ribosome-inactivating proteins. *Journal of drug targeting* **8,** 281–288; 10.3109/10611860008997906 (2000).

178. Bolognesi, A. *et al.* Anti-CD30 immunotoxins with native and recombinant dianthin 30. *Cancer immunology, immunotherapy : CII* **40,** 109–114; 10.1007/BF01520292 (1995).

179. Gilabert-Oriol, R. *et al.* Combinatorial approach to increase efficacy of Cetuximab, Panitumumab and Trastuzumab by dianthin conjugation and co-application of SO1861. *Biochemical pharmacology* **97,** 247–255; 10.1016/j.bcp.2015.07.040 (2015).

180. Bhargava, C. *et al.* Targeted dianthin is a powerful toxin to treat pancreatic carcinoma when applied in combination with the glycosylated triterpene SO1861. *Molecular oncology* **11,** 1527–1543; 10.1002/1878-0261.12115 (2017).

181. Gilabert-Oriol, R. *et al.* Small structural differences of targeted anti-tumor toxins result in strong variation of protein expression. *Protein expression and purification* **91,** 54–60; 10.1016/j.pep.2013.07.004 (2013).

182. Weng, A. *et al.* The toxin component of targeted anti-tumor toxins determines their efficacy increase by saponins. *Molecular oncology* **6,** 323–332; 10.1016/j.molonc.2012.01.004 (2012).

183. Zarinwall, A. *et al.* Magnetic Nanoparticle-Based Dianthin Targeting for Controlled Drug Release Using the Endosomal Escape Enhancer SO1861. *Nanomaterials* **11**; 10.3390/nano11041057 (2021).

184. Piret, J. & Boivin, G. Pandemics Throughout History. *Frontiers in microbiology* **11,** 631736; 10.3389/fmicb.2020.631736 (2020).

185. Dobson, A. P. *et al.* Ecology and economics for pandemic prevention. *Science (New York, N.Y.)* **369,** 379–381; 10.1126/science.abc3189 (2020).

186. Kim, D. *et al.* The Architecture of SARS-CoV-2 Transcriptome. *Cell* **181,** 914-921.e10; 10.1016/j.cell.2020.04.011 (2020).

187. Yoshimoto, F. K. The Proteins of Severe Acute Respiratory Syndrome Coronavirus-2 (SARS CoV-2 or n-COV19), the Cause of COVID-19. *The protein journal* **39,** 198–216; 10.1007/s10930-020-09901-4 (2020).

188. Shu, T. *et al.* SARS-Coronavirus-2 Nsp13 Possesses NTPase and RNA Helicase Activities That Can Be Inhibited by Bismuth Salts. *Virologica Sinica* **35,** 321–329; 10.1007/s12250-020-00242-1 (2020).

189. Gao, Y. *et al.* Structure of the RNA-dependent RNA polymerase from COVID-19 virus. *Science (New York, N.Y.)* **368,** 779–782; 10.1126/science.abb7498 (2020).

190. Kern, D. M. *et al.* Cryo-EM structure of SARS-CoV-2 ORF3a in lipid nanodiscs. *Nature structural & molecular biology* **28,** 573–582; 10.1038/s41594-021-00619-0 (2021).

191. Flower, T. G. *et al.* Structure of SARS-CoV-2 ORF8, a rapidly evolving immune evasion protein. *Proceedings of the National Academy of Sciences of the United States of America* **118**; 10.1073/pnas.2021785118 (2021).

192. Miorin, L. *et al.* SARS-CoV-2 Orf6 hijacks Nup98 to block STAT nuclear import and antagonize interferon signaling. *Proceedings of the National Academy of Sciences of the United States of America* **117,** 28344–28354; 10.1073/pnas.2016650117 (2020).

193. Rosenthal, S. H. *et al. Identification of eight SARS-CoV-2 ORF7a deletion variants in 2,726 clinical specimens* (2020).

194. Yang, R. *et al.* SARS-CoV-2 Accessory Protein ORF7b Mediates Tumor Necrosis Factor-α-Induced Apoptosis in Cells. *Frontiers in microbiology* **12,** 654709; 10.3389/fmicb.2021.654709 (2021).

195. Hassan, S. S. *et al.* Notable sequence homology of the ORF10 protein introspects the architecture of SARS-CoV-2. *International Journal of Biological Macromolecules* **181,** 801–809; 10.1016/j.ijbiomac.2021.03.199 (2021).

196. Pancer, K. *et al.* The SARS-CoV-2 ORF10 is not essential in vitro or in vivo in humans. *PLoS pathogens* **16,** e1008959; 10.1371/journal.ppat.1008959 (2020).

197. Schloßhauer, J. L., Cavak, N., Zemella, A., Thoring, L. & Kubick, S. Cell Engineering and Cultivation of Chinese Hamster Ovary Cells for the Development of Orthogonal Eukaryotic Cell-free Translation Systems. *Front. Mol. Biosci.* **9,** 832379; 10.3389/fmolb.2022.832379 (2022).

198. Banerjee, A. K. *et al.* SARS-CoV-2 Disrupts Splicing, Translation, and Protein Trafficking to Suppress Host Defenses. *Cell* **183,** 1325-1339.e21; 10.1016/j.cell.2020.10.004 (2020).

199. van Schaeybroeck, S. *et al.* Chemotherapy-induced epidermal growth factor receptor activation determines response to combined gefitinib/chemotherapy treatment in non-small cell lung cancer cells. *Mol Cancer Ther* **5,** 1154–1165; 10.1158/1535-7163.MCT-05-0446 (2006).

200. Zhang, F. *et al.* Quantification of epidermal growth factor receptor expression level and binding kinetics on cell surfaces by surface plasmon resonance imaging. *Anal. Chem.* **87,** 9960–9965; 10.1021/acs.analchem.5b02572 (2015).

201. Promega. *Technical Manual - CellTox™ Green Cytotoxicity* (2020).

202. Song, L. *et al.* Structure of staphylococcal alpha-hemolysin, a heptameric transmembrane pore. *Science (New York, N.Y.)* **274,** 1859–1866; 10.1126/science.274.5294.1859 (1996).

203. Jessberger, N. *et al.* Binding to The Target Cell Surface Is The Crucial Step in Pore Formation of Hemolysin BL from Bacillus cereus. *Toxins* **11**; 10.3390/toxins11050281 (2019).

204. Kaser, D. *Research Internship - Cell-free synthesis and characterization of the enterotoxin Cytotoxin K from Bacillus cereus* (2020).

205. Kaser, D. *Masterarbeit, Funktionelle Charakterisierung des Enterotoxins Cytotoxin K aus Bacillus cereus: Entwicklung einer Nanopore* (2021).

206. Jack, L. *Master thesis, Synthesis and functional characterization of AB5 toxins: Applications for toxin-based therapies using cell-free systems* (Technical University of Berlin; Fraunhofer Institute for Cell Therapy and Immunology (IZI), Branch Bioanalytics and Bioprocesses (IZI-BB), Potsdam-Golm, Germany, 2020).

207. Zrimi, J., Ng Ling, A., Giri-Rachman Arifin, E., Feverati, G. & Lesieur, C. Cholera toxin B subunits assemble into pentamers--proposition of a fly-casting mechanism. *PloS one* **5,** e15347; 10.1371/journal.pone.0015347 (2010).

208. Yamamoto, S. *et al.* Mutants in the ADP-ribosyltransferase cleft of cholera toxin lack diarrheagenicity but retain adjuvanticity. *The Journal of Experimental Medicine* **185,** 1203–1210; 10.1084/jem.185.7.1203 (1997).

209. Kennedy, D. C. *et al.* Cellular consequences of copper complexes used to catalyze bioorthogonal click reactions. *Journal of the American Chemical Society* **133,** 17993–18001; 10.1021/ja2083027 (2011).

210. Bachran, C. *et al.* Chimeric toxins inhibit growth of primary oral squamous cell carcinoma cells. *Cancer biology & therapy* **7,** 237–242; 10.4161/cbt.7.2.5264 (2008).

211. Lapointe, C. P. *et al.* Dynamic competition between SARS-CoV-2 NSP1 and mRNA on the human ribosome inhibits translation initiation. *Proceedings of the National Academy of Sciences of the United States of America* **118**; 10.1073/pnas.2017715118 (2021).

212. Tan, Y., Schneider, T., Leong, M., Aravind, L. & Zhang, D. Novel Immunoglobulin Domain Proteins Provide Insights into Evolution and Pathogenesis of SARS-CoV-2-Related Viruses. *mBio* **11**; 10.1128/mBio.00760-20 (2020).

213. Shang, J. *et al.* Cell entry mechanisms of SARS-CoV-2. *Proceedings of the National Academy of Sciences of the United States of America* **117,** 11727–11734; 10.1073/pnas.2003138117 (2020).

214. Grant, B. D. *et al.* A SARS-CoV-2 coronavirus nucleocapsid protein antigen-detecting lateral flow assay. *PloS one* **16,** e0258819; 10.1371/journal.pone.0258819 (2021).

215. Grifoni, A. *et al.* A Sequence Homology and Bioinformatic Approach Can Predict Candidate Targets for Immune Responses to SARS-CoV-2. *Cell host & microbe* **27,** 671-680.e2; 10.1016/j.chom.2020.03.002 (2020).

216. Surya, W., Li, Y., Verdià-Bàguena, C., Aguilella, V. M. & Torres, J. MERS coronavirus envelope protein has a single transmembrane domain that forms pentameric ion channels. *Virus Research* **201,** 61–66; 10.1016/j.virusres.2015.02.023 (2015).

217. Ramm, F. *et al.* The Potential of Eukaryotic Cell-Free Systems as a Rapid Response to Novel Zoonotic Pathogens: Analysis of SARS-CoV-2 Viral Proteins. *Front. Bioeng. Biotechnol.* **10,** 617; 10.3389/fbioe.2022.896751 (2022).

218. Anderson, P. D. Bioterrorism: toxins as weapons. *Journal of pharmacy practice* **25,** 121–129; 10.1177/0897190012442351 (2012).

219. Berger, T. *et al.* Toxins as biological weapons for terror-characteristics, challenges and medical countermeasures: a mini-review. *Disaster and Mil Med* **2,** 7; 10.1186/s40696-016-0017-4 (2016).

220. Zemella, A., Thoring, L., Hoffmeister, C. & Kubick, S. Cell-Free Protein Synthesis: Pros and Cons of Prokaryotic and Eukaryotic Systems. *Chembiochem : a European journal of chemical biology* **16,** 2420–2431; 10.1002/cbic.201500340 (2015).

221. Stech, M. *et al.* Cell-free synthesis of functional antibodies using a coupled in vitro transcription-translation system based on CHO cell lysates. *Sci Rep* **7,** 12030; 10.1038/s41598-017-12364-w (2017).

222. Chemla, Y. *et al.* Simplified methodology for a modular and genetically expanded protein synthesis in cell-free systems. *Synthetic and systems biotechnology* **4,** 189–196; 10.1016/j.synbio.2019.10.002 (2019).

223. Hershewe, J. M. *et al.* Improving cell-free glycoprotein synthesis by characterizing and enriching native membrane vesicles. *Nature communications* **12,** 2363; 10.1038/s41467-021-22329-3 (2021).

224. Stech, M. *et al.* Synthesis of Fluorescently Labeled Antibodies Using Non-Canonical Amino Acids in Eukaryotic Cell-Free Systems. *Methods in molecular biology (Clifton, N.J.)* **2305,** 175–190; 10.1007/978-1-0716-1406-8_9 (2021).

225. Gillet, D. & Barbier, J. 4 - Diphtheria toxin. In *The comprehensive sourcebook of bacterial protein toxins,* edited by J. E. Alouf, D. Ladant & M. R. Popoff (Elsevier, Amsterdam, 2015), pp. 111–132.

226. Fogeron, M.-L. *et al. SARS-CoV-2 ORF7b: is a bat virus protein homologue a major cause of COVID-19 symptoms?* (2021).

227. Altincekic, N. *et al.* Large-Scale Recombinant Production of the SARS-CoV-2 Proteome for High-Throughput and Structural Biology Applications. *Frontiers in Molecular Biosciences* **8,** 653148; 10.3389/fmolb.2021.653148 (2021).

228. Riss, T. L. *et al.* Assay Guidance Manual. Cell Viability Assays (2004).

229. Crowley, L. C. *et al.* Measuring Cell Death by Propidium Iodide Uptake and Flow Cytometry. *Cold Spring Harbor protocols* **2016**; 10.1101/pdb.prot087163 (2016).

230. Rebecca Buxton. *Blood agar plates and hemolysis protocols* (American Society for Microbiology, 2005).

231. Delcour, A. H. Function and modulation of bacterial porins: insights from electrophysiology. *FEMS microbiology letters* **151,** 115–123; 10.1111/j.1574-6968.1997.tb12558.x (1997).

232. Berrier, C. *et al.* Cell-free synthesis of a functional ion channel in the absence of a membrane and in the presence of detergent. *Biochemistry* **43,** 12585–12591; 10.1021/bi049049y (2004).

233. Bornhorst, J. A. & Falke, J. J. Purification of proteins using polyhistidine affinity tags. *Methods in enzymology* **326,** 245–254; 10.1016/s0076-6879(00)26058-8 (2000).

234. Rajkovic, A. *et al.* Detection of toxins involved in foodborne diseases caused by Gram-positive bacteria. *Comprehensive reviews in food science and food safety* **19,** 1605–1657; 10.1111/1541-4337.12571 (2020).

235. Ligler, F. S. *et al.* Array biosensor for detection of toxins. *Analytical and bioanalytical chemistry* **377,** 469–477; 10.1007/s00216-003-1992-0 (2003).

236. Dias-Lopes, C., Paiva, A. L., Guerra-Duarte, C., Molina, F. & Felicori, L. Venomous Arachnid Diagnostic Assays, Lessons from Past Attempts. *Toxins* **10**; 10.3390/toxins10090365 (2018).

237. Gherezgihier, B. *et al.* DETECTION SHELLFISH POISONING, MARINE TOXINS, OF FOOD BY HPLC:PARALYTIC SHELLFISH POISONING. *IJAR* **5,** 1551–1558; 10.21474/IJAR01/5671 (2017).

238. Reverté, L., Soliño, L., Carnicer, O., Diogène, J. & Campàs, M. Alternative methods for the detection of emerging marine toxins: biosensors, biochemical assays and cell-based assays. *Marine drugs* **12,** 5719–5763; 10.3390/md12125719 (2014).

239. Krause, N. *et al.* Performance characteristics of the Duopath® cereus enterotoxins assay for rapid detection of enterotoxinogenic Bacillus cereus strains. *International journal of food microbiology* **144,** 322–326; 10.1016/j.ijfoodmicro.2010.10.008 (2010).

240. Han, M. S., Byun, J.-H., Cho, Y. & Rim, J. H. RT-PCR for SARS-CoV-2: quantitative versus qualitative. *The Lancet Infectious Diseases* **21,** 165; 10.1016/S1473-3099(20)30424-2 (2021).

241. Wernike, K. *et al.* Pitfalls in SARS-CoV-2 PCR diagnostics. *Transboundary and emerging diseases* **68,** 253–257; 10.1111/tbed.13684 (2021).

242. Dykhuizen, D. Species Numbers in Bacteria. *Proceedings. California Academy of Sciences* **56,** 62–71 (2005).

243. Henkel, J. S., Baldwin, M. R. & Barbieri, J. T. Toxins from bacteria. *EXS* **100,** 1–29; 10.1007/978-3-7643-8338-1_1 (2010).

244. Liu, J. *et al.* Sequential CRISPR-Based Screens Identify LITAF and CDIP1 as the Bacillus cereus Hemolysin BL Toxin Host Receptors. *Cell host & microbe* **28,** 402-410.e5; 10.1016/j.chom.2020.05.012 (2020).

245. Beecher, D. J. & Macmillan, J. D. A novel bicomponent hemolysin from Bacillus cereus. *Infection and immunity* **58,** 2220–2227; 10.1128/iai.58.7.2220-2227.1990 (1990).

246. Hurtado, I. de & Layrisse, M. A quantitative method for the assay of snake venom hemolytic activity. *Toxicon* **2,** 43–49; 10.1016/0041-0101(64)90029-7 (1964).

247. Zhu, K. *et al.* Formation of small transmembrane pores: An intermediate stage on the way to Bacillus cereus non-hemolytic enterotoxin (Nhe) full pores in the absence of NheA. *Biochemical and biophysical research communications* **469,** 613–618; 10.1016/j.bbrc.2015.11.126 (2016).

248. Haug, T. M. *et al.* Formation of very large conductance channels by Bacillus cereus Nhe in Vero and GH(4) cells identifies NheA + B as the inherent pore-forming structure. *The Journal of Membrane Biology* **237,** 1–11; 10.1007/s00232-010-9298-6 (2010).

249. Heilkenbrinker, U. *et al.* Complex formation between NheB and NheC is necessary to induce cytotoxic activity by the three-component Bacillus cereus Nhe enterotoxin. *PloS one* **8,** e63104; 10.1371/journal.pone.0063104 (2013).

250. Liu, X. *et al.* Non-hemolytic enterotoxin of Bacillus cereus induces apoptosis in Vero cells. *Cellular microbiology* **19**; 10.1111/cmi.12684 (2017).

251. Tinker, J. K., Erbe, J. L. & Holmes, R. K. Characterization of fluorescent chimeras of cholera toxin and Escherichia coli heat-labile enterotoxins produced by use of the twin arginine translocation system. *Infection and immunity* **73,** 3627–3635; 10.1128/IAI.73.6.3627-3635.2005 (2005).

252. Stech, M., Hust, M., Schulze, C., Dübel, S. & Kubick, S. Cell-free eukaryotic systems for the production, engineering, and modification of scFv antibody fragments. *Engineering in Life Sciences* **14,** 387–398; 10.1002/elsc.201400036 (2014).

253. Dondapati, S. K. *et al.* Membrane assembly of the functional KcsA potassium channel in a vesicle-based eukaryotic cell-free translation system. *Biosensors & bioelectronics* **59,** 174–183; 10.1016/j.bios.2014.03.004 (2014).

254. Tinker, J. K., Erbe, J. L., Hol, W. G. J. & Holmes, R. K. Cholera holotoxin assembly requires a hydrophobic domain at the A-B5 interface: mutational analysis and development of an in vitro assembly system. *Infection and immunity* **71,** 4093–4101; 10.1128/IAI.71.7.4093-4101.2003 (2003).

255. Matsuda, T., Watanabe, S. & Kigawa, T. Cell-free synthesis system suitable for disulfide-containing proteins. *Biochemical and biophysical research communications* **431,** 296–301; 10.1016/j.bbrc.2012.12.107 (2013).

256. Zawada, J. F. *et al.* Microscale to manufacturing scale-up of cell-free cytokine production--a new approach for shortening protein production development timelines. *Biotechnology and bioengineering* **108,** 1570–1578; 10.1002/bit.23103 (2011).

257. Jobling, M. G., Yang, Z., Kam, W. R., Lencer, W. I. & Holmes, R. K. A single native ganglioside GM1-binding site is sufficient for cholera toxin to bind to cells and complete the intoxication pathway. *mBio* **3**; 10.1128/mBio.00401-12 (2012).

258. Park, E. J., Chang, J. H., Kim, J. S., Chung, S. I. & Yum, J. S. Development of two novel nontoxic mutants of Escherichia coli heat-labile enterotoxin. *Experimental & molecular medicine* **31,** 101–107; 10.1038/emm.1999.17 (1999).

259. Tessier, D. C., Thomas, D. Y., Khouri, H. E., Laliberié, F. & Vernet, T. Enhanced secretion from insect cells of a foreign protein fused to the honeybee melittin signal peptide. *Gene* **98,** 177–183; 10.1016/0378-1119(91)90171-7 (1991).

260. Zhou, N. *et al.* A novel fluorescent retrograde neural tracer: cholera toxin B conjugated carbon dots. *Nanoscale* **7,** 15635–15642; 10.1039/c5nr04361a (2015).

261. Hirsch, J. D. *et al.* Easily reversible desthiobiotin binding to streptavidin, avidin, and other biotin-binding proteins: uses for protein labeling, detection, and isolation. *Analytical biochemistry* **308,** 343–357; 10.1016/s0003-2697(02)00201-4 (2002).

262. Townsend, S. A. *et al.* Tetanus toxin C fragment-conjugated nanoparticles for targeted drug delivery to neurons. *Biomaterials* **28,** 5176–5184; 10.1016/j.biomaterials.2007.08.011 (2007).

263. Lichtenstein, B. R. & Höcker, B. Engineering an AB5 Protein Carrier. *Sci Rep* **8,** 12643; 10.1038/s41598-018-30910-y (2018).

264. Roux, S. *et al.* Internalization of a GFP-tetanus toxin C-terminal fragment fusion protein at mature mouse neuromuscular junctions. *Molecular and cellular neurosciences* **30,** 572–582 (2005).

265. O'Neal, C. J., Amaya, E. I., Jobling, M. G., Holmes, R. K. & Hol, W. G. J. Crystal structures of an intrinsically active cholera toxin mutant yield insight into the toxin activation mechanism. *Biochemistry* **43,** 3772–3782; 10.1021/bi0360152 (2004).

266. Bowman, C. C. & Clements, J. D. Differential biological and adjuvant activities of cholera toxin and Escherichia coli heat-labile enterotoxin hybrids. *Infection and immunity* **69,** 1528–1535; 10.1128/IAI.69.3.1528-1535.2001 (2001).

267. Freise, A. C. & Wu, A. M. In vivo imaging with antibodies and engineered fragments. *Molecular immunology* **67,** 142–152; 10.1016/j.molimm.2015.04.001 (2015).

268. Phillips-Jones, M. K., Watson, F. J. & Martin, R. The 3' codon context effect on UAG suppressor tRNA is different in Escherichia coli and human cells. *Journal of molecular biology* **233,** 1–6; 10.1006/jmbi.1993.1479 (1993).

269. Link, A. J. & Tirrell, D. A. Cell surface labeling of Escherichia coli via copper(I)-catalyzed 3+2 cycloaddition. *Journal of the American Chemical Society* **125,** 11164–11165; 10.1021/ja036765z (2003).

270. Kostova, V. *et al.* Targeted Shiga toxin-drug conjugates prepared via Cu-free click chemistry. *Bioorganic & medicinal chemistry* **23,** 7150–7157; 10.1016/j.bmc.2015.10.010 (2015).

271. Sánchez, J. & Holmgren, J. Cholera toxin structure, gene regulation and pathophysiological and immunological aspects. *Cellular and molecular life sciences : CMLS* **65,** 1347–1360; 10.1007/s00018-008-7496-5 (2008).

272. Majd, S. *et al.* Applications of biological pores in nanomedicine, sensing, and nanoelectronics. *Current opinion in biotechnology* **21,** 439–476; 10.1016/j.copbio.2010.05.002 (2010).

273. Schmidt, J. Membrane platforms for biological nanopore sensing and sequencing. *Current opinion in biotechnology* **39,** 17–27; 10.1016/j.copbio.2015.12.015 (2016).

274. Kasianowicz, J. J., Brandin, E., Branton, D. & Deamer, D. W. Characterization of individual polynucleotide molecules using a membrane channel. *Proceedings of the National Academy of Sciences of the United States of America* **93,** 13770–13773; 10.1073/pnas.93.24.13770 (1996).

275. Winters-Hilt, S. The alpha-hemolysin nanopore transduction detector - single-molecule binding studies and immunological screening of antibodies and aptamers. *BMC bioinformatics* **8 Suppl 7,** S9; 10.1186/1471-2105-8-S7-S9 (2007).

276. Tu, B., Bai, S., Lu, B. & Fang, Q. Conic shapes have higher sensitivity than cylindrical ones in nanopore DNA sequencing. *Sci Rep* **8,** 9097; 10.1038/s41598-018-27517-8 (2018).

277. Bhattacharya, S. *et al.* Molecular dynamics study of MspA arginine mutants predicts slow DNA translocations and ion current blockades indicative of DNA sequence. *ACS nano* **6,** 6960–6968; 10.1021/nn3019943 (2012).

278. Maglia, G., Restrepo, M. R., Mikhailova, E. & Bayley, H. Enhanced translocation of single DNA molecules through alpha-hemolysin nanopores by manipulation of internal charge. *Proceedings of the National Academy of Sciences of the United States of America* **105,** 19720–19725; 10.1073/pnas.0808296105 (2008).

279. Walker, B., Krishnasastry, M., Zorn, L. & Bayley, H. Assembly of the oligomeric membrane pore formed by Staphylococcal alpha-hemolysin examined by truncation mutagenesis. *The Journal of biological chemistry* **267,** 21782–21786 (1992).

280. Sugawara, T. *et al.* Structural basis for pore-forming mechanism of staphylococcal α-hemolysin. *Toxicon : official journal of the International Society on Toxinology* **108,** 226–231; 10.1016/j.toxicon.2015.09.033 (2015).

281. Beattie, S. H. & Williams, A. G. Detection of toxigenic strains of Bacillus cereus and other Bacillus spp. with an improved cytotoxicity assay. *Letters in applied microbiology* **28,** 221–225; 10.1046/j.1365-2672.1999.00498.x (1999).

282. Glasset, B. *et al.* The cytotoxic potential of Bacillus cereus strains of various origins. *Food microbiology* **98,** 103759; 10.1016/j.fm.2021.103759 (2021).

283. Elzonris. *European Medicines Agency (EMA)* (2021).

284. Lumoxiti. *European Medicines Agency (EMA)* (2021).

285. Matasci, M., Hacker, D. L., Baldi, L. & Wurm, F. M. Recombinant therapeutic protein production in cultivated mammalian cells: current status and future prospects. *Drug discovery today. Technologies* **5,** e37-42; 10.1016/j.ddtec.2008.12.003 (2008).

286. Collart, M. A. & Weiss, B. Ribosome pausing, a dangerous necessity for co-translational events. *Nucleic Acids Research* **48,** 1043–1055; 10.1093/nar/gkz763 (2020).

287. Alves de Vasconcelos, M. *et al.* Fruticulosin: A novel type 2 ribosome-inactivating protein from Abrus fruticulosus seeds that exhibits toxic and antileishmanial activity. *Archives of biochemistry and biophysics* **658,** 46–53; 10.1016/j.abb.2018.09.001 (2018).

288. Bolognesi, A. *et al.* A comparison of anti-lymphocyte immunotoxins containing different ribosome-inactivating proteins and antibodies. *Clinical and experimental immunology* **89,** 341–346; 10.1111/j.1365-2249.1992.tb06959.x (1992).

289. Chandler, L. A. *et al.* Targeting tumor cellsvia EGF receptors: Selective toxicity of an HBEGF-toxin fusion protein. *Int. J. Cancer* **78,** 106–111; 10.1002/(SICI)1097-0215(19980925)78:1<106::AID-IJC17>3.0.CO;2-9 (1998).

290. Arkhipov, A. *et al.* Architecture and membrane interactions of the EGF receptor. *Cell* **152,** 557–569; 10.1016/j.cell.2012.12.030 (2013).

291. European Medicines Agency (EMA). *Clinical investigation of the pharmacokinetics of therapeutic proteins | European Medicines Agency* (2007).

292. *Immunogenicity assessment of biotechnology-derived therapeutic proteins | European Medicines Agency* (2017).

293. Stroochi, P., Barbieri, L. & Stirpe, F. Immunological properties of ribosome-inactivating proteins and a saporin immunotoxin. *Journal of immunological methods* **155,** 57–63; 10.1016/0022-1759(92)90271-t (1992).

294. FDA. *S6(R1) Preclinical Safety Evaluation of Biotechnology-Derived Pharmaceuticals* (2012).

295. *Potency testing of cell-based immunotherapy medicinal products for the treatment of cancer | European Medicines Agency* (2016).

296. Conduct of pharmacokinetic studies in target animal species | European Medicines Agency. *European Medicines Agency (EMA)* (2000).

297. Yin, G. *et al.* Aglycosylated antibodies and antibody fragments produced in a scalable in vitro transcription-translation system. *mAbs* **4,** 217–225; 10.4161/mabs.4.2.19202 (2012).

298. Jackson, K., Khnouf, R. & Fan, Z. H. Cell-free protein synthesis in microfluidic 96-well plates. *Methods in molecular biology (Clifton, N.J.)* **1118,** 157–168; 10.1007/978-1-62703-782-2_10 (2014).

299. Zhu, B., Mizoguchi, T., Kojima, T. & Nakano, H. Ultra-high-throughput screening of an in vitro-synthesized horseradish peroxidase displayed on microbeads using cell sorter. *PloS one* **10,** e0127479; 10.1371/journal.pone.0127479 (2015).

300. World Health Organization. Coronavirus disease (COVID-19). Available at https://www.who.int/emergencies/diseases/novel-coronavirus-2019 (2022).

301. Beyer, R. M., Manica, A. & Mora, C. Shifts in global bat diversity suggest a possible role of climate change in the emergence of SARS-CoV-1 and SARS-CoV-2. *The Science of the total environment* **767,** 145413; 10.1016/j.scitotenv.2021.145413 (2021).

302. Skegg, D. *et al.* Future scenarios for the COVID-19 pandemic. *Lancet (London, England)* **397,** 777–778; 10.1016/S0140-6736(21)00424-4 (2021).

303. Thoradeniya, T. & Jayasinghe, S. COVID-19 and future pandemics: a global systems approach and relevance to SDGs. *Globalization and health* **17,** 59; 10.1186/s12992-021-00711-6 (2021).

304. Tran, K. *et al.* Cell-free production of a therapeutic protein: Expression, purification, and characterization of recombinant streptokinase using a CHO lysate. *Biotechnology and bioengineering* **115,** 92–102; 10.1002/bit.26439 (2018).

305. Molla, A., Paul, A. V. & Wimmer, E. Cell-free, de novo synthesis of poliovirus. *Science (New York, N.Y.)* **254,** 1647–1651; 10.1126/science.1661029 (1991).

306. Kubickova, B. *et al.* A broadly cross-reactive monoclonal antibody against hepatitis E virus capsid antigen. *Appl Microbiol Biotechnol* **105,** 4957–4973; 10.1007/s00253-021-11342-7 (2021).

307. Tarui, H., Imanishi, S. & Hara, T. A novel cell-free translation/glycosylation system prepared from insect cells. *Journal of bioscience and bioengineering* **90,** 508–514 (2000).

308. Lan, J. *et al.* Structure of the SARS-CoV-2 spike receptor-binding domain bound to the ACE2 receptor. *Nature* **581,** 215–220; 10.1038/s41586-020-2180-5 (2020).

309. Mohammad, S. *et al.* SARS-CoV-2 ORF8 and SARS-CoV ORF8ab: Genomic Divergence and Functional Convergence. *Pathogens (Basel, Switzerland)* **9**; 10.3390/pathogens9090677 (2020).

310. Benitez-Cantos, M. S. *et al.* Translation initiation downstream from annotated start codons in human mRNAs coevolves with the Kozak context. *Genome Research* **30,** 974–984; 10.1101/gr.257352.119 (2020).

311. Ahn, J.-H., Hwang, M.-Y., Lee, K.-H., Choi, C.-Y. & Kim, D.-M. Use of signal sequences as an in situ removable sequence element to stimulate protein synthesis in cell-free extracts. *Nucleic Acids Research* **35,** e21; 10.1093/nar/gkl917 (2007).

312. Schuster, N. A. *Characterization and structural prediction of the putative ORF10 protein in SARS-CoV-2* (2020).

313. Mena, E. L. *et al.* ORF10-Cullin-2-ZYG11B complex is not required for SARS-CoV-2 infection. *Proceedings of the National Academy of Sciences of the United States of America* **118**; 10.1073/pnas.2023157118 (2021).

314. Krammer, F. SARS-CoV-2 vaccines in development. *Nature* **586,** 516–527; 10.1038/s41586-020-2798-3 (2020).

315. Smits, V. A. J. *et al.* The Nucleocapsid protein triggers the main humoral immune response in COVID-19 patients. *Biochemical and biophysical research communications* **543,** 45–49; 10.1016/j.bbrc.2021.01.073 (2021).

316. Wilson, L., McKinlay, C., Gage, P. & Ewart, G. SARS coronavirus E protein forms cation-selective ion channels. *Virology* **330,** 322–331; 10.1016/j.virol.2004.09.033 (2004).

317. Verdiá-Báguena, C. *et al.* Coronavirus E protein forms ion channels with functionally and structurally-involved membrane lipids. *Virology* **432,** 485–494; 10.1016/j.virol.2012.07.005 (2012).

318. Pervushin, K. *et al.* Structure and inhibition of the SARS coronavirus envelope protein ion channel. *PLoS pathogens* **5,** e1000511; 10.1371/journal.ppat.1000511 (2009).

319. Mandala, V. S. *et al.* Structure and drug binding of the SARS-CoV-2 envelope protein transmembrane domain in lipid bilayers. *Nature structural & molecular biology* **27,** 1202–1208; 10.1038/s41594-020-00536-8 (2020).

320. Xia, B. *et al.* SARS-CoV-2 envelope protein causes acute respiratory distress syndrome (ARDS)-like pathological damages and constitutes an antiviral target. *Cell Research* **31,** 847–860; 10.1038/s41422-021-00519-4 (2021).

321. Karim, S. S. A. & Karim, Q. A. Omicron SARS-CoV-2 variant: a new chapter in the COVID-19 pandemic. *Lancet (London, England)* **398,** 2126–2128; 10.1016/S0140-6736(21)02758-6 (2021).

322. Meganck, R. M. & Baric, R. S. Developing therapeutic approaches for twenty-first-century emerging infectious viral diseases. *Nature medicine* **27,** 401–410; 10.1038/s41591-021-01282-0 (2021).

7 Directories

7.1 List of Figures

7.2 List of Tables

8 Appendix

8.1 Supplementary Materials

8.1.1 Python script

```
from datetime import datetime
import easygui as eg
import os
import warnings

# The Function "DataFrame.append" generates a warning, as it will be removed in future updates of pandas.
# FutureWarnings are suppressed through warnings.simplefilter
warnings.simplefilter(action="ignore", category=FutureWarning)
import pandas as pd

"""A script to calculate the conductance shift caused by pore insertion in planar lipid bilayer experiments.
It allows the analysis of conductance shift values caused by multiple pore insertions.

To ensure precise results, the script iterates multiple times through all values. The amount of iterations is adjustable.
The script requires a literature value.

Abbrivations:
stddev - standard deviation"""

def set_parameters():
    """Set parameters for the calculations.
    Please modify the values here."""

    global mean_lit, max_pores, deviation, iterations

    # Literature value in pS
    lit_value = 627 # in pS

    # Offset caused by the use of different buffer systems.
    # Set to 1 if same buffer is used or differences are negligible.
    Offset = 1.26
    # Percentual difference from 0.1 M NaCl used in lit_cal and 0.1 M KCl
        used in this thesis.
    # Offset was calculated from data from Hardy et al. 2001

    mean_lit = lit_value * Offset

    # Maximum number of simultaneous pores allowed.
    # Values representing more simultaneous pores are not considered
```

```
    max_pores = 9

    # Allowed deviation. 0.5 equals 50%.
    deviation = 0.25

    # Number of repeats for the calculation of the mean value in
          "calc_mean_multi_pore" function.
    iterations = 100

def get_file_information():
    """Get file and directory information to save the results."""

    global progpath, filepath, data_titel, time

    # Get current time to name savefile
    time = datetime.now().strftime("%m-%d %H:%M").replace(" ", "_").replace(":", "-")

    # Get directory of the script.
    progpath = os.path.dirname(os.path.abspath(__file__))

    # Request a csv-file through an explorer window and get the according filepath.
    filepath = eg.fileopenbox(default=f"{progpath}/*.csv",
          msg="Choose a csv-file.",filetypes="*.csv")
    filepath = filepath.replace("\\", "/")

    # Get name of chosen file.
    data_filename = os.path.splitext(os.path.basename(filepath))
    data_titel = data_filename[0]

    # Open the chosen file and store content to a DataFrame.
    with open(filepath, 'r') as file:
        data_df = pd.read_csv(file)

    return data_df

def calc_mean_ref(mean_lit, deviation, data_df):
    """Calculate the mean value of all values one pore, based on a given reference value.
    Returns lists containing the calculated mean and standarddeviation only."""

    global result_means, result_stds

    # Set the range of data used for the mean calculation.
    mean_lit_range = [mean_lit - (mean_lit * deviation), mean_lit + (mean_lit * deviation)]

    # Drop all values from data_df not in range and give this new DataFrame a new label.
    # data_df is not altered!
    mean_lit_data = pd.DataFrame()
    mean_lit_data = data_df.drop(
        data_df[
```

```
            (data_df['data'] < mean_lit_range[0])
            | (data_df['data'] > mean_lit_range[1])
        ].index
    )

    # Caclulate mean and standard deviaton and save them in the according list.
    mean = mean_lit_data['data'].mean()
    stddev = mean_lit_data['data'].std()
    result_means = [mean]
    result_stds = [stddev]
    print(f"Mean 1: {result_means[-1]}\n")

def sort_data(data_df, min_max_range):
    """Sorts values from a dataframe based on a given range.
    Ranges must be in form of one min and one max value in a list.
    Lists nested in a list are allowed."""

    # Create or clear dataframe for used data
    result_data = pd.DataFrame(columns=['data'])

    for entry in data_df['data']:
            for i, (lower_mean, upper_mean) in enumerate(min_max_range):

                # Check if a value is within the set range.
                if lower_mean < entry < upper_mean:
                    value = entry / (i + 1)
                    result_data = result_data.append({'data': value}, ignore_index=True)

    return result_data

def calc_mean_multi_pore(data_df, deviation):
    """calculate means"""

    # List all theoretical mean value ranges based on the last mean value calculated.
    # Amount of ranges used are defined by the "max_pores" value
    # All ranges are generated as a list and stored in the "theoretical_means" list.
    theoretical_means = [
        [i * result_means[-1] - (mean_lit * deviation), i * result_means[-1] +
                    (mean_lit * deviation)]
        for i in range(1, max_pores + 1)
    ]

    # Sort data through function "sort_data"
    result_data = sort_data(data_df, theoretical_means)

    # Append calculated mean and stddev to the result_means and result_stds lists,
          respectively.
    mean = float(result_data.mean())
    stddev = float(result_data.std())
```

```
    # result_means, result_stds are set to global in "calc_mean_ref"
    result_means.append(mean)
    result_stds.append(stddev)

def store_data():
    """Store output data in a csv-file."""

    # Store calculated mean- and stddev values in one DataFrame.
    results = pd.DataFrame(list(zip(result_means, result_stds)), columns=['mean','stddev'])

    # Create savepath directory if not present.
    savepath = f"{progpath}/results"
    if not os.path.exists(savepath):
        os.makedirs(savepath)

    # Save calculated data to a csv-file.
    # File is located in the script directory in "/results".
    # Result file is named with date and name of the choosen data file.
    with open(f"{savepath}/{time}_{data_titel}.csv", 'w') as file:
                results.to_csv(file,    float_format='%.4f',    sep=";",    index_label="iterations",
line_terminator='\n')

def run_script():
    """Run script if it is not importet.
    This script may be used as a package."""
    if __name__ == "__main__":

        set_parameters()

        data_df = get_file_information()

        calc_mean_ref(mean_lit, deviation, data_df)

        # Repeat calculation any number of times given through "iterations" value.
        for loop in range(iterations):
            calc_mean_multi_pore(data_df, deviation)

            # Print script progress.
            print(f"Loop {loop + 1}/{iterations} compelted!")

        store_data()

run_script()
```

8.2 Supplementary Results

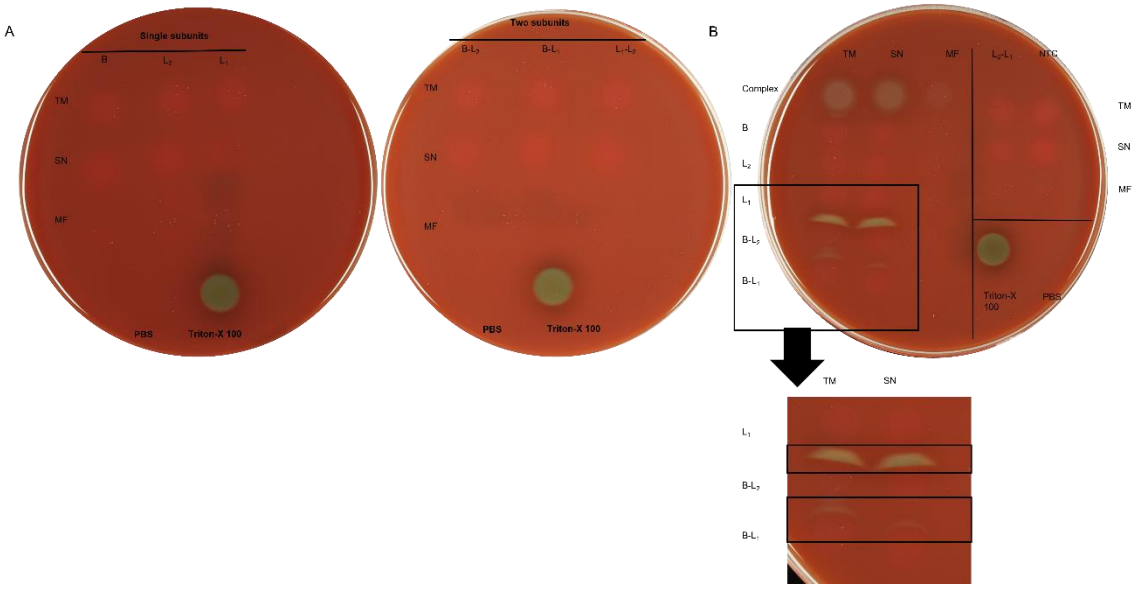

Supplementary Figure 1: Hemolytic activity assessment of Hbl.
Hbl subunits B, L_1 and L_2 were synthesized either separately or in a co-expression of either two or three subunits in CHO lysate. (A) Uncropped 5% sheep blood agar plates from Figure 10 C. (B) Hemolytic activity of the single subunits and two co-expressed subunits was assessed on one single 5% sheep blood agar plate. Crescent formation was emphasized by the black box and enlarged corresponding to Figure 10 D. Taken from Ramm *et al.*, 2021.

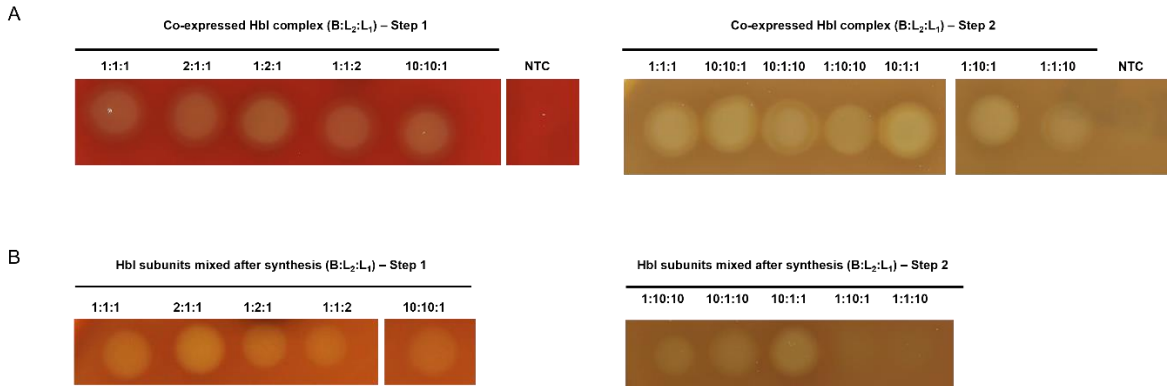

Supplementary Figure 2: Hbl subunit interaction on 5% sheep blood agar plates.
Subunit interactions were assessed by hemolytic activity on 5% sheep blood agar plates. 10 µl of either the reaction mixture of co-expressed Hbl subunits in different molas plasmid ratios (A) or subunits mixed after the individual syntheses (B) were spotted onto the 5% sheep blood agar plates. Modified from Ramm *et al.*, 2021.

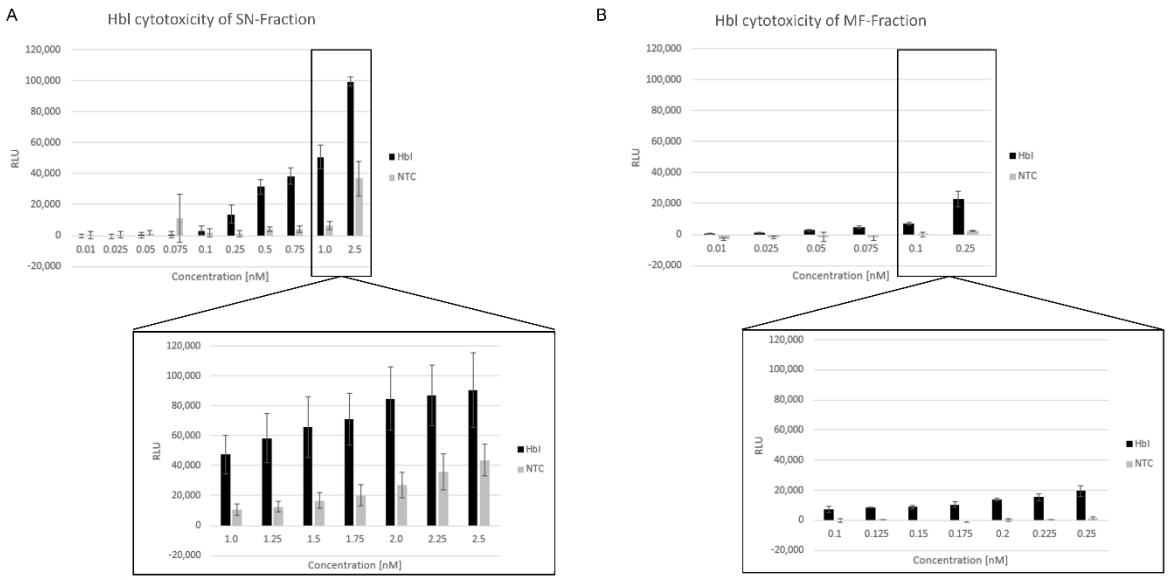

Supplementary Figure 3: Membrane integrity assay for Hbl using propidium iodide.

Hbl subunits B, L1 and L2 were a co-expression in CHO lysate was assessed and tested for its cytotoxic effect on Caco2 cells. Upon Hbl induced membrane rupture, the DNA intercalating agent PI enters the cell's cytoplasm. DNA bound PI was detected at 616 nm using the Mithras^2 LB 943. Hbl tripartite toxin was coexpressed and the SN fraction (A) and the MF fraction (B) were analyzed. An NTC consisting of a volume equivalent reaction without a coding DNA template was used as a negative control. Hbl protein concentrations ranging from 0.01 nM up to 2.5 nM were tested. Standard deviations were calculated from triplicate samples of three independent experiments (n= 9) with the exception of the MF NTC at 0.25 nM as indicated by * (n=5). Figure published in Ramm et al., 2021.

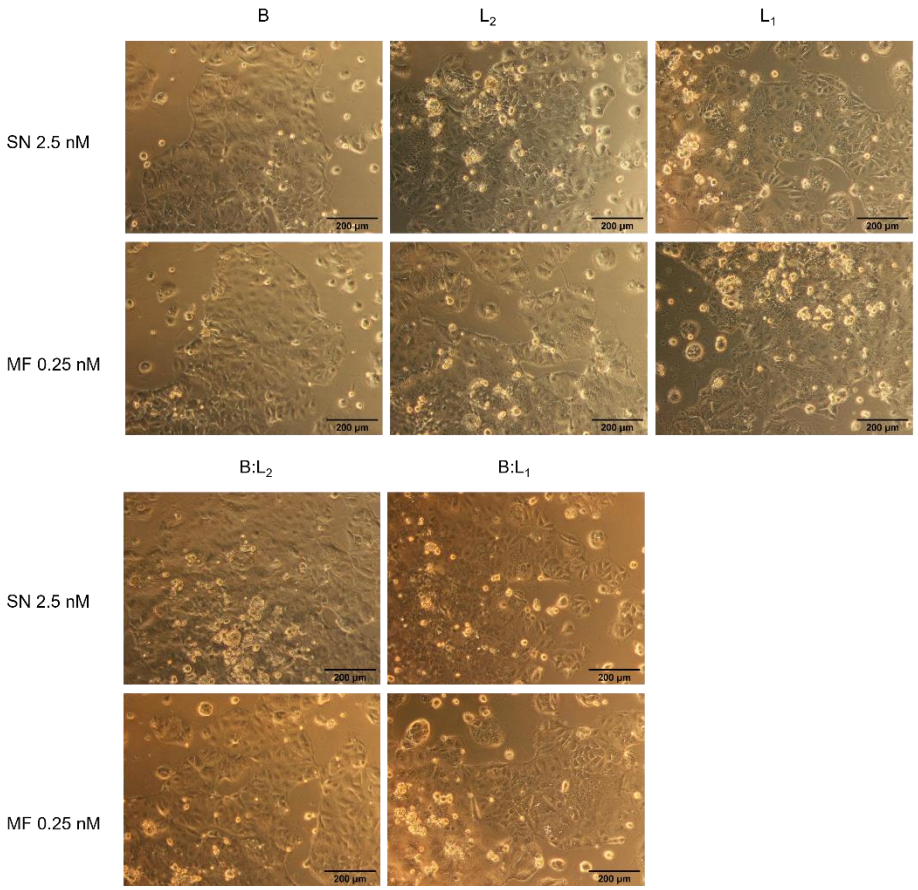

Supplementary Figure 4: Morphological assessment of Caco2 cells after supplementation of Hbl subunits. Hbl subunits were synthesized in CHO lysate either separately or in a co-expression of two subunits. Subsequently, proteins or protein complexes were administered to Caco2 cells (15,000 cells/well) and assessed for their cytotoxic effects. Scale bar indicated 200 µm.

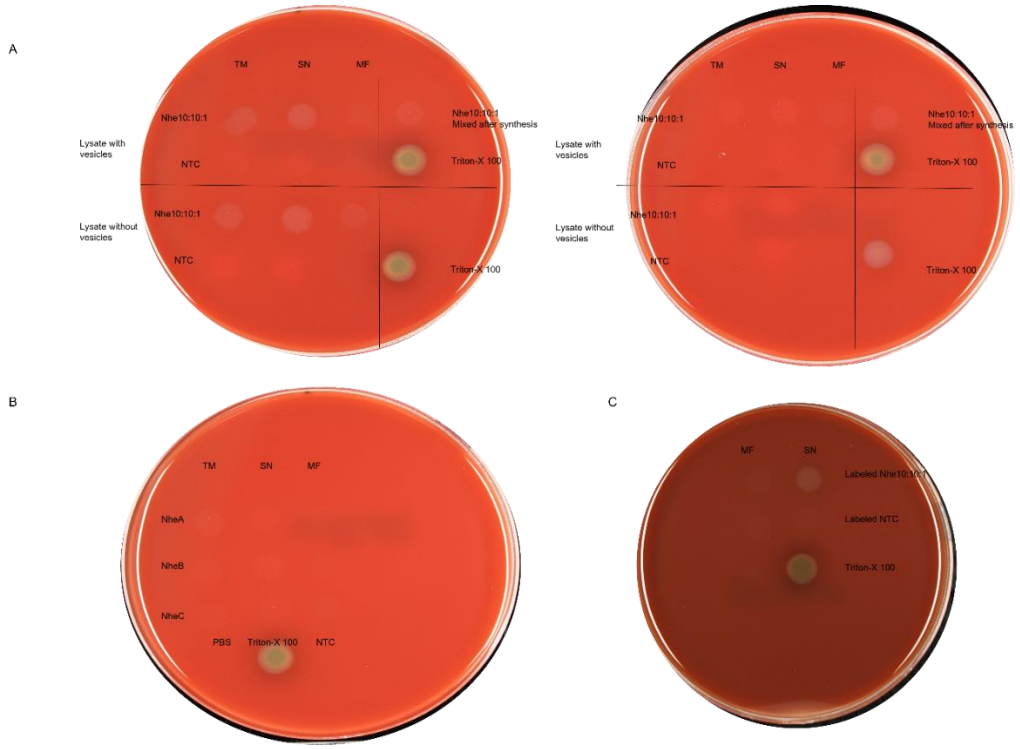

Supplementary Figure 5: Uncropped 5% sheep blood agar plates for the establishment of the cell-free synthesis of Nhe.

Nhe subunits A, B and C were synthesized in CHO lysate either separately or co-expressed to form the tripartite toxin using molar plasmid concentrations of 10:10:1 and 1:1:1 ratios. (A) Hemolytic activity of the Nhe tripartite toxins was assessed on 5% sheep blood agar plates in TM, SN, MF fractions. (B) Hemolytic assessment of Nhe single subunits. (C) Bodipy-labelled Nhe toxin was assessed by in-gel fluorescence and functional activity was assessed by 5% sheep blood agar plates. TM, SN or MF fractions were analyzed. PBS, Triton-X 100 and an NTC were used as controls.

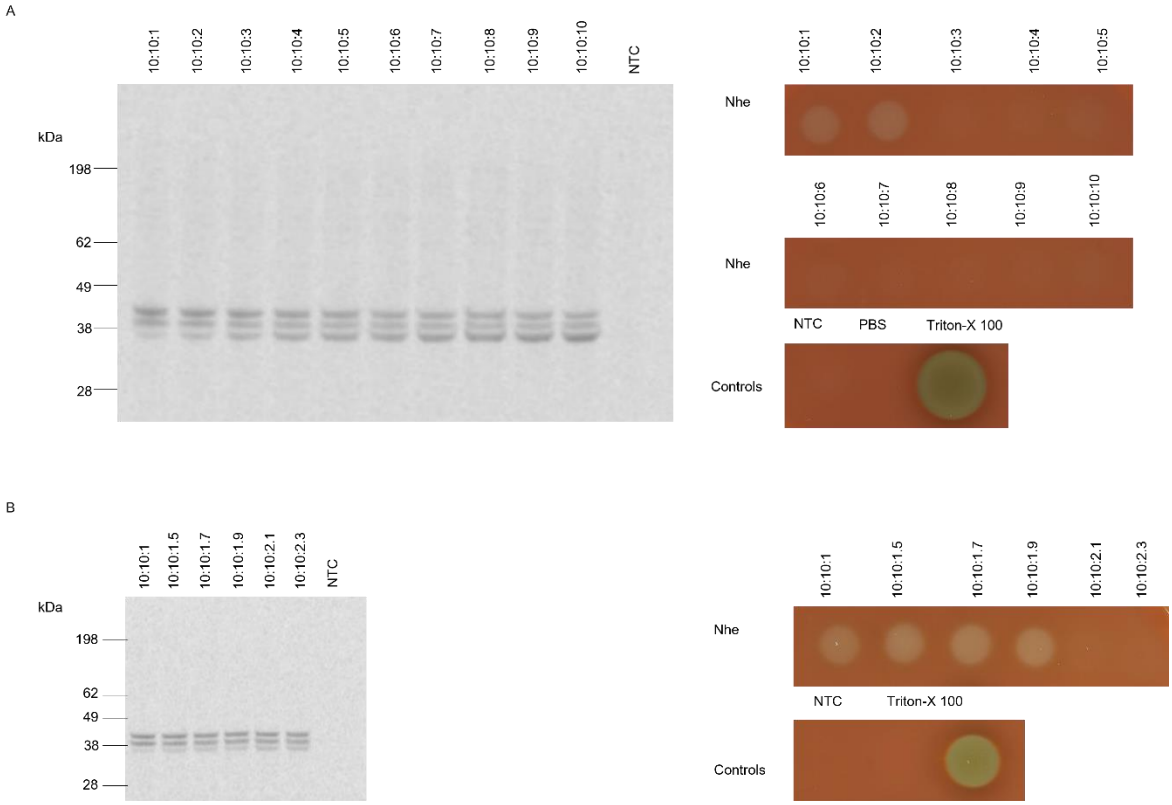

Supplementary Figure 6: Synthesis and hemolytic activity of different molar plasmid ratios for Nhe tripartite toxin.

Co-expressed Nhe subunits A, B and C were synthesized in CHO lysate, an autoradiograph was performed as a quality control and their hemolytic activity was assessed on 5% sheep blood agar plates. PBS and a non-template control (NTC) were used as negative controls and Triton-X 100 as a positive control. (A) First experiment with molar plasmid ratios of 10:10:1, 10:10:2, 10:10:3, 10:10:4, 10:10:5, 10:10:6, 10:10:7, 10:10:8, 10:10:9, 10:10:10. (B) Second experiment with molar plasmid ratios of 10:10:1, 10:10:1.5, 10:10:1.7, 10:10:1.9, 10:10:2.1, 10:10:2.3. Data published and further reproduction of data in different lysates shown in Ramm et al.,2020.

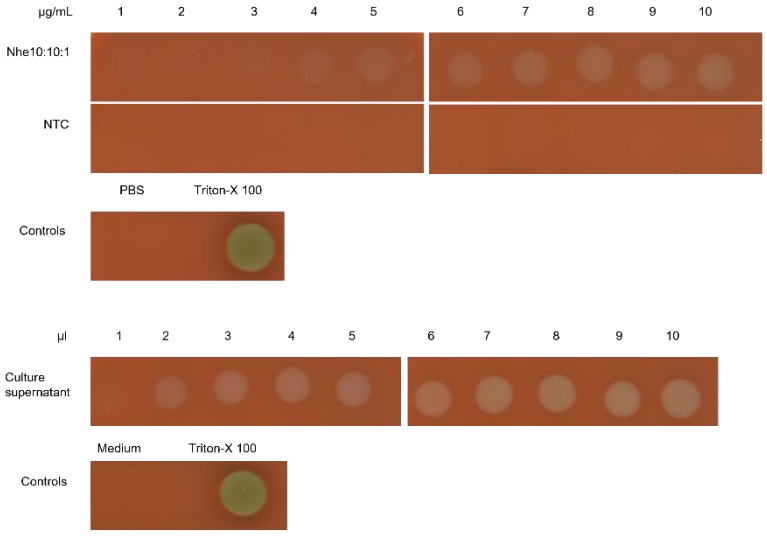

Protein	µg/mL	Measured Pixels	Calculated length [cm]
Cell-free Nhe	10	120.04	0.69
	9	120.00	0.69
	8	105.17	0.60
	7	102.00	0.59
	6	108.00	0.62
	5	102.00	0.59
	4	108.04	0.62
	3	87.05	0.50

Protein	µl	Measured Pixels	Calculated length [cm]
Culture Supernatant	10	126.04	0.72
	9	114.00	0.66
	8	123.00	0.71
	7	117.00	0.67
	6	105.04	0.60
	5	96.05	0.55
	4	96.00	0.55
	3	93.05	0.54
	2	108.00	0.62
Triton-X 100	10	150.03	0.86
1 cm		174.00	1

Supplementary Figure 7: Hemolytic activity of cell-free and cell-based Nhe.

Nhe subunits A, B and C were synthesized in a CHO lysate at a molar plasmid ratio of 10:10:1. The hemolytic activity was assessed on 5% sheep blood agar plates. A serial dilution in PBS of the total reaction mixture containing *de novo* synthesized Nhe toxin was spotted on the blood agar plate. Cell-free synthesized toxin was spotted in a serial dilution of 1 to 10 µg/mL. Different dilutions of Nhe containing culture supernatant from *B. cereus* (s.l.)-strain BfR-BA-01088 were spotted onto 5% sheep blood agar plates to compare the functional activity of cell-free expressed to cell-based expressed Nhe toxin. Culture supernatant was diluted in culture medium. Culture medium, PBS and Triton-X 100 served as controls. Comparison of hemolytic zones was performed by a pixel analysis of the photographs of the blood agar plates using ImageJ. Figure modified from Ramm *et al.,* 2020.

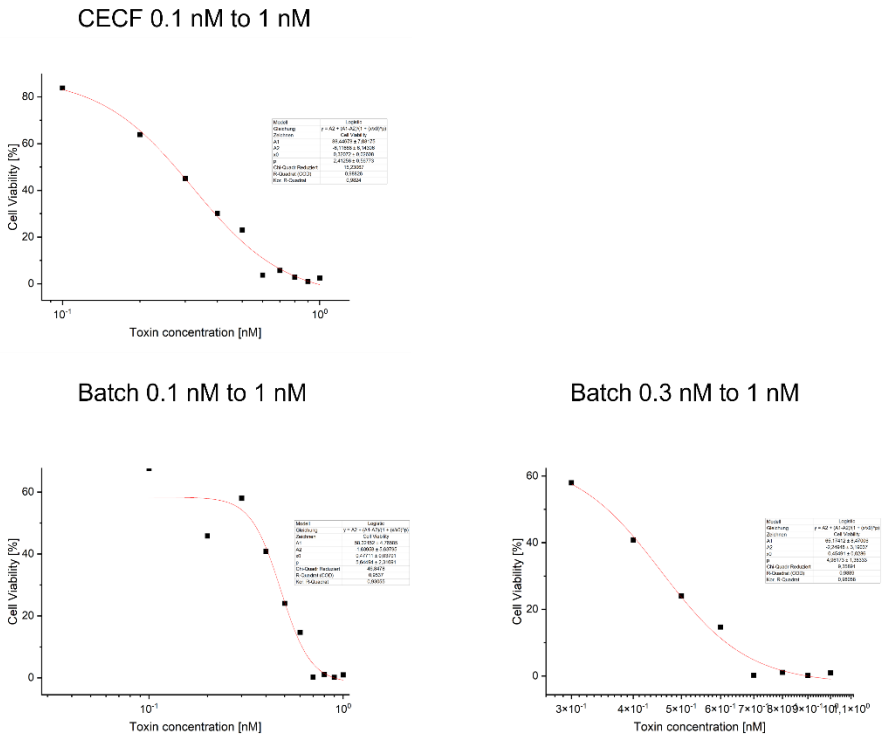

Supplementary Figure 8: Non-linear regression for IC_{50} value determination of Nhe.
Non-linear regression and IC_{50} value determination were performed using Origin 2021.IC_{50} is stated as the EC_{50} value in Origin 2021.

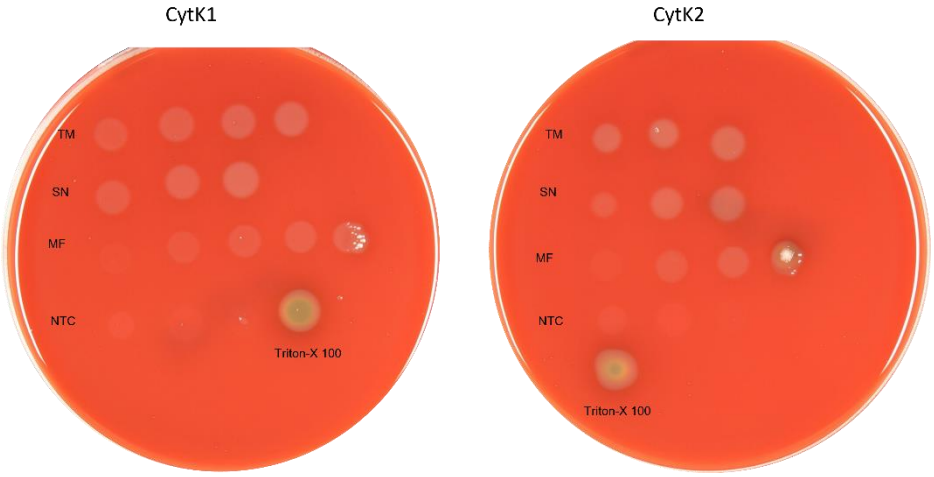

Supplementary Figure 9: Hemolytic activity of CytK1 and CytK2 of each individual fraction.

CytK1 and CytK2 were synthesized in CHO lysate. Samples were fractionated in the translation mixture (TM), the soluble supernatant (SN) and microsomal fraction (MF). Triton-X 100 and a no template control (NTC) were used as controls.

Supplementary Table 1: CytK mutant design.

Mutant	**Modification**	**Suspected effect**
CytK1-A196P	Integration of loop 196-PLY-198	In aHL this loop important for multimerization, thus change of multimerization
CytK1-Q13S	β-strand integration 11-IGSN-14	In aHL this strand is part of multimerization site, thus change of multimerization
CytK1-D191del	α-helix break 190-RDS-192	Potential knock-out, in aHL this mutation resulted in different lipid bilayer interactions
CytK1-I91F	Headgroup modification	β-sheet formation changed, information on the robustness of the pore
CytK1-I91G	Headgroup modification	β-sheet formation changed, information on the robustness of the pore
CytK2-S196P	Integration of loop 196-PLY-198	In aHL this loop important for multimerization, thus change of multimerization
CytK2-Q13S	β-strand integration 11-IGSN-14	In aHL this strand is part of multimerization site, thus change of multimerization
CytK2-D191del	α-helix break 190-RDS-192	Potential knock-out, in aHL this mutation resulted in different lipid bilayer interactions
CytK2-V91F	Headgroup modification	β-sheet formation changed, information on the robustness of the pore
CytK2-V91G	Headgroup modification	β-sheet formation changed, information on the robustness of the pore

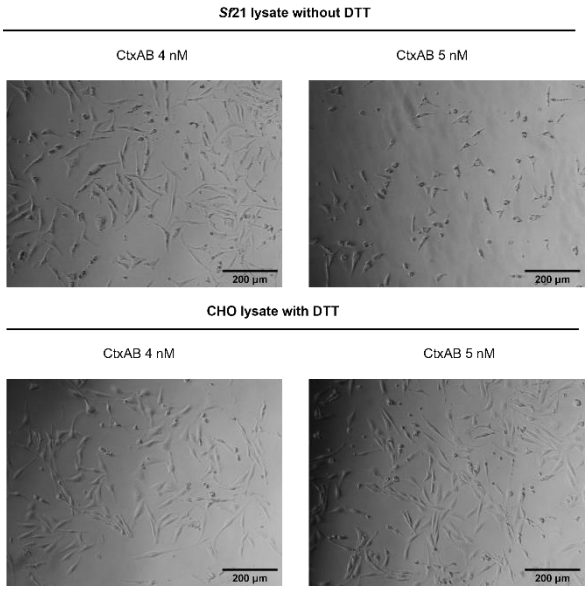

Supplementary Figure 10: Toxicity of Ctx influenced by DTT.
Cell-free synthesized CtxAB supplemented to CHO-K1 cells in a 96-well plate. Morphological changes were investigated after 48 h after the supplementation of CtxAB co-expressed in *Sf*21 lysate not containing DTT and CHO lysate containing DTT. Scale bar indicated 200 µm.

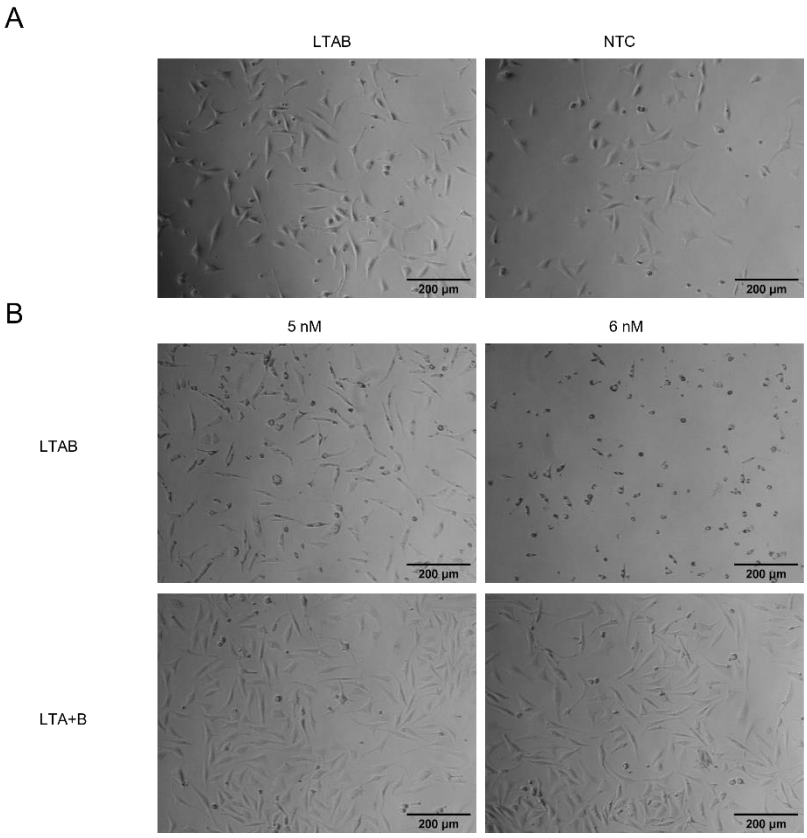

Supplementary Figure 11: Functional activity of LT.
Cell-free synthesized LTAB supplemented to CHO-K1 cells in a 96-well plate. (A) Morphological changes were investigated after 24 h after the supplementation of LTAB co-expressed in *Sf*21 lysate. (B) Morphological changes were investigated after 48 h after the supplementation of LTAB. LTAB was co-expressed in *Sf*21

lysate or the single subunits were pre-synthesized and mixed in a 1:5 molar protein ratio after the synthesis (LTA+B). Scale bar indicated 200 µm. Figure modified from Ramm *et al*., 2022.

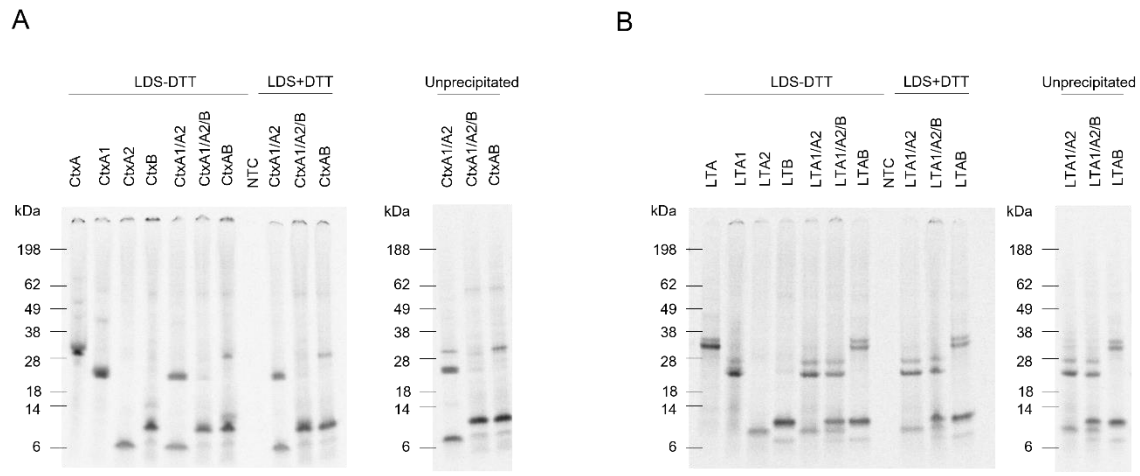

Supplementary Figure 12: Holotoxin formation of Ctx and LT in *Sf*21 lysate.

Single subunits and co-expressed subunits of Ctx (A) and LT (B) were synthesized in *Sf*21 lysate. Autoradiographs depicting the ^{14}C-labelled protein bands after a synthesis. A no template control (NTC) was used as a negative control. Figure modified from Ramm *et al.,* 2022.

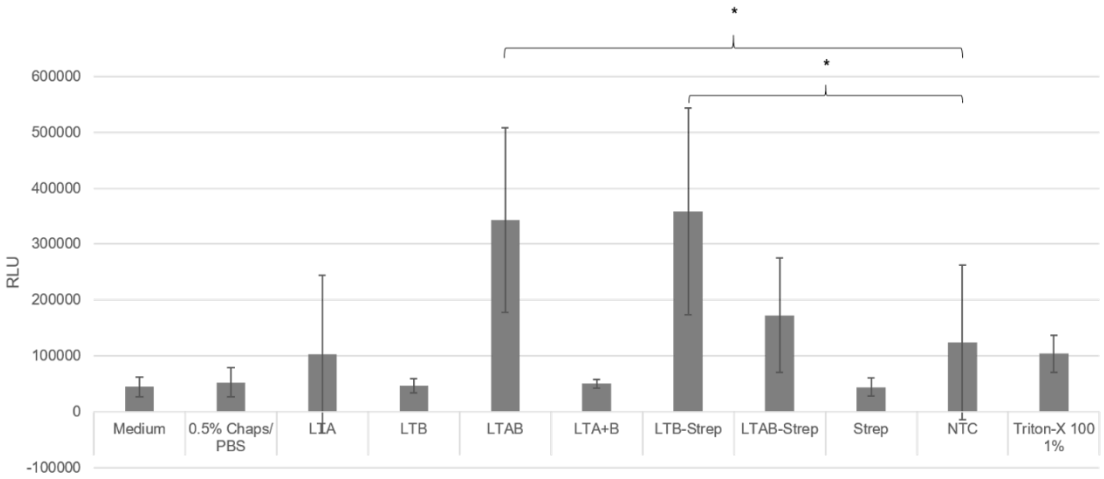

Supplementary Figure 13: Cytotoxicity assessment of LT.

Analysis of cytotoxic effects of LT multimers and single subunits supplemented to CHO-K1 cells after 48 h incubation. Toxins were synthesized in *Sf*21 lysate. CHO-K1 cell were seeded in a 96-well plate (10,000 cells/well). Cytotoxicity was anaylzed using the CellTox CyGreen assay after 48 h. Relative light units (RLU) detected apoptotic effects. Cells supplemented with medium, 0.5% CHAPS/PBS, an NTC in an volume equivalent served as controls. 1% Triton-X 100 was a positive control. Standard deviation derived from three assays with triplicate analysis (n=9). Statistical significance indicated by *. Figure modified from Ramm *et al.,* 2022 .

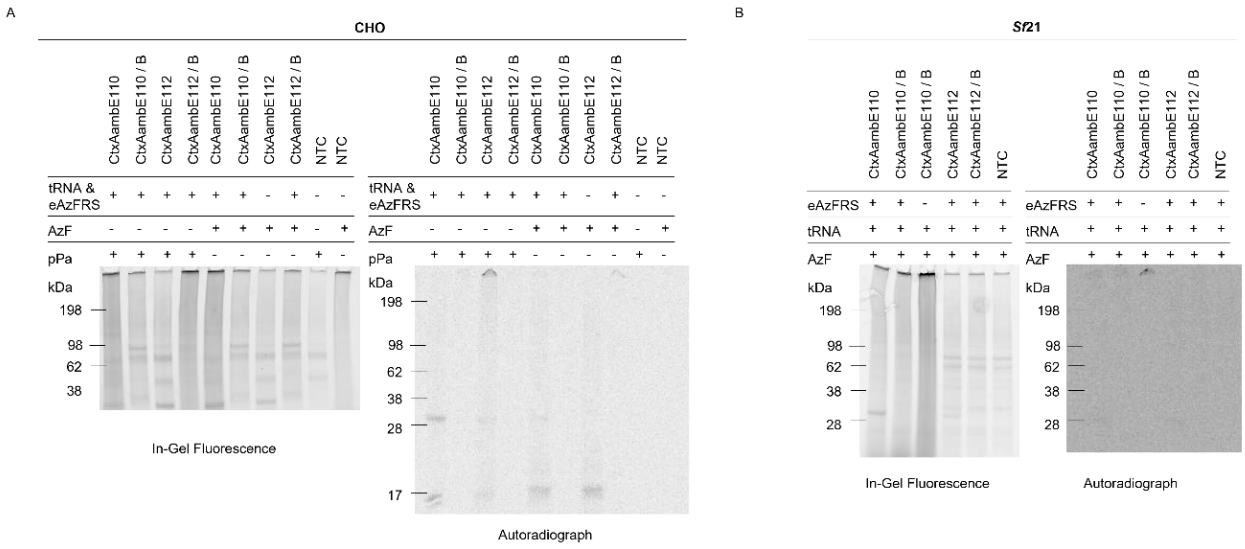

Supplementary Figure 14: CtxAamb co-expression with CtxB in cell-free systems.
Synthesis of CtxAamb mutants and their co-expression with CtxB in (A) CHO and (B) *Sf*21 lysate. Shown are in-gel fluorescence and autoradiography of modified subunits and co-expressed multimer after the incorporation of AzF and pPa and subsequent labelling with DyLight-632 phosphine and Sulfo-Cy5-Azide.

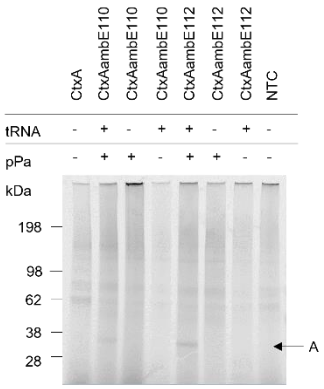

Supplementary Figure 15: Incorporation of pPa to CtxAamb using the modified CHO system.
Synthesis of CtxAamb mutants in the modified CHO lysate. Shown is the in-gel fluorescence of modified subunits after the incorporation of pPa and subsequent labelling with Sulfo-Cy5-Azide.

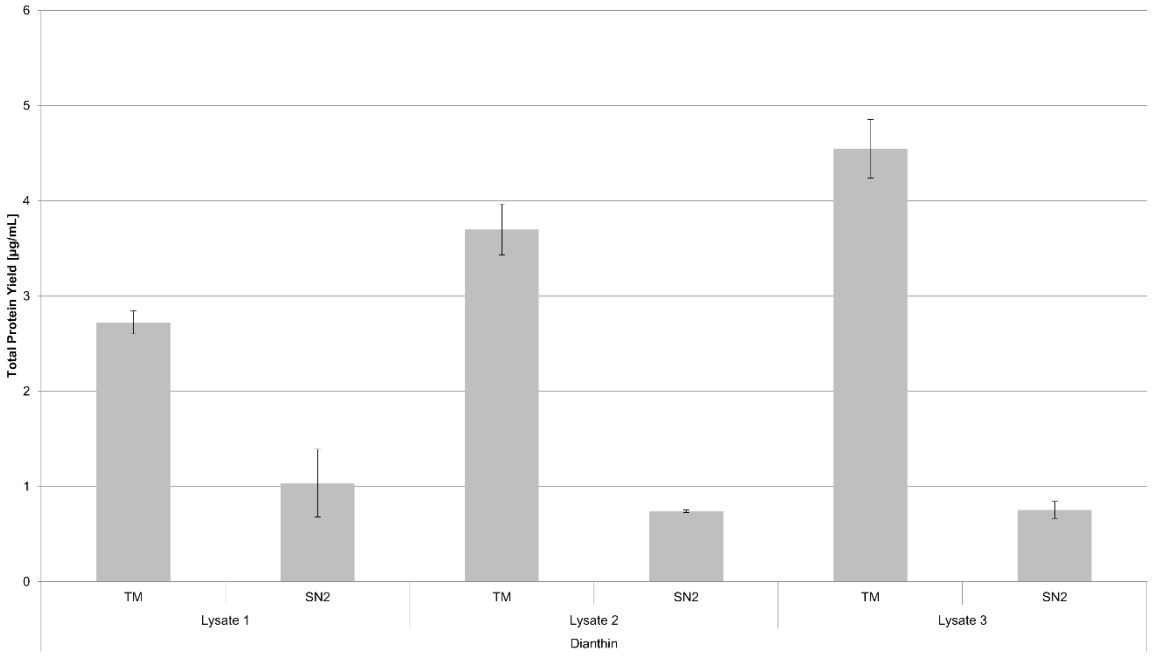

Supplementary Figure 16: Translocation efficiency of Dianthin in three CHO lysates.
Dianthin was synthesized in three CHO lysates and quantitatively analyzed. Quantitative analysis of cell-free Dianthin by liquid scintillation counting. Standard deviations were calculated from duplicate analysis. The crude translation mixture (TM) and the translocated soluble protein (SN2) were analyzed.

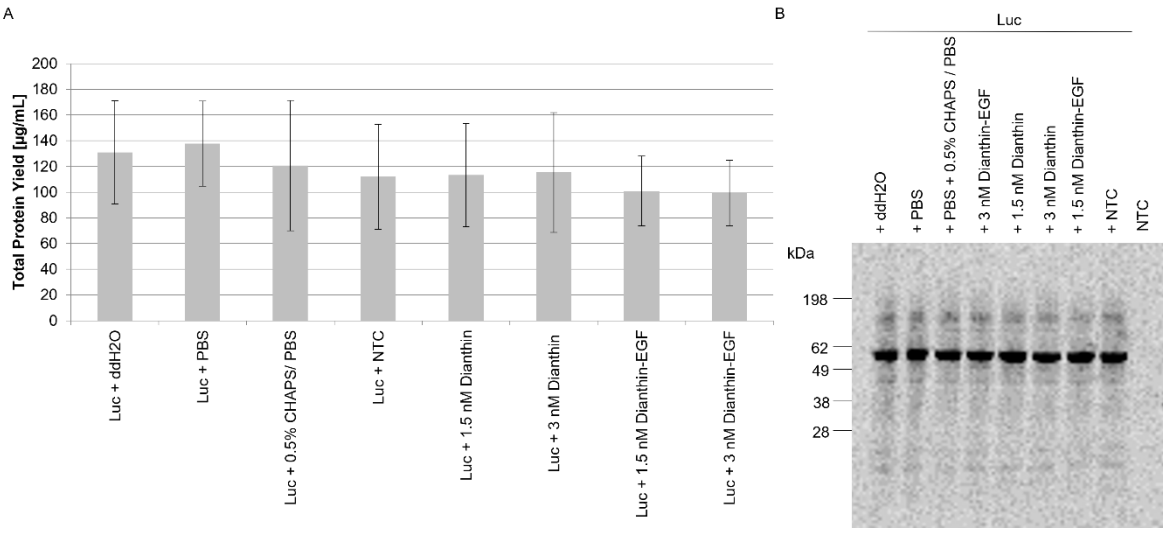

Supplementary Figure 17: *In vitro* inhibition of LUC synthesis in *E. coli*.
Dianthin and Dianthin-EGF were pre-synthesized in CHO lysate and added to the cell-free synthesis of LUC in an *E. coli* system. (A) Quantitative analysis of cell-free synthesized LUC in the presence of Dianthin and Dianthin-EGF or control supplements by liquid scintillation counting. Standard deviations were calculated from duplicate analysis of three individual experiments. Statistical analysis using an ANOVA based on Bonferroni. (B) Exemplary autoradiograph showing ^{14}C-leucine labelled TM fraction of LUC after the supplementation of Dianthin and Dianthin-EGF as well as control supplements.

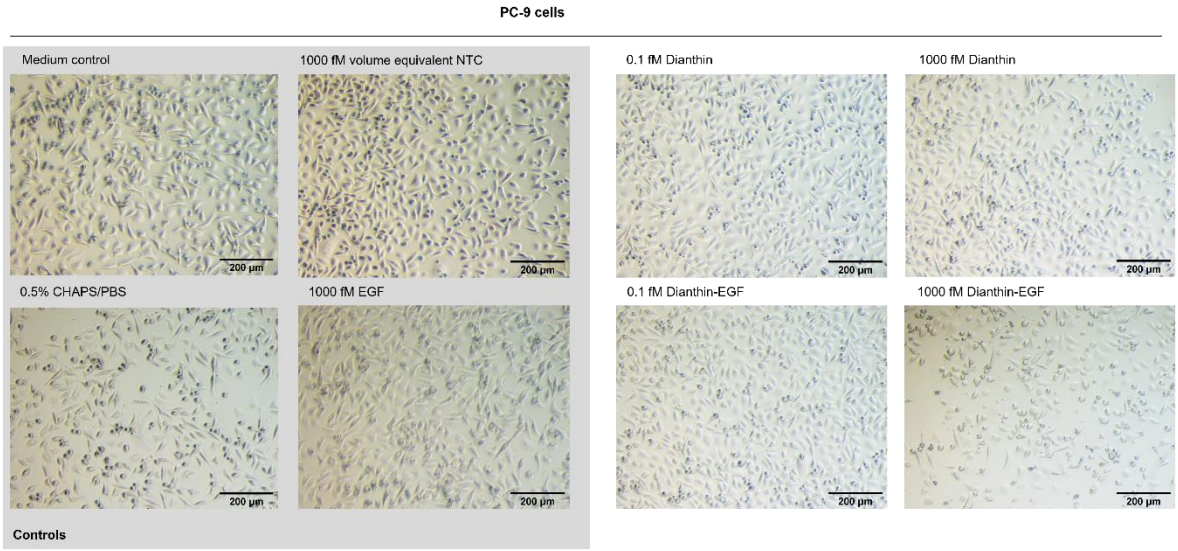

Supplementary Figure 18: PC-9 cells supplemented with Dianthin and Dianthin-EGF .
Cell-free synthesized Dianthin and Dianthin-EGF supplemented to PC-9 cells in a 24-well plate. Morphological changes of PC-9 cells after supplementation of Dianthin and Dianthin-EGF concentrations of 0.1 fM and 1000 fM without SO1861 were investigated. Untreated cells, cells supplemented with CHAPS/PBS, cells supplemented with an NTC and cells supplemented with cell-free synthesized EGF were used as controls. Scale bar indicated 200 µm.

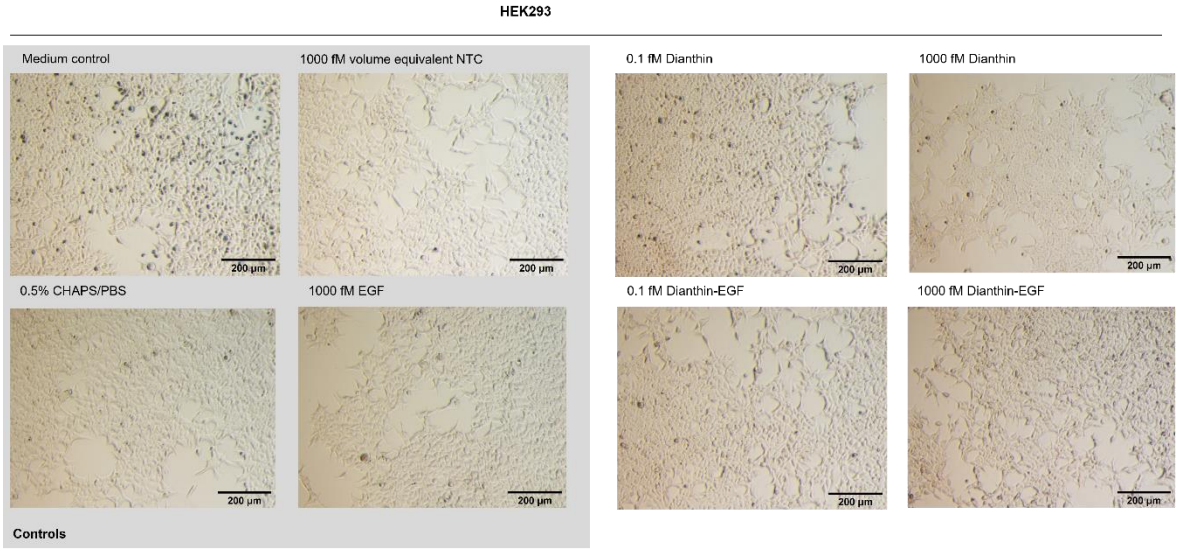

Supplementary Figure 19: HEK293 cells supplemented with Dianthin and Dianthin-EGF.
Cell-free synthesized Dianthin and Dianthin-EGF supplemented to HEK293 cells in a 24-well plate. Morphological changes of HEK293 cells after supplementation of Dianthin and Dianthin-EGF concentrations of 0.1 fM and 1000 fM without SO1861 were investigated. Untreated cells, cells supplemented with CHAPS/PBS, cells supplemented with an NTC and cells supplemented with cell-free synthesized EGF were used as controls. Scale bar indicated 200 µm.

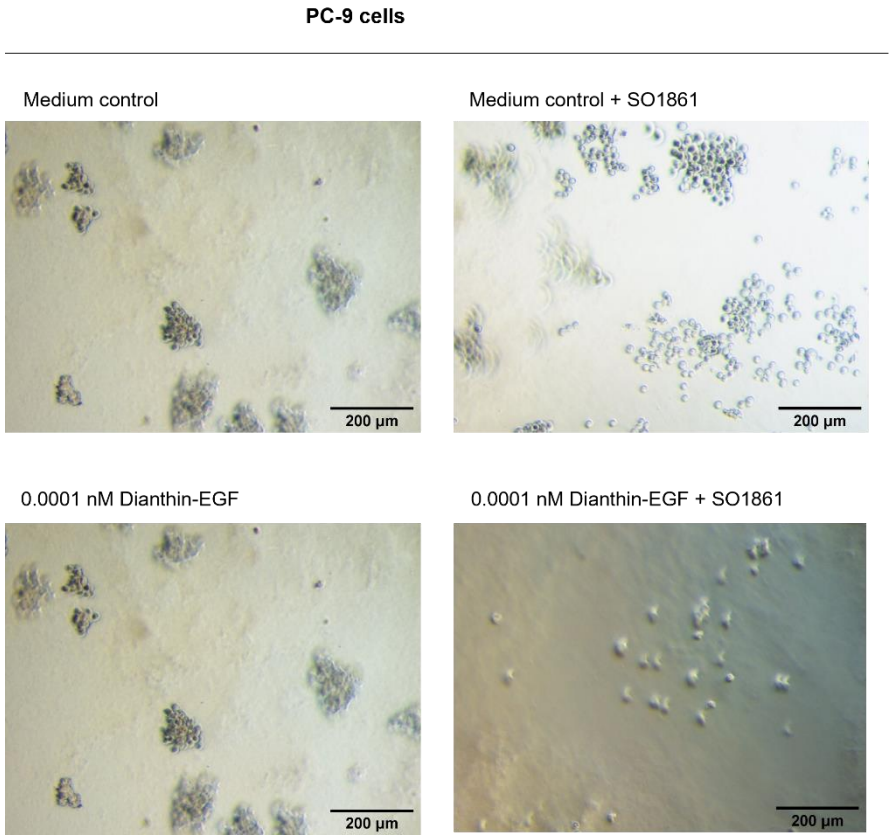

Supplementary Figure 20: Soft-agar assay using PC-9 cells.
Cell-free synthesized Dianthin-EGF was supplemented to PC-9 cells embedded in a Soft-agar set up. Untreated cells were used as controls. Scale bar indicated 200 µm.

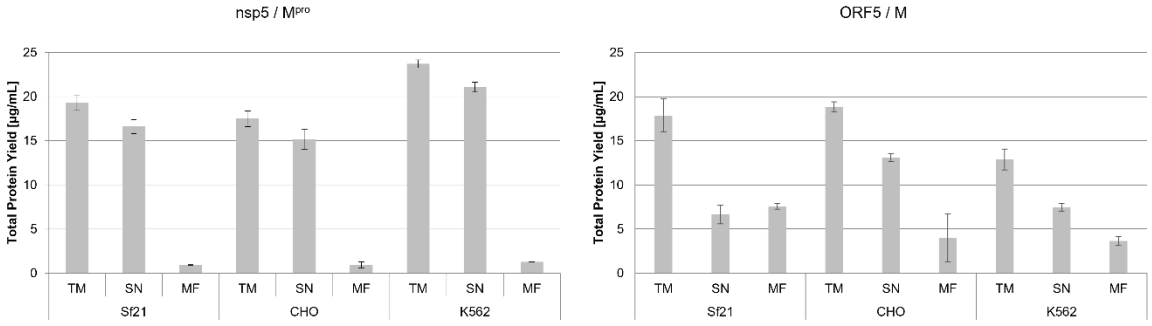

Supplementary Figure 21: Fractionation of nsp5 and the M protein in three lysates.
Nsp5 and the M protein were synthesized in batch-based reactions with *Sf*21, CHO and K562 lysate. Quantitative analysis of ^{14}C-labelled proteins was performed by liquid scintillation counting. Standard deviations were calculated from triplicate analysis. The translation mixture (TM) was separated into the soluble proteins in the supernatant (SN) and the microsomal fraction (MF).

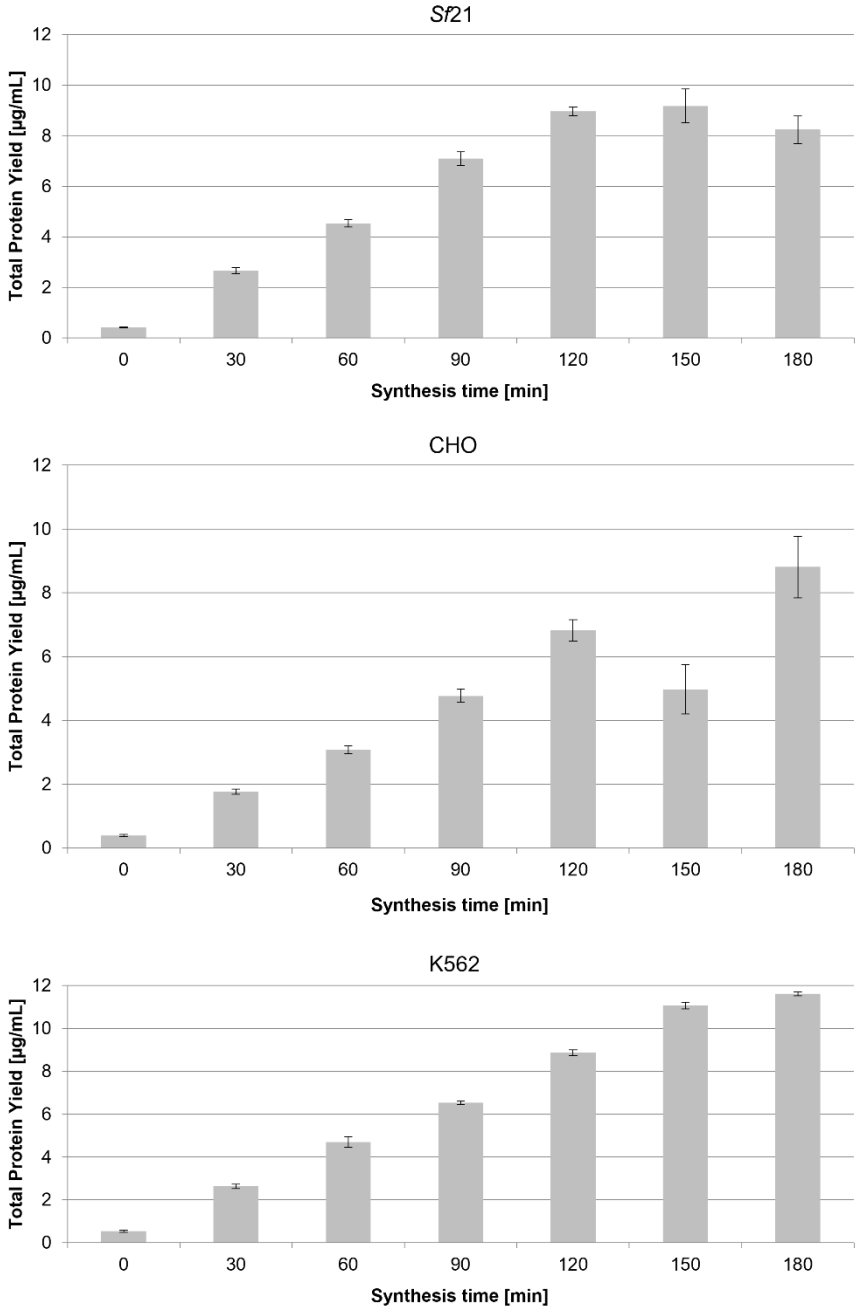

Supplementary Figure 22: Synthesis time row of the E protein.

The E protein was synthesized in batch-based reactions with *Sf*21, CHO and K562 lysate. Quantitative analysis of ^{14}C-labelled proteins was performed by liquid scintillation counting. Standard deviations were calculated from triplicate analysis. Total protein yield at different times during the reaction was determined.

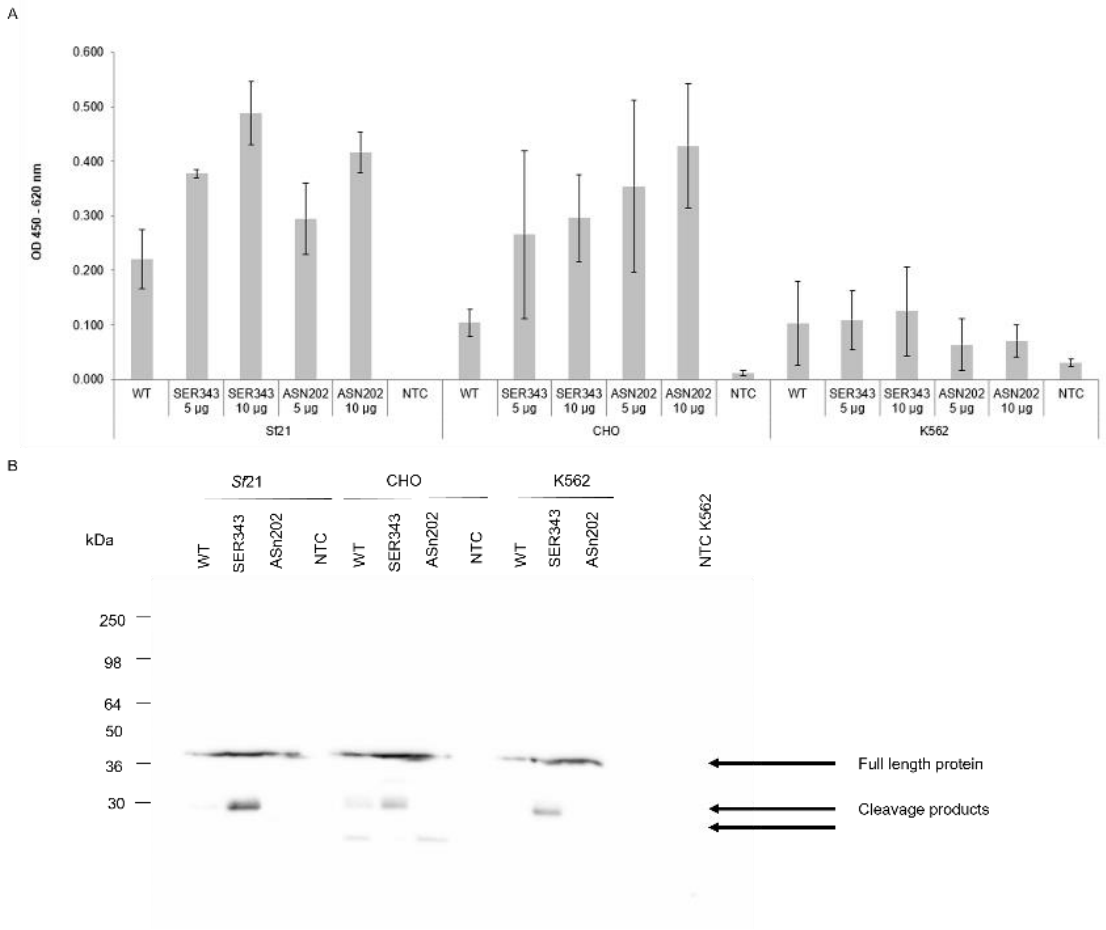

Supplementary Figure 23: Detection of SARS-CoV2 N protein in three lysates.

The nucleocapsid WT protein as well as both mutants (SER343 & ASN202) were synthesized in *Sf*21, CHO and K562 cell-free systems. Detection of cell-free synthesized nucleocapsid protein in an in-solution ELISA (A), and Western Blot (B).

Curriculum vitae

Personal details are not available in the online version of this doctoral thesis.

List of publications, oral and poster presentations

Publications, peer reviewed

Ramm F., Dondapati SK., Trinh, HA., Wenzel D., Walter, RM., Zemella A., Kubick S.: The Potential of Eukaryotic Cell-Free Systems as a Rapid Response to Novel Zoonotic Pathogens: Analysis of SARS-CoV-2 Viral Proteins. Front. Bioeng. Biotechnol. 10, 617; 10.3389/fbioe.2022.896751 (2022).

Ramm, F., Jack, L., Kaser, D., Schlosshauer JL., Zemella, A., Kubick, S.: Cell-Free Systems Enable the Production of AB5 Toxins for Diagnostic Applications. Toxins 14, 233; 10.3390/toxins14040233 (2022).

Ramm, F., Stech, M., Zemella, A., Frentzel, H., Kubick, S.: The Pore-Forming Hemolysin BL Enterotoxin from Bacillus cereus: Subunit Interactions in Cell-Free Systems. Toxins 13, 807; 10.3390/toxins13110807 (2021).

Kubickova B., Schenk JA., Ramm F., Markuškienė K., Reetz J., Dremsek P., Tamosiunas PL., Laima Cepulyte L., Trinh HA., Johannes Scholz J., Memczak H., Hovestädt M., Ryll R., Petraityte-Burneikiene R., Corman VM., Andersson A., Becher D., Groschup MH., Kubick S., Sellrie F., Johne R., Ulrich RG.: A broadly cross-reactive monoclonal antibody against hepatitis E virus capsid antigen. *Appl Microbiol Biotechnol* 105, 4957–4973; 10.1007/s00253-021-11342-7 (2021).

Ramm, F., Dondapati SK., Thoring L., Zemella A., Wüstenhagen DA., Frentzel H., Stech M., Kubick S.: Mammalian cell-free protein expression promotes the functional characterization of the tripartite non-hemolytic enterotoxin from Bacillus cereus. *Sci Rep* 10, 2887; 10.1038/s41598-020-59634-8 (2020).

Oral presentation

Qualifying cell-free systems for the characterization of toxic proteins
7th German Pharm-Tox Summit (March 2022)

Poster presentations

AB_5 toxins as tools for diagnostic and therapeutic applications using eukaryotic cell-free systems
7th German Pharm-Tox Summit (March 2022)

Cell-free production and functional characterization of pore-forming proteins
New and Emerging Technologies (September 2021)

Cell-free synthesis as a rapid response to COVID-19
Werkstattberichte Anti-Corona-Programm (September 2021)

The Assessment of cytotoxic Proteins using Cell-Free Protein Synthesis
New and Emerging Technologies (September 2019)

Eukaryotic Cell-free Systems: A novel Platform Technology for Production and functional Characterization of Pore-forming Toxins
4th German Pharm-Tox Summit (February 2019)

Harvesting functional Dianthin from a microsome based cell-free system.
Annual Congress Biotechnology 2020+ (October 2018)

Cell-free production of proteinogenic toxins for future medical treatments: Harvesting functional Dianthin from a vesicle based eukaryotic system
2nd International Symposium -Cutting Edge Concepts in Molecular Pharmacology and Toxinology (September 2018)

Synthesis and functional characterization of toxins using cell-free systems as a novel protein production platform
Statusseminar des glyconet Berlin Brandenburg e.V. (April 2018)

Cell-free protein synthesis as a new platform technology for toxin synthesis and functional characterization
3rd German Pharm-Tox Summit (February/March 2018)